Discovery and Study of Exotic Radio Pulsars

by

Jason William Thomas Hessels

Department of Physics
McGill University
Montréal, Québec, Canada

A thesis submitted to McGill University
in partial fulfilment of the requirements of the degree of
Doctor of Philosophy

(Submitted August 25th, 2006)

Your file Votre référence
ISBN: 978-0-494-32194-2
Our file Notre référence
ISBN: 978-0-494-32194-2

Abstract

We have conducted both targeted and wide-field surveys for exotic radio pulsars using the Arecibo, Green Bank, and Parkes telescopes. A survey of 22 globular clusters with Arecibo has discovered 11 millisecond pulsars, almost doubling the number known in these clusters. Ten of the new pulsars are in binaries, and 3 show eclipses. This survey has discovered significantly more very fast-spinning pulsars ($P_{\rm spin} \lesssim 4\,$ms) and short orbital period systems ($P_{\rm orb} \lesssim 6\,$hr) than previous surveys of the same clusters. We discuss some characteristics of the globular cluster pulsar population in general, particularly the luminosity function.

In observations of the rich, massive cluster Terzan 5 with the Green Bank Telescope we have discovered the 1.396-ms pulsar J1748−2446ad, which is now the fastest-spinning neutron star known. The difficulty in detecting this pulsar, due to its very low flux density and high eclipse fraction (∼40% of the orbit), suggests that even faster-spinning neutron stars exist. If the pulsar has a mass less than $2\,M_\odot$, then its non-rotating radius is constrained by the spin period to be $< 16\,$km. The short period of this pulsar also constrains models that suggest gravitational radiation, through an r-mode instability, limits the maximum spin frequency of neutron stars.

Arecibo and Parkes searches of 5 potential *ASCA* X-ray counterparts to unidentified *EGRET* γ-ray sources have revealed the young, energetic pulsar J2021+3651. PSR J2021+3651 is associated with the X-ray source AX J2021.1+3651, which in turn is likely associated with the *COS B* γ-ray source

2CG 075+00, also known as GeV J2020+3658 and 3EG J2021+3716. This solves the long-standing mystery of this source's nature. Subsequent X-ray imaging and timing of PSR J2021+3651 with the *Chandra* observatory revealed a pulsar wind nebula whose morphology is reminiscent of the equatorial tori seen around some young pulsars, along with thermal emission from an embedded point source ($kT_\infty = 0.15 \pm 0.02\,\mathrm{keV}$). An observation in continuous-clocking mode reveals a possible pulse detection from the point source.

Finally, we discuss two on-going, untargeted surveys of the Galactic Plane. These surveys hope to find exotic pulsars whose properties will elucidate the physics of pulsars, or which can potentially be used to study ultra-dense matter and strong gravity. The PALFA survey at Arecibo is using a 7-beam receiver at 1.4 GHz to cover the Arecibo-visible Galactic Plane. 28 pulsars have been discovered so far, including a few young, energetic pulsars and the youngest pulsar binary system known, PSR J1906+0746. The GBT350 survey at Green Bank is covering the Galactic Plane north of $\delta = 40°$. Despite the 350-MHz observing frequency, the high resolution of these data allows us to maintain sensitivity to fast pulsars. Thus far, 14 pulsars have been discovered, 3 of which were found in time-domain searches for bright, dispersed bursts.

Résumé

Nous avons éffectué des recherches de pulsars éxotiques en utilisant les téléscopes d'ondes radio Arecibo, Green Bank, et Parkes. Au cours d'une recherche qui visait 22 amas globulaires à l'aide du téléscope Arecibo, nous avons découvert 11 pulsars millisecondes, ce qui n'est pas loin de doubler la population de pulsars connus dans ces amas. Dix de ces nouveaux pulsars sont dans des systèmes binaires, dont 3 démontrent des éclipses. Au cours de cette recherche, nous avons découvert plus de pulsars tournant très rapidement ($P_{\rm rot} \lesssim 4\,{\rm ms}$) et de systèmes compacts ($P_{\rm orb} \lesssim 6\,{\rm hr}$) qu'au cours des recherches précédantes qui visaient ces amas. Nous discutons de certaines charactéristiques de la population de pulsars dans les amas globulaires, particulièrement de la distribution de luminosités.

Les observations de l'amas massif Terzan 5 faites à l'aide du téléscope de Green Bank ont révélé l'existence de PSR J1748−2446ad, qui, avec une période de rotation de 1.396 ms, est le pulsar connu tournant le plus rapidement. La difficulté de détection d'un pulsar comme PSR J1748−2446ad, qui a un flux faible et qui est éclipsé pendant 40% de la durée de son orbite, implique que d'autres pulsars tournant encore plus rapidement existent. Si PSR J1748−2446ad a une masse $< 2\,{\rm M}_\odot$, sa période de rotation implique que son rayon est $< 16\,{\rm km}$. La courte période de rotation de ce pulsar met aussi des contraintes sur les modèles qui disent que le taux de rotation maximale d'une étoile à neutron est limité par l'émission d'ondes gravitationelles.

Les recherches de pulsations radio faites à l'aide des téléscopes Arecibo

et Parkes dans les directions de 5 sources de rayons-X *ASCA* associées avec des sources de rayons-γ non-identifiés d'*EGRET* ont révélé l'existence de PSR J2021+3651, un jeune pulsar énergétique. PSR J2021+3651 est associé avec la source de rayons-X AX J2021.1+3651, qui est elle même associée avec la source de rayons-γ *COS B* 2CG 075+00, aussi connue sous les noms GeV J2020+3658 et 3EG J2021+3716. Nous montrons ainsi l'imagerie et le chronométrage de ce pulsar réalisés à l'aide de l'observatoire *Chandra*. Ces observations ont révélé l'existence d'une source ponctuelle thermique ($kT_\infty = 0.15 \pm 0.02\,\mathrm{keV}$) se trouvant à la position du pulsar, et d'une nébuleuse à vent de pulsar de morphologie toroidale. Ces observations ont aussi révélé de possibles pulsations en rayons-X provenant de ce pulsar.

Finalement, nous discutons de deux recherches de pulsations dans le plan de la galaxie. Le but de ces recherches est de découvrir des pulsars éxotiques qui pouront nous aider à mieux comprendre la physique des pulsars, ou qui pouraient servir comme outils pour étudier la matière ultra-dense et la gravité forte. La recherche PALFA réalisé à l'aide d'Arecibo se sert d'un récepteur de 7 faisceaux à 1.4 GHz pour couvrir le plan galactique visible d'Arecibo. À date, 28 pulsars ont été découverts, incluant quelques jeunes pulsars énergétiques et le plus jeune système binaire connu, PSR J1906+0746. La recherche GBT350 réalisé à l'aide de Green Bank couvre le plan galactique au nord de $\delta = 40°$. En dépit de la fréquence d'observation de 350 MHz, la haute résolution de ces données nous permet de garder une haute sensibilité aux pulsars rapides. À date, 14 pulsars ont été découverts, dont 3 ont été découverts uniquement dans les recherches des séries temporelles pour les éclats dispersés.

Preface

Statements of Originality and Contributions of Co-Authors

A summary of the background literature pertinent to this thesis is given in Chapters 1−3. Original work is presented in Chapters 4−8. These chapters are the collection of three previously published papers in *Science*, the *Astrophysical Journal Letters*, and the *Astrophysical Journal*, as well as one manuscript in preparation for the *Astrophysical Journal* and a description of two major projects in progress. What links these chapters is that they all present surveys for radio pulsars, newly discovered pulsars resulting from these searches, and in some cases follow-up work on these discoveries.

Here I give bibliographic information for parts of this thesis which have been published elsewhere, a statement pertaining to the originality of the research presented in each of Chapters 4−8, as well as statements addressing the contributions to this work made by myself and my collaborators/co-authors.

Chapter 4 - A 1.4-GHz Survey for Pulsars in Globular Clusters with Arecibo:

Hessels, J. W. T., Ransom, S. M., Stairs, I. H., Kaspi, V. M., & Freire, P. C. C., A 1.4-GHz Survey for Pulsars in Globular Clusters with Arecibo, to be submitted to the Astrophysical Journal.

This draft paper presents searches for pulsars in 22 globular clusters with the Arecibo telescope. It is the deepest search of these clusters ever conducted. Our survey employed a higher observing frequency and higher resolution data-recording than the only previous major survey of these clusters with Arecibo, which was conducted 10 years prior to the start of our survey. We used the most sensitive and computationally efficient algorithms available for detecting pulsars in binary systems. Our survey discovered 11 millisecond pulsars, almost doubling the known population in these globular clusters. 10 of these new pulsars are in binary systems, and 3 show eclipses. We find a significantly higher proportion of binaries and pulsars with very short spin periods ($P_{\rm spin} < 4\,{\rm ms}$) than previous searches of these clusters. We also investigate the characteristics of the total observed population of pulsars in globular clusters and determine their luminosity distribution.

This survey and the follow-up studies of our discoveries were a major undertaking, which required 6 proposals to the Arecibo observatory and over 400 hr of observations with the Arecibo telescope. I have been involved in this project since the very first observation and have played a major role throughout the project. I have made significant contributions to every aspect of this project, including the writing of telescope proposals and divising observation strategy. I performed the majority of the required observations. I also did the majority of the preparatory data reduction and searching for pulsars. I was directly responsible for the discovery of 6 of the 11 new sources and aided in the discovery of the other 5, which were found by my collaborator Dr. Scott Ransom. Dr. Ransom is the author of the software suite PRESTO, used to perform these searches. Roughly 40 *years* of computer processing time were required to thoroughly search these data for pulsations. This was accomplished in much less than 40 years by analyzing the data in parallel using a large computer cluster called "The Borg", which our group constructed specifically for

this purpose. This computer system was largely designed and constructed by Dr. Ransom, but I played an increasingly large role in the maintenance of the system as time went by. I also made contributions to the development and refinement of the data reduction pipeline. While the majority of the timing analysis of the new pulsars was performed by Dr. Ransom, Dr. Ingrid Stairs, and Dr. Paulo Freire, I still played an active role in this part of the work as well by obtaining orbital solutions for three of the pulsars. The draft paper presented in Chapter 4 was written by myself with important suggestions on the content of the manuscript provided by all co-authors. I have presented this work both orally and in poster form at several national and international conferences.

Chapter 5 - A 716-Hz Pulsar in Terzan 5

Hessels, J. W. T., Ransom, S. M., Stairs, I. H., Freire, P. C. C., Kaspi, V. M., & Camilo, F., A Radio Pulsar Spinning at 716 Hz, Science, 311, 1901, 2006.

This paper presents deep observations of the rich, dense globular cluster Terzan 5 with the Green Bank Telescope at 2 GHz. Searches of these observations resulted in the discovery of PSR J1748−2446ad, which has a spin period of 1.396 ms (spin frequency of 716 Hz). PSR J1748−2446ad is now the fastest-spinning pulsar known, breaking the 24-yr record held by PSR J1937+21, which has a spin period of 1.558 ms. The maximum spin rate that a neutron star can achieve has potentially important implications for the supra-nuclear equation of state, accretion physics, and the prevalence of gravitational radiation from super-fast-spinning neutron stars. Because of the strong observational bias against finding systems similar to PSR J1748−2446ad, the discovery of this pulsar suggests that even faster-spinning pulsars exist. We use the spin rate of PSR J1748−2446ad to constrain its radius as a function of assumed

mass and discuss implications for the period distribution of millisecond pulsars.

Dr. Ransom created the software suite PRESTO, used to perform these searches. I have meticulously searched many observations of Terzan 5 in order to discover PSR J1748−2446ad. The searches I conducted also discovered 4 other pulsars, which are presented in Ransom et al. 2005, Science, 307, 892 (see List of Refereed Publications). All authors have participated in the data-taking process, with Dr. Ransom performing the majority of the observations. Myself, Dr. Freire, Dr. Ransom, and Dr. Stairs were all involved in the refinement of PSR J1748−2446ad's orbital parameters. I did a significant amount of background literature research in the process of writing the paper presented in Chapter 5. Valuable suggestions on the content of this manuscript have been provided by all co-authors. I have presented this work both orally and in poster form at several national and international conferences.

Chapter 6 - A New Candidate Gamma-Ray Pulsar

Roberts, M. S. E., **Hessels, J. W. T.**, Ransom, S. M., Kaspi, V. M., Freire, P. C. C., Crawford, F., & Lorimer, D. R., PSR J2021+3651: A Young Radio Pulsar Coincident with an Unidentified EGRET γ-ray Source, Astrophysical Journal Letters, 577, 19L, 2002.

This paper presents deep searches for radio pulsations towards 5 X-ray counterparts to *EGRET*-identified γ-ray sources. The young, energetic Vela-like radio pulsar J2021+3651 was discovered coincident with one of the sources, and presents a likely low-energy counterpart to both the X-ray source AX J2021.1+3651 and γ-ray source 3EG J2021+3716. This discovery likely solves the long-standing mystery of what is creating the γ-rays observed from this source. PSR J2021+3651 is thus likely a rare γ-ray emitting pulsar, of which only 6 have been confirmed. Such pulsars provide a different window on

pulsar physics than that provided by the radio pulsars.

The X-ray source list which we searched was compiled by Dr. Mallory Roberts, who also did the X-ray analysis included in this paper. Dr. Ransom created the software suite PRESTO, used to perform these searches. I was responsible for carefully searching all the sources for radio pulsations and discovered PSR J2021+3651. Dr. Fronefield Crawford performed an independent search of the three Parkes sources with different search software. No new sources were discovered in that analysis. I wrote the paper presented in Chapter 6, with Dr. Roberts providing significant guidance in the writing of the discussion section. I have presented this work both orally and in poster form at several national and international conferences.

Chapter 7 - Discovery of an X-ray Pulsar Wind Nebula Associated with PSR J2021+3651

Hessels, J. W. T., Roberts, M. S. E., Ransom, S. M., Kaspi, V. M., Romani, R. W., Ng, C.-Y., Freire, P. C. C., & Gaensler, B. M., Observations of PSR J2021+3651 and its X-ray Pulsar Wind Nebula G75.2+0.1, Astrophysical Journal, 612, 389, 2004.

This paper presents follow-up X-ray timing and imaging of the area around PSR J2021+3651 (whose discovery is presented in Chapter 6) with the *Chandra X-ray Observatory*. These observations resolve the previously known *ASCA* X-ray source and reveal a point source surrounded by a compact nebula. The point source is coincident with the radio timing position of PSR J2021+3651, and the nebula is likely a pulsar wind nebula, powered by the pulsar's relativistic wind. Such nebula are rare (roughly only 20 are known), but can provide important physical insights into the nature of the pulsar. We also present potential X-ray pulsations from the pulsar and long-term phase coherent radio

timing, which revealed a glitch.

I performed the X-ray imaging, with guidance provided by Dr. Mallory Roberts. The majority of the basic analysis tools are provided by the Chandra X-ray Center. Dr. Roger Romani performed the spatial fitting of the nebula using a model created by himself and Dr. C.-Y. Ng. I did both the radio and X-ray timing analysis with assistance from Dr. Scott Ransom. I wrote the paper presented in Chapter 7. Dr. Roberts provided significant help in the writing of the discussion and the description of the spatial fitting was written by Dr. Romani. All other co-authors provided valuable comments and critiques throughout the writing process.

Chapter 8 - Continuing Surveys of the Galactic Plane

Work from Cordes et al. 2006, Lorimer et al. 2006, and Hessels et al. in preparation for publication.

This chapter describes two on-going large-scale surveys of the Galactic Plane for pulsars: the PALFA and GBT350 surveys.

PALFA is the first multibeam survey with Arecibo, and the deepest large-scale survey for pulsars ever undertaken. Given the high time and frequency resolution of the data recorder, it is likely that this survey will significantly increase the number of known millisecond pulsars in the Galactic Plane. The first results from the PALFA survey have been presented in Cordes et al. 2006 and Lorimer et al. 2006 (see List of Refereed Publications). 28 pulsars have been discovered in this survey so far.

The PALFA survey is run by a collaboration of roughly 30 pulsar astronomers. As such, the observations and pulsar discoveries of this survey have been made by a number of people. Drs. Dunc Lorimer and David Champion created the "quicklook" search processing program, which has been used

to discover all the pulsars so far. Despite the large size of this collaboration, I have contributed significantly to this project. I have spearheaded the planning and cataloguing of observations through the creation of a customized survey database and associated software and performed dozens of observing sessions, in which seven new pulsars have been found. I have also taken the lead in planning and proposing follow-up studies of some of the sources, including X-ray observations of the young, energetic pulsar PSR J1856+02. I have also had a hand in the planning and development of full-resolution search processing.

GBT350 is the first Galactic Plane survey to be conducted using the GBT. It is the deepest survey of the northern Galactic Plane ever done. The results of the GBT350 survey will be published as Hessels et al. after the survey is completed. So far, 14 pulsars have been discovered, including three "sporadic" pulsars which were discovered via their bright single pulses.

Compared with the PALFA project, the GBT350 survey is a much smaller collaboration. This projects is a collaboration between myself and Dr. Scott Ransom, Dr. Vicky Kaspi, Dr. Mallory Roberts, and Dr. David Champion. I have taken the leading role in this project. I have written telescope proposals, and planned and performed a large fraction of the survey and follow-up observations. Dr. Ransom is the author of the software suite, PRESTO, which contains the core routines used to perform these searches. Given the need to automate the processing of this large dataset, I have constructed a full reduction pipeline and customized database to analyze this data efficiently using the power of our large computer cluster. I have performed all the searching and discovered all the 14 pulsars found in the survey thus far. I have also taken the leading role in follow-up observations and timing analysis of these new sources.

List of Refereed Publications

1. **Hessels, J. W. T.**, Ransom, S. M., Stairs, I. H., Freire, P. C. C., Kaspi, V. M., & Camilo, F., A Radio Pulsar Spinning at 716 Hz, Science, 311, 1901–1904, 2006.

2. Lorimer, D. R., Stairs, I. H., Freire, P. C. C., Cordes, J. M., Camilo, F., Faulkner, A. J., Lyne, A. G., Nice, D. J., Ransom, S. M., Arzoumanian, Z., Manchester, R. N., Champion, D. J., van Leeuwen, J., Mclaughlin, M. A., Ramachandran, R., **Hessels, J. W. T.**, Vlemmings, W., Deshpande, A. A., Bhat, N. D., Chatterjee, S., Han, J. L., Gaensler, B. M., Kasian, L., Deneva, J. S., Reid, B., Lazio, T. J., Kaspi, V. M., Crawford, F., Lommen, A. N., Backer, D. C., Kramer, M., Stappers, B. W., Hobbs, G. B., Possenti, A., D'Amico, N., & Burgay, M., Arecibo Pulsar Survey Using ALFA. II. The Young, Highly Relativistic Binary Pulsar J1906+0746, Astrophysical Journal, 640, 428–434, 2006.

3. Cordes, J. M., Freire, P. C. C., Lorimer, D. R., Camilo, F., Champion, D. J., Nice, D. J., Ramachandran, R., **Hessels, J. W. T.**, Vlemmings, W., van Leeuwen, J., Ransom, S. M., Bhat, N. D. R., Arzoumanian, Z., McLaughlin, M. A., Kaspi, V. M., Kasian, L., Deneva, J. S., Reid, B., Chatterjee, S., Han, J. L., Backer, D. C., Stairs, I. H., Deshpande, A. A., & Faucher-Giguere, C.-A., Arecibo Pulsar Survey Using ALFA. I. Survey Strategy and First Discoveries, Astrophysical Journal, 637, 446–455, 2006.

4. Lorimer, D. R., Xilouris, K. M., Fruchter, A. S., Stairs, I. H., Camilo, F., Vazquez, A. M., Eder, J. A., McLaughlin, M. A., Roberts, M. S. E., **Hessels, J. W. T.**, & Ransom, S. M., Discovery of 10 Pulsars in an Arecibo Drift-Scan Survey, Monthly Notices of the Royal Astronomical Society, 359, 1524-1530, 2005.

5. Ransom, S. M., **Hessels, J. W. T.**, Stairs, I. H., Freire, P. C. C., Camilo, F., Kaspi, V. M., & Kaplan, D. L., Twenty-One Millisecond Pulsars in Terzan 5 Using the Green Bank Telescope, Science, 307, 892–896, 2005.

6. Freire, P. C. C., **Hessels, J. W. T.**, Nice, D. J., Ransom, S. M., Lorimer, D. R., & Stairs, I. H., The Millisecond Pulsars in NGC 6760, Astrophysical Journal, 621, 959–965, 2005.

7. **Hessels, J. W. T.**, Roberts, M. S. E., Ransom, S. M., Kaspi, V. M., Romani, R. W., Ng, C.-Y., Freire, P. C. C., & Gaensler, B. M., Observations of PSR J2021+3651 and its X-Ray Pulsar Wind Nebula G75.2+0.1, Astrophysical Journal, 612, 389–397, 2004.

8. Ransom, S. M., Stairs, I. H., Backer, D. C., Greenhill, L. J., Bassa, C. G., **Hessels, J. W. T.**, & Kaspi, V. M., Green Bank Telescope Discovery of Two Binary Millisecond Pulsars in the Globular Cluster M30, Astrophysical Journal, 604, 328–338, 2004.

9. Roberts, M. S. E., **Hessels, J. W. T.**, Ransom, S. M., Kaspi, V. M., Freire, P. C. C., Crawford, F., & Lorimer, D. R., PSR J2021+3651: A New γ-Ray Pulsar Candidate, Advances in Space Research, 33, 577–580, 2004.

10. Roberts, M. S. E., **Hessels, J. W. T.**, Ransom, S. M., Kaspi, V. M., Freire, P. C. C., Crawford, F., & Lorimer, D. R., PSR J2021+3651: A Young Radio Pulsar Coincident with an Unidentified EGRET γ-Ray Source, Astrophysical Journal Letters, 577, L19–L22, 2002.

Acknowledgements

First of all, I would like to heartily thank my supervisor Vicky Kaspi, who is a world-class astrophysicist and amazingly also finds time to be a devoted mother to three young children. I honestly can't imagine having chosen a better supervisor. Vicky's vast knowledge, experience and kindness were a constant help during my doctoral work. Vicky was also very generous in providing funds for attending international conferences and observing runs, where I met many colleagues and friends. In the five years I spent at McGill, I have seen Vicky build a large pulsar research group and, furthermore, bring McGill's physics department to the forefront of Canadian astrophysics. I was also extremely fortunate that Vicky hired fantastic post-doctoral fellows to work in the group. In particular, I must mention Scott Ransom and Mallory Roberts, both of whom imparted no small measure of their experience and expertise to me. Scott, thank you for writing PRESTO, constructing the original Borg, and sharing so much of your knowledge about Linux and computers with me. I've learned so much from you. Mallory, thank you for giving me a broader view of astronomy by involving me in topics outside my nominal research project. Two of my regular collaborators outside McGill also deserve special mention: Ingrid Stairs and Paulo Freire, both excellent researchers and kind human beings.

Of course, I must also thank my fellow grad students in the pulsar group, and some of our hijinx should be recorded here for the sake of posterity. To my office-mates Fotis, Cindy, Rim, and Maggie: you people are hilarious. How much more enriching work can be because of your co-workers. I will never

forget the Creole swearing we learned from Mike the 3rd floor janitor, our secret office liquor cabinet (mostly stocked by Mike), the secret television for watching the Simpsons (hidden behind a white lab coat), or watching cars sliding back down the hill of rue Université on snowy days. Also our office plants, François and Madeleine. François: I hope you live on without me; Madeleine: you died too young, and it's my fault for poor watering habits. It was also a pleasure to work with the other past and present members of the McGill pulsar group: René Breton, David Champion, Claude-André Faucher-Giguerre, Marjorie Gonzalez, and Maxim Lyutikov. Thank you everyone... the beer is on me!

My parents Wiggert and Tina and sister Liz deserve extra-special thanks for all the years they have encouraged and patiently put up with me.

The papers included in this thesis benefitted from the great contributions and guidance of my co-authors: F. Camilo, F. Crawford, P. C. C. Freire, B. M. Gaensler, V. M. Kaspi, D. R. Lorimer, C.-Y. Ng, S. M. Ransom, M. S. E. Roberts, R. W. Romani, and I. H. Stairs. For the work presented in Chapter 8, I would like to thank all the members of the PALFA consortium, especially D. J. Champion.

The research presented in this thesis has been generously funded by a number of Canadian and international agencies including the FQRNT, NSF, and CFI. I am very thankful to the Natural Science and Engineering Research Council of Canada (NSERC) for funding me through undergraduate, masters, Ph.D., and now a post-doctoral fellowship. These funds have given me the freedom to focus on my studies. The Canadian Foundation for Innovation (CFI), through New Opportunities Grants, provided the necessary funds to construct both the Borg and Next Generation Borg computer clusters, which were critical in obtaining almost all the results presented here.

In doing this research, I was very fortunate to have access to the best telescopes in the world. The Arecibo Observatory is part of the National Astronomy and Ionosphere Center, which is operated by Cornell University under a

cooperative agreement with the National Science Foundation. I am very grateful to all the telescope operators at Arecibo and to Arun Venkataraman, Jeff Hagen, Ganesh R, and Bill Sisk for their work in creating and maintaining the WAPP data recorders. The National Radio Astronomy Observatory (NRAO) is a facility of the National Science Foundation and is operated under a cooperative agreement by Associated Universities, Inc.. At NRAO Green Bank, I would like to acknowledge the telescope operators, as well as Carl Bignell and Frank Ghigo for support with observations. The Parkes radio telescope is part of the Australia Telescope, which is funded by the Commonwealth of Australia for operation as a National Facility managed by CSIRO. The Chandra X-ray Observatory is operated by the National Aeronautics and Space Administration (NASA). Over the years I have made extensive use of NASA's Astrophysics Data System (ADS).

To my parents.
Wiggert Hein Johannes and Tina Hendrika Hessels

Contents

List of Figures

List of Tables

Chapter 1

Introduction

Space, the final frontier...
– From a popular 1960's television series.

1.1 Neutron Stars and Pulsars

1.1.1 Neutron Stars and the Discovery of Pulsars

Not long after the discovery of the neutron in 1932 by James Chadwick, Walter Baade and Fritz Zwicky predicted that a star composed chiefly of this newly found particle could be an endpoint of stellar evolution, created in a supernova (Baade & Zwicky, 1934). They postulated that these incredibly dense stars would be supported from gravitational collapse only by the degenerate pressure of their neutrons, which, according to the Pauli exclusion principle for fermions, must inhabit distinct energy states, rather than all settling into the ground state. This enticing theoretical prediction remained relatively unexplored, however, as the tiny size ($< 20\,\mathrm{km}$ radius) of these stars would make them very difficult to detect via their optical surface emission.

It was not until 1967 that Jocelyn Bell, a graduate student working under

the supervision of Anthony Hewish at Cambridge University, discovered what would ultimately be recognized as the first observational evidence for a neutron star[1]. Using a dipole array she and Hewish had constructed to discover distant radio galaxies, Bell noticed a curious "bit of scruff" on her chart recorder one night at 19:19 right ascension. Hewish was skeptical that the signal was anything other than terrestrial interference, because it initially failed to repeat at the same right ascension (most likely because of scintillation). But, after repeated observations, the signal reappeared and showed the correct 4 minute per day sidereal drift indicative of astronomical sources. Increased time resolution showed that the "scruff" was in fact highly regular pulsations repeating every 1.3 s. Initially the regularity of these pulsations seemed unnatural, and the possibility that the signal was from an extra-terrestrial civilization was discussed along with plausible astronomical explanations. After careful consideration, however, Hewish, Bell, and their collaborators eventually concluded that there was indeed some natural process at work, likely associated with the rotation or pulsation of some kind of very compact source (Hewish et al., 1968). The term "pulsar", which is now used to describe these objects, is short for pulsating star. Thomas Gold was the first to correctly recognize that the unprecentedly short time scales of the pulsations identified by Hewish and Bell result from the rotation of a neutron star (Gold, 1968). Anthony Hewish was awarded the 1974 Nobel prize in physics for the discovery of pulsars. This prize was shared with Sir Martin Ryle, who developed the aperture synthesis technique.

1.1.2 Formation and General Description

Simply speaking, there are three established endpoints of stellar evolution which main-sequence stars will ultimately become: white dwarfs, neutron stars, and black holes. White dwarfs are the end product of main-sequence stars with

[1]Note however that earlier the same year Pacini (1967) suggested that a neutron star could be the source of energy powering the Crab Nebula.

masses below $\sim 8\,M_\odot$. They are formed in a relatively quiet collapse of the core of the parent star, after it has consumed the nuclear fuel in its core. Conversely, the most massive stars ($M \gtrsim 40\,M_\odot$) create black holes at the end of their relatively short lifetimes in extremely powerful supernova (or perhaps hypernova) explosions. Stars with masses between roughly $8 - 40\,M_\odot$ (the exact mass range is hotly debated, and also depends strongly on metallicity) will eventually become neutron stars[2]. A neutron star is also formed during a supernova explosion. During the explosion, the outer layers of the star are violently expelled, while the stellar core collapses. The collapsed core becomes so dense that the majority of the protons and electrons combine to form neutrons through inverse beta decay ($p^+ + e^- \longrightarrow n + \nu_e$). This process also results in the creation of a large number of neutrinos, which escape because of their extremely low cross-section for interaction. This scenario is strongly supported by the detection of neutrinos from supernova 1987A by the Irvine-Michigan-Brookhaven and Kamiokande II underground water Cherenkov detectors (Bionta et al., 1987; Hirata et al., 1987). The resulting neutron star is too dense to be supported by thermal pressure, which is how normal main-sequence stars support themselves against gravitational collapse, and is instead supported by neutron degeneracy pressure.

Pulsars are rapidly rotating, highly magnetized neutron stars that show pulsations mostly at radio wavelengths $\lambda \sim 10 - 100\,\mathrm{cm}$, but sometimes also in optical, X-rays, and γ-rays. Based on the rotation rate of neutron star progenitors, conservation of angular momentum suggests that a newly formed neutron star should be spinning very rapidly, with a spin period $P_{\rm spin} \sim 10 - 100\,\mathrm{ms}$. Likewise, magnetic flux conservation suggests that the star's original magnetic field should be greatly amplified. Most pulsars have inferred surface magnetic fields $B_{\rm surf} = 10^{11} - 10^{13}\,\mathrm{G}$, which are assumed, for the purposes of roughly calculating fundamental physical characteristics, to be dipolar in the region close

[2]The recent discovery of a magnetar candidate in the massive star cluster Westerlund 1 by Muno et al. (2006) suggests that magnetars (see §1.1.3), a type of neutron star, have very massive ($\sim 40\,M_\odot$) progenitors.

to the pulsar. A pulsar carries with it a co-rotating magnetosphere, which is populated by plasma (Goldreich & Julian, 1969). The characteristic size of the magnetosphere is defined by the light cylinder, the radius out to which corotation with the pulsar is sub-luminal. For a 1.4-ms (1-s) pulsar, the radius of the light cylinder is 67 (48000) km. Particle acceleration above the magnetic poles creates beams of radiation, possibly via curvature or synchrotron emission. Beyond the light cylinder, charged particles will stream out along the "open" field lines. This process is still not well understood, and it is fair to say that one of the greatest outstanding problems in pulsar astrophysics is the emission mechanism itself. The spin and magnetic axes of a pulsar are generally misaligned. If the magnetic axis points towards the Earth, one may observe pulsations as the pulsar beam sweeps by, much like a lighthouse (see Figure 1.1 for a cartoon model of a pulsar). This pulsed emission is what characterizes some neutron stars as pulsars.

The majority of pulsars are found within only a few degrees of the Galactic Plane. In fact, roughly a third of all the known pulsars are within only one degree of the Plane. This is not surprising given that the massive stars that become pulsars are also formed here. With the exceptions of pulsars that have been found in the Large and Small Magellanic Clouds, and those in Galactic globular clusters (see §1.2.2), no pulsars have been discovered outside of the Milky Way. This is because pulsars are intrinsincally faint sources with fluxes at 1400 MHz that can be less than 0.1 mJy. Furthermore, there are a host of propagation effects in the interstellar medium that further complicate finding distant pulsars (see §2.1.3).

The range of well measured pulsar masses is roughly $1.2 - 2.2\,M_\odot$ (Stairs, 2004), with quite a few of these close to the Chandrasekhar mass limit[3] of $1.35\,M_\odot$ (Chandrasekhar, 1931). Theory and observation indicate that the neutron star radius is $R_{NS} \sim 10 - 20$ km, with a moment of inertia $I \sim 10^{45}$ g

[3]This is the maximum mass a white dwarf, which is supported by *electron* degeneracy pressure, can have before collapsing to a neutron star.

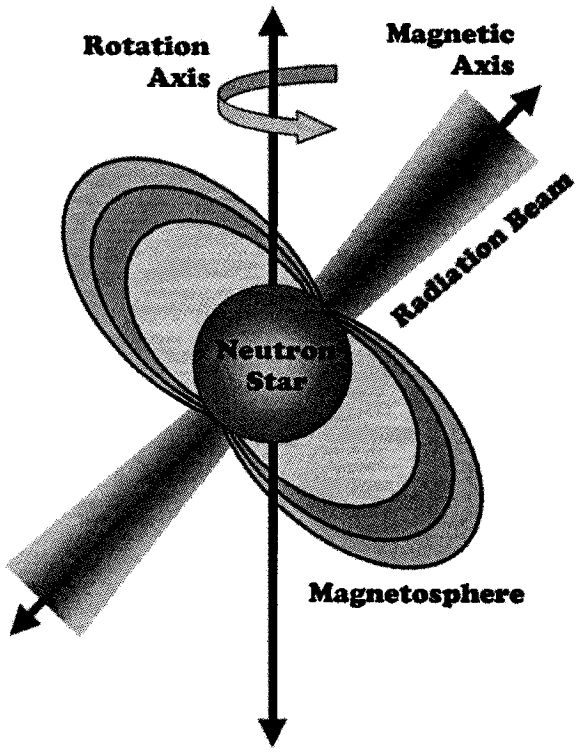

Figure 1.1: A cartoon pulsar diagram showing the neutron star's rotation axis, the magnetic axis of the dipole field, the radiation beam, which is along the magnetic axis, and the magnetosphere. To be observed as a pulsar, some part of the radiation beam must intersect the observer's line of sight.

cm^2. Note that the Schwarzschild radius[4], $R_S = 2GM/c^2$, of a $1.35\,M_\odot$ body is $\sim 4\,\mathrm{km}$, comparable to the neutron star radius. The gravitational binding energy $E_{\mathrm{grav}} = 3GM^2/5R$ (assuming a sphere of uniform density) is roughly 10% of the rest-mass energy Mc^2. Spacetime is highly curved in the vicinity of a neutron star, and General Relativity is necessary to describe the dynamics in this environment. The acceleration due to gravity at the neutron star surface is roughly 14 orders of magnitude higher than on Earth, corresponding to a gravitational redshift $z_{\mathrm{grav}} \sim 0.35$ (Cottam et al., 2002).

The internal structure of the neutron star is of particular interest for studying the physics of matter at supranuclear densities, but is still poorly constrained (see §1.1.5 for a short discussion of the neutron star equation of state). In the simplest picture, the neutron star has a crystalline iron crust, $1 - 2\,\mathrm{km}$ thick, on top of which is an envelope and a thin (spatially, not optically) atmosphere. The envelope has a marked effect on the release of thermal energy from the surface, while the atmosphere strongly influences the observed photon spectrum (Lattimer & Prakash, 2004). Inside, there is an inner core and an outer core. The outer core may contain a neutron superfluid and a proton superconductor. The composition of the inner core, which likely reaches densities a few times larger than the nuclear equilibrium density, is more debatable, and may host an exotic state of matter such as deconfined quarks, hyperons, or Bose condensates (Lattimer & Prakash, 2004).

1.1.3 Types of Pulsars

Based on the source of the energy they release, pulsars can be classified into three broad categories:

- **Rotation-Powered Pulsars (RPPs)**: Because a time-varying magnetic field releases energy, so will a rotating neutron star with a misaligned magnetic axis. This energy comes at the expense of the pulsar's

[4]For a *non-rotating* black-hole, this is the radius at which the escape velocity is the speed of light.

rotational kinetic energy, an effect which is known as magnetic braking. Thus, all RPPs are slowing down with time, which is to say they have positive period derivative, $\dot{P}$. In general, this slow-down is very regular, although some young pulsars show "glitches", where there is a sudden decrease in the spin period and change in $\dot{P}$, which later relaxes to the pre-glitch value (see Lattimer & Prakash, 2004, and references therein, for the physical theory of glitches). The RPPs are the most commonly observed type of pulsar, with approximately 1700 currently known. The vast majority of these are observed as radio pulsars, and thus the terms "radio pulsar" and RPP are sometimes used interchangeably. This is not strictly correct, as rotation can also power higher-energy pulsations (typically X-ray and sometimes γ-ray) and some X-ray and γ-ray RPPs are radio quiet (e.g. Geminga). The range of observed rotation periods spans three decades, from the fastest millisecond pulsars (see §1.2) to slow RPPs rotating once every few seconds. The intrinsic distribution at both the low and high limit of the spin period range is poorly constrained because of observational biases (see Chapter 3). Still, beyond a spin period of $\sim 8 - 10\,\mathrm{s}$, the radio emission appears to shut off, possibly because the electric potential in the emission zone is no longer great enough to cause pair production (Hibschman & Arons, 2001). In the radio, the RPPs are broad-band (most are visible between $0.2 - 2\,\mathrm{GHz}$) and generally have steep power-law spectra:

$$S \propto \nu^{-\alpha}, \tag{1.1}$$

where S is the flux density at the observing frequency ν. α, which is called the spectral index, can range from $\sim 0.0{-}4.0$, and is on average 1.8 (Maron et al., 2000a). Although there is a dearth of pulsar observations below 300 MHz, there is evidence that the radio luminosity peaks and then turns over somewhere between $100 - 200\,\mathrm{MHz}$ (Malofeev et al.,

1994).

- **Accretion-Powered Pulsars (APPs)**: If a neutron star has a binary companion that has filled its Roche Lobe, then it can accrete matter from its companion star (this process will be discussed more completely in §1.2). If the neutron star's magnetic field is strong enough, the accreting material is channeled by it and accumulates at the magnetic poles. The material continues to aggregate, eventually reaching a pressure and density at which thermonuclear fusion is possible. The resulting burst is modulated at the neutron star's spin period, a fact that was originally proven for the low mass X-ray binary (LMXB) SAX J1808.4−3658, which also shows transient coherent pulsations from accretion hot-spots (Chakrabarty et al., 2003). There are currently 13 LMXBs known that show bursts and 7 that show transient coherent pulsations (see §1.2.1). APPs are sometimes referred to as X-ray pulsars, although this term is imprecise because some X-ray pulsars are rotation-powered. Unlike the RPPs, which are all (mostly steadily) spinning down, APPs can show period changes, caused by accretion torque, and in most cases are observed to be spinning up. Some APPs are spinning as fast as the fastest RPPs, but they can also spin much more slowly. While the slowest-spinning RPP, PSR J2144−3933, has a spin period of 8.5 s, some APPs have spin periods of hundreds of seconds (Bildsten et al., 1997).

- **Magnetic-Powered Pulsars (Magnetars)**: It has been theorized that some neutron stars are powered by the decay of their magnetic field (Thompson & Duncan, 1995, 1996), and there is strong observational evidence supporting this idea (see Woods & Thompson, 2004, and references therein). These neutron stars, termed magnetars, are believed to have surface magnetic fields two or three orders of magnitude larger than regular RPPs ($B_{\rm surf} \sim 10^{14} - 10^{15}$ G). Both the classes of neutron stars termed soft-gamma repeaters (SGRs) and anomalous X-ray pul-

sars (AXPs) are believed to be magnetars (Gavriil et al., 2002; Woods & Thompson, 2004). For these stars, the X-ray flux is considerably larger than can be accounted for by their spin-down energy. Reconfigurations of the magnetic field lines can lead to massive releases of magnetic energy. The last major outburst was on December 27th, 2004, when SGR 1806−20 released enough energy to change the ionization levels in the Earth's upper atmosphere from night to day. There are only about a dozen known magnetars, as well as roughly a half-dozen radio pulsars that are inferred to have magnetar-like magnetic field strengths. Why these high-magnetic-field radio pulsars do not also show magnetar-like X-ray emission is unclear.

1.1.4 Measurable Properties

One can construct a precise rotational ephemeris and derive other valuable properties for a pulsar through a technique referred to as "pulsar timing". In the case of a binary pulsar, this technique is also used to derive a precise orbital ephemeris (including in some cases post-Keplerian effects included in the General Theory of Relativity). This is one of the most powerful techniques for studying pulsar physics. Pulsar timing works by measuring the time of arrival (TOA) of the pulsation at numerous epochs, spanning at least a year, and sometimes a few decades. A TOA is generated by taking a high signal-to-noise template of the pulse profile and fitting it to the observed average pulse profile integrated over some length of time. Generally, a single TOA comes from the sum of many hundreds to thousands of individual pulsations. For pulsars that are very dim and spinning particularly fast, it is sometimes necessary to average a few million individual pulsations per TOA. Once a list of topocentric TOAs is generated, one can fit them to a timing model that incorporates period, period derivative, position, dispersion measure (see §2.1.3), and sometimes other secondary (although very interesting when they can be measured) effects like proper motion, dispersion measure variation, and

higher-order period derivatives. The solution is "coherent" in the sense that the rotational phase of the pulsar is unambiguously determined between observing epochs (i.e. one accounts for every single rotation of the pulsar between TOAs). This results in extremely precise measurements of the model parameters. For instance, the period at a given epoch can sometimes be measured to a precision of one part in a trillion, and timing positions typically have uncertainties well below an arcsecond.

Simply by measuring period and period derivative, one can infer some of the pulsar's fundamental physical properties. The pulsar's rate of rotational kinetic energy loss through magnetic braking, $\dot{E}$, is found by taking the rotational kinetic energy $E = \frac{1}{2}I\omega^2 = 2\pi^2 I P^{-2}$ and differentiating it with respect to time:

$$\left|\frac{dE}{dt}\right| = |\dot{E}| = 4\pi^2 I \frac{\dot{P}}{P^3} = 4\pi^2 I \nu \dot{\nu} \tag{1.2}$$

This is often referred to as the pulsar's "spin-down luminosity". From Equation 1.2 we see that the most energetic rotation-powered pulsars have either a large period derivative or a very small period. For rotation-powered pulsars, this represents the pulsar's total energy budget, of which most takes the form of a relativistic wind (see §1.3), with the pulsations typically accounting for only a small fraction of the total energy output.

The time derivative of the spin frequency can be expressed as

$$\dot{\nu} \propto \nu^n, \tag{1.3}$$

where n is called the braking index and $n = 3$ for a pure magnetic dipole. If one assumes that the spin-down is due entirely to magnetic braking by a dipolar field and that the pulsar's initial spin period was much shorter than its current spin period ($P_{\rm birth} << P_{\rm now}$), then one can integrate Equation 1.3 to infer the pulsar's age. This value is termed the pulsar's "characteristic age",

$$\tau_c = \frac{P}{2\dot{P}} \text{ s}. \tag{1.4}$$

This does not necessarily reflect the pulsar's true age, particularly if the current spin period is close the initial spin period, or if the braking index deviates significantly from 3. In fact, independent age estimates based on, for instance, supernova remnant expansion measurements (e.g. Tam & Roberts, 2003; Bietenholz et al., 2001) show that there is often a discrepancy for young pulsars. Historically documented supernovae such as the Crab (1054 CE) and 3C 58 (plausibly, but not certainly associated with a supernova in 1181 CE) provide extremely precise ages, which are always inconsistent with the naively derived characteristic age.

In the case of very young pulsars it is sometimes also possible to measure a second frequency derivative, $\ddot{\nu}$, although this is often difficult because of glitches and timing noise[5]. Nonetheless, if $\ddot{\nu}$ can be measured, then, along with the spin frequency and first derivative, it provides an estimate of the braking index (and hence the configuration of the magnetic field):

$$n = \frac{\nu\ddot{\nu}}{\dot{\nu}^2}. \tag{1.5}$$

Assuming the magnetic field is dipolar, and equating the spin down energy with the luminosity of a dipole, one can also infer the pulsar's surface magnetic field strength,

$$B_{\text{surf}} = 3.2 \times 10^{19} \sqrt{\left(\frac{P}{\text{s}}\right)\left(\frac{\dot{P}}{\text{s/s}}\right)} \text{ G}. \tag{1.6}$$

A common way to display the properties of the observed pulsar population

[5]Timing noise is an apparently random (there is certainly no known way to model it physically) meandering of the pulse phase. It has a very "red" spectrum, which is to say that most of the power is at low frequencies. The wandering in phase occurs on month to year timescales and can make it very difficult to accurately determine intrinsic long-term higher-order period derivatives.

is to plot the measured periods and period derivatives, along with lines of constant characteristic age and surface magnetic field (Figure 1.2). From this, one sees that the majority of pulsars have $P_{\rm spin} = 0.1 - 2.0\,{\rm s}$, $B_{\rm surf} = 10^{11} - 10^{13}\,{\rm G}$, and $\tau_c = 100\,{\rm kyr} - 1\,{\rm Gyr}$. To the upper-left of this main population are the young, energetic pulsars, which can be loosely grouped into being either Crab-like ($\tau_c \sim 10^3\,{\rm yr}$, $\log(\dot{E}) \sim 37 - 38$), Vela-like ($\tau_c \sim 10^4\,{\rm yr}$, $\log(\dot{E}) \sim 36 - 37$), or Geminga-like ($\tau_c \sim 10^5\,{\rm yr}$, $\log(\dot{E}) \sim 35 - 36$). To the upper-right are the high-magnetic-field radio pulsars and the magnetars (SGRs and AXPs). A striking feature is the tail of faster pulsars with larger characteristic ages and weaker surface magnetic fields, the majority of which are in binary systems and/or reside in globular clusters. These are the "recycled" pulsars, whose spin rates have been affected by accreted material from a companion star (although they are currently rotation-powered, see §1.2).

1.1.5 Equation of State

Neutron stars are by far the densest known stars, and challenge our knowledge of how matter behaves under such extreme conditions. Identifying the neutron star equation of state (EOS) is thus potentially critical for understanding the properties of matter at supranuclear densities. An EOS describes the relationship between pressure P, temperature T, and density ρ in a system. If the true EOS for the matter inside neutron stars was known, one would be able to calculate the star's radius as a function of its mass, as well as its density profile, by solving the equations of hydrostatic equilibrium, which describe the balance between the outward pressure and the inward pull of gravity:

$$\frac{dP}{dr} = -\frac{G(m(r) + 4\pi r^3 P/c^2)(\rho + P/c^2)}{r(r - 2Gm(r)/c^2)} \tag{1.7}$$

and

$$\frac{dm(r)}{dr} = 4\pi\rho r^2. \tag{1.8}$$

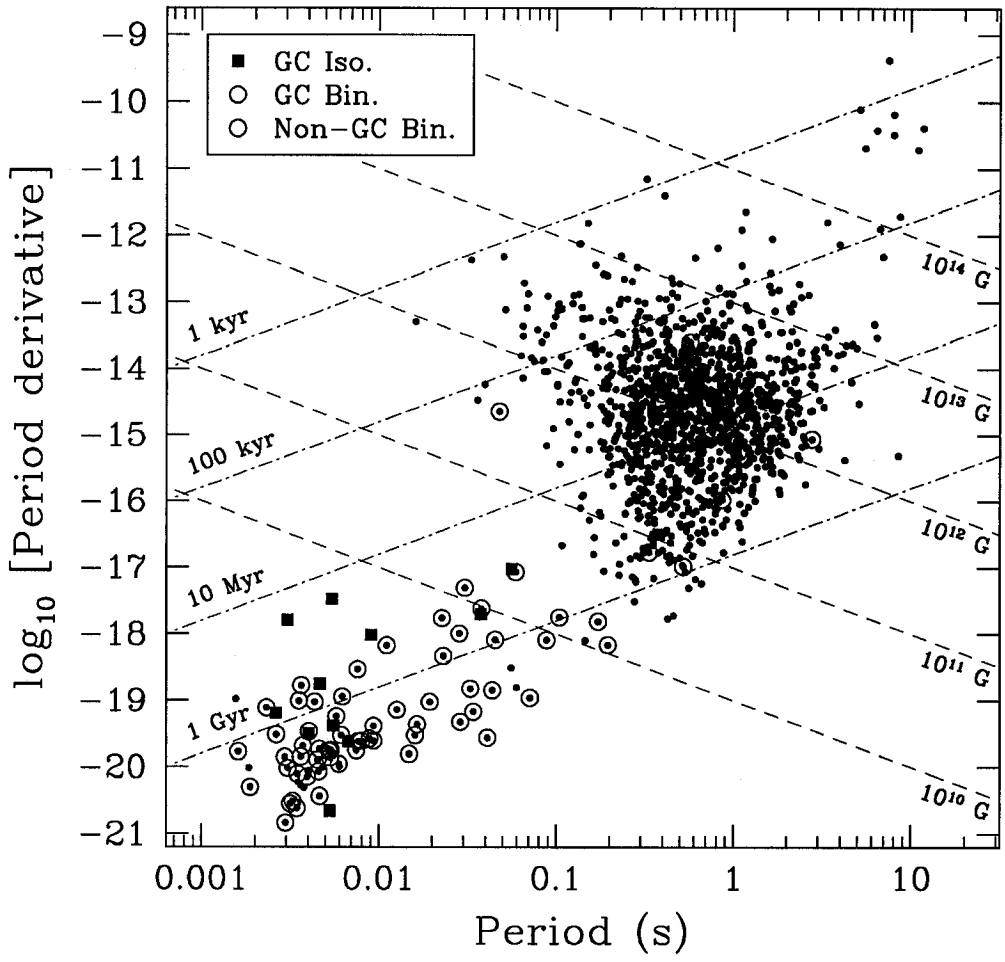

Figure 1.2: A $P - \dot{P}$ diagram including $\sim$ 1700 known pulsars. The dot-dashed lines are lines of constant characteristic age (Equation 1.4), from 1 kyr to 1 Gyr. The dashed lines are lines of constant surface magnetic field strength (Equation 1.6), from $10^{10} - 10^{14}$ G. Circled points are pulsars in binary systems. Binary and isolated pulsars found in Galactic globular clusters are indicated by magenta-colored circles and squares, respectively. Many of the known globular cluster pulsars are not plotted here because it is difficult to disentangle their intrinsic $\dot{P}$ from their observed spin-down, which is contaminated by their acceleration in the gravitational potential of the host cluster. The data plotted here is from the online pulsar catalogue of the Australia Telescope National Facility (Manchester et al., 2005, available at http://www.atnf.csiro.au/research/pulsar/psrcat). Figure provided by Cindy Tam.

These are referred to as the Tolman-Oppenheimer-Volkov equations and are valid for a sphere in general relativity (see Lattimer & Prakash, 2004, and references therein). Note that Equation 1.8 is simply a statement of conservation of mass, where $m(r)$ is the enclosed mass within a radius r.

Lattimer & Prakash (2004) note that the size of a neutron star will depend most importantly on how the pressure of matter behaves around the nuclear equilibrium density $\rho_{\rm nuc} \sim 2.7 \times 10^{14}\,{\rm g\ cm^{-3}}$. This is still poorly understood, as the pressure predicted near $\rho_{\rm nuc}$ varies by a factor of 6 among different models (Lattimer & Prakash, 2004). If pressure remains steady above nuclear densities, the neutron star radius will depend only weakly on mass, and almost entirely on the scale of this pressure. Alternatively, if pressure drops above the nuclear density, then radius will decrease with increasing mass. Recall that for a white dwarf $MR^3 = const.$ (Carroll & Ostlie, 1996, and references therein), and thus more massive white dwarfs will also be more compact (up until the Chandrasekhar mass limit).

It is still unclear what the exact composition of a neutron star is. While it is likely that most of the normal matter is in the form of neutrons (with the remaining $5-10\%$ being protons and electrons), some EOSs invoke exotic species such as hyperons, kaon condensates, or strange quark matter in the inner core. The EOS for stars composed of strange quark matter[6] (SQM) have also been calculated. In opposition to the normal matter EOSs, the SQM models give a nearly incompressible star (i.e. well below the maximum masses of these models, $R \propto M^{1/3}$).

We call EOSs in which the radius is mostly insensitive to mass "hard", whereas "soft" EOSs are those for which radius is a strong function of mass. Figure 1.3, adapted from Lattimer & Prakash (2004), plots some representative EOSs for normal matter and hybrid models. The viable mass range of neutron stars is likely between $\sim 1.0 - 3.0\,{\rm M_\odot}$. The upper limit of this range is based

[6]As an interesting sidenote, it is worth mentioning that Edward Witten has proposed that SQM is the ultimate ground state of matter. Also noteworthy is that SQM stars (if they exist) are self-bound, and do not require gravity to remain bound.

on the criterion that the speed of sound be less than the speed of light in the material. This is a statement that causality is respected, and is indicated by the orange $R \lesssim 3GM/c^2$ shaded region of Figure 1.3. A less constraining bound on the mass comes from the Schwarzchild condition of general relativity $R \lesssim 2GM/c^2$, and is shown by the red-shaded region of Figure 1.3. The lower limit on the neutron star mass comes from considering the supernova explosion itself, and the argument that any stable neutron star progenitor will have a mass of at least $1\,\mathrm{M}_\odot$. Another constraint in the mass-radius plane comes from the rotation rates of the fastest-rotating pulsars (the blue-shaded region of Figure 1.3, see §1.2.3).

Given the range of observed pulsar masses, most viable EOSs predict a neutron star radius $R \sim 8 - 15\,\mathrm{km}$ (Lattimer & Prakash, 2004). Determining the true EOS is very difficult because a very high level of precision in the measurement of radii is needed in order to discriminate between models. However, given the scientific payoff of discerning the true EOS, precisely measuring the masses and radii of neutron stars is an extremely worthy observational goal. Neutron star masses can be measured with great precision in binary systems where post-Keplerian effects are observed. For instance, the masses of the two components of the double pulsar J0737−3039 are $1.337 \pm 0.005\,\mathrm{M}_\odot$ and $1.250 \pm 0.005\,\mathrm{M}_\odot$ (Lyne et al., 2004). Measuring radii has been a less precise venture, as uncertainty in pulsar distances and the atmospheric composition of neutron stars introduce large systematic errors. Large magnetic fields also play a role in these measurements, as they will affect the opacity of the atmosphere, and hence alter the observed spectrum (for instance Pavlov & Bezchastnov, 2005). Rutledge et al. (2002) measure a radius at infinity[7] $R_\infty = 15.9^{+0.8}_{-2.9}(\mathrm{d}/5\,\mathrm{kpc})\,\mathrm{km}$ for the neutron star in the LMXB Aquila X-1. Such a measurement is possible because of the assumptions that the magnetic field of the neutron star is low and the atmosphere will be purely composed of

[7]Because spacetime is so strongly curved in the vicinity of a neutron star, a distant observer is partially able to see the far side of the neutron star. The radius at infinity, R_∞, is related to the actual physical radius of the star, R_{NS}, by $R_\infty = R_{\mathrm{NS}}/\sqrt{1 - 2GM/R_{\mathrm{NS}}c^2}$.

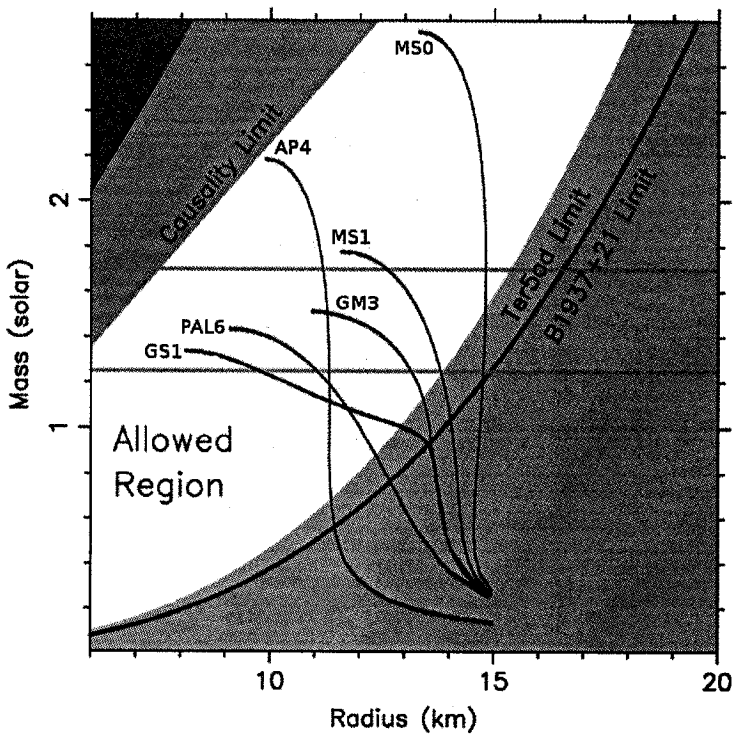

Figure 1.3: The mass-radius plane for neutron stars. The red region is excluded by General Relativity. For these combinations of mass and radius, the neutron star would be smaller than its Schwarzchild radius. The orange region is excluded by causality. In this region, the speed of sound would exceed that of light. The overlapping blue regions are disallowed specifically for PSRs J1748−2446ad (also known as Ter5ad) and B1937+21 (though not necessarily for other more slowly rotating pulsars) because of their rotation rate (see §1.2.3 for further details). The horizontal green lines indicate masses of $1.7\,M_\odot$ (top) and $1.25\,M_\odot$ (bottom). Representative EOSs are plotted in black. These models do not in reality end at a radius of 15 km; that is simply an artifact of the adaptation of the figure from another source. Adapted from Figure 2 of Lattimer & Prakash (2004).

hydrogen (due to accretion from the companion star). Measuring the gravitational redshift of spectral lines in the photosphere of a neutron star is another way to constrain mass and radius (Cottam et al., 2002). Recently, Ozel (2006) claims to have eliminated the soft EOSs by simultaneously measuring the mass and radius of the neutron star EXO 0748-676. This was done by combining constraints on the mass and radius that come from gravitational redshift and broadening of spectral lines, the Eddington luminosity, and surface emission. If the underlying assumptions made in this modelling are correct, then this greatly reduces the number of viable EOSs and potentially rules out exotic forms of matter in the core.

1.2 Millisecond Pulsars

1.2.1 Properties and Formation

Millisecond pulsars (MSPs), as their name suggests, are pulsars that spin once every few milliseconds ($P_{\rm spin} = 1-30\,{\rm ms}$), or, equivalently, up to a few hundred times a second ($\nu_{\rm spin} = 30 - 1000\,{\rm Hz}$). Given that the typical mass of a neutron star is $1.4\,{\rm M}_\odot$, this is truly remarkable. MSPs are by far the fastest-rotating stars known, and among the most rapidly rotating, naturally occuring macroscopic objects. It is only their intense gravity that allow MSPs to survive, even though their surface may have a transverse velocity $> 0.2\,{\rm c}$ at the equator. Just how fast an MSP can spin is a matter of intense debate, and is discussed in this thesis.

Although it may be that some pulsars are *born* with a spin period of a few milliseconds, their large magnetic field ($10^{11} - 10^{13}\,{\rm G}$) will slow the spin period to a few tens of milliseconds within only a few tens of years. MSPs have much smaller period derivatives than normal pulsars, and hence much larger characteristic ages ($\tau_c \gtrsim 100\,{\rm Myr}$) and much lower inferred surface magnetic fields ($B_{\rm surf} \lesssim 10^{10}\,{\rm G}$). Clearly, they are not young objects. Unlike most normal

pulsars, the majority of MSPs (roughly 80% of the MSPs in the Galactic Plane) are in binary systems, an important clue to their formation.

PSR B1937+21 ($P_{\rm spin} = 1.558\,{\rm ms}$, $\nu_{\rm spin} = 642\,{\rm Hz}$) was the first MSP to be discovered (Backer et al., 1982). Remarkably, it held the record for fastest-spinning pulsar for 24 years (Hessels et al., 2006). Prior to the discovery of PSR B1937+21, no one had predicted that such a rapidly spinning pulsar could exist, as the fastest-spinning pulsar known at the time was the Crab pulsar (PSR B0531+21, $P_{\rm spin} = 33.1\,{\rm ms}$, $\nu_{\rm spin} = 30.2\,{\rm Hz}$). Alpar et al. (1982) and Radhakrishnan & Srinivasan (1982a) were the first to propose the "recycling" scenario to explain PSR B1937+21's existence. In this model, an old, slowly rotating neutron star that is no longer an active pulsar can be spun-up to millisecond periods by the accretion of matter from a companion star. A similar idea had previously been considered to explain the original binary PSR B1913+16 (Smarr & Blandford, 1976), whose pulsar is relatively fast ($P_{\rm spin} = 59\,{\rm ms}$) but slowing down far less quickly than a young pulsar.

In the recycling scenario for MSPs (see Bhattacharya & van den Heuvel (1991) for a detailed discussion), a neutron star is in a binary system with a less-massive main sequence star. As the companion star evolves off of the main sequence, it will expand, eventually reaching a radius at which the gravitational force from both stars is equal. At this point, the companion star has filled its Roche Lobe, the equipotential surface that defines the extent of the star's gravitational influence over its own matter. At this point, matter flows from the companion star towards the pulsar, creating an inspiraling accretion disk around the compact object (Figure 1.4). The accretion disk transfers matter as well as angular momentum to the pulsar, thereby increasing its spin rate. This angular momentum comes at the expense of the orbital angular momentum of the system, and thus the orbit becomes more compact. The orbit is also tidally circularized (the eccentricity of most MSPs in the Plane is $e < 10^{-5}$). After the mass transfer period, the companion will in most cases evolve into a white dwarf.

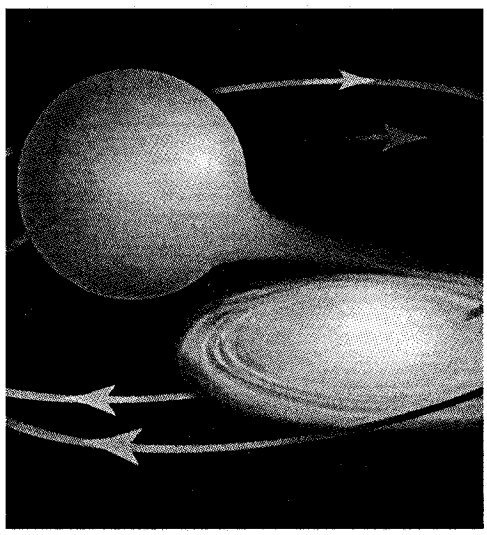

Figure 1.4: An artist's rendition of a neutron star accreting from a companion that has filled its Roche Lobe. Material is stripped from the bloated companion star and creates an accretion disk around the neutron star. This material will eventually accrete onto the neutron star itself, transfering its angular momentum and thereby increasing the neutron star's spin rate. Figure courtesy of Bill Saxton (NRAO).

During the accretion phase, the system is an LMXB[8] and can be a potentially bright X-ray source ($L_X = 10^{31} - 10^{38}\,\mathrm{erg\ s^{-1}}$, depending on whether the source is quiescent, actively accreting, or bursting). Although LMXBs are the most likely progenitors for the MSPs, not all LMXBs will necessarily become MSPs.

For at least seven LMXBs (Wijnands, 2005; Morgan et al., 2005), transient coherent X-ray pulsations have been detected during periods of accretion (the first by Wijnands & van der Klis, 1998, and the others in only the last 5 years). These "X-ray millisecond pulsars" provide a direct indication of the neutron star's rotation rate while it is being spun-up, although, because they are transient, they cannot be timed over a long period in the way radio pulsars are. As yet, no radio pulsations have been detected from such a system, despite concerted efforts (for example, Burgay et al., 2003). It seems that only after the LMXB phase is over will the recycled neutron star be observed as a radio pulsar, although this may be because the radio emission is obscured by material local to the binary. In the case of at least 13 LMXBs, burst oscillations have been detected. These bursts come from accreted material that is channeled to the magnetic poles, accumulates, and eventually reaches the critical density necessary for nuclear fusion. The discovery of both burst oscillations and transient coherent pulsations in the same source, SAX J1808.4−3658 (Chakrabarty et al., 2003), was the first firm evidence that the burst oscillations also measure the neutron star's rotation rate.

The lifetime of an LMXB is much shorter than the lifetime of the MSP it forms. Using simple arguments about the transfer of angular momentum, one can estimate that a $1.4\,\mathrm{M}_\odot$ neutron star needs to accrete only $\sim 0.1\,\mathrm{M}_\odot$ of material from its companion in order to reach a spin period of 1.5 ms. In principle, the neutron star may be able to reach much faster rotation rates, perhaps even sub-millisecond spin periods, during the accretion process. It has

[8]Recycling can also occur in a high mass X-ray binary, where the companion is massive enough to undergo a supernova. Although, in this case the pulsar is unlikely to be spun-up to a period of a few milliseconds.

been argued that the lack of pulsars observed spinning this fast suggests some physical process acts to limit spin-up (see §1.2.4). The initial strong magnetic field of a neutron star undergoing recycling is an important consideration in the accretion process, as it is responsible for setting the location of the inner edge of the accretion disk. For the inner edge of the accretion disk to reach the star's surface, the magnetic field must be dynamically negligible ($B_{\rm surf} < 10^8\,{\rm G}$). In principle, the closer the inner edge of the accretion disk to the star, the shorter the resulting spin period, since in equilibrium the star approaches corotation with the disk (Cook et al., 1994).

For the recycling scenario to occur in the Galactic Plane, a neutron star must be born in a binary system and the latter must survive the supernova explosion that creates the neutron star. This happens in only about 10% of supernovae (Bailes, 1989), and hence MSPs in the Plane are rare. There are only 45 MSPs among the approximately 1700 radio pulsars known in the Galactic Plane. Other formation channels for MSPs, that are not viable in the Galactic Plane, exist in globular clusters and are discussed in §1.2.2.

Not all recycled pulsars are MSPs, which is to say that the recycling process does not always spin-up a neutron star to millisecond periods. There is a population of partially-recycled pulsars with spin periods $\sim 30 - 300\,{\rm ms}$. One reason why a pulsar may be only partially recycled is if the companion is massive (i.e. $M \gtrsim 8\,{\rm M}_\odot$) and undergoes a supernova explosion before the original neutron star in the system is fully recycled. If the binary survives this second supernova, the system will be a double neutron star binary, where one of the components is observed as a partially recycled pulsar, for example PSRs B1913+16 and B1534+12 (Hulse & Taylor, 1975b; Wolszczan, 1991). These systems are formed from *high* mass X-ray binaries, where the companion is massive enough to undergo a supernova, and accretion comes from the massive companion's wind. Other partially recycled MSPs with low-mass companions may be the result of accretion-induced collapse, or may be formed from neutron stars with higher than average magnetic fields (Breton et al., 2007).

1.2.2 Pulsars in GCs

Globular clusters (GCs) are spherical conglomerations of $\sim 10^5 - 10^6$ stars, orbiting the Galactic Plane. Their cores have stellar densitities $\sim 10^4 - 10^6\,\mathrm{pc}^{-3}$, many orders of magnitude higher than in the disk of the Galaxy. There are roughly 150 GCs associated with the Milky Way, ranging in galacto-centric distance from $0.6 - 123\,\mathrm{kpc}$ (Harris, 1996). They contain some of the oldest stars in the Galaxy, with ages $\gtrsim 10^{10}\,\mathrm{yr}$. GCs are tidally truncated by the Milky Way; as such, the highest velocity of a star in the cluster is not what is needed to escape to infinity, but rather what is needed to reach the finite edge of the cluster itself (King, 1966), typically $v_{\mathrm{esc}} \lesssim 50\,\mathrm{km\ s}^{-1}$.

The extreme stellar densities in the cores of GCs make them excellent breeding grounds for MSPs and LMXBs. Stellar collisions and binary exchange interactions - in which a binary system interacts with an outside star or binary and switches one of its members for the new star - are far more common in the cores of GCs than in the Galactic Plane (see Camilo & Rasio, 2005, and references therein). Neutron stars have masses greater than the mean stellar mass of the cluster. Because of energy equipartition, they fall into the dense core of the cluster, along with the other most massive systems. In the core, isolated neutron stars, or neutron stars in a binary with an evolved companion, can end up in a binary system with an un-evolved companion star and then undergo the standard recycling scenario.

Fully recycled MSPs may even be able to exchange their companion in this crowded environment, potentially resulting in highly exotic MSP binaries. There is evidence that the bloated companion of the eclipsing binary PSR J1740−5340 in NGC 6397 is not the companion star that originally recycled the pulsar, but rather was exchanged for, subsequent to the creation of the MSP (D'Amico et al., 2001b). A similar situation may be responsible for the binary PSRs J1748−2446P and J1748−2446ad in Terzan 5 (Ransom et al., 2005c; Hessels et al., 2006). Furthermore, GCs may be the only place in the Galaxy where potential MSP-MSP or MSP-black-hole binaries can be formed.

The discovery of such a system has the potential for providing an unparalleled venue for testing gravitational theories.

Not only do GCs provide a propitious environment for the creation of close binaries, these binaries have, in turn, a noticeable influence on the dynamics of the host cluster through their gravitational binding energy (Pooley et al., 2003). This store of binding energy greatly exceeds the kinetic energy of the isolated stars in the cluster. It can be released through interactions with isolated stars or wider binaries, because these interactions will generally increase the compactness of the binary (Heggie, 1975).

The angular sizes of GC cores are generally small enough to comfortably fit within the half-power diameter of a large single-dish radio telescope's main beam. The core radii range from a few arcseconds to a few arcminutes, with a mean of $0.54'$ and a median of $0.34'$. With a single telescope pointing, one can perform a deep multi-hour observation of a GC and detect multiple faint pulsars. As of this writing, there are 129 pulsars known in 24 globular clusters[9]. Many of these have been discovered in only the last few years. The sudden resurgence in discoveries is due principally to new and refitted large radio telescopes like the GBT, Parkes and Arecibo, large and relatively affordable computer clusters, and large dedicated surveys.

1.2.3 Rotational Constraints on the Neutron Star Radius

One can place an upper limit on the radius of a neutron star, and by extension constrain the EOS, by requiring that the gravitational force $F_g = GM_1M_2/R^2$ holding the star together is not exceeded by the centrifugal force $F_c = Mv^2/R$ induced by the star's rotation. For a rigid Newtonian sphere, we can equate these and solve for the maximum radius as a function of spin period and mass:

[9]An online catalogue of GC pulsars is maintained by Paulo Freire at http://www.naic.edu/~pfreire/GCpsr.html.

$$R_{\rm max} = \left(\frac{GMP^2}{4\pi^2}\right)^{1/3} = 12.0 \left(\frac{M}{\rm M_\odot}\right)^{1/3} \left(\frac{P}{\rm ms}\right)^{2/3} \rm km. \quad (1.9)$$

This can be rearranged to give the Keplerian spin rate, which is the rotation rate of a particle orbiting just above the neutron star's surface:

$$\nu_{\rm K} = \frac{1}{2\pi}\sqrt{\frac{GM}{R^3}} = 1833 \left(\frac{M}{\rm M_\odot}\right)^{1/2} \left(\frac{R}{10\ \rm km}\right)^{-3/2} \rm Hz. \quad (1.10)$$

Unsurprisingly, the fastest-spinning pulsars provide the tightest rotational limits on the neutron star radius. Taking the fastest-spinning pulsar known, PSR J1748−2446ad ($P_{\rm spin} = 1.396\,\rm ms$), and assuming a mass of $1.4\,\rm M_\odot$, Equation 1.9 gives $R_{\rm max} = 21.0\,\rm km$.

However, because neutron stars are highly relativistic objects, one needs to consider general relativistic effects. Deformation is also an important consideration, if the star is spinning close to the Keplerian rate. Lattimer & Prakash (2004) find that the following equation approximates the maximum *non-rotating* radius of a neutron star independent of the true EOS (assuming the stellar mass is not close to the maximum mass of the true EOS):

$$R_{\rm max} = 10.3 \left(\frac{M}{\rm M_\odot}\right)^{1/3} \left(\frac{P}{\rm ms}\right)^{2/3} \rm km. \quad (1.11)$$

Using Equation 1.11, the revised upper limit on PSR J1748−2446ad's radius is 14.4 km (16.2 km) assuming a mass of $1.4\,\rm M_\odot$ ($2.0\,\rm M_\odot$). This rotational constraint is plotted as a function of mass in Figure 1.3. The light-blue region of the mass-radius diagram is forbidden for PSR J1748−2446ad, although pulsars with slower rotation rates are still permitted to have masses and radii within this region. For comparison, the rotational constraint for PSR B1937+21 ($P_{\rm spin} = 1.558\,\rm ms$), the second fastest rotating pulsar, is also shown. For this pulsar, the region below the solid dark-blue line is excluded. If the mass of PSR J1748−2446ad were known, it could be possible to eliminate some of the proposed EOSs. Finding an even faster-spinning pulsar, where the mass can

also be precisely measured, is a worthy goal, as it could very strongly constrain the EOS.

1.2.4 Accretion Torque, Gravitational Radiation, and the Maximum Spin Period

Simple models of accretion suggest that enough angular momentum can be imparted to a neutron star during the recycling process (§1.2.1) that it can, in principle, reach a *sub*-millisecond spin period (although see Andersson et al., 2005). The equilibrium spin period that a pulsar will reach depends on the external magnetic field, B, and mass-transfer rate, $\dot{M}$ (Ghosh & Lamb, 1979; Bildsten et al., 1997):

$$P_{\rm eq} \sim 1 \left(\frac{B}{10^{12}\ {\rm G}}\right)^{6/7} \left(\frac{\dot{M}}{10^{-9}\ {\rm M}_\odot\ {\rm yr}^{-1}}\right)^{-3/7} {\rm s}. \qquad (1.12)$$

The magnetic field limits how close the inner edge of the accretion disk is to the neutron star. Only if $B \lesssim 10^8\,{\rm G}$ will the accretion disk reach the surface.

Cook et al. (1994) devise evolutionary tracks and calculate the final spin period for 13 EOSs, assuming a simple recycling scenario where accretion occurs from the inner edge of a Keplerian disk onto a bare neutron star. They find that the post-accretion spin period, $P_{\rm f}$, ranges between 0.6 ms and 1.5 ms for the different EOSs, whose minimum achievable periods range from 0.47 ms and 0.85 ms.

However, no neutron star spinning this fast has been found. The observed population of MSPs has a sharp cut off around $1.4 - 1.6$ ms and the fastest-spinning neutron star observed in an LMXB also has a spin period of 1.6 ms. Although there are severe selection effects against finding the fastest radio pulsars (especially binaries, see §3.2), there is evidence that accretion is not the only factor in determining the final spin period of a recycled pul-

sar. Chakrabarty et al. (2003) (see also Chakrabarty, 2005a), consider the population of 13 LMXBs showing burst oscillations (sources where persistent pulsations have also been detected are excluded from the sample), whose inferred spin frequencies lie between 270 Hz and 619 Hz. They conclude, on the basis of a Bayesian statistical analysis, that the distribution is consistent with a maximum spin frequency $\nu_{\rm high} = 730\,{\rm Hz}$ (95% confidence). Similar systems are likely to evolve into radio MSPs, and thus the conclusions about the limiting spin frequency of LMXBs potentially has bearing for these objects as well.

Gravitational radiation has been proposed as a possible braking mechanism (Wagoner, 1984) which limits the ultimate spin period a pulsar can reach during accretion. Gravitational radiation may act through an accretion-induced quadrupolar moment in the crust (Bildsten, 1998), an r-mode instability in the core (Andersson et al., 1999a,b; Bildsten & Ushomirsky, 2000; Levin & Ushomirsky, 2001), or a large interior toroidal magnetic field, which deforms the neutron star (Cutler, 2002). We now describe the accretion-induced quadrupole and r-mode instability scenarios in more detail.

- **Crustal Quadrupole:** General Relativity predicts that a time-varying quadrupolar mass distribution will radiate gravitional waves. Because of their intense gravity, neutron stars should be extremely spherical objects. Even a 1-cm bump on the crust of a neutron star would be a significant deformation. There is the possibility that, during accretion, a neutron star can gain a quadrupolar moment. The scale of the quadrupole required to limit the spin frequency to a few hundred Hertz is only about $10^{-7}MR^2$. One way in which an accretion-induced quadrupole may be generated is through a large-scale temperature asymmetry (perhaps caused by a weak magnetic field), which is misaligned with the spin axis (Bildsten, 1998). This can engender the required quadrupole through temperature sensitive electron capture in the crust. This anisotropy is expected to disappear after accretion ceases. The rate

of energy loss via gravitational waves is a strong function of the spin rate $\nu_{\rm spin}$: $\dot{E}_{\rm gw} \propto Q^2 \nu_{\rm spin}^6$, where Q is the quadrupole moment. Following Bildsten (1998), equating the time-averaged spin-up torque due to accretion $N_{\rm acc} \approx \dot{M}(GMR)^{1/2}$ with the spin-*down* torque cause by gravitational radiation $N_{\rm gw} \approx \dot{E}_{\rm gw}/\nu_{\rm spin}$, one can estimate the critical spin frequency, $\nu_{\rm crit}$ above which energy losses due to gravitational radiation overcome accretion torque:

$$\nu_{\rm crit} \approx 300 \left(\frac{Q}{4.5 \times 10^{37}\ {\rm g\ cm^2}} \right)^{-2/5} \left(\frac{\dot{M}}{10^{-9}\ {\rm M_\odot\ yr^{-1}}} \right)^{1/5} {\rm Hz}. \quad (1.13)$$

Bildsten (1998) notes that the weak dependence that $\nu_{\rm crit}$ has on Q and $\dot{M}$ may explain why so many neutron stars in LMXBs have such similar spin frequencies ($\nu_{\rm spin} \approx 200-600$ Hz). Also, the required $Q \approx 4.5 \times 10^{37}$ g cm^2, is roughly seven orders of magnitude smaller than the total moment of inertia of the star, which is assumed to be approximately 10^{45} g cm^2. If such a quadrupole is created, it will be very difficult to achieve a rotation rate of 1000 Hz. Bildsten (1998) also suggests that the highest rotation rates may be achievable via long-term accretion at a low rate, because the temperature asymmetries may subside at lower accretion rates, creating a correspondingly lower Q.

- **r-mode Instability:**

  r-modes are excited by gravitational radiation emission in a rotating star (Andersson, 1998; Friedman & Morsink, 1998). Andersson et al. (1999b) suggest these can limit the spin rate of accreting neutron stars. Whether r-modes will grow in a neutron star depends on whether their excitation via gravitational radiation can overcome their damping by viscous forces. Viscous damping within the interior fluid, due to neutron-neutron scattering, was considered by Lindblom et al. (1998). They found that

this source of damping alone was not sufficient to dissipate the r-modes. Bildsten & Ushomirsky (2000) consider the additional damping created in the thin (few cm) viscous boundary layer between the inner fluid and a rigid crust. They find it to be a $10^5\times$ larger effect than that caused by shear in the interior of the star. As the crust will exist for temperatures less than 10^{10} K, this effect should dissipate the r-modes enough to negate their effect on neutron star spin periods. However, Levin & Ushomirsky (2001) consider a "toy model" *elastic* crust, in which, unlike in the *rigid* crust case, the r-modes can penetrate the crust. This leads them to reduce by $10^2 - 10^3\times$ the amount of damping attributed to the interaction between the inner fluid and crust. Thus, depending on one's model of the crust (i.e. its rigidity), r-modes may or may not be sufficiently damped to have an effect on the neutron star spin period.

1.3 Pulsar Wind Nebulae

The spin period of every non-accreting pulsar is increasing with time due to magnetic braking. While radio (and sometimes high-energy X-ray or γ-ray) pulsations are a striking result of this release of rotational kinetic energy, they generally represent only a small fraction ($\lesssim 10\%$) of the pulsar's total energy budget. The majority of the pulsar's spin-down energy is released in the form of a relativistic, magnetized wind, which interacts with the surrounding environment. The resulting nebula is termed a pulsar wind nebula (PWN), which may be visible from radio to γ-ray wavelengths, although in most cases PWN have only been observed in X-rays energies between about $1 - 10\,\mathrm{keV}$ and/or at radio frequencies between roughly $1-3\,\mathrm{GHz}$. In general, a high spin-down energy, $\dot{E} \gtrsim 10^{36}\,\mathrm{erg\ s^{-1}}$ (Equation 1.2), is necessary to create a bright PWN. Thus, PWNe are generally associated with only the youngest pulsars, or sometimes with nearby MSPs, which can also have relatively high $\dot{E}$ because of their high rotation rate (for example PSR B1957+20, Stappers et al., 2003).

Pulsars with high spatial velocities ($\gtrsim 400\,\mathrm{km/s}$), or those moving through a particularly dense medium, may sometimes show Hα and/or X-ray bow-shock nebulae (for example "The Mouse" nebula associated with PSR J1747−2958, Gaensler et al., 2004), which are also referred to as PWNe. In this case, the pulsar wind is balanced by ram pressure from the material the pulsar is plowing into. A significant fraction of PWNe have no detected pulsar counterpart, which may simply be due to viewing geometry.

The pulsar is the central engine of the PWNe and continuously injects high-energy particles and magnetic field into its surrounding environment. Highly relativistic electrons and positrons stream out with the magnetic field, which becomes predominantly toroidal at a few times the radius of the light cylinder (Kaspi et al., 2006). In the case of the youngest pulsars, which have ages $\lesssim 1000\,\mathrm{yr}$, the surrounding environment is likely to be at the centre of an expanding supernova shell (consider for instance the PWN in the supernova remnant G11.2−0.3; Roberts et al., 2003). Somewhat older pulsars may have left their supernova shell and are imbedded in the interstellar medium. The pulsar wind creates a forward shock (sharp increase in matter density) where it meets the outflowing supernova ejecta or interstellar medium. There is a corresponding reverse shock at the inner edge of the nebula, where the wind is terminated (Kaspi et al., 2006).

PWNe can have complex morphologies, especially in X-ray, with fine structure on angular scales as small as $\lesssim 1''$. This has been strikingly revealed in X-rays by recent high-spatial-resolution observations with *Chandra* (Figure 1.5): consider for instance the Crab (Weisskopf et al., 2000), Vela (Helfand et al., 2001), and PSR B1509−58 (Gaensler et al., 2002) PWNe. Kaspi et al. (2006) divide X-ray PWN into three broad morphological classifications: 1) torus with weak jet, 2) jet or tail dominated, and 3) mixed or uncertain. They note that the morphology of a PWN depends on the energy release history and environment of the pulsar. Furthermore, because the flow is relativistic, Doppler boosting also has a significant effect on the *observed* brightness distri-

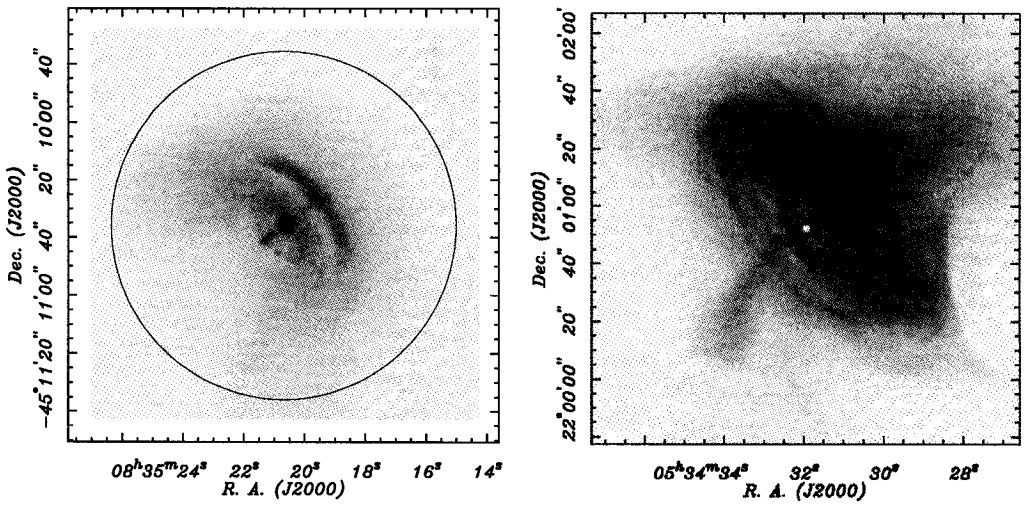

Figure 1.5: Two high-resolution *Chandra* observations of PWNe. *Left:* The PWN associated with the 10-kyr-old Vela pulsar. *Right:* The PWN associated with the 1-kyr-old Crab pulsar. The circles in each image have equal physical size assuming distances of 2 kpc and 250 pc to the Crab and Vela respectively. From Helfand et al. (2001).

bution in the nebula. X-ray PWNe are generally smaller than their associated radio nebula, with the X-ray nebula often embedded in the centre of the radio nebula. PWNe can have jets and other structures which vary on time-scales as short as a few months to years (Pavlov et al., 2003; Weisskopf et al., 2000). The particles that emit X-rays in the nebula have synchrotron lifetimes that are small compared with the lifetime of the nebula, while the converse is true for radio-emitting particles. Thus, X-rays trace the most recent history of the nebula, while radio traces the long-term evolution.

In both X-ray and radio wavelengths, the spectra of PWNe are non-thermal and can be described by a power law. In X-ray, the photon index Γ ($S \propto E^{-\Gamma}$) runs between $1.5-2.2$. In the radio, the spectral index $\alpha \equiv \Gamma - 1$ ($S \propto \nu^{-\alpha}$) is quite flat, and runs between $0.0 - 0.3$. The linear polarization fraction of the radio nebula is $\gtrsim 10\%$. One or more spectral breaks, accounting for a total change in the spectral index of $\Delta\alpha = 0.5 - 0.9$, are required to piece together

the X-ray and radio spectra (Kaspi et al., 2006).

1.4 Outline of Thesis

The remainder of this thesis is organized as follows:

Chapter 2, "Techniques and Instrumentation", describes the observational techniques employed in the radio and X-ray observations presented in this thesis, as well as a description of the telescopes that were used. Propagation effects induced on the pulsar signal by the interstellar medium are also described.

Chapter 3, "Pulsar Search Techniques", summarizes the various techniques that have been devised to search for pulsars, many of which have been applied in this thesis. These include basic Fourier domain periodicity searches, single pulse searches, and more advanced algorithms that compensate for binary motion.

Chapter 4, "A 1.4-GHz Survey for Pulsars in Globular Clusters with Arecibo", presents a survey for new pulsars in 22 globular clusters visible with the Arecibo telescope. 11 new millisecond pulsars were found in this survey, 10 of which are in binary systems, and three of which show eclipses. The observational properties of the globular cluster pulsar population as a whole are also discussed.

Chapter 5, "A 716-Hz Pulsar in Terzan 5", presents the GBT discovery of PSR J1748−2446ad, which is now the fastest-spinning neutron star known. We discuss the implications of this discovery.

Chapter 6, "A New Candidate Gamma-Ray Pulsar", presents Arecibo

and Parkes searches for radio pulsations from the possible X-ray counterparts to 5 unidentified *EGRET* γ-ray sources. These searches culminated in the discovery of PSR J2021+3651, a Vela-like pulsar that is the likely counterpart to the *EGRET* γ-ray source 3EG J2021+3716.

Chapter 7, "Discovery of an X-ray Pulsar Wind Nebula Associated with PSR J2021+3651", presents *Chandra* X-ray observations of the field around the young, energetic pulsar J2021+3651, as well as radio timing observations with Arecibo. These data revealed a compact pulsar wind nebula, possible X-ray pulsations, and a pulsar glitch.

Chapter 8, "Continuing Surveys of the Galactic Plane", Describes two complimentary surveys of the Galactic Plane for pulsars and radio transients. The Arecibo PALFA survey is covering the Galactic Plane at 1.4 GHz, between longitudes $32° < l < 77°$ and $168° < l < 214°$. The GBT350 survey is using the GBT at 350 MHz to cover the Galactic Plane between longitudes $65° < l < 170°$. Both surveys have high sensitivity to millisecond and binary pulsars.

Chapter 9, "Conclusions and Future Work" speculates on what future directions the work presented in this thesis may take.

Chapter 2

Techniques and Instrumentation

What you do is, you have your drawing board and a pencil in hand at the telescope. You look in and you make some markings on the paper and you look in again.
– Clyde Tombaugh, discoverer of Pluto.

In this chapter, we describe the observational techniques and telescopes used to gather data for this thesis. A much broader introduction to the techniques of pulsar astronomy is the "Handbook of Pulsar Astronomy" (Lorimer & Kramer, 2004). A summary of pulsar search techniques is left for Chapter 3.

2.1 Radio Observations

In order to maximize sensitivity, observations of radio pulsars require huge collecting area, low-temperature receivers, large observing bandwidth, as well as high time and frequency resolution data recording. Here we decribe some of the basic techniques and instrumentation used in the radio observations presented in this thesis. A classic, comprehensive reference for the basic techniques of radio astronomy is "Radio Astronomy" by John Krauss.

2.1.1 Antennae

Radio telescopes can range from simple dipole antennae to smooth spherical or parabolic reflecting dishes.

Dipole antennae are often used at the largest observing wavelengths ($\lambda_{\rm obs} >$ 1 m). When an electromagnetic (EM) wave is incident on a dipole antenna, it causes the electrons inside the antenna to oscillate along the direction of the electric component of the wave, inducing a time-varying voltage. This voltage is down-converted to an intermediate frequency (IF), and amplified before being recorded or sent to a spectrometer. To maintain sensitivity to the various polarizations of the EM wave, two dipoles, placed perpendendicular to each other, are used. Collecting area may be increased by constructing arrays with many hundreds of dipole antennae. The First Cambridge Array, constructed by Anthony Hewish, Jocelyn Bell and others in England is comprised of $\sim$ 2000 dipoles, and was the first intrument to detect a pulsar. Dipole arrays remain in use today. A consortium of Dutch radio astronomers is currently constructing the Low Frequency Array (LOFAR), which is comprised of 10,000 dipole antennae.

At much shorter observing wavelengths, it is more practical to use reflecting dishes[1]. They work in the same way as conventional optical reflecting telescopes, by focusing light, in this case to a radio receiver. Unlike terrestrial-based optical telescopes, whose imaging resolution is limited by atmospheric turbulence, large radio dishes are always diffraction limited (in the low-frequency limit). The finest angular resolution, $\theta_{\rm min}$, one can achieve at an observing wavelength $\lambda_{\rm obs}$ with a dish of diameter D is: $\theta_{\rm min} = \lambda_{\rm obs}/D$. Even for the largest single-dish radio telescopes on Earth, this corresponds to an angular resolution of only a few arcminutes, which is poor in comparison to the sub-arc*second* resolution achievable with some optical telescopes. Angular

[1]The lowest achievable observing wavelength depends on the quality of the surface. At observing wavelengths below $\sim$ 1 cm, atmospheric absorption also becomes an important factor, and observations may only take place on clear, dry days.

resolution at radio wavelengths can be greatly improved by using multiple telescopes as an interferometer. Here it is the *distance* between telescopes which dictates the resolution. By employing widely spaced dishes (in some cases, by coordinating telescopes on separate continents) angular resolutions of roughly 0.001 arcseconds can be achieved.

2.1.2 Radio Frequency Interference (RFI)

Interference from human-made radio signals, "Radio Frequency Interference" (RFI), is an increasing hindrance to successful radio-astronomical observations. Sources of RFI include airport and military radars, telecommunication towers for televisions and cell-phones, and artificial satellites. RFI from artificial satellites can be particularly pernicious as these are overhead and sometimes in relatively close proximity to the field of view one is observing. Only a few narrow bands of the radio spectrum are reserved for radio astronomy, for instance a $\sim$ 20-MHz-wide band centered around the 1420-MHz (21-cm) neutral hydrogen hyperfine splitting line. Despite the remote locations of most major radio observatories, RFI can still have a strong effect on astronomical observations, sometimes completely overwhelming the signal one is trying to detect (Figure 2.1). The flux from human-made radio signals is many orders of magnitude stronger than that from distant astronomical sources. For instance, if one were to place a cell-phone on the moon, it would be almost the brightest source of radio waves in the sky.

While contamination from RFI is almost unavoidable, fortunately it is often narrow-band or has a short duty cycle. Such signals can be removed from the data by masking individual frequency channels, clipping peaks in the time domain, or removing known frequencies from the power spectrum (for instance the 60-Hz "line" noise). These techniques aim to remove the maximum amount of RFI from the data, while still leaving most of the observing bandwidth and integration time intact. In the case of pulsar searches, effective RFI excision is crucial. Periodic RFI can greatly increase the number of false candidates found

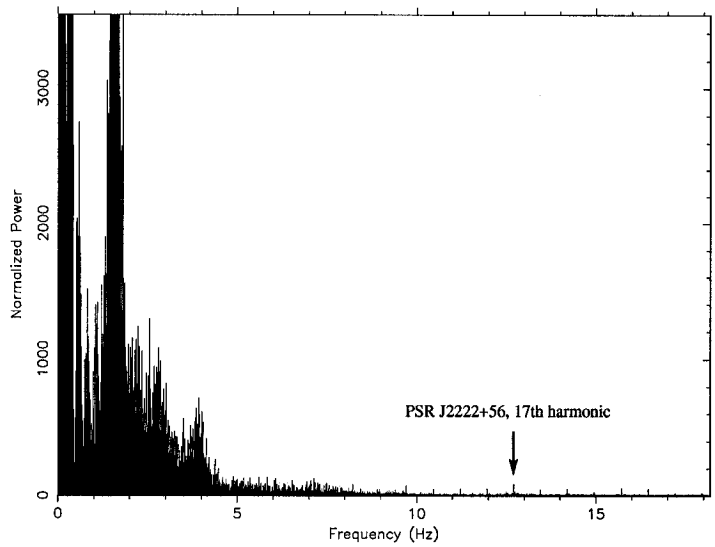

Figure 2.1: Power spectrum from a 0.5-hr observation with the GBT at 820 MHz showing very strong, periodic RFI. For comparison, the 17^{th} harmonic of the new 1.34-s pulsar J2222+56 (Chapter 8) is indicated.

in a pulsar search, severely complicating the identification of real astronomical signals. If it is narrow-band, RFI can be masked in the power spectrum so it does not appear in candidate lists, but one must be careful to minimize the chances that pulsar signals are not also being removed from the data.

2.1.3 Propagation Effects

The interstellar medium (ISM) is turbulent, inhomogeneous, magnetized, and ionized (Lorimer & Kramer, 2004). Radio pulsar signals are affected by a variety of propagation effects while travelling through the ISM. We summarize some of the major effects here.

- **Dispersion:** The ionized component of the ISM (principally free electrons) disperses radio waves, which is to say that the signal's group velocity is a function of frequency. Over a finite observing bandwidth,

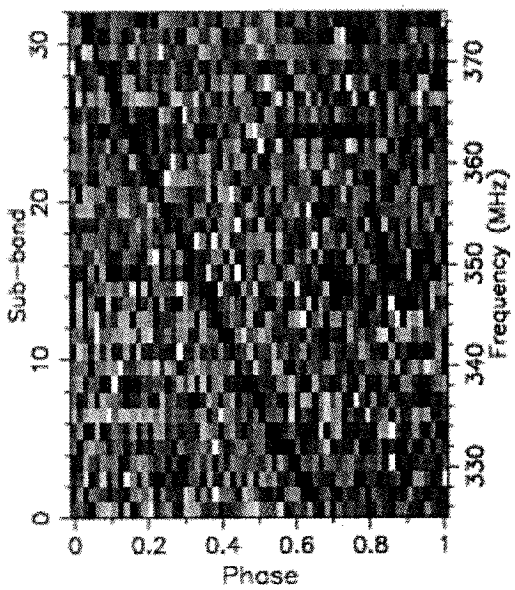

Figure 2.2: Signal from the newly discovered pulsar J2345+62 (Chapter 8) as a function of frequency and pulse phase. The 50 MHz bandwith is divided into 32 subbands. The dispersive effect of the interstellar medium has not been corrected for, and thus the lower frequency subbands arrive at later pulse phase.

the higher frequencies will arrive before the lower frequencies in a well-defined way (Figure 2.2). The time delay, $\Delta t_{\rm DM}$, between the arrival of the upper ($\nu_{\rm high}$) and lower ($\nu_{\rm low}$) frequencies in an observing bandwidth is

$$\Delta t_{\rm DM} = 4.15 \times 10^6\,{\rm ms} \left[\frac{\rm DM}{\rm cm^{-3}\ pc}\right] \left[\left(\frac{\nu_{\rm low}}{\rm MHz}\right)^{-2} - \left(\frac{\nu_{\rm high}}{\rm MHz}\right)^{-2}\right], \quad (2.1)$$

where DM is the "dispersion measure" towards the source. The DM is the integrated column density of free electrons, n_e, towards a source at distance d:

$$\mathrm{DM} = \int_0^d n_e\, dl. \quad (2.2)$$

For a modest DM of 100 pc cm^{-3} and a typical bandwidth of 100 MHz centered at a typical observing frequency of 1400 MHz, $\Delta t_{\rm DM} = 30$ ms. This is comparable to the pulse width of slow pulsars, and is significantly longer than the periods of millisecond pulsars. Unless this effect is compensated for, the pulse will be washed out. Dispersion can be mostly corrected for by channelizing the observed bandwidth and applying the appropriate time delays between channels before summing (see also §2.1.4). In this way, dispersive smearing occurs only within the much smaller bandwidth of the individual channels.

Although dispersion is generally a nuisance to radio pulsar observations, it nicely provides a way of estimating distance. Given a model of the free electron distribution in the Galaxy (i.e. n_e along different lines of sight: Taylor & Cordes, 1993; Cordes & Lazio, 2002b), one can use Equation 2.2 to estimate a pulsar's distance from its DM. Given the uncertainties in the n_e models, these distances have large uncertainties however, and can sometimes be off by a factor of two or more. Dispersion also has the

benefit of washing out RFI, which peaks in strength at DM = 0 pc cm^{-3}. For this reason, it can be easier to find slow pulsars at moderate to high DM, where the number of candidates is generally lower.

- **Scattering:** The pulsar signal can also be scattered by clumps of neutral dust in the ISM, which cause the signal to arrive via multiple paths (Lorimer & Kramer, 2004). This effectively convolves the emitted (unscattered) pulse profile with a one-sided exponential tail $e^{-t/\tau_{sc}}$, where τ_{sc} is called the scattering time (for instance, Figure 7.4). The amount of scattering is a strong function of observing frequency, with the lowest frequencies showing the most scattering: $\tau_{sc} \propto \nu^{-\alpha}$, where $\alpha \sim 4$ (Bhat et al., 2004). Unsurprisingly, the amount of scattering is positively correlated with DM (Bhat et al., 2004). Unlike dispersion, this effect cannot be corrected for. For distant, short period pulsars in the Galactic Plane, scattering can completely wash out the pulse at low observing frequencies, forcing one to observe at ~ 1.4 GHz or higher.

- **Scintillation:** Anisotropies in the ISM can also cause phase delays in the signal, which can then lead to constructive or destructive interference (Lorimer & Kramer, 2004). This results in a modulation of the observed signal brightness on a timescale Δt, and within a scintillation bandwidth, $\Delta\nu$ (Figure 2.3). A simple way of modelling this effect is by considering a thin, irregular screen halfway between the source and the Earth (Scheuer, 1968). In this model, the timescale of fluctuation will depend on the relative motion between the pulsar, screen and observer, and the scintillation bandwidth will be a strong function of frequency: $\Delta\nu \propto \nu^4$ (this dependence is related to the scattering time as a function of frequency). This is similar to the twinkling of stars, and relies on the fact that the pulsar is effectively a perfect point source. In the extreme case, a pulsar that is intrinsically too faint to be detected will become visible, or a relatively bright pulsar will become too faint to detect.

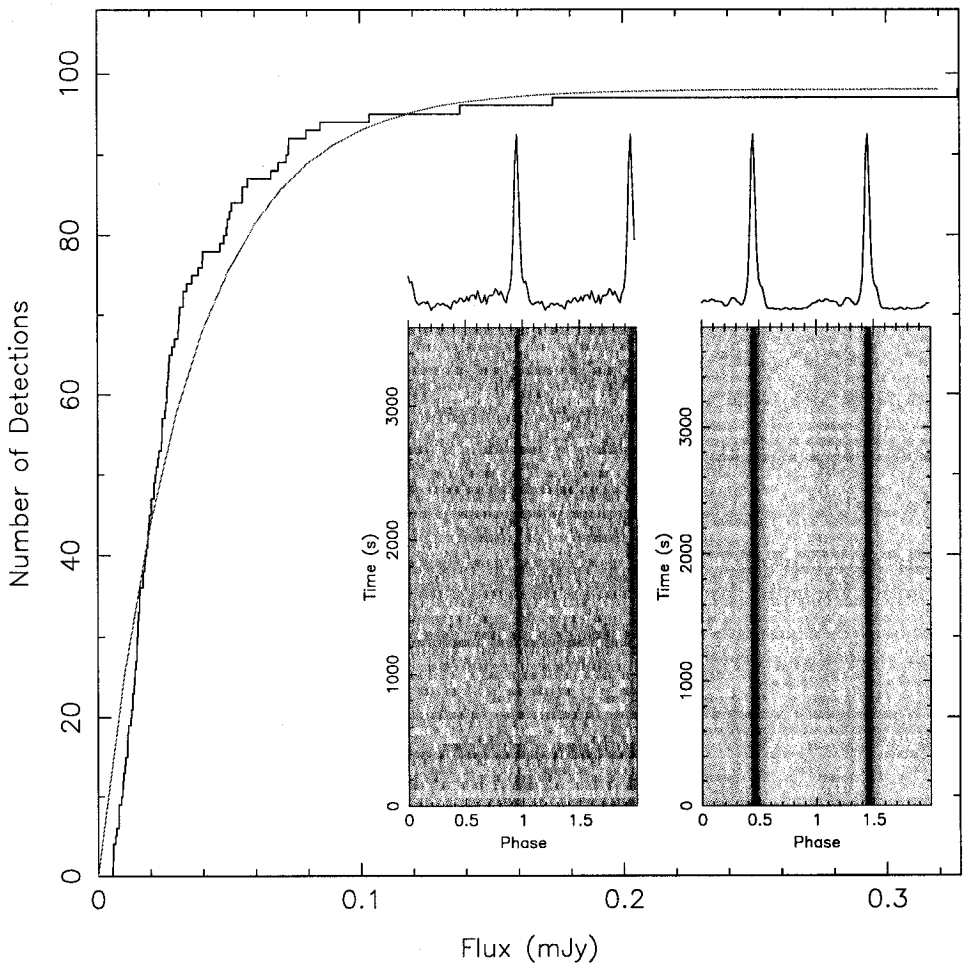

Figure 2.3: A cumulative distribution of the observed fluxes of PSR J1641+3627C from nearly 100 individual $\sim$ 1 hr observations with Arecibo. The discovery of this pulsar is presented in Chapter 4. The smooth green curve is the best-fit cumulative exponential distribution, and has a median of 34 μJy. The inset plots show two invidual detections as a function of observing time. The left plot shows the pulsar increasing in brightness drastically during the observation. The right plot shows the pulsar at its highest flux yet observed. Significant emission can be seen prior to the main pulse.

2.1.4 Signal Detection

In its rawest form, the signal is a time-varying complex voltage, one for each of the two orthogonal polarizations of the incident EM wave. These voltages carry all the information contained in the original wave itself. To record this information in its entirety requires sampling the voltages at the Nyquist rate $\nu_{\rm Nyq} = 2B$, where B is the observing bandwidth. In such a situation, assuming 8-bit (1-byte) samples and an observing bandwidth of 100 MHz, the combined data rate for both polarizations is 400 MB/s (1.4 TB/hr), a phenomenal amount of data. To mitigate the amount of data that is actually recorded and stored, several options are available. For known pulsars, one can apply a tranformation to dedisperse the data[2] and then record only the pulse profile (folded using the rotational ephemeris) in pseudo real time. This results in pulse profiles that do not suffer from any smearing due to finite frequency channelization of the observing bandwidth, although scattering tails will remain. Machines that can Nyquist-sample the voltage signal are called coherent baseband machines, because they first mix the observing band down to baseband ($0 - B$ MHz) before sampling at the Nyquist rate.

Several non-coherent techniques (i.e. where the phase information of the signal is lost) also exist. The conceptually simplest is the filterbank. A filterbank employs many narrow-bandpass filters to channelize the total observing bandpass. Such systems are impractical for creating very large numbers of channels because each filter must be individually tuned. They are also inflexible, as the filter frequencies and bandwidths cannot be quickly changed to dynamically support a variety of observing modes. An autocorrelation machine employs the autocorrelation theorem of the Fourier transform to channelize the data. Following Bracewell (2000), consider a function $f(t)$ that has Fourier transform:

[2]This is referred to as a "chirp function". It is the inverse of the frequency-dependent lag introduced by the ISM.

$$F(\nu) = \int_{-\infty}^{\infty} f(t)\, e^{-i2\pi\nu t}\, dt. \tag{2.3}$$

The autocorrelation function is defined as:

$$f(t) * f(t) = \int_{-\infty}^{\infty} f^*(t')\, f(t'+t)\, dt'. \tag{2.4}$$

The autocorrelation theorem states:

$$|F(\nu)|^2 = \int_{-\infty}^{\infty} f(t) * f(t)\, e^{-i2\pi\nu t}\, dt, \tag{2.5}$$

where $|F(\nu)|^2$ is the power spectrum of the original function $f(t)$. Thus, by taking the Fourier transform of the autocorrelation function, one retrieves the power spectrum. This is a special case of the convolution theorem. Note that all phase information about the Fourier components of $f(t)$ is lost (i.e. this is an incoherent method). In autocorrelators, this is done by applying a finite number of time lags n_{lags} to the signal, each time multiplying it with itself, in order to create the autocorrelation function. This is then Fourier-transformed to derive the power spectrum. The frequency resolution increases with n_{lags}. Modern autocorrelators can achieve $n_{\text{lags}} = 100 - 1000$s, where the maximum number of lags is limited by the maximum data rate of the system and the sampling time.

2.2 Arecibo Radio Telescope

The Arecibo radio telescope (Figure 2.4), operated by Cornell University and part of the National Astronomy and Ionosphere Center (NAIC), is a 305-m single-dish radio telescope located approximately 20 km south of the city of Arecibo in the inland hills of Puerto Rico. The site was chosen because a naturally occuring limestone sinkhole in the karst terrain was conducive to constructing a large sedentary reflector, with less need for excavation. The

original structure was completed in 1963 and upgraded in the mid 1970s and the late 1990s. Arecibo is the largest single telescope ever built, and may remain the largest single reflecting surface on Earth for a considerable time in the future.

The primary reflector is a spherical section and is composed of $\sim$ 39000 perforated aluminum panels suspended above the jungle floor by steel cables. A spherical reflector does not focus incident rays to a single point, but rather into a line[3]. Hence, one must employ either a line feed or a set of supplementary optics in order to collect the radio waves over a finite bandwidth. Arecibo features both: a 30-m long 430-MHz line feed and a Gregorian dome that houses secondary and tertiary reflectors that focus the radio waves to a receiver cabin, which contains a variety of higher frequency ($1 - 10\,\mathrm{GHz}$) receivers. The disadvantage of the Gregorian system, although it provides much larger bandwidths than the 430-MHz line feed, is that it illuminates only a fraction of the primary reflector. Thus while the gain of the 430-MHz line feed is $20\,\mathrm{K\ Jy^{-1}}$, the gain of the Gregorian is reduced to $11\,\mathrm{K\ Jy^{-1}}$.

Unlike more conventional single-dish radio telescopes, Arecibo's primary reflector is stationary. Pointing is achieved not by moving the main reflector, but rather by moving the receivers themselves, which are mounted on a platform suspended 150-m above the centre of the dish. Part of the platform is able to move the receivers in azimuth and zenith angle so they can track a source. Different fractions of the primary reflector are illuminated at different zenith angles, with the effective collecting area being reduced by a factor of 2 at the maximum achievable zenith angle of 19.8°. When the illumination spills over the edge of the dish, heat from the ground can significantly increase the system temperature (reducing the gain of the telescope). This problem was somewhat mitigated by an upgrade in the 1990s, when an extra ground screen was added to the periphery of the primary dish. Because it can only reach zenith angles up to 19.8°, Arecibo can only see objects within the declination

[3]This effect is referred to as "spherical aberration".

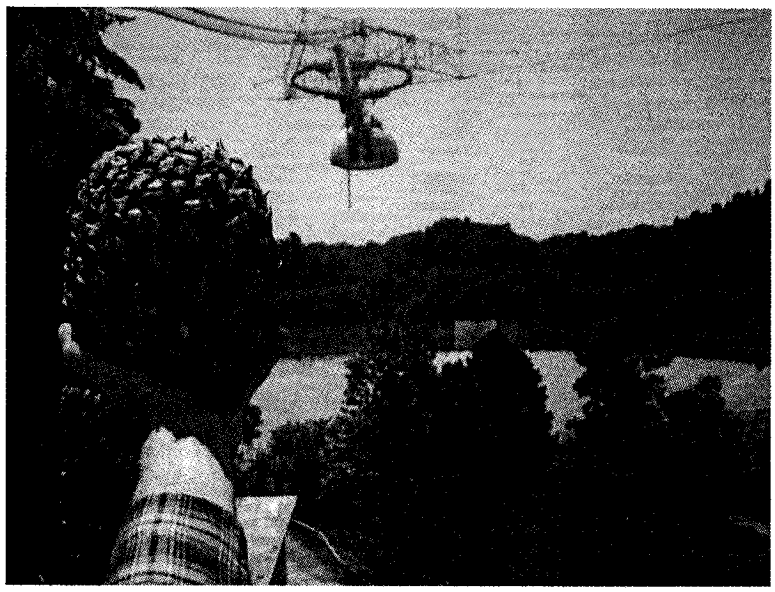

Figure 2.4: Still life with pineapple. The Arecibo feed structure is seen suspended above the 305-m reflector. Photo credit: Jason Hessels.

range $-1° < \delta < +38°$. The maximum tracking time (for sources that pass close to zenith) is ~ 2.5 hrs.

Recently, Arecibo has been equiped with a seven-receiver multibeam system, the Arecibo L-band Feed Array (ALFA), which allows one to sample the focal plane in seven locations simultaneously, and hence point the telescope in seven directions at once. This system can cover the sky more quickly during large-field surveys. Arecibo was used in the 1.4 GHz globular cluster survey presented in Chapter 4, the observations of PSR J2021+3651 presented in Chapters 6 and 7, and the on-going multibeam survey of the galactic plane, PALFA, described in Chapter 8.

2.2.1 Wideband Arecibo Pulsar Processor

The Wideband Arecibo Pulsar Processors[4] (WAPPs, of which there are now four identical machines) are digital autocorrelators designed and constructed at NAIC (Dowd et al., 2000). With a limiting data rate of 16 MB/s, the WAPPs can be configured to provide time sampling from $16 - 1024\,\mu s$ and between $16 - 512$ lags, with a maximum bandwidth of 100 MHz. The user is free to choose any combination of $t_{\rm samp}$, $n_{\rm lags}$, and sample size, provided the data rate does not exceed 16 MB/s, which is a limit set by the ring buffer. These backends were used to collect all the Arecibo data presented in this thesis.

2.3 Robert C. Byrd Green Bank Telescope

The Robert C. Byrd Green Bank Telescope (GBT, Figure 2.5), operated by the National Radio Astronomy Observatory (NRAO), is a 100 × 110-m single-dish reflector located near the small town of Green Bank, West Virginia in the United States National Radio Quiet Zone. It is the largest fully steerable telescope, as well as the largest movable land object ever constructed. The dish can dip to as low as 5.5° above the horizon, allowing the GBT to observe within the declination range $-46° < \delta < +90°$. While conventional dishes are azimuthally symmetric, with the focal point and receiver located along a central axis of symmetry, the GBT dish is shaped in order to produce a focal point which is offset from the centre of the main dish. This novel approach improves the overall gain of the telescope by not obscuring the collecting area with support arms for the feed cabin, and makes the beam pattern much simpler. The surface is much smoother and more precisely formed than that of many other radio telescopes, allowing the GBT to observe at frequencies between $0.3 - 100$ GHz. Note that at frequencies above ~ 20 GHz, observations

[4]See http://www2.naic.edu/~wapp.

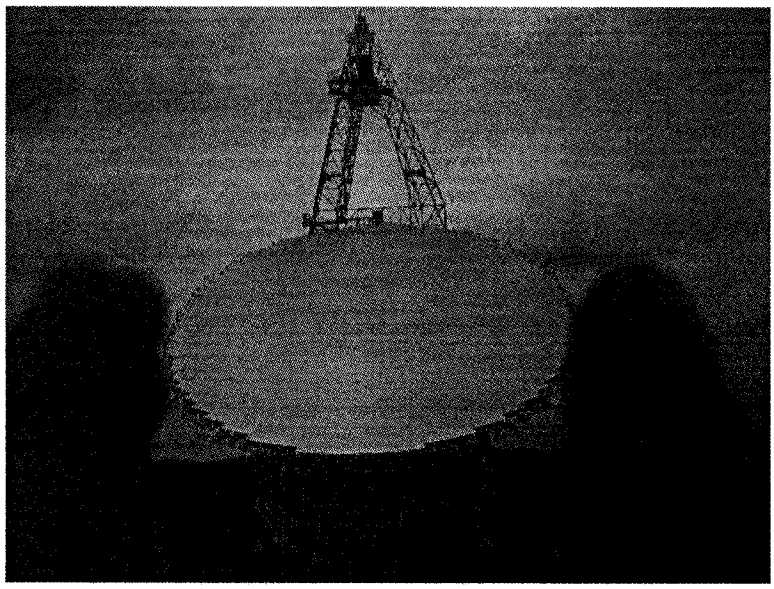

Figure 2.5: Green Bank Telescope shown framed by the photographer's hand. Photo credit: Jason Hessels.

become weather-sensitive and require dry, cloudless conditions. The precise shape of the surface is actively maintained by actuators beneath the corners of the 2000 panels that form the dish. GBT was used in the observations of the globular cluster Terzan 5 presented in Chapter 5 as well as the on-going survey of the northern Galactic plane, GBT350, presented in Chapter 8.

2.3.1 Pulsar Spigot

The GBT Pulsar Spigot[5] is a custom-designed circuit board with a Xilinx XCV300 Field Programmable Gate Array (FPGA) chip which receives and packs signals from the GBT spectrometer (Kaplan et al., 2005). It is a flexible machine, which is capable of outputting 50, 200, or 800-MHz of observing bandwidth with $256 - 2048$ lags and $2.56 - 81.92\,\mu$s sampling. The maximum data rate is 25 MB/s, which limits what combination of spectral and

[5]See http://www.astro.caltech.edu/~dlk/gbtcard/index.html.

time resolution one can use. A list of tested observing modes is available at http://www.gb.nrao.edu/GBT/spectrometer/spigot_card/modes.shtml. The Pulsar Spigot was used in the GBT observations of Terzan 5 presented in Chapter 5 and the GBT350 survey presented in Chapter 8.

2.4 Parkes Radio Telescope

Operated by the Australia Telescope National Facility (ATNF), the Parkes Radio Telescope (Figure 2.6) is a 64-m single-dish parabolic reflector near the town of Parkes in New South Wales, Australia. Built in 1961, it was the largest fully-steerable radio telescope in the southern hemisphere until 1987 when it was superseded by an extension to the DSS-43 telescope at Tidbinbilla. As such, it is one of very few large radio telescopes capable of seeing the extensive portion of the Galactic Plane which lies at southern declinations. It is equipped with a 13-beam multibeam receiver (for details, see Staveley-Smith et al., 1996), which was used to conduct a very successful survey of the southern Galatic Plane for pulsars, the "Parkes Multibeam Survey" (Manchester et al., 2001). Although it is an altitude-azimuth mounted telescope, it is steered by following the motion of a small equatorially mounted telescope located within the structure of the main telescope. Parkes was used in the observations of *EGRET* error boxes for radio pulsations, presented in Chapter 6.

2.4.1 Multibeam Filterbank

The multibeam filterbank (for further details, see Manchester et al., 2001) collects data from the two polarizations of each of the 13 beams in the Parkes multibeam receiver. For each beam, it provides 96 3-MHz channels (for a total bandwidth of 288 MHz) stored as 1-bit samples each 250 μs. The central beam of this system was used in the observations presented in Chapter 6.

Figure 2.6: The Parkes telescope at sunset. Photo credit: Cindy Tam.

2.5 X-ray Observations

Wave-particle duality states that light has the properties of both a wave and a particle. In certain contexts, it is most intuitive to consider light as a wave, in others as a particle. At radio energies, light is most naturally treated as a wave. At X-ray energies, one normally thinks of light as photons. Here we briefly discuss some specifics of X-ray observations, which pertain to the work presented in this thesis.

2.5.1 Focussing

Unlike radio receivers, X-ray detectors, such as a charge coupled device (CCD), detect individual photons. X-ray sources are weak. Even a "bright" X-ray source will have a flux of only about one photon per square centimeter per second at the Earth. A multi-hour observation of a fainter point source may only detect a few dozen photons. Focusing X-rays is very difficult compared

with lower-energy light. X-rays are generally absorbed rather than reflected by a mirror when they hit it. Also, X-rays cannot be easily focused by a lens, because at X-ray wavelengths the index of refraction is very close to 1 for all materials. This would require a cumbersomely long focal length. It is however possible to reflect X-rays using a mirror, if the angle of incidence is very shallow. This technique has been used very sucessfully in the *Chandra* (§2.6) and *XMM-Newton* satellites.

2.5.2 Propagation Effects

X-rays do not suffer from the same dispersive, scattering and scintillation effects described in §2.1.3 for radio waves. However, X-rays do still strongly interact with the ISM. Soft X-rays ($E \lesssim 1\,\mathrm{keV}$) are attenuated by photoelectric absorption in heavy metals. Hydrogen is used as a tracer for these elements. The column density is quantified in terms of the amount of hydrogen, N_{H}, along the line of sight, generally assuming solar abundance for all the heavier species. In analogy with the DM-derived distance method of radio pulsars, one can also estimate the distance of an X-ray source from its N_{H}, although this method is even more imprecise than the DM method. Photoelectric absorption almost completely blocks X-rays below $\sim 0.3\,\mathrm{keV}$, making it more difficult to measure the black-body spectra of neutron stars, which often peak around about $50 - 200\,\mathrm{eV}$ (Kaspi et al., 2006).

2.6 Chandra X-ray Observatory

Originally dubbed the *Advanced X-ray Astrophysics Facility* (*AXAF*), the *Chandra X-ray Observatory* was later renamed in honour of the renowned Indian astrophysicist Subramanyan Chandrasekhar. Launched July 23, 1999 by NASA, *Chandra* provides virtually an order-of-magnitude improvement in angular resolution over past imaging X-ray telescopes like *ROSAT* and *Einstein*. *Chandra* is capable of achieving $0.5''$ on-axis resolution (which is comparable

to angular resolutions achieved in optical observations) through the use of four iridium-coated pairs of nested hyperbolic and parabolic mirrors, which reflect the incoming X-ray photons at a very shallow angle. *Chandra* is sensitive to X-rays in the energy range $\sim 0.1 - 10.0\,\mathrm{keV}$. This energy range allows measurements of the black-body tail of objects with T$\sim 0.15\,\mathrm{keV}$, steep power-law spectra, and the $6 - 7\,\mathrm{keV}$ iron line seen in some sources.

There are two imaging detectors on-board, as well as two transmission gratings, which are used for very-high-resolution spectroscopy. The High Resolution Camera (HRC) provides the best angular resolution as well as time resolution of $16\,\mu\mathrm{s}$. The disadvantages of the HRC are that it does not provide spectroscopic information, and has a lower effective area than the other imaging detector, the Advanced CCD Imaging Spectrometer (ACIS). ACIS has the requisite spectral resolution needed to fit the black-body and power-law components of a source, as well as the amount of photo-electric absorption. ACIS's standard time resolution is 3.2 s, which can be improved by running the detector in a windowing mode which uses only a subsection of the dectector (this is often done to prevent pile-up from brighter sources). ACIS can also be run in a continuous clocking (CC) mode, in which spatial information is reduced to a single dimension in order to improve the timing resolution to $\sim 3\,\mathrm{ms}$.

Chandra was used here in the detection of an X-ray point source and pulsar wind nebula associated with the young, energetic pulsar J2021+3651. This work is presented in Chapter 7.

2.7 "The Borg" Computer Cluster

"The Borg" (Figure 2.7) is a 92-node computer cluster built by the McGill Pulsar Group[6] in order to provide sufficient computational power to conduct large-scale searches for pulsars. The original Borg consisted of 52 dual-node 1.4 GHz,

[6]Special acknowledgements are due to Dr. Scott Ransom and Mr. Paul Mercure, who have done the bulk of the system administration.

32-bit AMD Athlon machines as well as a master node and two 500 GB file servers, "data1" and "data2". This system was operational by the end of 2001. In the summer of 2005, the original system was expanded with the construction of the "Next Generation Borg". This included the addition of 40 dual-node 2.4 GHz, 64-bit AMD Opteron machines, a master node, and two 8.3 TB file-servers, "lore1" and "lore2"[7]. A block diagram of the full system is shown in Figure 2.8. The Borg resides in a specially designed air-conditioned[8] computer nursery on the third floor of the Rutherford Physics Building at McGill.

[7]In the TV series "Star Trek the Next Generation", Lore is Data's long-lost evil brother.

[8]The cooling of a large computer cluster is an important consideration, as a hundred computers can easily heat a room to above 30 degrees centigrade. At such a temperature, the computers will lock-up and the processors can be damaged. Before the installation of air-contioning in the Borg's current location, the Borg was placed next to a slightly open window during the bleak months of the Canadian winter. Although this was the cheapest and easiest solution to the cooling problem, it had some disadvantages. In the spring, before the Borg was moved to its permanent home, some birds left "residue" on the casing of one of the nodes.

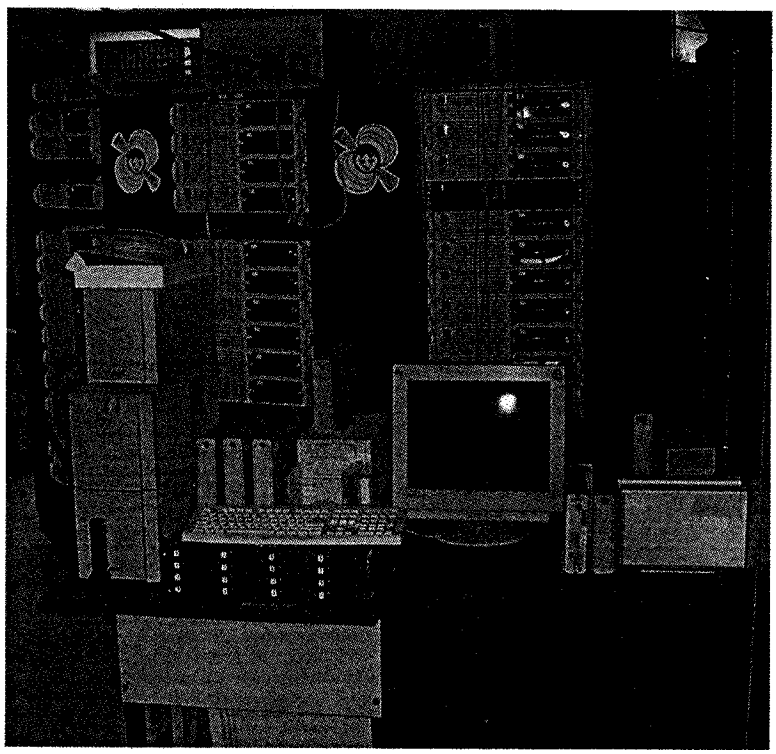

Figure 2.7: The Borg beowulf cluster and ancilliary equipment. Photo credit: Andrew Archibald.

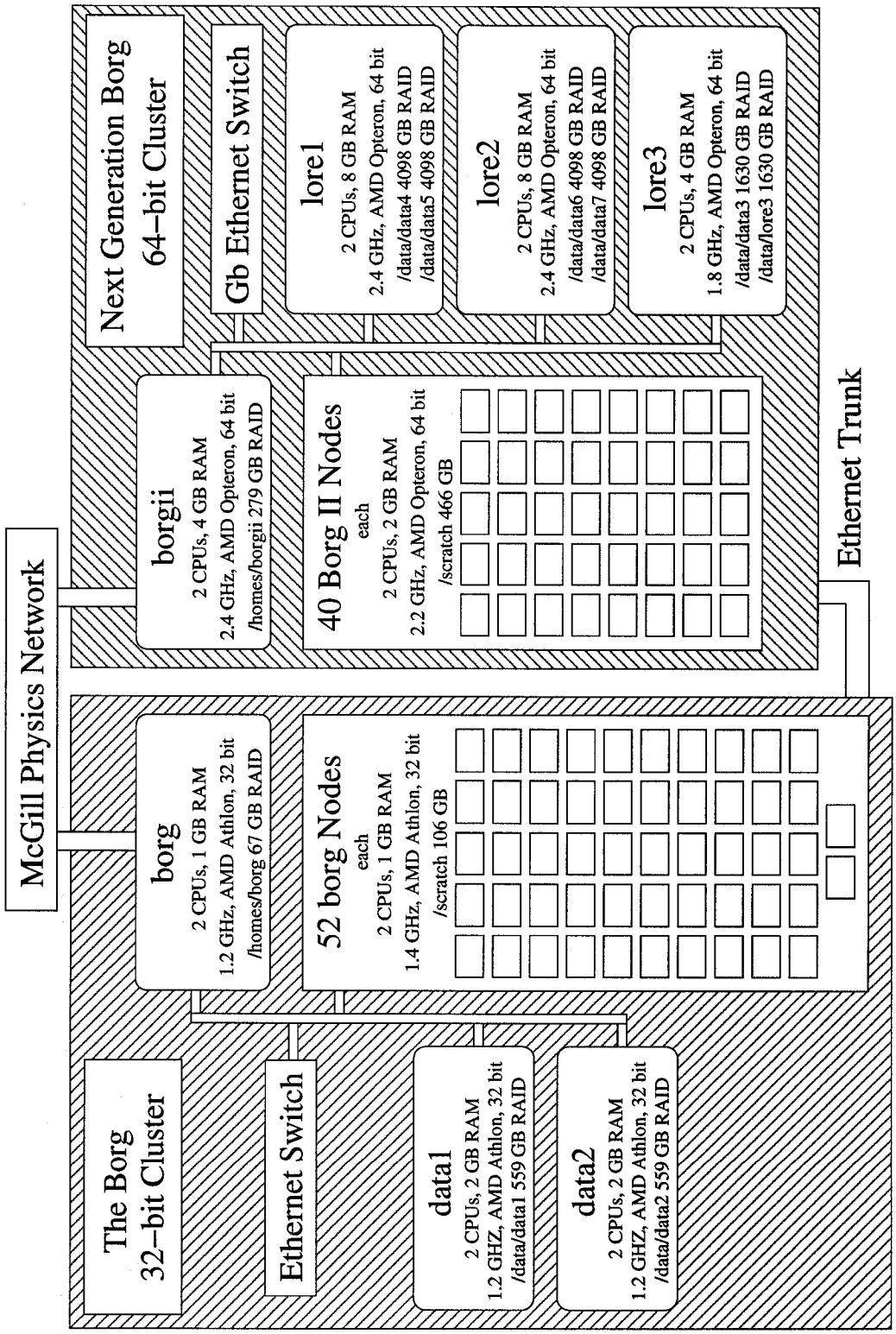

Figure 2.8: Block diagram showing the original "Borg" and "Next Generation Borg".

Chapter 3

Pulsar Search Techniques

In this chapter, we give an overview of pulsar search techniques. Searches have always been an important part of pulsar astrophysics. As the number of known pulsars has increased, so has our understanding of the physics behind their behaviour. With an increasing sample of pulsars to study, we are better able to discern the underlying properties of the population, such as birthrate and distributions in spin period, luminosity, and magnetic field strength. Furthermore, occasionally a pulsar is found whose characteristics make it exceptional for addressing specific physical problems, such as strong gravity, the equation of state, and the pulsar emission mechanism itself. In this sense, some of what we know is derived from the study of a few novel pulsars, and finding more of these could lead to breakthroughs in our understanding of pulsars and related science.

Radio pulsar search observations record the sky signal over some bandwidth, divided into a number of frequency channels and sampled at a constant time interval. Because radio pulsar signals are dispersed by the interstellar medium (§2.1.3), this effect must first be removed before one can search the data. A dedispersed time series is the signal as a function of time, dedispersed at some constant dispersion measure (DM). A standard pulsar signal is char-

acterized by extremely periodic dispersed pulsations[1]. As the pulsations are often too faint to be seen individually, one must rely on the integrated signal of many hundreds to millions of single pulses. The periodicity corresponding to the pulsar's rotation rate is typically discovered by examining the Fourier transform of the time series, which is highly sensitive to regular pulsations, even if the pulsations are individually very weak. In a search for new radio pulsars, the DM is not known *a priori*, and thus many trial dedispersed time series must be created over a range of DMs and searched seperately. This greatly magnifies the computational burden of searching for radio pulsars. Furthermore, if the pulsar is in a binary system, then the *observed* spin period will be variably Doppler shifted. This can lead to a significant loss of signal in the Fourier domain. Such pulsars may only be detectable using advanced techniques that partially compensate for the period drift created by orbital motion.

Given a set of dedispersed time series, which have been cleaned to remove man-made interference (see §2.1.2 and §4.3.1), we review the various techniques that are then employed to detect isolated, binary, and sporadic pulsars. These techniques can be used at higher observing wavelengths as well, for instance X-ray, where the dedispersion step is not necessary. Table 3.1 summarizes these techniques and provides a more detailed reference for each. This chapter does not provide an exhaustive list of all possible search techniques, but does identify the most commonly used methods in pulsar searches. The discussion generally follows that of Lorimer & Kramer (2004), which is a somewhat more detailed reference. The techniques presented here form the basis for the search results presented in the remaining chapters of this thesis.

[1]See also §3.3 for a discussion of searches for more sporadic emission from objects like the rotating radio transients (RRATs).

Technique	Section	Domain of Applicability	Coherent or Incoherent	Ref.
Un-accelerated Fourier	§3.1.1	Isolated	Coherent	1
Stack Search	§3.1.3	Isolated	Incoherent	1
Time domain Acceleration	§3.2.2	Binary $P_{\rm orb} \gtrsim 3 - 5T_{\rm obs}$	Coherent	2
Fourier domain Acceleration	§3.2.2	Binary $P_{\rm orb} \gtrsim 3 - 5T_{\rm obs}$	Coherent	3
Slide Search	§3.2.2	Binary $P_{\rm orb} \gtrsim 3 - 5T_{\rm obs}$	Incoherent	4
Phase Modulation	§3.2.3	Binary $P_{\rm orb} \lesssim 1.5T_{\rm obs}$	Coherent	5
Dynamic Power Spectrum	§3.2.4	Binary $P_{\rm orb} \sim T_{\rm obs}$	Incoherent	6
Single Pulse	§3.3	Strong pulses or bursts	Coherent	7

Table 3.1: A summary of the pulsar search techniques described in this chapter, their domain of applicability, whether they are a coherent or incoherent technique, and a standard reference. The references are: 1) Lorimer & Kramer (2004), 2) Camilo et al. (2000), 3) Ransom et al. (2002), 4) Faulkner et al. (2004), 5) Ransom et al. (2003), 6) Chandler (2003), and 7) Cordes & McLaughlin (2003).

3.1 Search Techniques for Isolated Pulsars

3.1.1 Fourier-Based Periodicity Searches

The Fourier transform[2]

$$F(\nu) = \int_{-\infty}^{\infty} f(t)\, e^{-i2\pi\nu t}\, dt \tag{3.1}$$

of a continuous function $f(t)$ is a well known, and sensitive method for detecting periodicities. In the case of a discretely sampled time series, like those used in pulsar searching, one must employ a Discrete Fourier Transform (DFT)

$$F(r) = N^{-1} \sum_{\tau=0}^{N-1} f(\tau)\, e^{-i2\pi(r/N)\tau}, \tag{3.2}$$

where τ ($\tau = 0, 1, \ldots, N$) is the n$^{\text{th}}$ sample of the time series $f(\tau)$, with N total samples, and r ($r = 0, 1, \ldots, N$) is the n$^{\text{th}}$ Fourier (frequency) component. The DFT is used in most pulsar searches (although see §3.3). For a time series which is uniformly sampled at an interval t_{samp}, the Fourier components are related to physical frequencies by $\nu_r = r/(Nt_{\text{samp}}) = r/T_{\text{obs}}$, and the frequency resolution is $1/T_{\text{obs}}$. $r = N/2$ corresponds to the Nyquist frequency $\nu_{\text{Nyq}} = 1/(2t_{\text{samp}})$. In the case of a real valued time series, the transform is symmetric around ν_{Nyq}, with Fourier components above ν_{Nyq} being the complex conjugates of their mirror component ($F_{N-r} = (F_r)^*$). The maximum frequency detectable in the time series is then simply ν_{Nyq}. An efficient algorithm for computing the DFT is the Fast Fourier Transform (FFT), which requires $N\log_2 N$ operations to calculate as opposed to the brute-force N^2 method.[3]

[2]For an exhaustive discussion of the Fourier transform, along with derivations of associated results and theorems, see Bracewell (2000).

[3]In this thesis, we have used the FFTW package ("Fastest Fourier Transform in the West"), which is a popular implementation of the FFT algorithm.

3.1.2 Additional Search Considerations

With the Fourier transform computed, one can then search for pulsar periodicities by looking for local peaks in the Fourier amplitudes $|F(r)|$ or power spectrum $|F(r)|^2$. However, to maximize sensitivity, a few additional steps must be taken:

- **Frequency Response.** The DFT produces a non-uniform response as a function of frequency, commonly referred to as "scalloping", because of the finite frequency resolution introduced by the finite time sampling. For a signal of frequency ν, which has a corresponding Fourier component $F(r')$ (where we let r' be real-valued), the corresponding Fourier component calculated from a DFT $F(r)$ (where r is strictly an integer) is reduced in the following way: $F(r) = F(r')/\mathrm{sinc}[\pi(r - r')]$ (Ransom et al., 2002). In the worst case, where a signal falls directly between spectral bins (i.e. $|r - r'| = 0.5$), the resulting loss in sensitivity is 60%. This can be mostly corrected for in a number of ways (see Lorimer & Kramer, 2004, and references therein), including interpolation using the nearby Fourier amplitudes, or simply by padding the end of the time series with zeros.

- **Renormalizing the Spectrum.** The spectrum must also be renormalized so that significant periodicities can be properly identified. While the response of the DFT to Gaussian or "white" noise is uniform, real pulsar data usually contain significant low-frequency or "red" noise, which greatly increases the background Fourier amplitudes at low frequencies and is detrimental to discovering slow pulsars (Figure 3.1). This can be mostly removed by dividing the amplitudes by a running median. The number of bins used to calculated the local median is typically a function of frequency. One uses only a few bins at the lowest frequency, where the slope of the red noise is changing most rapidly, and then increases the number of bins logarithmically with frequency. The median

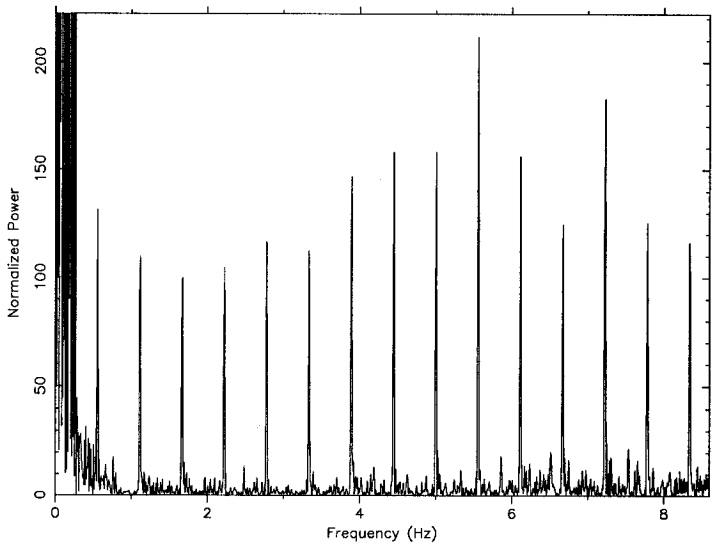

Figure 3.1: Zoomed-in power spectrum from a 60-s GBT observation of the 1.799-s (0.556-Hz) pulsar J2345+62, discovered in the GBT350 survey presented in Chapter 8. Numerous regularly spaced harmonics are visible; the pulse profile has a FWHM of roughly 5%. Also visible in the spectrum is low frequency "red" noise, increasing in strength with decreasing frequency.

rather than the mean is used so that the contribution of outlying amplitudes, which may represent a real astronomical signal, is reduced. With the amplitudes also normalized by the root mean square of the data, the signal-to-noise ratio of any amplitude is simply equal to its value. Furthermore, assuming the noise is appropriately Gaussian, the peak strengths in the power spectrum follow an exponential probability distribution, such that the probability of a particular peak being noise is proportional to $\exp(-P_{\rm min})$, where $P_{\rm min}$ is some threshold power.

- **Harmonic Summing.** The vast majority of radio pulsars have highly non-sinusoidal pulse profiles, with duty cycles typically of only a few percent of the pulse phase (see for instance the discoveries made in the GBT350 survey of Chapter 8, Figure 8.8). Such sharp pulses have the

majority of their spectral power in their harmonics (Figure 3.1), which must be taken into account to maximize search sensitivity. As a general rule of thumb, the number of harmonics present is roughly the inverse of the pulse duty cycle (Lorimer & Kramer, 2004). For example, roughly 20 harmonics should be present given a pulse duty cycle of 5%. Harmonic summing adds the Fourier components of harmonics with that of the fundamental to increase the signal-to-noise. One way in which this can be done is by stretching the spectrum by factors of 2, 4, 8, etc., each time adding the stretched spectrum onto the original. This has the effect of adding 2^{nd}, 4^{th}, 8^{th}, etc. harmonics to the fundamental. Harmonic summing will increase the signal-to-noise ratio for pulse duty cycles of roughly 30% or less, assuming a typical pulsar pulse shape (which can be described by a modified von Mises distribution, see Ransom et al., 2002, for details), and is critical for detecting faint, narrow pulsars. Note that even a profile that is broad overall can have many harmonics if it contains narrower substructure.

- **Barycentering.** In multi-hour observations, the observatory's motion with respect to the pulsar can smear the periodic signal over multiple spectral bins. To avoid this loss in sensitivity, the time series is transformed from its non-inertial topocentric reference frame to the roughly inertial reference frame of the solar system barycentre. In practice, this is done by comparing topocentric and barycentric arrival times and adding or deleting whole samples as necessary to bring the difference in the two time standards to less than the sampling time. Barycentering is also useful for comparing search candidates from the same direction on the sky, but at different epochs. This way, one can determine whether two candidates are related, or whether a candidate is potentially in a binary system. Cross-referencing candidate lists in this way is also useful for rejecting RFI.

3.1.3 Stack Searches

A coherent time series contains no gaps between samples, and hence the phase of a periodic signal is known unambiguously throughout the observation. For a coherent time series, the signal-to-noise of a signal increases with the square-root of the observation time. One can increase the total observing time, and hence the sensitivity to periodic signals, by combining multiple observations of a given direction on the sky. However, summing the power spectra from separate observations is an *incoherent* sum, which scales as time to the *fourth* root. For instance, summing the power spectra of four one-hour integrations will increase the sensitivity by $\sqrt{2}$. This technique works best for isolated pulsars, which will have a roughly constant period between observations. An important consideration is the time span between observations, $T_{\rm span}$. If $T_{\rm span}$ is comparable to the timescale on which the pulsar's observed period is changing, then the signal will drift by a spectral bin or more and the technique will not provide a real gain in sensitivity. Following Anderson (1993), the maximum useful $T_{\rm span}$ can be written in terms of the potential pulsar's spin period P and observed derivative $\dot{P}$, and the duration of the individual observations that are being combined, $T_{\rm obs}$:

$$T_{\rm span} < \frac{1}{T_{\rm obs}} \frac{P^2}{|\dot{P}|}. \tag{3.3}$$

Here, $|\dot{P}|$ can be due to the pulsar's intrinsic spin-down, acceleration in the gravitational potential of a host globular cluster, and binary motion. If the pulsar is significantly offset from the central pointing position, then it will not be properly barycentred. This will also contribute to $|\dot{P}|$ in Equation 3.3. In practice, for millisecond pulsars, only binary motion puts a strong constraint on $T_{\rm span}$. As an example, this method was successful in discovering four of the eight known pulsars in the globular cluster M15 (Anderson, 1993), which were too faint to be blindly detected in searches of individual observations. We have applied this method to observations of the cluster M71 (Chapter 4), but found

no new pulsars.

3.2 Search Techniques for Binary Pulsars

3.2.1 Orbital Modulation of the Pulsar Signal

Discovering binary pulsars is more exacting, and much more computationally intensive, than finding isolated pulsars because the observed periodicity of the pulsar is modulated by its orbital motion (Figure 3.2). Consequently, if the observing time, $T_{\rm obs}$, is a non-neglible fraction of the orbital period, $P_{\rm orb}$, then the pulsar signal will be smeared across numerous Fourier components, severely decreasing the chances of detecting such a pulsar in a blind search (see Johnston & Kulkarni, 1991, for a quantitative discussion of sensitivity loss due to binary motion). While one can mitigate the effects of binary motion by restricting the integration time of the observation to a negligible fraction of the likely binary orbital periods, it is still highly desirable to search long data-sets ($T_{\rm obs} \gtrsim 1\,{\rm hr}$), in order to find faint pulsars (e.g. the deep searches of globular clusters presented in Chapters 4 and 5).

The "brute-force" method of searching the entire orbital parameter space is not feasible given current computing resources, as the five-dimensional parameter space required to fully describe a Keplerian orbit is far too large to search in a reasonable amount of time. Here we review several computationally efficient algorithms which partially search over orbital parameter space in order to increase search sensitivity to binaries. These methods have greatly increased the known population of binary pulsars (e.g. Anderson, 1993; Camilo et al., 2000; Ransom et al., 2005c; Faulkner et al., 2004). The methods detailed here are complimentary in that, for a fixed $T_{\rm obs}$, they are more sensitive than the other methods for different $P_{\rm orb}$ (Table 3.1). By applying each method to a given data set, one has sensitivity to binary pulsars in a wide range of orbits.

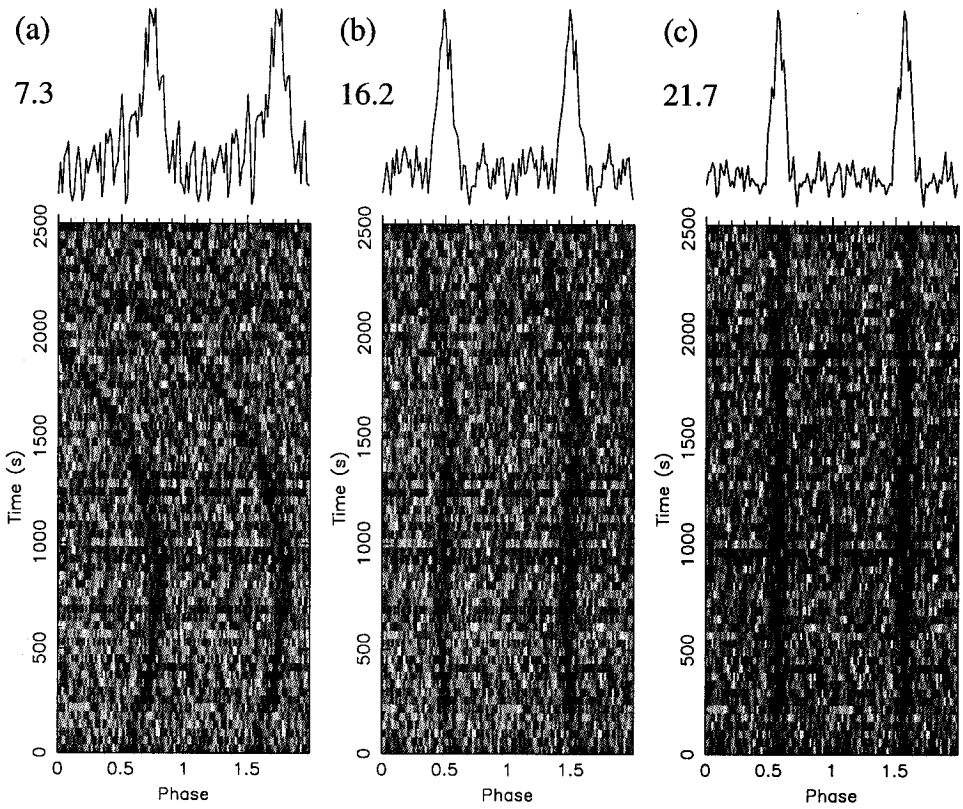

Figure 3.2: Three folds of the same Arecibo observation of the 4.89-ms binary pulsar J1953+1846A, whose discovery is presented in Chapter 4. The pulse intensity as a function of observing time and pulse phase (repeated twice for clarity) is shown in greyscale, with the cumulative profile plotted at the top. PSR J1953+1846A is in a 4.2-hr orbit with a $0.036\,M_\odot$ (minimum mass) companion. The three plots demonstrate the effect of PSR J1953+1846A's binary motion during the observation which, in this case, is 16% the length of the orbital period. (a): the pulsar is folded using only a constant period. The large apparent period derivative causes very significant phase drifts, which smear the cumulative pulse profile and increase the root-mean-square in the off-pulse region. The equivalent Gaussian sigma of the profile is 7.3σ, less than the threshold typically used in blind pulsar searches. (b): a period derivative is incorporated in the fold. The cumulative profile is sharper and is now 16.2σ. There is still a residual S-shaped curve as a function of observing time, which indicates that a second period derivative is required. (c): the effects of binary motion are now almost entirely removed by folding the data with the appropriate period and first two period derivatives. The significance of the detection is now 21.7σ.

3.2.2 Acceleration Searches

If the orbital period of a pulsar is sufficiently long compared to the observation time, then one can approximate the orbital motion of the pulsar as a constant acceleration. This method is most appropriate when $P_{\rm orb} \gtrsim 3 - 5T_{\rm obs}$.

This technique has been implemented equivalently in both the time and frequency domains:

- **Coherent time domain acceleration search.**

  If one resamples the time series to remove the radial motion of the pulsar with respect to the observer, then one is again in an inertial frame with respect to the pulsar and the search is reduced to the standard isolated search technique. In general, the time samples can be shifted using the Doppler equation:

$$\tau(t) = \tau_{\rm o}(1 + v_{\rm rad}(t)/c), \tag{3.4}$$

  where $v_{\rm rad}(t)$ is the radial velocity of the pulsar along the line of sight, c is the speed of light, and $\tau_{\rm o}$ is a normalization factor. While $v_{\rm rad}(t)$ can be determined given the five Keplerian orbital parameters, it is not computationally feasible to search over such a large parameter space. Instead, the problem is reduced to a one dimensional search by assuming $v_{\rm rad} = a_{\rm rad}t$ over the course of the observation, where $a_{\rm rad}$ is a constant radial acceleration (see, for instance, Camilo et al., 2000). In a blind search, a range of $a_{\rm rad}$ is searched, with a step size such that the drift of the pulsar signal is less than one bin. The number of bins a signal will drift,

$$N_{\rm drift} = a_{\rm rad}\nu_{\rm o}T_{\rm obs}^2/c, \tag{3.5}$$

  is a function of $a_{\rm rad}$, the intrinsic spin rate $\nu_{\rm o}$, and $T_{\rm obs}$ (Lorimer &

Kramer, 2004).

- **Coherent frequency domain acceleration search.**

  An equivalent method, developed by Ransom et al. (2002), can be performed in the frequency domain. This technique is more computationally efficient than the time series method, because it does not necessitate a new Fourier transform for each trial acceleration. In Fourier space, the pulsar's orbital motion is equivalent to taking a constant frequency and convolving it with a finite impulse response (FIR) filter. By applying the inverse filter to the Fourier transform, the signal power that was formerly spread across many bins is swept into a single bin. Templates are calculated for a range of frequency derivatives, out to some maximum number of bins that the pulsar signal can drift during the observation, $Z_{\rm max}$. This is related to the maximum acceleration by:

$$a_{\rm max} = \frac{Z_{\rm max} c P}{{T_{\rm obs}}^2}. \tag{3.6}$$

  Note that if the fundamental harmonic of a signal drifts by $N_{\rm drift}$ bins, its $n^{\rm th}$ harmonic will drift by $nN_{\rm drift}$ bins. Hence, significant harmonics can drop out of the search unless a sufficiently large $Z_{\rm max}$ is used.

- **Incoherent frequency domain acceleration search.**

  An *incoherent* frequency domain acceleration search also exists (for a detailed discussion, see Faulkner et al., 2004), which is basically an extension of the stack search method discussed in §3.1.3. Short chunks of the time series are individually Fourier transformed and the power spectra are summed. Smearing of the signal within individual power spectra is mitigated by the fact that the shorter time length of each chunk decreases the frequency resolution of the bins, and also allows less time for the signal to drift. To simulate various accelerations, the spectra are offset in frequency with respect to each other before summing. Although

this method is 20% less sensitive than the coherent acceleration methods (Faulkner et al., 2004), it is the most computationally inexpensive of the three.

3.2.3 Phase Modulation Search

This method, which is described in detail by Ransom et al. (2003) (see also Jouteux et al., 2002), works best when $T_{\rm obs} \gtrsim 1.5 P_{\rm orb}$. In fact, the technique's sensitivity *improves* as the ratio $T_{\rm obs}/P_{\rm orb}$ increases, which is not the case for acceleration searches (Figure 3.3). Given that the shortest orbital period known for a binary radio pulsar is 96 minutes (PSR J0024−7204R in the globular cluster 47 Tucanae, Camilo et al., 2000), and deep observations are typically > 2 hr in length, this technique is well motivated.

During a long observation of a binary pulsar, the phase of the pulsar signal has a periodic modulation, which produces sidebands in the Fourier domain around the intrinsic pulsar spin frequency and its harmonics (Figure 3.4). In the case of a circular orbit, the phase modulation is sinusoidal. The sidebands are regularly spaced at the orbital period, which is then detectable by Fourier transforming short chunks of the original power spectrum. Furthermore, by analyzing the complex amplitudes and phases of the sidebands, one can recover the other Keplerian orbital parameters for use in folding the data. This method was employed in the searches presented in Chapter 4, but discovered no new pulsars. However, given the < 3 hr integrations used in that survey, the phase modulation search was most sensitive to orbital periods < 1 hr. No such systems are currently known in the radio pulsar population.

3.2.4 Dynamic Power Spectrum

The dynamic power spectrum method (see Chandler, 2003, for a detailed discussion) employs the same stacked power spectra as in §3.1.3, but with the intention of identifying signals that are drifting due to binary motion. As

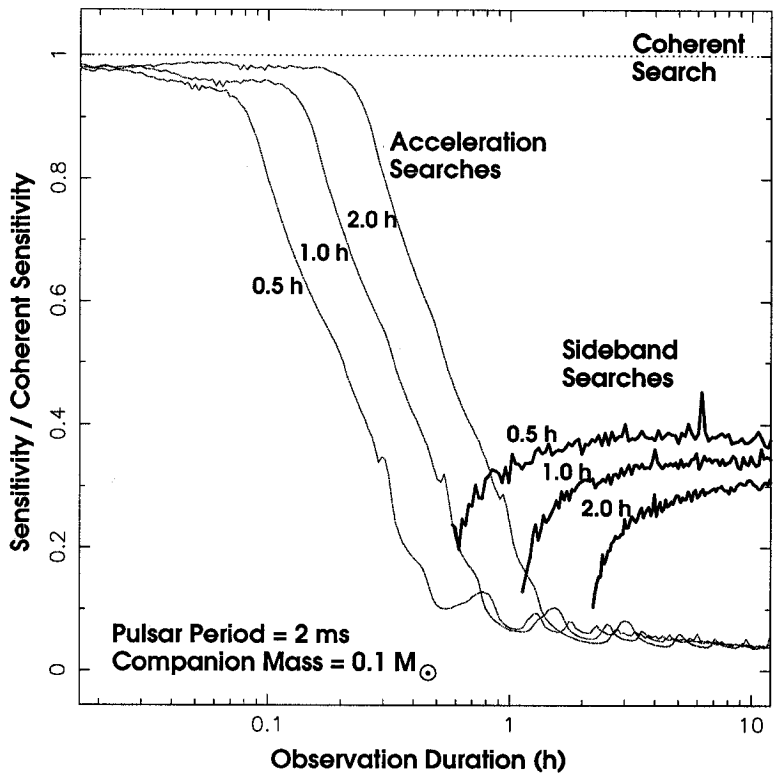

Figure 3.3: The sensitivities of the coherent Fourier domain acceleration search (§3.2.1) and sideband search (§3.2.2) are plotted as a function of observing time for a simulated 2-ms pulsar in a 0.5, 1, and 2-hr circular orbit with a $0.1\,M_\odot$ companion. The sensitivities are normalized to that of a hypothetical coherent search, which has *completely* compensated for the pulsar's orbital motion. Figure from Ransom et al. (2003).

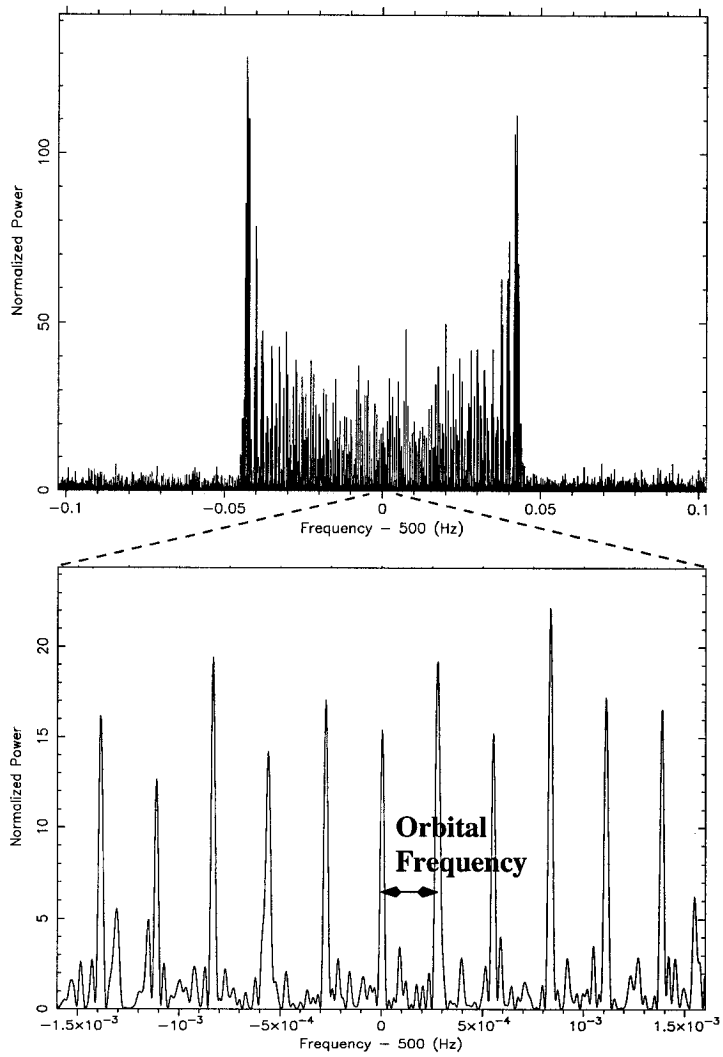

Figure 3.4: A simulated 11-hr observation, showing the effect of phase modulation for a bright 2-ms pulsar in a 1-hr circular binary orbit with a $0.055\,M_\odot$ (minimum mass) companion. *Top:* the characteristic "double-horned" pattern created in the power spectrum by the pulsar's binary motion. The two horns correspond to times when the pulsar is moving directly along the line of sight, and hence its apparent period has changed the most. *Bottom:* a zoomed view of the spectrum around the intrinsic pulsar spin rate of 500 Hz. Regularly spaced sidebands are present at intervals corresponding to the pulsar's orbital frequency. The orbital period can be determined by taking a short Fourier transform of the sidebands.

such, the power spectra are not summed, but rather are plotted on top of each other to create a frequency versus time plane (harmonic summing can be included). A pulsar signal that is orbitally modulated will appear as a curve - sinusoidal in the case of a circular orbit - in this plane (Figure 3.5). Although it is an incoherent method, it is potentially more sensitive - assuming the pulsar is not bright enough to be detectable in a shorter integration - than the acceleration search or phase modulation search, when $P_{\rm orb} \sim T_{\rm obs}$.

Creating the dynamic power spectrum is computationally simple; however, identifying curves is more difficult. One way in which this can be done is by scrolling through small windows of the spectrum and identifying curves by eye. Automated line-finding algorithms can also be implemented, although it is difficult to compete with the eye's natural ability to detect faint curves. This technique can of course also be used to find isolated pulsars, which will appear as straight lines. Although it is theoretically less sensitive than a coherent transform of the entire data-set, examining the dynamic power spectrum can sometimes help identify signals that would otherwise be obscurred by a strong RFI environment.

3.3 Single Pulse Search

Up until now, we have considered search techniques that use the power of the Fourier transform for detecting faint periodic signals. However, not all pulsars are persistent, steady emitters. Some show giant pulses ($\sim 10^2 - 10^3$ the mean pulse strength) and others may null for extended periods of time. There is also the recently identified class of rotating radio transients (RRATs; McLaughlin et al., 2006), which show strong pulses with repeat times from minutes to hours. In this regime, identifying signals in the time series can be the more sensitive method or, in extreme cases, there will be no signal in the Fourier transform at all (Figure 3.6).

To detect such signals, one inspects the dedispersed time series for signifi-

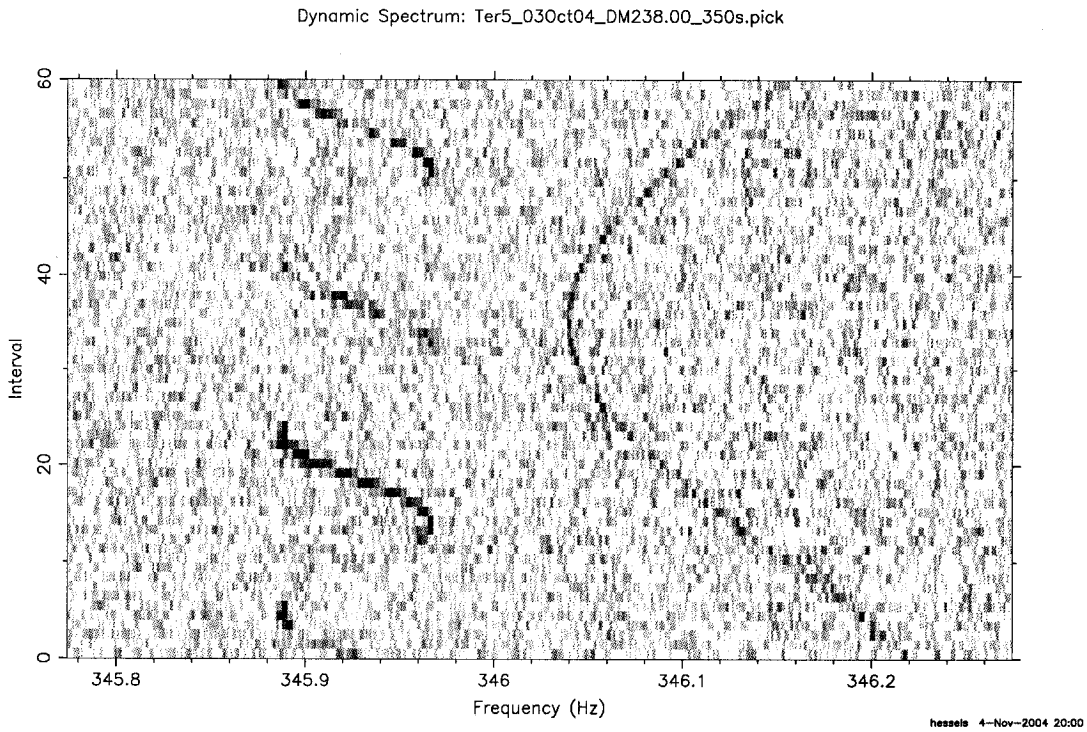

Figure 3.5: Example dynamic power spectrum from a 5.8-hr GBT observation of the globular cluster Terzan 5. Each interval is the power spectrum of a 350-s chunk of the total time series, which is dedispersed at DM = 238.0 pc cm^{-3}. Only 0.5 Hz of the spectrum is shown so that the binary motion of two of the pulsars known in the cluster is visible. The curve on the left is the 4$^{\text{th}}$ harmonic of PSR B1744−24A, which has an intrinsic spin frequency $\nu_{\text{spin}} = 86.48$ Hz and an orbital period $P_{\text{orb}} = 1.8$ hr. The gaps in the curve are due to both regular and irregular eclipses of the pulsar by its companion and intra-binary material. The curve on the right is the 3$^{\text{rd}}$ harmonic of PSR J1748−2446N, which has an intrinsic spin frequency $\nu_{\text{spin}} = 115.38$ Hz and an orbital period $P_{\text{orb}} = 9.3$ hr. It is a coincidence that these particular harmonics of these two pulsars have approximately the same frequency. Plot generated using code written by the author.

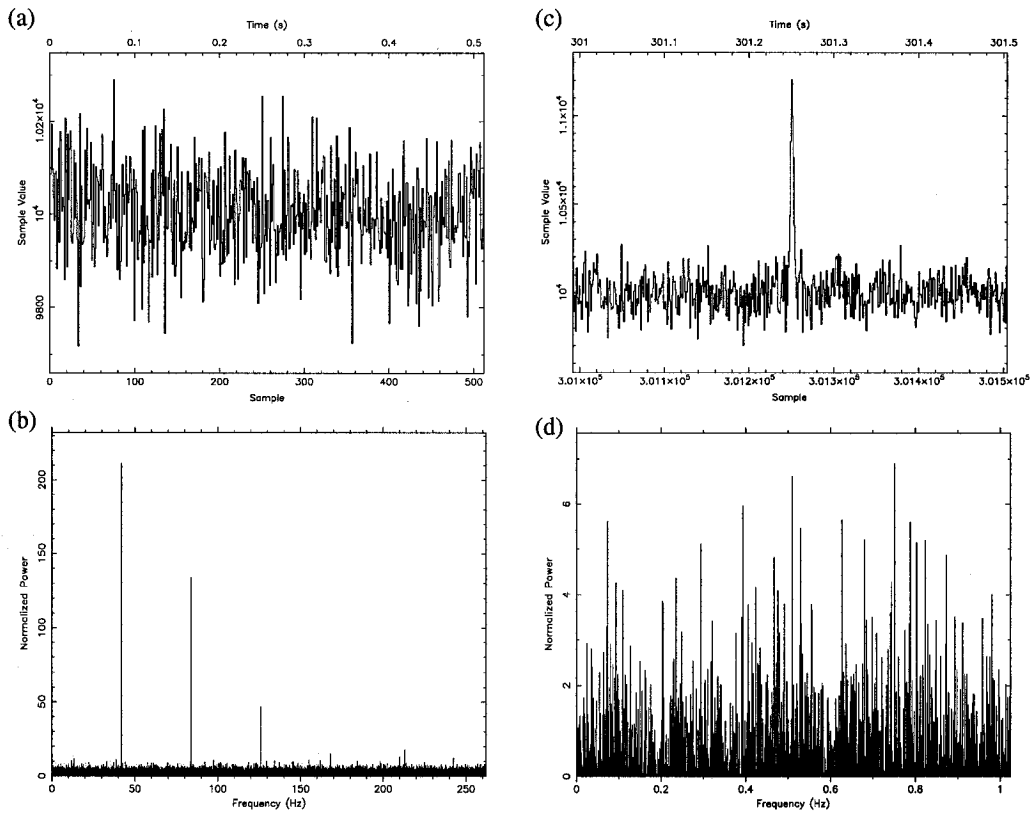

Figure 3.6: Two regimes of pulsar searches: 1) the individual pulses are persistent but are at too low a level to be seen in the time series 2) individual pulses can be very significant, but the emission is highly sporadic. (a): a 0.5-s segment of a simulated 1000-s time series containing persistent, low-level, 42-Hz gaussian pulses with a duty cycle of 15%. (b): the power spectrum of the (a) time series, clearly showing the 42-Hz signal and harmonics. (c): a 0.5-s segment of a different simulated 1000-s time series containing only a single strong pulse from a 5-s pulsar. The pulse is clearly visible above the noise. (d): the power spectrum of the (c) time series; no significant signal can be seen at the 0.2 Hz spin frequency of the pulsar, or at its harmonics.

cant peaks, which will have finite widths. To maintain sensitivity to a variety of pulse widths, the time series is smoothed to a variety of coarser binnings. The results from time series at different trial DMs can be stacked on top of each other to make the identification of dispersed pulses easier (Figure 3.7). Such plots, which contain other statistics on the ensemble of detected pulses, are important as many single pulse candidates will likely be RFI, which will peak at DM = 0 pc cm^{-3}.

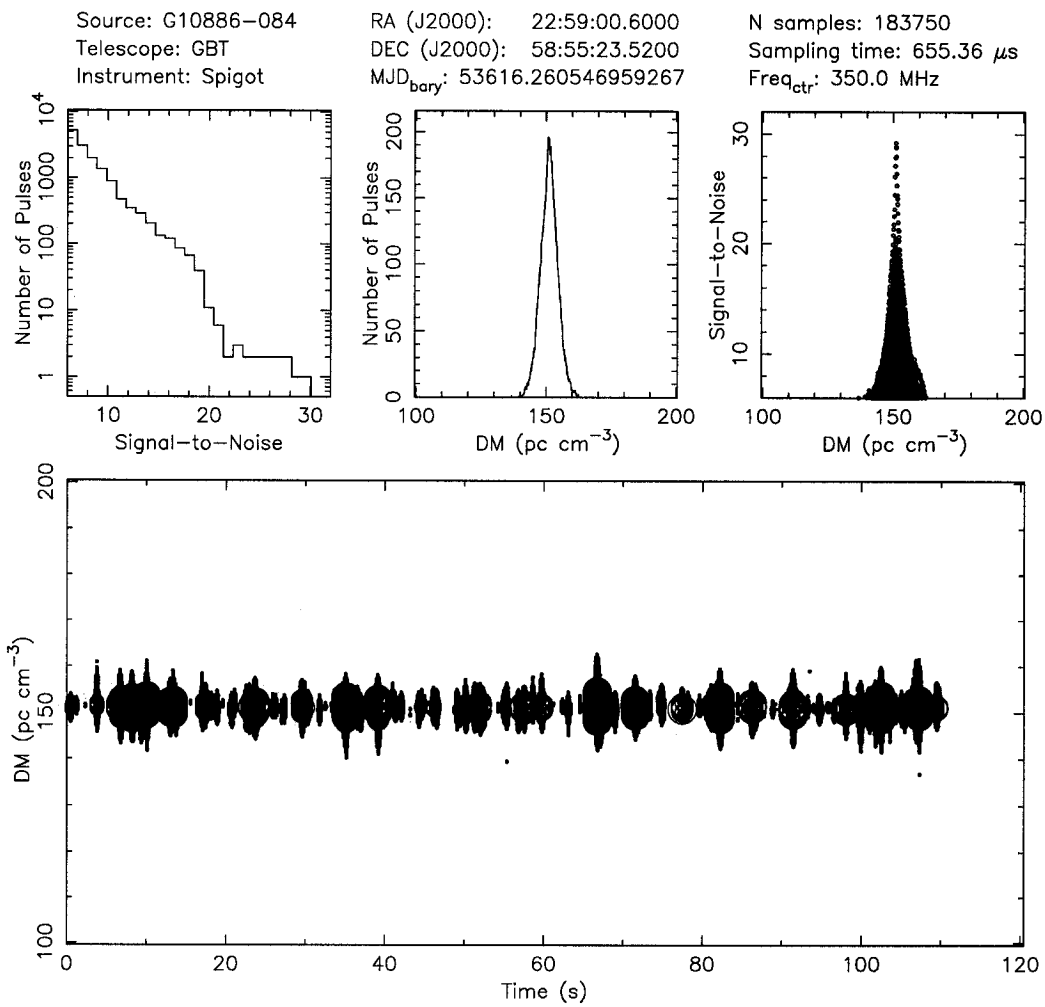

Figure 3.7: Single pulses from the 368-ms pulsar B2255+58 observed with the GBT at 350 MHz as part of the survey described in Chapter 8. The pulsar has a flux density at 400 MHz $S_{400} = 34$ mJy and is offset by 16′ with respect to the centre of the telescope beam, which has a half power radius of $\sim 18'$. *Top left:* number of pulses as a function of signal-to-noise. *Top centre:* number of pulses detected as a function of DM, showing a strong peak at DM ~ 151 pc cm^{-3}. *Top right:* pulse signal-to-noise as a function of DM, again showing a strong peak at DM ~ 151 pc cm^{-3}. *Bottom:* pulses are plotted as circles proportional in size to their signal-to-noise. The detected pulses are clustered in DM, and appear throughout the ~ 110-s observation. This pulsar was also easily detected by the Fourier-based search. For an example of a single pulse detection where far fewer pulses were detected, and no significant signal is present in the Fourier transform, see Figure 8.9.

Chapter 4

A 1.4-GHz Survey for Pulsars in Globular Clusters with Arecibo

Science has to be accountable to the tax payers. Not unlike my L-band globular cluster survey.
– From the movie "Contact".

The first set of searches we present in this thesis are deep searches for radio pulsations in globular clusters with the Arecibo telescope. Because they are faint and often in binary systems, these are some of the hardest pulsars to find. Nonetheless, this chapter presents the discovery of 11 millisecond pulsars, most of which were found using the acceleration search technique presented in Chapter 3.

The work presented in this chapter will be submitted for publication as: *Hessels, J. W. T., Ransom, S. M., Stairs, I. H., Kaspi, V. M., & Freire, P. C. C., A 1.4-GHz Survey for Pulsars in Globular Clusters with Arecibo, to be submitted to the Astrophysical Journal.*

4.1 Introduction

Currently, there are approximately 130 known pulsars in globular clusters (GCs)[1], of which about 60% are observed to be in binary systems[2]. Roughly two thirds of all the pulsars known in GCs have been discovered in only the last five years by surveys (e.g. Possenti et al., 2003; Ransom et al., 2005a; Hessels et al., 2006) using low-temperature receivers ($T_{\rm rec} \lesssim 35\,{\rm K}$) at central observing frequencies between $\nu_{\rm center} = 1{-}2\,{\rm GHz}$, large bandwidth and high time and frequency-resolution backends (e.g. the Wideband Arecibo Pulsar Processor, Dowd, Sisk, & Hagen 2000, and the Spigot, Kaplan et al. 2005), advanced search techniques for binaries (e.g. Ransom, Eikenberry, & Middleditch, 2002; Ransom, Cordes, & Eikenberry, 2003), and copious amounts of processing time on dedicated computer clusters. The 150 known GCs[3] orbiting the Milky Way contain roughly three orders of magnitude more observed millisecond pulsars (MSPs) per unit mass than the Galactic plane, which contains approximately 60 known MSPs. GCs have proven to be the most fruitful place to look for MSPs partly because of the enormous stellar densities in their cores, which exceed those in the Galactic plane by up to six orders of magnitude. These conditions promote many different formation processes that create binary systems in which a neutron star can be spun-up, or "recycled" (Alpar et al., 1982; Radhakrishnan & Srinivasan, 1982b), through the accretion of matter from its companion star (see Camilo & Rasio, 2005, and references therein, for a review of the formation and evolutionary processes at work in the cores of GCs). Furthermore, the cores of GCs, where most of the MSPs reside, typically have radii less than an arcminute, small enough to be covered by a single telescope

[1] A catalogue of GC pulsars is maintained by P. C. C. Freire at http://www.naic.edu/~pfreire/GCpsr.html.

[2] Note however that, because binary pulsars are more difficult to detect than isolated pulsars, the observed binary fraction is a lower limit on the intrinsic binary fraction of the population.

[3] An online catalogue of Milky Way GCs (Harris, 1996) is maintained at http://physun.physics.mcmaster.ca/Globular.html.

pointing. This affords the possibility of making single, deep multi-hour integrations for multiple faint MSPs in GCs, something that is not feasible in large area surveys of the field.

Some clusters contain many pulsars: Terzan 5 and 47 Tucanae harbor 33 and 22 known pulsars, respectively. Together, they contain $\sim 42\%$ of the total known GC pulsar population (Camilo et al., 2000; Ransom et al., 2005a; Hessels et al., 2006). Finding numerous pulsars in a single cluster allows interesting studies of the cluster itself, in addition to the individual pulsars contained therein. Such studies have included the detection of intra-cluster ionized gas (Freire et al., 2001), high mass-to-light ratios (D'Amico et al., 2002), and hints at the cluster's dynamical history (Possenti et al., 2003). However, many clusters still contain no known pulsars at all, despite sensitive searches. In some cases, this may simply be because MSPs are intrinsically weak objects and GCs are often distant (approximately 90% of the GCs orbiting the Milky Way are $> 5\,\mathrm{kpc}$ from the Sun). Interstellar scattering, which broadens pulsations because of multi-path propagation, can also be a major obstacle, particularly for clusters close to the Galactic plane. At low radio frequencies ($\lesssim 500\,\mathrm{MHz}$), scattering can completely wash out the signal of fast-spinning pulsars.

While GCs are clearly the most profitable targets for finding MSPs, these searches remain non-trivial. First, the requisite short sampling times ($< 100\,\mu\mathrm{s}$), high frequency resolution ($< 0.5\,\mathrm{MHz}$ channels), long integrations (few hours), and large bandwidth ($> 100\,\mathrm{MHz}$) of these data can make data acquisition and storage formidable (data rates $\sim 30{-}100\,\mathrm{GB/hr}$). Recent surveys with relatively good sensitivity to binary pulsars have revealed that the majority of GC MSPs are in binaries. The pulsed signal from these binary pulsars is smeared in Fourier space by their orbital motion, and thus even a bright pulsar can go undetected if nothing is done to correct for this modulation over the course of a long observation. Advanced and computationally intensive techniques, which partially search orbital parameter space, are required to recover the majority of the lost signal. The extra effort required to find binaries is

well justified however, as some of the most exotic pulsar binaries known have been found in GCs. For instance, PSR B1620−26 in the cluster M4 is in a hierarchical triple system with a white dwarf and a $1-3\,M_{Jup}$ planet, the only planet known in a GC (Thorsett et al., 1999; Sigurdsson & Thorsett, 2005); PSR J0514−4002 in NGC 1851, with an eccentricity of 0.89, is one of the most eccentric binary pulsars known (Freire et al., 2004); PSR B2127+11C in M15 is a rare double neutron star binary (Anderson et al., 1990); PSR J1748−2446ad in Terzan 5 is the fastest-spinning neutron star known (Hessels et al., 2006); and a few pulsars with possible main-sequence companions have been found (e.g. PSR J1740−5340, D'Amico et al., 2001b, similar systems have not been found in the Galactic plane). Other exotic binaries, perhaps even an MSP-MSP binary or a MSP-black-hole binary, may have effective formation channels only in GCs (but see Sipior, Portegies Zwart, & Nelemans, 2004).

Here we present searches for radio pulsations from 22 GCs, using Arecibo at central observing frequencies between 1.1−1.6 GHz. Roughly half of these clusters have been searched previously with Arecibo at 430 MHz (Anderson, 1993; Wolszczan et al., 1989a,b). The highly successful Anderson (1993) survey found 11 of the 14 pulsars known in these clusters prior to the survey presented here. Our searches have uncovered 11 new MSPs and 2 promising candidates in five clusters: M3, M5, M13, M71, and NGC 6749. Acceleration searches were crucial in finding all but 2 of these systems. 10 of the new pulsars are in binaries, 3 of which are eclipsing, with orbital periods of only a few hours. 9 of the 11 new pulsars have $P_{\rm spin} < 4$ ms. Only 2 of the 14 previously known pulsars in these clusters have $P_{\rm spin} < 4$ ms, clearly demonstrating the improved sensitivity of this survey over past surveys to the fastest MSPs. In §4.2 we describe the sources, observational setup, and sensitivity of the survey. In §4.3 we outline the search procedure and analysis pipeline. In §4.4 we present the results of the survey. Finally, in the discussion of §4.5, we comment on the characteristics of the GC pulsar population in general, particularly its luminosity distribution.

4.2 Observations

4.2.1 Sources

We observed every known Galactic GC visible from Arecibo[4] and within 70 kpc of the Sun without any selection bias towards larger or denser clusters. The sample of 22 GCs is listed in Table 4.1, along with basic and derived cluster parameters (Harris, 1996, unless otherwise indicated, all GC quantities used in this paper are from the 2003 February revision of the catalogue). The numbers of known isolated and binary pulsars in each cluster are indicated, with figures in parentheses denoting the number of pulsars found by this survey. For clusters containing known pulsars, the average dispersion measure (DM) of the pulsars is indicated, as well as their spread in DM, which is in parentheses (for clusters where two or more pulsars have been found). For clusters with no known pulsar, the DM is also unknown; the value listed (in italics) is derived from the Cordes & Lazio (2002a) "NE2001" model for the distribution of free electrons in the Galaxy, using the Harris (1996) position and distance to the cluster.

4.2.2 Data Acquisition

Each cluster was observed at least twice for the full time it is visible with Arecibo (Table 4.1). The clusters were observed in one of two campaigns in the summers of 2001 and 2002 using the Gregorian L-band Wide receiver[5] ($T_{\rm rec} \sim 35\,{\rm K}$). Depending on the known or predicted DM of the cluster, the central observing frequency was either 1175 MHz (DM $\lesssim 100\,{\rm pc\ cm^{-3}}$) or 1475 MHz (DM $\gtrsim 100\,{\rm pc\ cm^{-3}}$). Our observations were made using the Wideband Arecibo Pulsar Processor (WAPP, see Dowd et al., 2000, for details), a digital auto-correlator with configurable sampling time (3 or 9-level samples) and number of lags. Generally, 3-level samples were autocorrelated

[4]The declination range visible from Arecibo is approximately $-1°$ to $+38°$.
[5]This is not the L-band Wide receiver currently available at Arecibo.

Catalogue ID	Other Name	Distance (kpc)	ρ_o[a] (log $M_\odot$/kpc^3)	Concentration[b] (log r_c/r_t)	DM(ΔDM)[c] (pc cm^{-3})	Time Visible[d] (hrs)	Isolated[e] Pulsars	Binary[e] Pulsars	Lum. Limit (mJy kpc^2)
NGC 4147*	...	19	3.48	1.80	*24*	2.8	...	...	6.8
NGC 5024*	M53	18	3.05	1.78	24	2.8	...	1	6.1
NGC 5053	...	16	0.53	0.84	*25*	2.7	...	...	5.0
NGC 5272*	M3	10	3.51	1.84	26.4(0.2)	2.5	...	4(4)	2.1
NGC 5466	...	17	0.88	1.32	*22*	2.4	...	...	5.7
NGC 5904	M5	7.5	3.91	1.83	29.5(0.8)	1.5	1	4(3)	1.4
NGC 6205*	M13	7.7	3.33	1.51	30.2(1.1)	1.2	2(1)	3(2)	1.7
NGC 6426*	...	20	2.35	1.70	*121*	1.7	...	...	11
NGC 6535*	...	6.7	2.69	1.30	*170*	0.8	...	...	1.9
NGC 6749	Be42	7.9	3.33	0.83	193(2)	1.5	...	2(2)	2.0
NGC 6760*	...	7.4	3.84	1.59	200(6)	1.3	...	1	2.0
NGC 6779	M56	10	3.26	1.37	*163*	2.3	...	...	2.5
NGC 6838	M71	4.0	3.04	1.15	117	2.8	...	1(1)	0.3
NGC 6934*	...	17	3.43	1.53	*83*	2.2	...	...	6.6
NGC 7006*	...	42	2.46	1.42	*74*	2.7	...	...	34
NGC 7078*	M15	10	5.38	2.50	66.9(2.2)	2.6	7	1	2.1
NGC 7089	M2	12	3.90	1.80	*46*	0.6	...	...	5.3
Pal 2	...	28	3.76	1.45	*136*	2.3	...	...	18
Pal 5	...	23	-0.81	0.70	*34*	0.9	...	...	17
Pal 10	...	5.9	3.50	0.58	*166*	2.8	...	...	0.8
Pal 13	...	27	0.40	0.68	*38*	2.6	...	...	14
Pal 15	...	45	-0.27	0.60	*77*	0.7	...	...	76

Table 4.1: Survey Source List

[a] Central density of the cluster.
[b] Ratio of the core radius to the tidal radius of the cluster.
[c] Italicized DMs are predicted values based on the Cordes & Lazio (2002b) electron density model of the Galaxy. There is no formal uncertainty on these values, although the predicted DM can sometimes differ from the true value by a factor of two or more.
[d] Time visible with the Arecibo telescope, which can only track sources while they are within 20° of the zenith.
[e] Values in parentheses indicate the number of pulsars in the cluster that were found in this survey.
Note - Clusters marked with an asterisk (*) were also searched by Anderson (1993) with Arecibo at 430 MHz. Anderson (1993) also searched NGC 6218 (M12, no pulsars found), which is not visible using the Arecibo Gregorian dome. All previously known pulsars were found by Anderson (1993), with the exceptions of PSR J1911+0101B (Freire et al., 2005, in NGC 6760), PSRs B1516+02A and B (Wolszczan et al., 1989a, in M5), and PSR B2127+11A (Wolszczan et al., 1989b, in M15).

with 256 lags, accumulated every 64-μs, and summed in polarization before being written to the WAPP disk array as 16-bit numbers. For the few clusters with known or predicted DMs greater than 100 pc cm^{-3}, we used 128-μs sampling and 512 lags, to reduce DM smearing. This configuration was chosen in order to minimize dispersive pulse smearing and take full advantage of the WAPP's maximum sustainable data rate (16 MB/s, or $\sim$ 30 GB/hr). Data were transferred to DLT magnetic tape for offline analysis and archiving. These observations resulted in about 4 TB of data on about 100 tapes.

At the time of our original cluster search observations, only one WAPP backend was available, providing 100 MHz of bandwidth. In more recent observations of M3, M5, M13, M71, and NGC 6749 (after December 2002), which were made as part of the timing observations of the new discoveries, we used three of the four available WAPP backends, each with 100 MHz of bandwidth centered at 1170, 1420 and 1520 MHz. The frequency gap between the lower and upper bands was to avoid persistent and intense radio frequency interference (RFI) in the frequency ranges 1220–1360 MHz and $>$ 1570 MHz. Using the PRESTO[6] pulsar software suite, these data were partially dedispersed into a reduced number of subbands (generally 16 or 32 subbands) at the average DM of the cluster pulsars before further timing or search analysis. This process affords an order-of-magnitude reduction in data size (enabling transfer of these data over the internet from Puerto Rico to Canada), while still providing the possibility of creating dedispersed time series at a variety of DMs around the average DM of the cluster.

4.2.3 Search Sensitivity

We can estimate the typical minimum flux density to which our searches were sensitive, as a function of the radiometer noise and observed pulsar duty cycle,

[6]See http://www.cv.nrao.edu/~sransom/presto.

using the equation

$$S_{\rm min} = \frac{\sigma \xi T_{\rm sys}}{G\sqrt{n\Delta\nu T_{\rm obs}}} \left(\frac{w_{\rm obs}}{P_{\rm spin} - w_{\rm obs}} \right)^{1/2} \quad (4.1)$$

(following Dewey et al., 1985). The minimum signal-to-noise ratio (S/N) of a search candidate is indicated by σ, and is taken to be 10 here (although when candidate lists were short, due to a lack of RFI, we investigated candidates below this threshold). ξ is a factor that incorporates both losses due to the 3-level quantization of the signal and other systemic effects. Zero lag and van Vleck corrections (see Lorimer & Kramer, 2004, and references therein) have been applied to our data. We use a value $\xi = 1.2$ to quantify the loss in sensitivity compared with infinite quantization. $T_{\rm sys}$ is the equivalent temperature of the observing system and sky (approximately 40 K toward our sources, which are predominantly at high Galactic latitudes). G is the telescope gain, which is a function of zenith angle, and is taken to have an average value of 10.5 K/Jy. For clusters that are only visible at zenith angles $\gtrsim 16°$, the gain (and hence the sensitivity) is reduced by 5−15%. This is the case for the clusters which are closest to the declination limit of the Arecibo-visible sky: M2, M5, M13, Pal5, Pal15, NGC6535, NGC6749, and NGC6760. n is the number of orthogonal polarizations that have been summed ($n = 2$ here). $\Delta\nu$ is the bandwidth of the backend, taken to be 100 MHz here. For clusters where subsequent timing observations were also performed (M3, M5, M13, M71, and NGC 6749), we were able to search a larger bandwidth by combining multiple WAPPs. $T_{\rm obs}$ is the integration time, which varies between clusters from 0.5−2.75 hr depending on the declination of the source, but is set to 2 hr for the purposes of these sensitivity calculations. $w_{\rm obs}$ is the observed pulse width, which is a function of the intrinsic pulse width $w_{\rm int}$ and other effects that smear the observed pulse profile (Equation 4.2). $P_{\rm spin}$ is the pulsar spin period.

When the DM of a cluster is not known, one must construct 100s of trial time series at a wide range of DMs, each of which must be searched. Even for

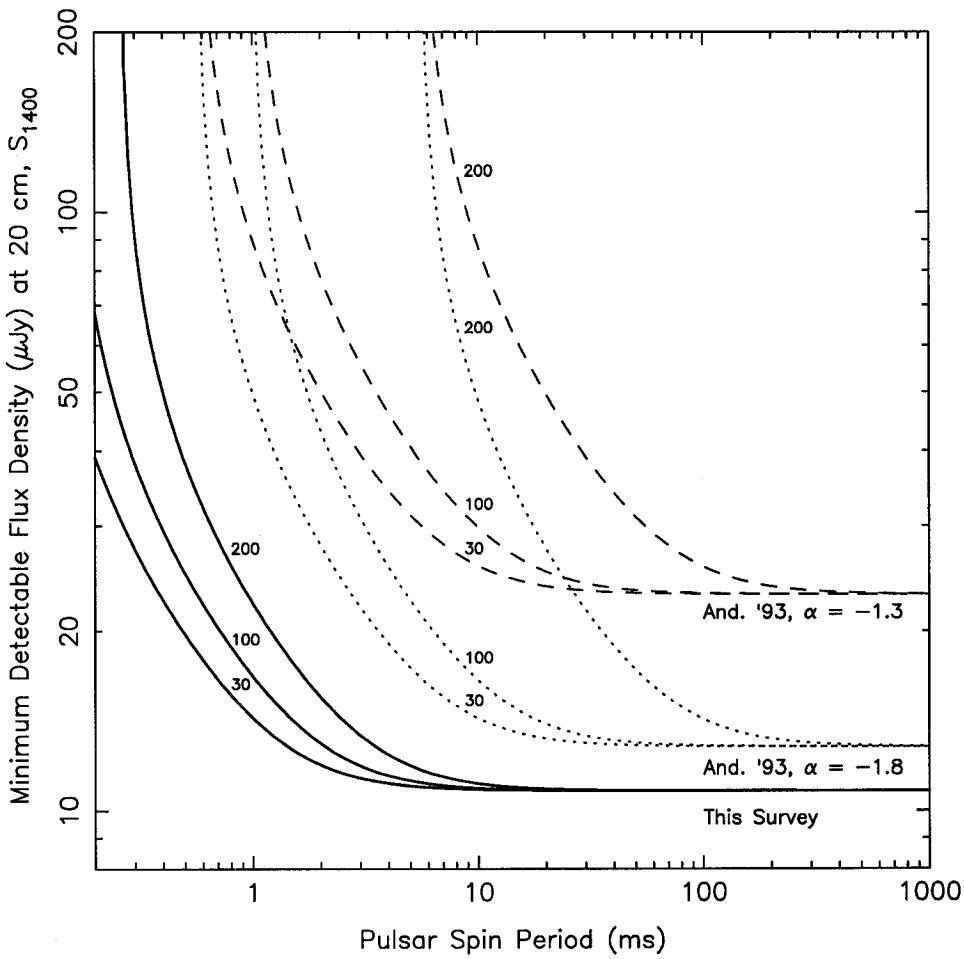

Figure 4.1: Survey sensitivity as a function of period and DM, assuming an intrinsic pulse width of 8% and an integration time of 2 hr. Each set of curves shows (from left to right) the sensitivity for DMs of 30, 100, and 200 pc cm^{-3}. The solid curve is the sensitivity of the survey described in this paper. The dotted (dashed) curve is the sensitivity of the 430 MHz survey of Anderson (1993) scaled to 1400 MHz assuming a spectral index of −1.8 (−1.3). For low-DM pulsars with periods $\gtrsim$ 10 ms and steep spectral indices, the Anderson (1993) survey has comparable sensitivity. However, the survey presented here is significantly more sensitive to pulsars with periods $\lesssim$ 4 ms, high DMs, and/or relatively flat spectral indices.

clusters with known DMs, the pulsars have a spread in DM, ΔDM, and several trial DMs must be searched in order to maintain maximum sensitivity. ΔDM increases roughly linearly with DM, and typically ΔDM/DM is a few percent (Freire et al., 2005).

The observed pulse width, $w_{\rm obs}$ in Equation 4.1, is always equal to or larger than the pulsar's intrinsic pulse width $w_{\rm int}$. Broadening is due to the finite time sampling of the data recorder, $t_{\rm samp}$, dispersive smearing across individual frequency channels, $t_{\rm DM}$, the deviation of a pulsar's true DM from the nominal DM of the time series used for searching or folding, $t_{\Delta\rm DM}$, and interstellar scattering, $t_{\rm scatt}$. One can express the observed width as the sum in quadrature of these terms:

$$w_{\rm obs}{}^2 = w_{\rm int}{}^2 + t_{\rm samp}{}^2 + t_{\rm DM}{}^2 + t_{\Delta\rm DM}{}^2 + t_{\rm scatt}{}^2, \tag{4.2}$$

where the dispersive smearing (assuming the channel bandwidth $\Delta\nu_{\rm chan} \ll \nu_{\rm center}$) across an individual channel is given by

$$t_{\rm DM} = 8.3 \left(\frac{\rm DM}{\rm pc\ cm^{-3}}\right) \left(\frac{\Delta\nu_{\rm chan}}{\rm MHz}\right) \left(\frac{\nu_{\rm center}}{\rm GHz}\right)^{-3} \mu{\rm s}, \tag{4.3}$$

the smearing due to an incorrect DM in the time series is

$$t_{\Delta\rm DM} = 4.1 \left[\left(\frac{\nu_{\rm low}}{\rm GHz}\right)^{-2} - \left(\frac{\nu_{\rm high}}{\rm GHz}\right)^{-2}\right] \left(\frac{\Delta\rm DM}{\rm pc\ cm^{-3}}\right) {\rm ms}, \tag{4.4}$$

(where $\nu_{\rm low}$ and $\nu_{\rm high}$ are the low and high frequency edges of the bandwidth respectively), and the scattering can be estimated by the empirical formula (Cordes & Lazio, 2003)

$$\log_{10}(t_{\rm scatt}) = -3.59 + 0.129 \log_{10}({\rm DM}) + 1.02 \left(\log_{10}({\rm DM})\right)^{2.0} - 4.4 \log_{10}\left(\frac{\nu_{\rm center}}{\rm GHz}\right) \mu{\rm s}. \tag{4.5}$$

For these data at 1.4 GHz, $t_{\rm DM} = 30{-}120\,\mu$s for DMs 25–200 pc cm^{-3} (using $\Delta\nu_{\rm chan} = 100/256$ MHz for DM < 100 pc cm^{-3} and $\Delta\nu_{\rm chan} = 100/512$ MHz

for DM $> 100\,\mathrm{pc\ cm^{-3}}$). In searches where the cluster DM was not known, we created dedispersed time series with DMs spaced by $1.0\,\mathrm{pc\ cm^{-3}}$. For clusters with known DMs, we typically used a spacing of $0.5\,\mathrm{pc\ cm^{-3}}$ or finer. Hence, the maximum DM deviation between a pulsar's true DM and that assumed in making the trial time series is $0.5\,\mathrm{pc\ cm^{-3}}$, resulting in a maximum smearing $t_{\Delta\mathrm{DM}} = 150\,\mu\mathrm{s}$. We have estimated t_{scatt} using Equation 4.5 (Cordes & Lazio, 2003), which predicts the scattering time based on the known (or predicted) DM and the observing frequency. t_{scatt} varies from source to source, but given the relatively high observing frequency of these data and the high Galactic latitudes of most of the sources observed here (most of which have relatively low known or predicted DMs), it does not significantly increase the smearing already present in the data.

Figure 4.1 shows the search sensitivity determined from Equations 1–5 as a function of DM and period.[7] We compare the sensitivity of our survey with that of the only other major survey of these clusters with Arecibo (Anderson, 1993). As the Anderson (1993) survey was conducted at 430 MHz, we use a typical pulsar spectral index of -1.8 (Maron et al., 2000b) as well as a flatter spectral index of -1.3 to scale that survey to 1400 MHz, so that the sensitivities of both surveys can be more directly compared. For low-DM pulsars with spin periods $\gtrsim 10\,\mathrm{ms}$ and a standard spectral index ($\alpha = -1.8$), the Anderson (1993) survey had a similar sensitivity to ours. However, for pulsars spinning faster than this, especially those at high DMs and with relatively flat spectral indices, our survey provides a significant increase in sensitivity. For example, we were roughly 3–6 times more sensitive to a 2-ms pulsar at a DM of $100\,\mathrm{pc\ cm^{-3}}$, assuming $-1.8 < \alpha < -1.3$.

[7]The degradation in sensitivity to binary pulsars caused by their orbital motion is *not* included in these estimates. We discuss our sensitivity to binary pulsars in §4.5.1.

4.3 Analysis

4.3.1 Radio Frequency Interference Excision

Periodicities due to terrestrial radio frequency interference (RFI) can swamp search candidate lists. Ultimately this reduces a survey's sensitivity by increasing the number of false positives. First, strong bursts of interference, principally from airport and military radars, were removed in the time domain by clipping samples found to be further than $6\,\sigma$ from the mean in the DM = 0 pc cm^{-3} time series. Secondly, we created time-frequency masks and applied them to all data before searching. These masks remove certain channels during specific time intervals when either the maximum Fourier power, standard deviation, or mean of the data surpass statistically determined thresholds. This method was very useful at excising strong narrow-band and transient RFI from the data before searching and typically only $\lesssim$ 10% of the data were masked. Lastly, we removed known "birdies" (weak but highly periodic broadband interference and bright known pulsars) from the power spectrum by setting the powers in these narrow frequency intervals to zero. We found that using these techniques and observing in the relatively RFI-clean frequency ranges of 1120−1220 MHz and 1370−1570 MHz kept the size of our candidate lists manageable, while minimizing the risk of rejecting potentially interesting candidates.

4.3.2 Search Techniques

In a standard Fourier-based search, which identifies pulsar harmonics above a certain threshold, binary pulsars are strongly selected against because of orbital modulation, which smears the signal power over many bins in frequency space. As the majority of MSPs in GCs are in binary systems, sometimes with orbital periods comparable to or shorter than the observation length, it is crucial to use more sophisticated techniques.

Our primary search method is a Fourier-based matched filtering technique (Ransom et al., 2002) which assumes that the pulsar's orbit can be described by a constant acceleration (i.e. constant frequency derivative) over the course of the observation. This technique is a frequency-domain version of a previously used constant acceleration technique (Middleditch & Kristian, 1984; Anderson et al., 1990; Camilo et al., 2000) in which the time series is stretched or compressed before it is Fourier transformed, in order to simulate different accelerations. The advantage of the Fourier-based technique used here is that it is computationally more efficient than the equivalent time-domain-based method, and provides even sampling of frequency derivative space. This method is typically sensitive to binaries where the orbital period is $\gtrsim 10\times$ the integration time of the observation, although very bright pulsars with orbital periods much shorter than this can often be detected (Johnston & Kulkarni, 1991). As our Arecibo observations were typically from 1–2.5 hr in length, for full tracks this search method is most sensitive to orbital periods $\gtrsim$ 10–25 hr. Using the same technique, we also searched overlapping subsections of the data sets (which were typically about one third the total observation length), in order to be sensitive to larger accelerations and tighter binaries ($P_{\rm orb} \gtrsim 3$–10 hr), as well as eclipsing systems.

To search for binaries with orbital periods a factor of ~ 2 or more shorter than the observation time, we used the "phase modulation" search of Ransom et al. (2003). This method makes use of the change in phase of the pulsations from a binary pulsar and the "comb" pattern created by such a signal in the Fourier power spectrum. By taking Fast Fourier Transforms (FFTs) of short subsections of the power spectrum from the full observation, one can detect the sidebands, which are evenly spaced at the orbital period and centered on the true frequency of the pulsar. This method is appropriate for binary pulsars with orbital periods less than half the observation length, and increases in sensitivity as the ratio $T_{\rm obs}/P_{\rm orb}$ increases. Given the 1–2.5 hr integration times used in this survey, this technique was sensitive to an area of orbital

parameter space in which no binary radio MSPs have yet been observed.

4.3.3 Data Pipeline

Here we summarize the data analysis pipeline applied to the observations of each cluster. The routines used in the pipeline are part of the PRESTO pulsar search and analysis package. First, we generated an RFI mask from the raw data (as described in §4.3.1). Applying this mask, a DM = 0 pc cm^{-3}, topocentric time series was created and the corresponding power spectrum was examined by eye for periodic interference. We added the worst of the interference to a "birdie list" of frequency intervals to be subsequently removed from the Fourier transform. Again applying the RFI mask, we then dedispersed the data at a number of trial DMs using DM steps ≤ 1 pc cm^{-3}, clipping samples found to be greater than 6σ from the mean in the DM = 0 pc cm^{-3} time series. The time series were transformed to the solar-system barycenter during dedispersion, which allowed us to compare directly candidate periods from separate observations. This was very useful for distinguishing likely pulsar periodicities from the RFI background, which can vary greatly between observations. For clusters with known pulsars, we dedispersed at a range of trial DMs equal to at least 10% of the cluster's average DM. For clusters with no known pulsars, we created time series at a range of DMs centered around the predicted DM of the cluster (Cordes & Lazio, 2002a), given its Galactic coordinates and distance in the Harris (1996) catalogue. We assumed a 100% error in the predicted DM value when choosing a DM search range. For example, for a cluster with a predicted DM of 100 pc cm^{-3}, we searched the time series from DM = 0–200 pc cm^{-3}. The dedispersion and subsequent analysis of the time series was conducted in parallel using multiple processors on a 52-node dual-processor Linux cluster called "The Borg", located at McGill University and constructed by our group specifically for pulsar searches. Once the dedispersion was complete, the time series were Fourier-transformed. Our analysis did not restrict the number of samples in the time series to be a power of

two[8]. We then set the frequency intervals of the birdie list to zero in the power spectra before searching the power spectra with both the phase-modulation and matched-filtering techniques described in §4.3.2.

As most pulsars have relatively short duty cycles, with spectral power divided between numerous harmonics, we summed harmonics in our match-filter search to increase sensitivity to such signals. For each candidate signal, sums of 1, 2, 4, and 8 harmonics were tried and the optimum combination was determined. In these searches, we looked for signals where the highest of the harmonics used in summing drifted by up to $z_{\rm max} = 170$ bins in the Fourier domain. Higher order harmonics will drift by $N_{\rm harm}$ times more bins than the fundamental, where $N_{\rm harm} = 1$ for the fundamental, $N_{\rm harm} = 2$ for the second harmonic, etc.. If, for example, 8 harmonics were summed in the identification of a particular candidate period, then the maximum number of bins the fundamental could drift by during the observation and still be detectable by our search would be 170/8. Conversely, for signals where the fundamental drifted by more than 170/2 bins during the observation, we were sensitive to at most one harmonic. The maximum number of bins a signal is allowed to drift corresponds to a maximum line-of-sight acceleration of $a_{\rm max} = z_{\rm max} c P_{\rm spin}/T_{\rm obs}^2/N_{\rm harm} \simeq 4 P_{\rm spin,ms}/T_{\rm obs,h}^2/N_{\rm harm}\,{\rm m\ s^{-2}}$, where $P_{\rm spin,ms}$ and $T_{\rm obs,h}^2$ are the spin period in milliseconds and the observation time in hours and $N_{\rm harm}$ is the highest order harmonic used in summing. Overlapping subsections of the observation, corresponding to about a third of the total observation length, were also searched using the matched-filtering technique and $z_{\rm max} = 170$ bins, in order to look for more highly accelerated pulsars.

The resulting candidate lists from the matched-filtering search were generally short enough that they could easily be examined by eye, although we also parsed candidate lists with a script that automatically folded candidates above an equivalent gaussian significance threshold of 7. Interesting candidates were

[8]Some minimal padding was added to the data-sets however, so that the number of samples could be factored into primes where the maximum factor size was ≤ 13.

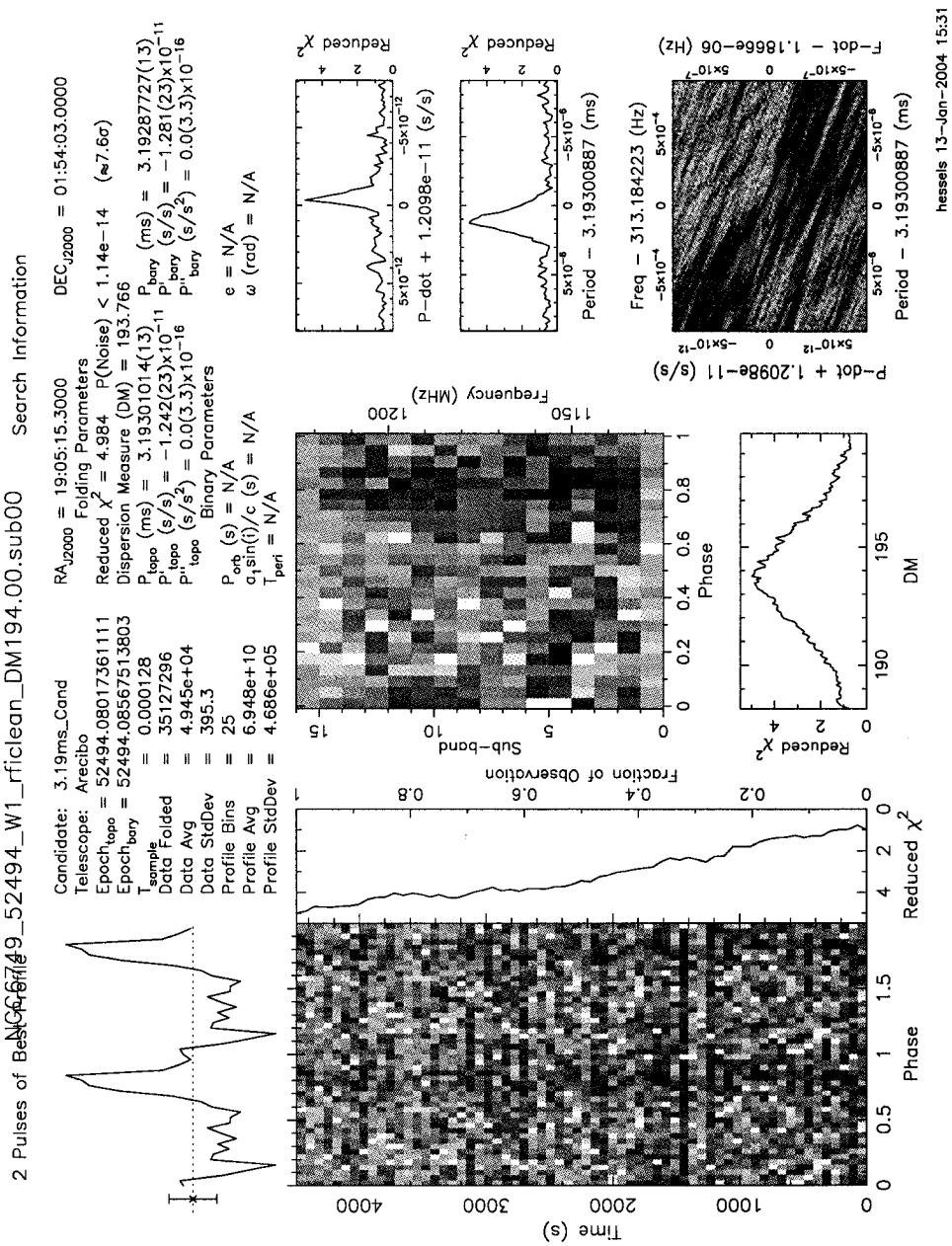

Figure 4.2: Sample candidate plot showing the various criteria on which a candidate is judged, including the signal strength as a function of observing time, DM, observing frequency, and period. This is the discovery observation of NGC 6749A. The subbands show effects due to the masking of some of their constituent channels to remove RFI.

folded using the estimated DM, period, and period derivative from the search and these parameters were optimized by the folding software to maximize the S/N ratio of the folded profile. The output plot from such a fold was used to determine whether a given candidate warranted further attention (see sample discovery plot and description in Figure 4.2). To identify potentially interesting candidates from the phase-modulation searches, we compared the search outputs from the different observing epochs of each cluster. The criteria for a promising phase-modulation candidate was a signal with a significance $> 10\sigma$ that did not peak in significance at DM $= 0\,\mathrm{pc\ cm^{-3}}$, had an orbital period $> 600\,\mathrm{s}$, and appeared, by virtue of a similar orbital period, in the candidate lists of at least two observing epochs.

4.4 Results

4.4.1 Redetections

Table 4.2 lists the 15 previously known pulsars in our survey clusters. The majority of these pulsars was easily detected by our search pipeline (Table 4.2). In fact, because many of these sources are relatively bright, masking these periodicities and their many significant harmonics was an important factor in reducing the length of candidate lists. The only previously known pulsars not detected in our searches are M15F, G, and H.[9] Although these are all isolated pulsars, and are well within the half-power radius of the 1.4-GHz Arecibo main beam, our non-detections are not very surprising: these are the dimmest pulsars in M15, and were all found in coherent searches of multiple observing epochs. Assuming standard spectral indices, they have flux densities right at the limit of our search sensitivity.

[9]Note however that M15F was easily detected in complementary searches we made using the WAPP at 327 MHz (see §4.2.2.).

Name	Period (ms)	Isolated (I) or Binary (B)	Redetected?
M5A / PSR B1516+02A	5.554	I	Y
M5B / PSR B1516+02B	7.947	B	Y
M13A / PSR B1639+36A	10.38	I	Y
M13B / PSR B1639+36B	3.528	B	Y
M15A / PSR B2127+11A	110.7	I	Y
M15B / PSR B2127+11B	56.13	I	Y
M15C / PSR B2127+11C	30.53	B	Y
M15D / PSR B2127+11D	4.803	I	Y
M15E / PSR B2127+11E	4.651	I	Y
M15F / PSR B2127+11F	4.027	I	N[a]
M15G / PSR B2127+11G	37.66	I	N
M15H / PSR B2127+11H	6.743	I	N
M53A / B1310+18	33.16	B	Y
NGC6760A / PSR B1908+00	3.619	B	Y
NGC6760B / PSR J1911+0101B	5.384	I	Y

Table 4.2: Previously Known Pulsars

[a]Detected in 327-MHz WAPP data, see §4.2.2..

4.4.2 New MSPs

We have discovered 11 MSPs and two promising candidates in five clusters. Three of the clusters with new pulsars (M3, M71, and NGC 6749) contained no known pulsars prior to our survey. All of the pulsars discovered in this survey were found using the matched-filtering acceleration search technique, and all but the newly-found isolated pulsar M13C (PSR J1641+3627C) and the long-orbital-period binary M3D (PSR J1342+2822D) required a non-zero trial frequency derivative in order to be detectable. Given the criteria outlined in §4.3.3, no interesting candidates were identified by the phase-modulation search. The spin periods of the new pulsars have a narrow range 2.4–5.4 ms. For comparison, the previously known pulsars in these clusters have spin periods in the range 3.5–110 ms, with only 2 pulsars having $P_{\rm spin} < 4$ ms. All but one of the new pulsars is in a binary system, with orbital periods ranging from $\sim$ 2 hr up to $\gtrsim$ 50 days. 3 of the new pulsars show eclipses. The basic characteristics of these pulsars are summarized in Table 4.3. Integrated pulse profiles, which are often the sum of numerous observations, are shown in Figure 7.4.

We have conducted monthly timing observations of these discoveries over the course of approximately two years using Arecibo and multiple WAPP backends. In fact, M3C (PSR J1342+2822C), M5E (PSR J1518+0204E), and M13E (PSR J1641+3627E) were all discovered in searches of timing data because of fortuitous scintillation. The timing results for the M5 and M71 pulsars will be presented by Stairs et al. (2007, in preparation) and the timing of the M13 pulsars will be presented by Ransom et al. (2007, in preparation).

M3 (NGC 5272)

We have found the first three, and likely four, pulsars known in M3. All of these pulsars were detected in observations in which interstellar scintillation increased their flux to a detectable level and are not reliably detectable

Name[a]	Period (ms)	DM (pc cm^{-3})	$P_{\rm orbit}$ (hr)	$a_1 \sin(i)/c$ (lt-s)	Min M_2[b] ($M_\odot$)	w_{50}[c] (%)	Flux Density[d] (mJy)
M3A / PSR J1342+2822A	2.545	26.5	Unk.	Unk.	Unk.	9.3	7
M3B / PSR J1342+2822B	2.389	26.2	34.0	1.88	0.21	8.2	14
M3C[e] / PSR J1342+2822C	2.166	26.5	Unk.	Unk.	Unk.	11	$\lesssim 6$
M3D / PSR J1342+2822D	5.443	26.3	129 d	38.4	0.21	9.2	10
M5A[f] */ PSR B1516+02A*	5.554	30.1	...	...	...	6.7	120
M5B / PSR B1516+02B	7.947	29.5	165	3.05	0.13	20	25
M5C[g] / PSR J1518+0204C	2.484	29.3	2.08	0.0573	0.038	6.2	39
M5D / PSR J1518+0204D	2.988	29.3	29.3	1.60	0.20	18	8
M5E / PSR J1518+0204E	3.182	29.3	26.3	1.15	0.15	7.9	10
M13A[f] */ PSR B1639+36A*	10.38	30.4	...	...	...	11	140
M13B / PSR B1639+36B	3.528	29.5	30.2	1.39	0.16	13	22
M13C[f] / PSR J1641+3627C	3.722	30.1	...	...	...	5.5	30
M13D / PSR J1641+3627D	3.118	30.6	14.2	0.924	0.18	6.6	24
M13E[g] / PSR J1641+3627E	2.487	30.3	2.8 ± 0.2	0.037 ± 0.004	0.02	6.0	10
M71A[g] / PSR J1954+1847A	4.888	117	4.24	0.0782	0.032	10	59
NGC6749A / PSR J1905+0154A	3.193	194	19.5	0.588	0.090	16	23
NGC6749B[e] / PSR J1905+0154B	4.968	192	Unk.	Unk.	Unk.	7.8	$\lesssim 6$

Table 4.3: New Pulsars and Their Basic Parameters

Note - Unless otherwise indicated, errors on quantities are well below the level of the least significant figure quoted.
[a]Italicized names are previously known pulsars.
[b]Assuming a pulsar mass (M_1) of $1.4\,M_\odot$ and orbital inclination $i = 90°$.
[c]For profiles with multiple components, the width of the highest peak is given. As all the profiles suffer from residual dispersive smearing, these values represent upper limits on the intrinsic pulse width at this observing frequency.
[d]Flux density at 1400 MHz. The approximate uncertainty is 30%.
[e]Unconfirmed candidate pulsar.
[f]Isolated.
[g]Eclipses.

with Arecibo. Their average DM is 26.3 pc cm^{-3}, which compares very well with the 23 pc cm^{-3} DM predicted by the NE2001 model (Cordes & Lazio, 2002a). There is little doubt that these pulsars are members of M3. M3A (PSR J1342+2822A) is a 2.54-ms binary which has only been detected three times, on MJDs 52491, 52492 and 52770. Due to this paucity of detections, we do not currently know the orbital parameters for this pulsar, although its orbital period is likely on the order of a day. M3B (PSR J1342+2822B) is a 2.39-ms binary in a 34.0-hr orbit with a 0.2 $M_\odot$ (minimum mass) companion, which, in analogy to other systems with similar orbital parameters, may be a low-mass helium white dwarf. It is the most consistently detectable pulsar in M3, and is visible at least faintly in roughly half of our observations. On some occasions M3B has shown very large increases in flux (up to a flux density at 1400 MHz $S_{1400} \sim 0.1$ mJy), presumably due to diffractive scintillation. We have derived a phase-connected timing solution for M3B (Table 4.4), which places it 8.3″ from the center of the cluster.

M3D has a spin period of 5.44 ms and an orbital period $\sim$ 129 days. Though the detections of M3D are too sparse to derive a phase-connected timing solution for this pulsar, by inserting arbitrary phase jumps between observing epochs we have been able to derive accurate orbital parameters, and a relatively precise position (Table 4.4). M3D's orbital period is much longer than the typical orbital period of GC MSPs, most of which have $P_{\rm orb} < 3$ days, and may suggest a non-standard evolutionary history for the system. PSR B1310+18 in M53 ($P_{\rm orb} \sim 256$ d, Kulkarni et al., 1991), PSR B1620−26 in M4 ($P_{\rm orb} \sim 191$ d, Lyne et al., 1988), and PSR J1748−2446E in Terzan 5 ($P_{\rm orb} \sim 60$ d, Ransom et al., 2005a) are the only other GC MSPs known to have orbital periods longer than 50 d. Binaries with orbital periods $10 \lesssim P_{\rm orb} \lesssim 1000$ d may be efficiently formed by exchange interactions involving an isolated neutron star and "hard" primordial binaries (Hut et al., 1992; Sigurdsson & Phinney, 1993). However, such wide binaries also have large interaction cross-sections and may easily be disrupted in the high-density cores of GCs.

We also have one very good candidate (denoted M3C in Table 4.3) with a spin period of 2.16 ms that has been seen only once (presumably due to scintillation) with a S/N of ~ 6 during a ~ 3000-s portion of an observation with the Green Bank Telescope (GBT), but never in any of our Arecibo data. These GBT data were taken with the Berkeley-Caltech Pulsar Machine (BCPM) as part of a parallel survey by our group for pulsars in GCs visible by the GBT (see Ransom et al., 2004, 2005c, for more details on these survey observations).

A deep radio synthesis image of M3 made at 1.4 GHz with the VLA (Kulkarni et al., 1990) revealed a faint $S_{1400} \sim 180\,\mu$Jy source 7.4″ from the optical center of the cluster. This source does not coincide with the positions of M3B or M3D. In principal, the Kulkarni et al. (1990) source could be associated with M3A, M3C, or another unknown pulsar in the cluster, although this seems unlikely given that its flux density should have made it easily detectable in our searches.

Three 10-ks observations of the cluster with *Chandra* ACIS-S taken by Grindlay et al. reveal no obvious X-ray counterpart to the Kulkarni et al. (1990) radio source. There are however two obvious point sources within the half-mass radius of the cluster. One of these sources is coincident with the supersoft X-ray source 1E 1339.8+2837 (Dotani, Asai, & Greiner, 1999). The other is not coincident with the positions of either M3B or M3D.

M5 (NGC 5904)

In M5, we have found three new pulsars in addition to the isolated 5.5-ms pulsar M5A (PSR B1516+02A) and the binary 7.9-ms pulsar M5B (PSR B1516+02B) found by Wolszczan et al. (1989a), bringing the total population of this cluster to five. M5C (PSR J1518+0204C), with a spin period of 2.48 ms, is in a 2.1-hr orbit with a $0.04\,M_\odot$ (minimum mass) companion. It shows regular eclipses for $\sim 15\%$ of its orbit as well as eclipse delays at eclipse ingress and egress, which can be up to ~ 0.2 ms and are presumably due to dispersive delays as the pulsar passes through the ionized wind of its com-

	PSR J1342+2822B	PSR J1342+2822D
Observation and data reduction parameters		
Period Epoch (MJD)	52770	52770
Start time (MJD)	52763	52768
End time (MJD)	53542	53476
# of TOAs	168	83
TOA rms (μs)	9.2	24
Timing parameters		
α [a]	$13^h42^m11.08708(6)$ s	$13^h42^m10.2(3)$ s
δ	$+28°22'40.141(1)''$	$+28°22'36.2(77)''$
P (ms)	2.3894207577857(6)	5.44297516(3)
$\dot{P}_{\rm obs}$ (10^{-20})	1.858(2)	Unk.
DM ($\rm cm^{-3}\,pc$)	26.160(1)	26.358(9)
P_b [b](days)	1.417352299(1)	128.752(3)
$T_{\rm asc}$ (MJD)	52485.9679712(4)	52655.38(2)
x (s)	1.875655(1)	38.524(2)
e	Unk.	0.0753(3)

Table 4.4: Timing Solutions for two M3 Pulsars

[a]The uncertainties indicated for all parameters are 1-σ, and are twice the formal values given by `TEMPO`.

[b]The orbital parameters are: orbital period (P_b), time of passage through the ascending node ($T_{\rm asc}$), semi-major axis of the orbit of the pulsar, projected along the line-of-sight, divided by the speed of light (x) and orbital eccentricity (e). Since the latter quantity is too small to be measured, we can not estimate the longitude of the periastron relative to ascending node (ω). All other parameters are as described in the text.

panion. M5C is part of the growing class (Freire, 2005) of ~ 10 eclipsing GC binaries with orbital periods of only a few hours and very low mass companions ($M_c \lesssim 0.1\,M_\odot$). It is positionally coincident with a soft X-ray counterpart seen in a 45-ks *Chandra* ACIS-S observation of the cluster (Stairs et al. 2007, in preparation). M5D (PSR J1518+0204D) was originally discovered in Arecibo data taken by our group at 327 MHz (see also Mott & Freire, 2003), but it has also been seen at 1.4 GHz on numerous occasions because of scintillation. These 327-MHz data were obtained using the Gregorian 327-MHz receiver and the WAPP as part of a smaller set of search observations conducted at lower frequency on the clusters M3, M5, M13, and M15. M5D is in a 29.3 hr orbit with a $0.19\,M_\odot$ (minimum mass) companion. M5E was discovered in a search of our regular timing observations of M5 and was visible because of scintillation. M5E has an orbital period of 26.3 hr and a $0.14\,M_\odot$ (minimum mass) companion. It has a complex pulse profile and close to a 100% duty cycle (Figure 7.4).

M13 (NGC 6205)

In M13, we have found three new pulsars in addition to the isolated 10.4-ms pulsar M13A (PSR B1639+36A) and the binary 3.5-ms pulsar M13B (PSR B1639+36B) found by Kulkarni et al. (1991) and Anderson (1993), bringing the total population of this cluster to five. The pulsars in this cluster show $2-10\times$ changes in flux density because of scintillation on time scales shorter than an hour. M13C has a spin period of 3.72 ms and is the only isolated pulsar discovered in this survey. M13D (PSR J1641+3627D) is a 3.11-ms binary with a 14.2-hr orbital period and a $0.18\,M_\odot$ (minimum mass) companion. M13E has been detected in only two observations, likely because of favorable scintillation. It is highly accelerated and appears to be eclipsed for part of each of these two observations. We estimate that the orbital period is approximately 2.8 ± 0.2 hr, which is consistent with the interpretation that it is an eclipser similar to M5C. The short orbital period and likely eclipses of this system make

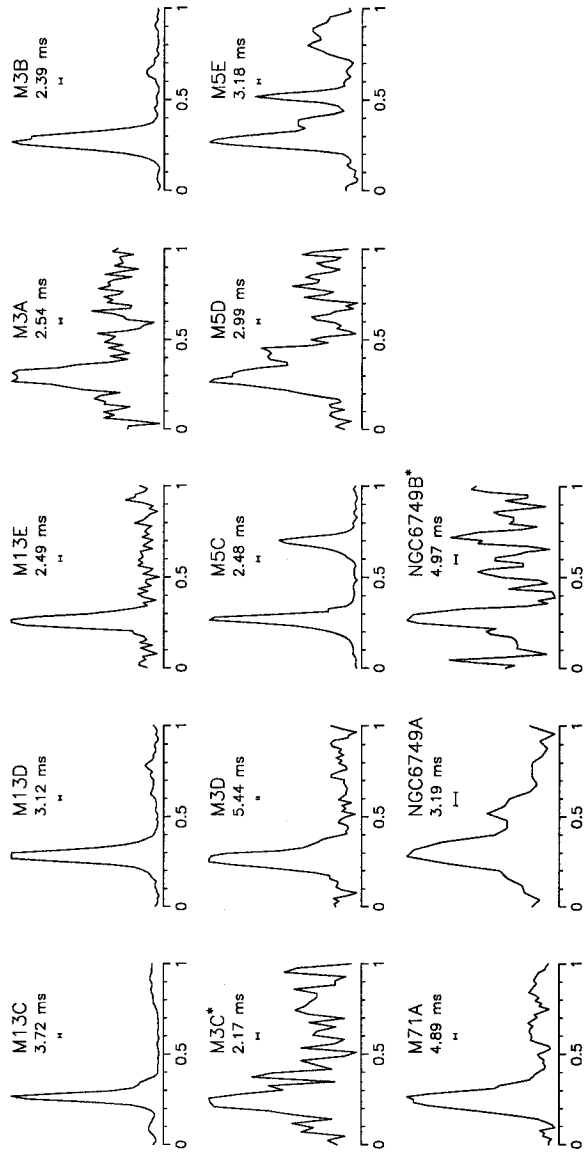

Figure 4.3: 1.4-GHz pulse profiles for the 11 millisecond pulsars and two promising candidates (marked with an asterisk) discovered in this survey. The profiles are the sum of numerous observations and in the case of clusters where there is significant scintillation (i.e. M3, M5, and M13) the profiles are the sum of a few (or only one) observations where the pulsar appears much brighter than on average. The profiles have been rotated in phase so that pulse maximum occurs at 0.25. In each case, there are 64 bins accross the profile. The horizontal bar indicates the effective time resolution of the data, taking into consideration dispersive smearing.

it difficult to blindly detect in a search. In analogy to other eclipsing MSPs, it is also likely that M13E will be visible as an X-ray source. Two roughly 30-ks *Chandra* observations of M13 were taken in March 2006, and may reveal an X-ray source coincident with this pulsar, or one of the others known in M13.

M71 (NGC 6838)

In M71, we have found M71A (PSR J1954+1847A), the first and only pulsar known in this cluster. M71A's DM of 117 pc cm^{-3} is reasonably close to the 86 pc cm^{-3} predicted by the NE2001 Galactic electron model (Cordes & Lazio, 2002a). It is also located ~ 0.6 core radii from the optical center of the cluster (see Stairs et al. 2007, in preparation), leaving little doubt it is associated with M71. M71A is a 4.89-ms pulsar in a 4.2-hr orbit with a $0.03\,M_\odot$ (minimum mass) companion. It shows regular eclipses for $\sim 20\%$ of its orbit, though no eclipse delays are seen at ingress or egress. A discussion of its identification with an X-ray counterpart will be published elsewhere. The low density and relative proximity of M71 (d = 4.0 kpc) make optical follow-up observations of M71A viable. The relatively high DM towards this cluster means diffractive scintillation has a small effect on the flux density of M71A. A stack search combining four contiguous days of data on this cluster revealed no new pulsars; searches combining more data sets will be undertaken.

NGC 6749 (Berkeley 42)

Lastly, we have found the first known pulsar in the direction of NGC 6749, as well as another promising pulsar candidate. The DM of NGC 6749A (PSR J1905+0154A) is 194 pc cm^{-3}, which is significantly lower than the 440 pc cm^{-3} DM predicted by the NE2001 model (Cordes & Lazio, 2002a). Given the rarity of MSPs, an association between this pulsar and NGC 6749 seems quite likely however, and the DM discrepancy could easily be due to uncertainties in the NE2001 model, or an overestimation of the cluster's distance. Assuming the association between NGC 6749A and the cluster is correct, then

NGC 6749 has the lowest concentration ($c = \log_{10}(r_t/r_c)$) and the second lowest central luminosity density of any GC with a known pulsar. NGC 6749A is a 3.19-ms binary pulsar with an orbital period of 19.5 hr and a 0.089 $M_\odot$ (minimum mass) companion. We have been unable to phase connect the 12 observations we have of this pulsar because they are spaced by intervals of $\gtrsim$ 1 month, and we have been unable to secure a more densely sampled set of observations at Arecibo. If a timing solution is obtained in the future, it will provide a precise position and observed period derivative. If the position is within the core of the cluster and/or the observed period derivative is negative (because it is accelerating towards us in the gravitational potential of the cluster) then the association of NGC 6749A with NGC 6749 will be more secure. NGC 6749B (PSR J1905+0154B) is a candidate 4.97-ms binary pulsar that has been seen only once, in data from MJD 52921. Although it is quite faint – the detection has a S/N of ~ 5 – the signal shows a clear peak in DM at roughly 192 pc cm^{-3}. The similarity in DM with NGC 6749A bolsters this candidate's identification as a real pulsar. The existence of a second pulsar in the direction of NGC 6749 with roughly the same DM as NGC 6749A would also secure the association of both pulsars with the cluster.

4.5 Discussion

4.5.1 Survey Limitations

Sensitivity to Fast and Binary Pulsars

The fastest-spinning pulsar known in a GC is PSR J1748−2446ad in Terzan 5, with a spin period of 1.396 ms (Hessels et al., 2006) and the shortest known orbital period of any binary MSP in a GC is 1.6 hr (PSR J0024−7204R in 47 Tucanae, Camilo et al., 2000). Here we discuss the sensitivity of this survey to very-fast-spinning pulsars ($P_{\rm spin} \sim 0.5$–3.0 ms) and/or pulsars in very tight orbits ($P_{\rm orb} \sim 0.5$–6.0 hr). The discovery of such systems is hampered by a

number of selection effects (Johnston & Kulkarni, 1991; Ransom et al., 2003), which strongly bias the observed spin and orbital period distributions to longer periods. We discuss the extent to which the observed spin period distribution of the total population of MSPs has been affected by selection effects in §4.5.2.

We have characterized the sensitivity of this survey, as a function of period and DM, in §4.2.3 and compare it to the sensitivity of the Anderson (1993) survey (Figure 4.1). For DM = 30 pc cm^{-3}, our sensitivity to a 1-ms pulsar is degraded by a factor of roughly 1.5 compared with a 4-ms pulsar. This degradation in sensitivity is a strong function of DM and increases to a factor of ~ 2.5 at a DM of 200 pc cm^{-3}. Some of the MSPs we have discovered in this survey were just barely detectable by our processing (e.g. NGC 6749A and M3D). We can thus not rule out the existence of pulsars with $P_{\rm spin} \lesssim 1.5$ ms in our survey data, if they have fluxes comparable to the dimmest sources we have discovered. However, a "reasonably bright" ($S_{1400} > 50\,\mu$Jy), *isolated* 1-ms pulsar would very likely have been detected. We discuss the *luminosity* limits achieved for individual clusters, which depend largely on the cluster distance, in the next section. Even higher time and frequency resolution data are required to maintain as flat a sensitivity response as possible out to spin periods below ~ 1 ms. This should be a goal of future surveys and is feasible given the current state of computer technology.

The shortest spin period found in this survey was 2.4 ms (M3B). Furthermore, 5 of the 11 pulsars found here have spin periods between 2–3 ms, significantly lower than the median period of the observed population of GC MSPs, which is ~ 4 ms. For comparison, the fastest-spinning pulsar known in these clusters prior to this survey is M13B, with a spin period of 3.5 ms. This demonstrates the increased sensitivity of this survey to fast-spinning pulsars, compared with previous surveys, and suggests that the observed spin-period distribution of GC pulsars is still artificially biased towards longer spin frequencies. This is unsurprising if one compares the sensitivity curves of this survey with those of Anderson (1993), as in Figure 4.1.

Our sensitivity to short orbital periods is difficult to quantify precisely. We compare the sensitivity of a coherent search of the data (i.e. one in which the orbital modulation of the pulsar signal can be completely corrected, and in which the sensitivity is proportional to $T_{\rm obs}^{-1/2}$) to that of our acceleration search technique, using the simulations of Ransom et al. (2003), which were made using the same search technique and software. These simulations assume a pulsar spin period of 2 ms and a companion mass of 0.1 $M_\odot$. We see that for a 2-hr binary period and a 0.5-hr observation duration that the sensitivity afforded by an acceleration search is roughly half that of the coherent sensitivity. A 0.5-hr observation duration is typical of the length used in our short subsection searches, and thus for all clusters we had good sensitivity to orbital periods down to a few hours. Specifically for the survey clusters with known pulsars (where the DM is thus also known), we searched a larger variety of short subsections of the total observation length, down to integration times as short as roughly 10 minutes. For these clusters, we were sensitive to even more compact systems and higher accelerations (assuming the pulsar's flux is high enough to show up in such short integrations).

As explained in §4.3.3, in our matched-filter acceleration technique we looked for signals where the highest order harmonic used in summing drifted by up to $z_{\rm max} = 170$ bins, corresponding to a maximum line-of-sight acceleration of $a_{\rm max} \simeq 4P_{\rm spin,ms}/T_{\rm obs,h}^2/N_{\rm harm}\,{\rm m\ s^{-2}}$. For comparison, we note that Camilo et al. (2000) were sensitive to a maximum acceleration of $< |30|\,{\rm m\ s^{-2}}$ in their searches of 47 Tucanae (where 0.3-h integration subsections were used) and that PSR B1744−24A in Terzan 5 has a maximum line-of-sight acceleration of $33\,{\rm m\ s^{-2}}$ (Lyne et al., 1990). For $P_{\rm spin} = 2$ ms and $T_{\rm obs} = 0.5$-h, which is typical of the integration times used in our short-subsection searches, we reach a limiting acceleration of $32\,{\rm m\ s^{-2}}$ (note however that this limit applies only to the fundamental and not to sums including higher-order harmonics). For clusters where we searched numerous timing observations, $z_{\rm max} = 500$ bins was sometimes used, providing an additional factor of three range in acceleration

space. Such high accelerations are worth exploring in order to maintain sensitivity to not only the accelerated fundamental of a pulsar signal but also its harmonics, which are needed to detect faint pulsars. Though no new pulsars were found in these searches, we note that the pulsars M13E and M71A were only detected with $1-2$ harmonics in our initial $z_{\rm max} = 170$ searches and would have been more easily identified in a $z_{\rm max} = 500$ search. Re-searching the data presented here with $z_{\rm max} = 1000$ has the potential to discover compact binaries that were previously missed.

The most extreme orbital systems we found in this survey were M5C, M13E, and M71A, with orbital periods between $\sim 2-4$ hr and minimum companion masses between $\sim 0.02-0.1\,{\rm M}_\odot$. As 10 of 11 pulsars found here are in binary systems, this survey did a good job of detecting the binaries that were missed by Anderson (1993) and other previous searches of these clusters[10]. With the exception of the long orbital period binary M3D, all the binaries presented here required the acceleration search technique in order to be detected. The fact that we found only 1 isolated pulsar suggests that previous surveys already found the vast majority of the reasonably bright isolated pulsars in these clusters.

Sensitivity to the Weakest Pulsars

Of the 22 clusters we have searched for pulsations, 14 still contain no known pulsar, although all of these (with the exception of M2) are > 15 kpc from the Sun and/or have very high predicted DMs ($> 150\,{\rm pc\ cm^{-3}}$). We have estimated the maximum luminosity of any undiscovered pulsars in the clusters we have searched, using the distance to the cluster, its DM (or predicted DM), and the sensitivity calculations of §4.2.3. These upper limits are given

[10]However, we note that five of the eight pulsars found in M15 by Anderson (1993) are especially faint, isolated pulsars discovered in searches of multiple M15 data sets. M15D and E were found in incoherent stack searches of multiple observations, while M15F, G, and H were found in coherent multi-day transforms. These searches are *much* less sensitive to binary systems.

in Table 4.1, and apply most directly to isolated pulsars. For comparison, the weakest-known pulsars in Terzan 5 have 1400-MHz luminosities[11] $L_{1400} \sim 2\,\mathrm{mJy\ kpc^2}$, and the weakest in 47 Tucanae are about $L_{1400} \sim 1\,\mathrm{mJy\ kpc^2}$. Furthermore, there are indications that the *intrinsic* lower limit for the MSPs in 47 Tucanae is $L_{1400}^{min} = 0.4\,\mathrm{mJy\ kpc^2}$ (McConnell et al., 2004). Because of their large distances, such weak pulsars are not excluded in any of the clusters we have searched here. For most of our clusters, the luminosity limits only exclude pulsars whose luminosity is comparable to the brightest MSPs known in the GC system ($L_{1400} \sim 100\,\mathrm{mJy\ kpc^2}$). Significantly more sensitive observing systems (using, for example, the Square Kilometer Array) will be required to fully probe the pulsar populations of these clusters down to the proposed low-luminosity cutoff.

Spatial Coverage

Here we investigate whether our single-pointing observations provided adequate spatial coverage to discover all the visible pulsars in our survey clusters. The vast majority of GC pulsars are found in the cores of their clusters due to mass-segregation of the massive neutron stars. The radius of the Arecibo beam at 1400 MHz is 1.5′. For the vast majority of GCs the core radii r_c are $< 1'$ and the half-mass radii are $< 2'$. For almost all of the clusters observed here, the core radius (and in most cases the half-mass radius) fell within the Arecibo beam. The exceptions are NGC 5053 ($r_c = 1.98'$), NGC 5466 ($r_c = 1.64'$), and Pal 5 ($r_c = 3.25'$). In the entire known population, all but three of the GC MSPs with measured positions lie within $\sim 1.5'$ of the optical center of their host cluster. The exceptions are PSRs J1911−5958A and J1911−5958C at 6.39′ and 2.70′, respectively, from the center of NGC 6752, and PSR B1718−19 at 2.30′ from the center of NGC 6342[12]. For these pulsars, it has been sug-

[11]This is a "pseudo-luminosity", defined as $L_{1400} = S_{1400}d^2$.

[12]Note however that this pulsar is offset from the optical center of the cluster by 46 times the core radius, and it is possible that it is not associated with the cluster.

gested that they have been ejected from the core of their cluster by a close interaction with another star or binary. Given the relatively small size of the Arecibo beam, it is possible that we missed similar systems. However, the beam radius of the 430-MHz Anderson (1993) survey, which observed 11 of the same sources, was 5′, and would likely have detected some sources further from the cluster centers, if they existed. Other GC surveys with Parkes and the GBT, which have larger beam sizes ($\sim 10-15'$), have failed to find a significant number of MSPs far from the core of their cluster. It is thus likely that the observed positions of GC MSPs with respect to the center of their host cluster come close to reflecting an intrinsic distribution, rather than an observational bias due to incomplete spatial coverage. If this is the case, then it is unlikely that a significant number of pulsars were missed in this survey because of spatial coverage.

4.5.2 MSP Spin Frequency Distribution

If one includes both the known MSPs in the field and those in GCs, the *observed* distribution of radio pulsar spin frequencies above 200 Hz roughly follows a power-law relationship with an index of -3, i.e. $N_{\rm psr} \propto {\nu_{\rm spin}}^{-3}$ (Figure 4.4). We do not suggest that the underlying spin period distribution is a power-law, or that a physical motivation for this choice exists, we merely use this functional form to quantify the sharp observed drop in observed pulsars as $\nu_{\rm spin}$ increases. In fact, considering the combined spin periods of MSPs in the field and in GCs is potentially problematic, as the period distribution between field MSPs and those in GCs might be intrinsically different. Furthermore, the period distribution between GC MSP populations also appears to vary (e.g. Terzan 5 has a much wider observed range of spin periods than 47 Tucanae). Nonetheless, we will consider the MSP population as a whole here.

There is no significant correlation currently observed between the radio luminosity of MSPs and their spin frequency. Because all other conceivable observational biases (e.g. scattering, dispersive smearing, self-obscuration) *in-*

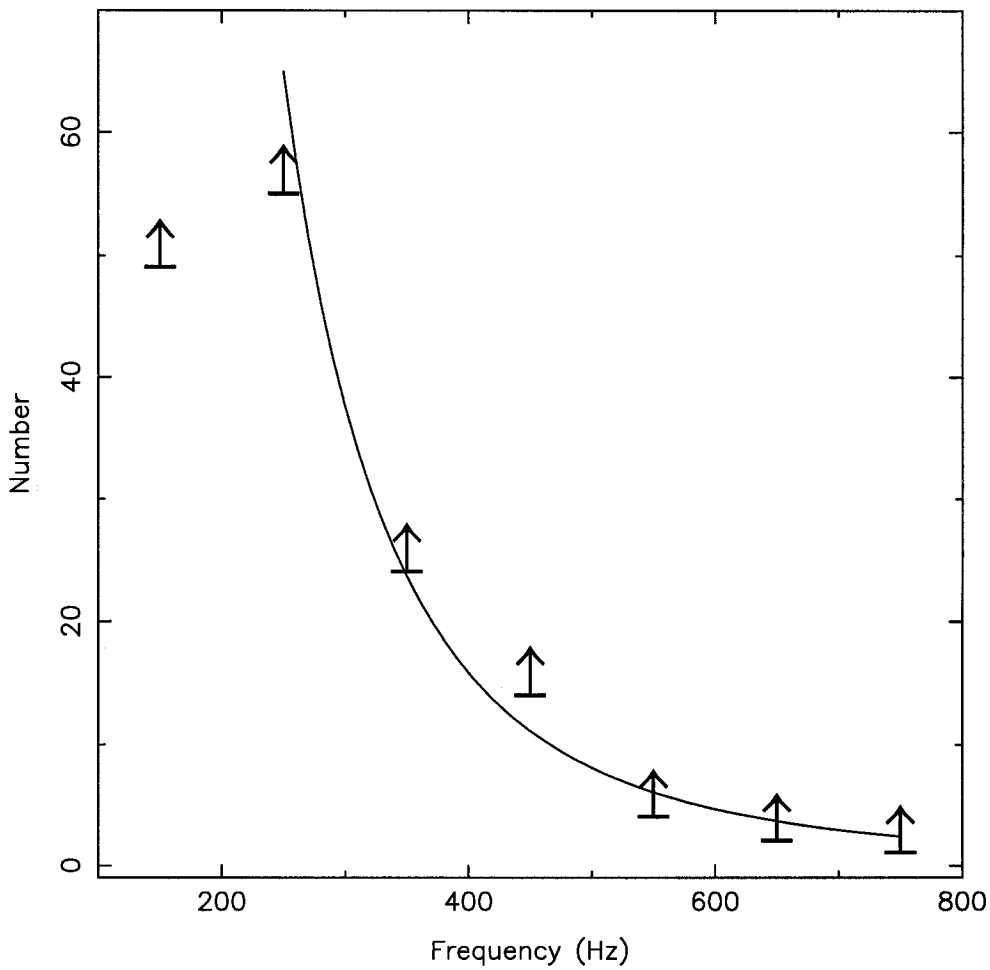

Figure 4.4: The combined population of MSPs in the field and GCs, plotted as a function of spin frequency. The points are binned in intervals of 100 Hz, and are show as lower limits to reflect the various observational biases against detecting millisecond pulsars. The number of observed pulsars drops rapidly with spin frequency above 200 Hz, roughly as $N_{\rm psr} \propto \nu_{\rm spin}{}^{-3}$ (solid line).

crease the difficulty in detecting the fastest pulsars, the observed spin-frequency distribution above 200 Hz places a limit on the steepness of the intrinsic spin frequency distribution at these frequencies (i.e. if $N_{\rm psr} \propto {\nu_{\rm spin}}^{-\alpha}$, then $\alpha_{\rm true} < \alpha_{\rm obs}$). Chakrabarty (2005a) (see also Chakrabarty et al., 2003) notes that the observed spin-frequency distribution of accreting LMXBs showing bursts (the "nuclear-powered" pulsars) is statistically consistent with a flat distribution between 270–619 Hz, and a cut-off at 730 Hz. Given that LXMBs are the most likely progenitors of the MSPs, do MSPs also have a roughly flat spin-frequency distribution up to some cut-off frequency?

To answer this, we consider the observational biases that contribute to the observed spin-frequency distribution of MSPs. First, we see from Equation 4.1 that the minimum detectable flux density depends on spin frequency because pulse smearing due to scattering and DM has a greater relative effect for fast pulsars. This accounts for part of the slope in the observed spin-frequency distribution. Second, as there is no indication that orbital period is strongly correlated with spin period, it is unlikely that many of the fastest MSPs are being missed because they are preferentially in the most compact orbits. However, the number of bins through which a binary-modulated pulsar signal will drift in the Fourier domain is directly proportional to its spin frequency. In other words, for the same orbital period, it is more difficult to detect a 1-ms pulsar than a 5-ms pulsar in an acceleration search, because the 1-ms pulsar (and its harmonics) will drift by a factor of 5 times more Fourier bins. Harmonics that drift by many bins are more susceptible to non-linear frequency drift terms (reducing their detectability) and may drift beyond the maximum number of bins probed by the search ($z_{\rm max}$). Thus, binary motion also accounts for part of the slope in the observed spin-frequency distribution, although this effect is difficult to quantify. Finally, because it is plausible that eclipse fraction increases with $\dot{E} = 4\pi^2 I \nu \dot{\nu} \propto B_{\rm surf}^2 \nu^3$ (assuming that the pulsar spindown is dominated by magnetic dipole radiation), fast-spinning pulsars in binary systems may be preferentially obscured by the material their strong winds ablate

from their companions (Tavani, 1991; Hessels et al., 2006).

Given this multitude of observational biases against detecting the fastest-spinning radio pulsars, it is difficult to identify what portion of the observed spin-frequency distribution is instrinsic to the population. Perhaps the best way to investigate this problem is by performing Monte Carlo simulations of various trial underlying populations and then searching these until one converges on the observed population. Terzan 5 and 47 Tucanae present excellent samples on which to perform such simulations, although one would have to be careful in generalizing the results to MSPs in the field or in other GCs. If the distribution of radio pulsar spin periods is even roughly similar to that of the LMXBs, which is roughly consistent with being flat over the observed range, then we have still only discovered a very small fraction of the fastest-spinning radio pulsars. Mapping the period distribution at the fastest spin periods depends crucially on finding these pulsars.

Radio surveys for rotation-powered pulsars will always be limited by scattering, but there is still room for higher time and frequency resolution backends (or coherent dedispersion) to improve sensitivity to the fastest-spinning pulsars. Surveys at higher observing frequencies than used here (i.e. $> 1.5\,\mathrm{GHz}$, e.g. Ransom et al., 2005a,b) mitigate the effects of scattering, which scales as ν_{obs}^{-4}, and inter-channel dispersive smearing, which scales as ν_{obs}^{-3}. Unfortunately, higher observing frequencies also require very large observing bandwidth to compensate for the typically steep spectral indices of pulsars. X-ray surveys are also potentially interesting, as they do not suffer from the adverse effects of dispersion or scattering (although there is absorption of soft X-rays by intervening matter). However, currently only one of the radio MSPs in GCs (PSR B1821−24A) is also detected as an X-ray pulsar. Furthermore, the strong bias against detecting binaries can be mitigated by the development of increasingly sophisticated (and computationally intensive) search techniques that more completely correct for the pulsar's binary motion. Another advantage of future instruments, which will have greater instantaneous sensitivity,

is that one may find faint pulsars in increasingly short data sets, where binary motion has less time to smear the signal.

4.5.3 Pulsar Luminosities

In Table 4.3, we list the flux densities of the pulsars discovered in this survey, as well as those of the previously known pulsars in these clusters. These were derived from the observed pulse profiles by integrating the pulse and scaling this flux using the off-pulse root mean square and the radiometer equation. For the pulsars found in M3, M5, and M13, scintillation has a strong effect on the observed flux of the pulsars, making it more difficult to estimate the underlying intrinsic brightness of the source. For these pulsars, we have used an approach similar to that used by Camilo et al. (2000) to estimate the fluxes of these pulsars: we fit the observed fluxes – using half the survey sensitivity limit as the flux in the case of non-detections – to an exponential distribution, whose median value we take as the intrinsic flux.

The luminosity distribution of MSPs, both in the field and in GCs, is difficult to constrain precisely because of the observational bias against detecting faint, fast, and binary pulsars. Furthermore, individual estimates of pulsar luminosity can suffer from large systematic errors because the distance is incorrect (this is particularly difficult in the field, where many distances are estimated from the DM). The small number of known MSPs is also a major hindrance. In this section, we take advantage of the many new pulsar discoveries that have been recently made in GCs. We combine the luminosities of the pulsars currently known in M5, M13, M15, M28, NGC 6440, NGC 6441, 47 Tucanae, and Terzan 5 and consider the resulting luminosity law for GC MSPs. These clusters were chosen because they contain at least 4 pulsars each. The clusters M3, M62, NGC 6624, and NGC 6752 were excluded from the analysis because reliable fluxes were not available for all the pulsars in these clusters.

In Figure 4.5 we plot the cumulative luminosity distribution of 29 isolated

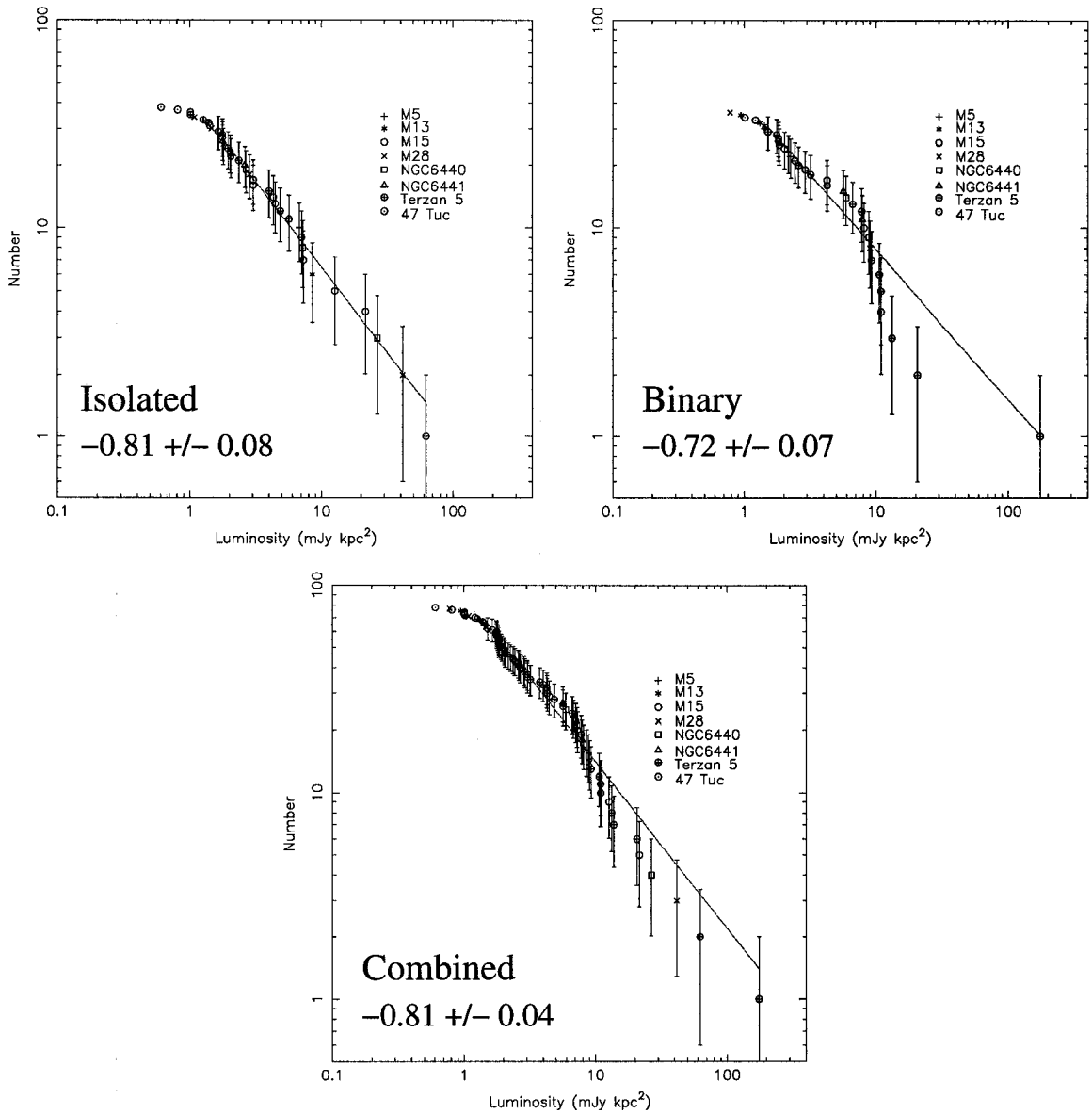

Figure 4.5: Cumulative distributions of 1.4-GHz luminosities of pulsars in M5, M13, M15, M28, NGC 6440, NGC 6441, 47 Tucanae, and Terzan 5. The minimum luminosity considered for fitting purposes is $L_{1400}^{\rm min} = 1.5\,{\rm mJy\ kpc^2}$. Error bars are the square-root of each value. The excluded points below $L_{1400}^{\rm min}$ are shown without error bars. *Top left:* luminosity distribution of 29 isolated pulsars in these clusters, which has a slope of -0.81 ± 0.08. *Top right:* luminosity distribution of 29 binary pulsars in these clusters, which has a slope of -0.72 ± 0.07. *Bottom:* combined luminosity distribution, including both isolated and binary pulsars, which has a slope of -0.81 ± 0.04.

(top left), 29 binary (top right), and all 58 pulsars combined (bottom) in our sample GCs. All luminosities were scaled to 1.4 GHz assuming a pulsar spectral index of $\alpha = -1.8$ (Maron et al., 2000b). The M5 and M13 fluxes are from the observations made in this survey, using the Harris (1996) distances to derive luminosities. The Terzan 5 fluxes come from Ransom et al. (2005a), using a distance of 8.7 kpc (Cohn et al., 2002) to convert to luminosities. The 47 Tucanae fluxes are from Camilo et al. (2000) and are converted to luminosities using a distance of 4.5 kpc (Zoccali et al., 2001). The luminosities of pulsars in M28, NGC 6440, and NGC 6441 come from recent 1950 MHz timing observations made by our group with the GBT (Ransom et al., 2005b). We fit $\log_{10}(N > L)$ versus $\log_{10}(L)$ to a line, using the square-root of $\log_{10}(N > L)$ as the uncertainties. No corrections have been made for any observational bias (as has been done for field MSPs in Lyne et al., 1998; Cordes & Chernoff, 1997).

For all isolated and binary pulsars combined, the best-fit slope is -0.81 ± 0.04. Below 1.5 mJy kpc^2 the observed distribution turns over, and thus we used a minimum luminosity cut-off of $L_{1400}^{\rm min} = 1.5$ mJy kpc^2 for fitting purposes. In combining luminosities from numerous clusters, we have assumed that the luminosity function does not vary significantly between clusters. We note that when the same analysis is applied separately to the Terzan 5 and 47 Tucanae pulsars that the slope in each case is consistent with the slope derived from all clusters in our sample combined, suggesting that indeed the radio luminosity law of GC pulsars is universal.

There are clearly ripples in the combined distribution, suggesting unmodeled effects. When the population is separated into isolated and binary pulsars, it is clear that these effects come predominantly from the binary pulsars. This is unsurprising, as the observational biases inherent in detecting such systems are significantly higher than for the isolated pulsars. Fitting only the 29 isolated pulsars in our sample, we find a slope (-0.81 ± 0.08) that is identical to the combined distribution, although now the distribution is much smoother.

Conversely, the cumulative distribution of the 29 binaries is poorly fit by a single slope (-0.72 ± 0.07) as there appears to be a dearth of pulsars in the high-luminosity end of the distribution.

Given the much lower bias against detecting isolated pulsars, we suggest that the slope derived from fitting only isolated pulsars is the most reliable. This distribution is somewhat flatter than the d $\log_{10}(N) = -$ d $\log_{10}(L)$ relation found for non-recycled field pulsars and MSPs (consider for instance Lyne, Manchester, & Taylor, 1985; Lyne, Manchester, Lorimer, Bailes, D'Amico, Tauris, Johnston, Bell, & Nicastro, 1998; Cordes & Chernoff, 1997), although, interestingly, it is consistent with the recently derived luminosity law of Lorimer et al. (2006a), who find d $\log_{10}(N) \sim -0.8$ d $\log_{10}(L)$ using a sample of 1008 normal (non-millisecond) pulsars. As the population of GC MSPs continues to increase, we will be better able to constrain their luminosity distribution. We consider the question of whether isolated and binary MSPs have the same luminosity distribution an outstanding question. It is hard to constrain the luminosity function of GC MSPs below 1 mJy kpc^2 because of the relatively large distances to GCs and selection effects, which are worse for weak pulsars.

Chapter 5

A 716-Hz Pulsar in Terzan 5

Although Arecibo is the most sensitive radio telescope in the world at the frequencies typically used to observe radio pulsars, it has a restricted range of visibility. Many of the densest, most massive globular clusters are not visible with Arecibo. The GBT is fully steerable and can see many of these rich clusters. In this chapter, we present deep GBT searches of the dense globular cluster Terzan 5, which have discovered the fastest-spinning pulsar known.

The work presented in this chapter originally appeared in: *Hessels, J. W. T., Ransom, S. M., Stairs, I. H., Freire, P. C. C., Kaspi, V. M., & Camilo, F. A Radio Pulsar Spinning at 716-Hz. Science, 2006.* References to this chapter should be considered references to Hessels et al. (2006) as well.

5.1 Introduction

While the majority of neutron stars are observed to rotate slower than a few times a second, those in binary systems can reach spin rates of hundreds of times a second through the transfer of angular momentum from their companion star (Alpar et al., 1982; Radhakrishnan & Srinivasan, 1982a). Some

of these neutron stars, termed millisecond pulsars, are persistent radio sources whose emission is modulated at the star's spin frequency. Determining the maximum achievable rotation rate of a neutron star is important for a variety of astrophysical problems, ranging from understanding the behaviour of matter at supra-nuclear densities, to estimating the importance of neutron stars as gravitational wave sources for current and upcoming gravitational wave detectors. For over 23 years, the 642-Hz pulsar B1937+21, the first millisecond pulsar ever found, has been the fastest-spinning neutron star known (Backer et al., 1982). It has been argued that faster ones are exceedingly rare, if they exist at all (Chakrabarty et al., 2003).

Per unit mass, globular clusters have many more millisecond pulsars than the Galactic disk. This is due to the extremely high stellar densities in their cores ($10^4 - 10^6\,\mathrm{pc}^{-3}$), which promote the creation of binary systems (Meylan & Heggie, 1997) where a neutron star is spun-up (or "recycled") to rotate hundreds of times a second (Alpar et al., 1982; Radhakrishnan & Srinivasan, 1982a). We have searched the massive and dense globular cluster Terzan 5 for millisecond pulsars using the National Radio Astronomy Observatory's 100-m Green Bank Telescope (GBT). Our searches have thus far uncovered 30 millisecond pulsars in Terzan 5[1], in addition to the three previously known pulsars in this cluster (Lyne et al., 1990, 2000; Ransom, 2001). The discovery of 21 pulsars in Terzan 5 was presented in (Ransom et al., 2005c). Following that paper, an additional nine pulsars have been found in searches of our monitoring observations. These will be reported elsewhere. Terzan 5 has the largest known population of millisecond pulsars of any globular cluster, roughly one quarter of the entire population of globular cluster millisecond pulsars, and the five fastest rotating pulsars in the Galactic globular cluster system. Among the newest discoveries in Terzan 5 is PSR J1748−2446ad, a 716-Hz eclipsing binary millisecond pulsar, which is the fastest-spinning neutron star ever found.

[1]For an updated list of GC pulsars see http://www.naic.edu/~pfreire/GCpsr.html.

5.2 Observations and data analysis

We discovered PSR J1748−2446ad in 10 November 2004 observations of Terzan 5 and confirmed it in 8 January 2005 observations using the Pulsar Spigot backend (Kaplan et al., 2005) on the GBT. All observations employed the Spigot with 600 MHz of usable bandwidth centered at 1950 MHz, 768 spectral channels, and 81.92-μs sampling. Observations were generally 6−7 hours in length and taken at roughly monthly intervals starting June 2004. In addition, there was a more closely spaced set of observations in early May 2005.

The discovery observation showed that the pulsar is part of a binary system and is eclipsed by its companion; both of these properties restricted our ability to detect the pulsar in our monitoring sessions. Nonetheless, we have now detected the pulsar in at least 18 out of the 30 multi-hour observations taken thus far (see Figure 5.1 for pulse profile). We have derived a reliable orbital ephemeris (Table 5.1) by initially modelling the pulse phase delays of a few good detections with a simple sine function and then refining the model by fitting pulse times of arrival to a simple Keplerian orbital model, with arbitrary pulse phase offsets between observing epochs. This ephemeris allowed us to detect the pulsar in many observations where it was not initially identified through a periodicity search.

The pulsar is in a highly circular 26-hr orbit with a $\gtrsim 0.14\,M_\odot$ companion, and is eclipsed for $\sim 40\%$ of its orbit at 2 GHz. Such a large eclipse fraction, corresponding to an eclipse region with physical size $\sim 5 - 6\,R_\odot$ is extremely rare for such a relatively wide orbit (separation between the pulsar and companion of $\sim 4 - 5\,R_\odot$). The companion may be a bloated main-sequence star, possibly still filling its Roche Lobe, as has been suggested for PSR J1740−5340, a 35-hr binary millisecond pulsar with a $\gtrsim 0.21\,M_\odot$ companion and $\sim 40\%$ eclipse fraction at 1.4 GHz (D'Amico et al., 2001b). The eclipse properties are also similar to those of PSR J1748−2446A, a 1.8-hr binary with a $0.089\,M_\odot$ minimum mass companion, also located in Terzan 5 (Lyne et al., 1990). Like

Parameter	Value
Rotational Parameters	
Pulse period P (s)	0.00139595482(6)
Period derivative $\lvert\dot{P}\rvert$ (s/s)	$\leq 6 \times 10^{-19}$
Pulse frequency ν (Hz)	716.35556(3)
Frequency derivative $\lvert\dot{\nu}\rvert$ (Hz/s)	$\leq 3 \times 10^{-13}$
Epoch (MJD)	53500
Orbital Parameters	
Orbital period $P_{\rm orb}$ (days)	1.09443034(6)
Projected semi-major axis x (lt-s)	1.10280(6)
Time of ascending node $T_{\rm ASC}$ (MJD)	53318.995689(12)
Eccentricity e	< 0.0001
Derived Quantities	
Companion minimum mass $M_{2,\rm min}$ ($\rm M_\odot$)	0.14
Dispersion measure DM (pc $\rm cm^{-3}$)	235.6(1)
Flux density at 1950 MHz S_{1950} (mJy)	0.08(2)
Characteristic age $\tau_{\rm c}$ (years)	$\geq 2.5 \times 10^7$
Surface magnetic field $B_{\rm surf}$ (G)	$\leq 1.1 \times 10^9$
Spin-down luminosity $\dot{E}$ erg/s	$\leq 1.3 \times 10^{37}$

Table 5.1: Measured and derived parameters of PSR J1748−2446ad. All measured spin and orbital parameters were determined using the TEMPO software package[3], using arbitrary phase offsets between observing epochs. Given the currently sparsely sampled data, it is impossible to phase connect separate observations. For this reason, we provide only an upper limit on the magnitude of the spin frequency derivative of the pulsar, which incorporates the maximum possible acceleration due to the gravitational potential of Terzan 5 assuming a position close to the cluster center. Likewise, we can currently only place limits on the derived characteristic age, surface magnetic field and spin-down luminosity. The minimum companion mass is derived assuming a pulsar mass of $1.4\,\rm M_\odot$. The dispersion measure was determined by measuring pulse arrival time delays in the different frequency channels across the 600-MHz observing bandwidth.

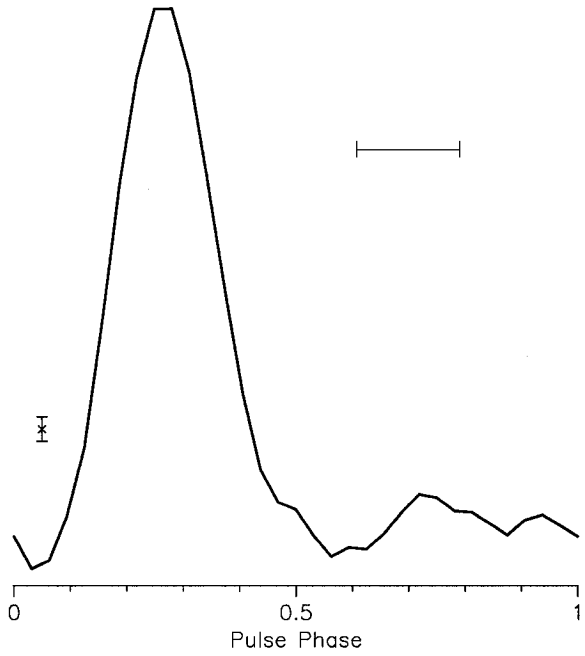

Figure 5.1: Master PSR J1748−2446ad pulse profile from the combination of eight GBT Pulsar Spigot observations at 2 GHz with particularly good detections of the pulsar. The cumulative integration time is ∼54 hrs. There are 32 phase bins across the profile, and the y-axis plots flux in arbitrary units. The one sigma error bar on the flux is shown in the lower left-hand corner. The effective time resolution of the data, $\sim 300\,\mu$s, which accounts for pulse smearing due to channelisation of the dispersed data and finite time sampling, is indicated by the horizontal bar. A weak, but statistically significant interpulse is seen at a phase of ∼0.75.

PSR J1740−5340 and PSR J1748−2446A, there is evidence that the eclipse duration of PSR J1748−2446ad is variable, and sometimes lasts longer than 40% of the orbit. On a least two epochs when our ephemeris predicts the pulsar should have been visible for several hours, it was not detected at all. The pulse signal-to-noise is too low to measure dispersion measure variations on short timescales. Future observations should allow a phase-coherent timing solution to be derived, which will provide a precise position and observed spin frequency derivative $\dot{\nu}$. Until then, we have provided an upper limit on $|\dot{\nu}|$

(Table 5.1).

We have verified that this signal is not harmonically related to any of the other known pulsars in Terzan 5. We have also carefully investigated the possibility that our searches have identified the second harmonic of a new 358-Hz pulsar. When we fold the data at 358 Hz, there are two identical peaks (within the resolution and RMS noise level of the Spigot data) separated by 180° in pulse phase. This is what we expect to see if the pulsar signal is folded at half its intrinsic spin frequency, and strongly suggests that 716 Hz is the true spin frequency of the pulsar. The results of folding the data at other harmonically related spin frequencies are also consistent with the pulsar having a true frequency of 716 Hz. There is also evidence (Figure 5.1) for a weak, but statistically significant interpulse (extra structure in addition to the main pulse peak) when the data are folded at 716 Hz. This interpulse, if real, is further evidence that the spin frequency is 716 Hz.

Lastly, we have simultaneously observed the pulsar using the GASP coherent dedispersion pulsar machine (Demorest et al., 2004; Ferdman et al., 2004), which records only $\sim 1/6$ the bandwidth achievable with Spigot but which removes all dispersive smearing due to the ionized interstellar medium, resulting in significantly sharper (i.e. narrower) pulse profiles[4]. When the GASP data are folded at 358 Hz, two peaks, consistent in shape with each other to within the RMS of the noise, are seen separated by 180° in pulse phase, again indicating that 358 Hz is half the true spin frequency. We conclude that PSR J1748−2446ad is indeed a 716-Hz pulsar.

[4]The SPIGOT pulse profile is significantly widened compared with the intrinsic pulse width of the pulsar because the finite number of channels used across the observing bandwidth does not allow for a complete removal of the dispersive effects of the interstellar medium.

5.3 Implications and Discussion

The equation of state of matter at supra-nuclear densities, and thus the mass-radius relation for neutron stars, is unknown. If a star is rotating too rapidly for a given radius, centrifugal forces will cause it to shed mass. Lattimer & Prakash (2004) derive the following equation which, independent of the true equation of state, gives the maximum spin frequency for a neutron star with a non-rotating radius R and mass M (assuming this is not close to the maximum mass allowed by the equation of state): $\nu_{\rm max} = 1045(M/{\rm M}_\odot)^{1/2}(10\,{\rm km}/{\rm R})^{3/2}\,{\rm Hz}$. Using this, and assuming a mass less than $2\,{\rm M}_\odot$ (which accomodates all measured neutron star masses (Lattimer & Prakash, 2004)) we find an upper limit of 16 km on PSR J1748−2446ad's radius. We note that this constraint applies specifically to PSR J1748−2446ad and that slower-spinning pulsars could have larger radii. Recently, Li & Steiner (2005) have derived a radius range of 11.5−13.6 km for a $1.4\,{\rm M}_\odot$ neutron star, based on terrestrial laboratory measurements of nuclear matter. For a $1.4\,{\rm M}_\odot$ neutron star, we find an upper limit of 14.4 km, which is in agreement with their result. These radius constraints are more robust than those obtained through observations of neutron star thermal emission, which is faint, difficult to measure, and whose characterization depends on uncertain atmosphere models (Kaspi et al., 2006). Although in principle a radius measurement could constrain the unknown equation of state of dense matter, PSR J1748−2446ad does not rule out any particular existing models, since the pulsar mass is unknown. It is unlikely that a mass measurement will be achievable through timing of the pulsar, as the orbit is too circular to measure the relativistic advance of the periastron, which would likely be contaminated by classical effects as well.

Although there are selection effects, especially at radio wavelengths, against finding fast, binary pulsars (Johnston & Kulkarni, 1991), we have maintained excellent sensitivity to these through the use of advanced search techniques (Ransom et al., 2002) and data with high time and frequency resolution. For

example, these searches blindly detect the 596-Hz binary pulsar PSR J1748−2446O ($P_{\rm orb} \sim 6$ hrs) at its second and fourth harmonic, which is equivalent to detecting a highly accelerating 1192-Hz pulsar and its second harmonic. While these searches are clearly sensitive to pulsars faster than 716 Hz, we note that obscuration of the pulsar signal by material blown off the companion by the pulsar wind may play an important role in reducing the chances of detecting such systems (Tavani, 1991). Of the five fastest known millisecond pulsars (including the two found in the Galactic Plane; see Table 5.2), four are eclipsing, and the fifth, PSR B1937+21, is unusual because, unlike ∼80% of Galactic Plane millisecond pulsars, it has no binary companion. Since rotational energy loss is inversely proportional to the cube of the spin period ($\dot{E} = 4\pi^2 I \dot{P}/P^3$, where $\dot{E}$ is the spin-down luminosity and $\dot{P}$ is the period derivative), it is plausible that a large fraction of the fastest binary pulsars are evading detection because their powerful winds are ablating their companions. Some of the ablated material remains in the vicinity of the system and obscures radio pulsations, particularly at lower radio frequencies. Although we have no detections of the pulsar at other frequencies, several other eclipsing pulsars are observed to have longer eclipse durations at lower radio frequencies (Ransom et al., 2004). If this is also the case for PSR J1748−2446ad, then the unusually high observing frequency used here (2 GHz, while most globular cluster surveys have been conducted at 1.4 GHz or lower) was likely crucial in detecting this pulsar. PSR J1748−2446ad is too weak (the flux density at 1950 MHz is ∼0.08 mJy) to be detectable by the vast majority of Galactic Plane surveys and its high eclipse fraction compounds this problem. This suggests that other even faster-spinning pulsars exist, but will require deeper surveys (perhaps at higher observing frequencies to mitigate obscuration of the pulsar signal by intra-binary material) and more concentrated efforts to be detected. In effect, the isolated nature and very large luminosity of PSR B1937+21 make it a unique object, rather than a representative member of the millisecond pulsar population.

Pulsar	Spin Frequency (Hz)	P_b (days)	$M_{2,\min}$ ($M_\odot$)	Eclipse Fraction	Location
J1748−2446ad	716.358	1.0944	0.14	0.4	Terzan 5
B1937+21	641.931		Isolated		Galaxy
B1957+20	622.123	0.3819	0.021	0.1	Galaxy
J1748−2446O	596.435	0.2595	0.035	0.05	Terzan 5
J1748−2446P	578.496	0.3626	0.37	0.4	Terzan 5
J1843−1113	541.812		Isolated		Galaxy
J0034−0534	532.714	1.5892	0.14	0	Galaxy
J1748−2446Y	488.243	1.17	0.14	0	Terzan 5
J1748−2446V	482.507	0.5036	0.12	0	Terzan 5
B0021−72J	476.048	0.1206	0.020	0.1*	47 Tucanae

Table 5.2: The ten fastest-spinning known radio pulsars. Data compiled from the ATNF pulsar database (Manchester et al., 2005). *B0021−72J is eclipsed only at radio frequencies < 1 GHz.

Low-mass X-ray binaries (LMXBs) with neutron star members are the likely progenitors of the radio millisecond pulsars. As the spin-up time for a neutron star to reach > 1000 Hz rotation via the accretion of matter in an LMXB is much shorter than the typical LMXB lifetime, one might naively expect many millisecond pulsars to be rotating at sub-millisecond periods. However, given the observed lack of pulsars spinning this fast, gravitational radiation has been proposed as a limiting mechanism, as it could be responsible for carrying away rotational kinetic energy from the star, thus spinning it down. Specifically, gravitational waves may be acting either through an accretion-induced mass quadrupole on the crust (Bildsten, 1998), a large toroidal magnetic field (Cutler, 2002), or an r-mode (Rossby wave) instability in the stellar core (Andersson et al., 1999a; Levin & Ushomirsky, 2001).

PSR J1748−2446ad provides interesting constraints on the r-mode possibility. These oscillations are believed to be present in all rotating neutron stars (Andersson, 1998; Friedman & Morsink, 1998). Due to gravitational radiation emission, the r-modes become unstable and grow exponentially. The

amplitude of the mode continues to grow as angular momentum is radiated away, and the star spins down. However, it is unclear whether the driving of these modes by gravitational waves can overcome viscous damping in the star. Damping depends on the core temperature of the star and its spin rate, as well as several other factors including the thickness of the neutron star crust and how it couples to the core. For a given core temperature, it is possible to derive a critical spin frequency above which the proposed mode is unstable and will cause the star to spin down rapidly. It has been predicted that the critical frequency is < 700 Hz for a wide range of core temperature ($10^7 - 10^{10}$ K) and a realistic model of the neutron star crust (Levin & Ushomirsky, 2001). Our discovery of a 716-Hz pulsar indicates that if the r-mode instability limits neutron star spin-up, then either it must become important only at more rapid spin rates or better modelling of the neutron star crust is required. The current upper limit on the frequency derivative of PSR J1748−2446ad is consistent with those measured for other millisecond pulsars, and does not suggest an anomalously rapid spin-down rate. Thus, while there is currently no evidence that PSR J1748−2446ad is spinning down due to gravitational radiation, the possible importance of systems like PSR J1748−2446ad as gravitational wave sources for detectors like LIGO makes improved modelling of neutron star structure and gravitational wave instabilities critically important.

The observed spin frequencies of LMXBs are all less than 620 Hz. The biases that exist at radio wavelengths against finding much faster pulsars do not exist for LMXBs, as X-rays do not suffer from the dispersive effects of the interstellar medium and are less obscured by intra-binary material. This suggests that faster-spinning neutron stars in LMXBs should be detectable if they exist. However, transient coherent pulsations are only observed in seven sources, and there may be unidentified sources of bias in the population that are preventing faster pulsations from being detected. Chakrabarty et al. (2003) performed a Bayesian statistical analysis on the spin frequencies of 11 nuclear-powered millisecond pulsars, those for which the spin frequency is

known from the detection of burst oscillations, and concluded that the sample is consistent (at the 95% confidence level) with a cutoff $\nu_{\rm max} = 760\,{\rm Hz}$. More recent work by the same authors (Chakrabarty, 2005b), which added 2 pulsars to the sample, has revised this limit to 730 Hz. Based on this, they conclude that something, possibly gravitational radiation, is limiting the spin frequency of neutron stars. If their statistically derived upper limit is realistic (and therefore some mechanism is limiting neutron star spin-up), then the 716-Hz pulsar presented here is likely an extremely rare object. However, we note that their Bayesian calculation is very sensitive to the neutron star with the slowest spin frequency included in the analysis. In addition, the assumption made by these authors that the pulsar spin rates are uniform in frequency (at least over some range $\nu_{\rm low}$ to $\nu_{\rm high}$) would likely not apply to the Terzan 5 pulsars, whose spin period distribution is clearly not uniform (Ransom et al., 2005c), even accounting for the observational bias against detecting the fastest pulsars. Hence, a recalculation of the maximum spin cutoff using the Terzan 5 sample of pulsars and the same statistical analysis would not be appropriate, although the existence of PSR J1748−2446ad already implies that the cutoff must be higher.

Chapter 6

A New Candidate Gamma-Ray Pulsar

In this chapter, we switch gears, from searches that target globular clusters to those that target high-energy sources that are potentially also radio pulsars.

The work presented in this chapter originally appeared in: *Roberts, M. S. E., Hessels, J. W. T., Ransom, S. M., Kaspi, V. M., Freire, P. C. C., Crawford, F., & Lorimer, D. R. PSR J2021+3651: A Young Radio Pulsar Coincident with an Unidentified EGRET γ-Ray Source. Astrophysical Journal Letters, 577, L19, 2002.* References to this chapter should be considered references to Roberts et al. (2002) as well.

6.1 Introduction

The majority of high energy γ-ray sources observed by *EGRET* and other telescopes have long escaped identification with lower energy counterparts (Hartman et al., 1999). Young pulsars remain the only Galactic source class (other than the Sun) unambiguously shown to emit radiation in the 100 MeV

– 10 GeV range (Thompson, 2001). It is likely that many of the unidentified γ-ray sources at low Galactic latitudes are young pulsars as well. Many of these sources have characteristics similar to those of the known γ-ray pulsars, but have no known pulsars within their error boxes. This fact, along with modelling of the multi-wavelength pulse profiles and the still singular example of Geminga (Halpern & Holt, 1992; Helfand, 1994), has led to the suggestion that a large fraction of the radio beams from γ-ray sources will miss the Earth and appear radio quiet (Romani, 1996).

Recently, a number of young pulsars coincident with known γ-ray sources have been discovered (D'Amico et al., 2001a; Camilo et al., 2001). These new discoveries are largely a result of greater sensitivity to pulsars with high dispersion measures (DM) obtainable with newer pulsar backends such as the Parkes multibeam system (Manchester et al., 2001). The recent detection of a young radio pulsar in the supernova remnant 3C58 with a 1400 MHz flux density of only ~ 50 μJy (Camilo et al., 2002) suggests many more faint radio pulsars await discovery in deep, targeted searches.

A major stumbling block in the identification of the *EGRET* sources is their large positional uncertainty, which can be greater than 1° across. We approach this problem by targeting potential hard X-ray counterparts, whose size and positional uncertainty are much smaller than the typical single dish radio beam. Using as our guide the *ASCA* catalog of potential X-ray counterparts of GeV sources (based on the Lamb & Macomb (1997) catalog of sources with significant flux above 1 GeV) by Roberts et al. (2001) (hereafter, RRK), we have searched five X-ray sources for radio pulsations using the 305-m Arecibo telescope and the 64-m Parkes telescope (see Table 6.1). Previous searches of these targets were limited. In particular, two of the three sources observed at Parkes (AX J1418.7−6058 and AX J1809.8−2332) were not previously the subject of any directed search and were only observed as a matter of course during the Parkes Multibeam Galactic Plane Survey (Manchester et al., 2001). A survey of *EGRET* sources by Nice & Sayer (1997) looked at two of

the sources searched here (AX J1826.1−1300 and AX J2021.1+3651) with a limiting flux density for slow pulsars of 0.5 – 1.0 mJy at frequencies of 370 and 1390 MHz, but found no new pulsars. Our search has led to the discovery of one young and energetic pulsar, PSR J2021+3658. We argue that it is a likely counterpart to AX J2021.1+3651 and GeV J2020+3658 / 2CG 075+00.

6.2 Observations and Analysis

On 2002 January 30 and 31, we observed the only two unidentified sources in the RRK catalog visible from the Arecibo radio telescope, AX J1907.4+0549 and AX J2021.1+3651, using the Wideband Arecibo Pulsar Processor (WAPP). The WAPP is a fast-dump digital correlator with adjustable bandwidth (50 or 100 MHz) and variable numbers of lags and sample times (for details see Dowd, Sisk, & Hagen 2000). Our observations were made at 1.4 GHz with 100 MHz of bandwidth and summed polarizations. The observational parameters are summarized in Table 6.1. The 16-bit samples were written to a disk array and then transfered to magnetic tape for later analysis.

On 2001 February 11−15, the three extended hard X-ray sources listed by RRK as potential pulsar wind nebulae, AX J1418.7−6058 (the Rabbit), AX J1809.8−2333, and AX J1826.1−1300, were searched for radio pulsations with the Multibeam receiver on the Parkes radio telescope. Each source was observed once at a central observing frequency of 1390 MHz with a 512 channel filterbank spectrometer covering 256 MHz of bandwith, and once at a central observing frequency of 1373 MHz with 96 channels and 288 MHz of bandwith (see Table 6.1). During each observation, signals from each channel were square-law detected and added in polarization pairs before undergoing high-pass filtering. The signals were one-bit digitized every 0.25 ms and recorded onto magnetic tape for later analysis.

Analysis of Arecibo observations was done using the PRESTO software

Source Name	RA (J2000) hh:mm:ss.s	DEC (J2000) dd:mm:ss	Epoch (MJD)	Telescope	ν_c^a (MHz)	$\Delta\nu^b$ (MHz)	N_{ch}^c	t_{sam}^d (μs)	T_{int}^e (s)	S_{min}^f (mJy)
AX J1418.7−6058 / GeV J1417−6100	14:18:41.5	−60:58:11	51951.63	Parkes	1390	256	512	250	16900	0.08
			51953.67	Parkes	1373	288	96	250	16900	0.08
AX J1809.8−2332 / GeV J1809−2327	18:09:50.2	−23:32:23	51951.83	Parkes	1390	256	512	250	16900	0.08
			51954.77	Parkes	1373	288	96	250	16900	0.08
AX J1826.1−1300 / GeV J1825−1310	18:26:04.9	−12:59:48	51952.83	Parkes	1390	256	512	250	13234	0.09
			51955.83	Parkes	1373	288	96	250	14832	0.09
AX J1907.4+0549 / GeV J1907+0557	19:07:21.3	+05:49:14	52305.58	Arecibo	1425	100	512	200	6480	0.02
AX J2021.1+3651 / GeV J2020+3658	20:21:07.8	+36:51:19	52304.67	Arecibo	1425	100	512	200	1627	0.04
			52305.66	Arecibo	1425	100	256	200	3000	0.03

Table 6.1: Observational Parameters

[a] Central observing frequency.

[b] Total bandwidth of the observation.

[c] Number of frequency channels.

[d] Sampling time.

[e] Length of the observation.

[f] Flux density sensitivity limit.

suite (Ransom, 2001)[1] by first removing obvious narrow band and/or short duration interference in both the time and frequency domains. We then dedispersed the data at 500 trial DMs between 10 and 510 pc cm^{-3} for AX J2021.1+3651 and 540 trial DMs between 0 and 2695 pc cm^{-3} for AX J1907.4+0549. Employing harmonic summing, the FFTs of each time series were searched, and interesting candidates were folded over a fine grid in DM, period, and period derivative space to optimize the signal-to-noise ratio.

The Parkes observations were analyzed using fvlsa/i (available from the ATNF) and a similar procedure by searching the 96 channel data at 279 trial DMs ranging from 0 to 1477 pc cm^{-3} and the 512 channel data at 501 trial DMs ranging from 0 to 670 pc cm^{-3}. We tested the system by observing a known bright pulsar (PSR B1124−60) for 300 s, which was clearly detected in the processing. Re-analysis of the data using PRESTO has not revealed any new candidates.

6.3 Results

A new highly dispersed 104-ms pulsar was detected in the Arecibo observations made of AX J2021.1+3651; it is clearly visible in both of the original search observations, and represents a $\sim 40\ \sigma$ detection in the longest observation. The pulse profile is shown in Figure 6.1.

A subsequent series of 7 observations performed between MJD 52405−52416 allowed us to determine a phase connected solution for some of the pulsar parameters. Integrated pulse profiles from these observations were convolved with a template profile to extract 12 topocentric times of arrival (TOA). Using TEMPO[2] and adopting the ROSAT position for the pulsar (§6.4.1), the topocentric TOAs were converted to TOAs at the solar system barycentre at infinite frequency and fit simultaneously for pulsar period, period derivative,

[1]See http://www.physics.mcgill.ca/~ransom.
[2]See http://pulsar.princeton.edu/tempo.

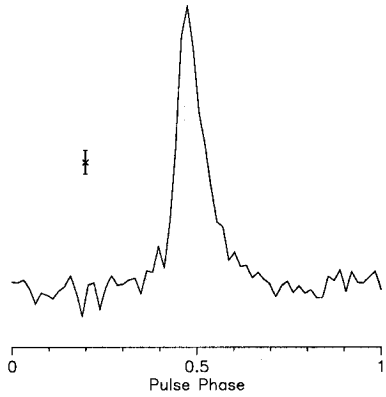

Figure 6.1: 1.4 GHz Pulse profile for PSR J2021+3651 from the MJD 52305 observation. The error bar represents the 1 σ uncertainty.

and DM, with a residual rms of 91 μs. The measured and derived parameters for this pulsar are listed in Table 6.3. If the X-ray source is not related to the pulsar, an error in position of up to 1/2 the Arecibo beam width of 3' will cause an inaccurate $\dot{P}$ with an error of approximately same magnitude as the TEMPO errors reported in Table 2. If the positional error is much smaller (i.e. the error of the ROSAT position, assuming it is the X-ray counterpart), the $\dot{P}$ error is dominated by statistical effects and the quoted TEMPO errors should apply.

No convincing pulsar candidates were detected in any of the search observations conducted at Parkes. We estimate upper limits of $S \cong 0.08$ mJy at 1.4 GHz for pulse periods $P \gtrsim 10$ ms for most of the 512 channel observations. A comparable sensitivity was obtained for long periods in the 96 channel observations. For DMs larger than about 100 pc cm^{-3}, the sensitivity to fast pulsars (P $\lesssim$ 50 ms) is significantly degraded in the 96 channel system. These sensitivity limits were estimated using a sensitivity modelling technique described in detail elsewhere (e.g., Manchester et al. 2001). Likewise, extensive searching of AX J1907.4+0549 yielded no convincing pulsar candidates. We estimate an upper limit of $S \simeq 0.02$ mJy at 1.4 GHz for a long-period pulsar

Parameter	Value
Right ascension α (J2000)	$20^{\rm h}\ 21^{\rm m}04^{\rm s}.5^{a}$
Declination δ (J2000)	$+36°\ 51'\ 27''.0^{a}$
Galactic longitude l	75.°23
Galactic latitude b	+0.°11
Pulse period P (s)	0.10372222480(17)
Period derivative $\dot{P}$	$9.563(48) \times 10^{-14}$
Pulse frequency ν (s^{-1})	9.641135271(16)
Frequency derivative $\dot{\nu}$ (s^{-2})	$-8.889(45) \times 10^{-12}$
Epoch (MJD)	52407.389
Dispersion Measure DM (pc cm^{-3})	371.2(3.2)
Pulse width at 50% of peak w_{50} (ms)	9.9
Pulse width at 10% of peak w_{10} (ms)	18
Flux density at 1425 MHz (mJy)	~ 0.1
Spin-down luminosity $\dot{E}^{b}$ (erg s^{-1})	3.4×10^{36}
Surface dipole magnetic field B^{c} (G)	3.2×10^{12}
Characteristic Age $\tau_c \equiv \frac{1}{2}P/\dot{P}$ (kyr)	17

Table 6.2: Measured and Derived Parameters for PSR J2021+3651.

[a] Coordinates of the *ROSAT* X-ray source 1RXS J202104.5+365127 with estimated positional error of 24″.
[b] $\dot{E} = 4\pi^2 I \dot{P}/P^3$ with $I = 10^{45}$ g cm^2.
[c] Assuming standard magnetic dipole spindown: $B = 3.2 \times 10^{19}(P\dot{P})^{1/2}$ Gauss (Lorimer & Kramer, 2004).
Note - Figures in parentheses represent uncertainty in the least-significant digits quoted equal to 3 times errors given by TEMPO.

assuming a 10% duty cycle.

6.4 Discussion

6.4.1 PSR J2021+3651

Our search targeted AX J2021.1+3651, which was identified as a potential high-energy counterpart to GeV J2020+3658 by RRK. The X-ray source is near the *ASCA* field edge and so the positional uncertainty from *ASCA* is $\gtrsim 1'$ (Gotthelf et al., 2000). A subsequent search of the *ROSAT* All-Sky Survey Faint Source catalog (Voges et al., 2000) revealed the source 1RXS J202104.5+365127 with a smaller positional error of $24''$. Given the rarity of such young, energetic pulsars and the small size of the Arecibo beam ($3'$ at full width at half-maximum), an association with the X-ray source is highly probable.

The DM of PSR J2021+3651 is by far the highest known in the Galactic longitude range $55° < l < 80°$ which is mainly an inter-spiral arm direction. Using the recent Cordes & Lazio (2002b) update to the Taylor & Cordes (1993) dispersion measure model gives a distance of $\sim$ 12.4 kpc, at the outer edge of the last spiral arm used in the model. It is possible that there are further contributions from clouds in the Cygnus region not included in the model, where there is known to be excess gas at $d \sim 1.5$ kpc (J. Cordes, private communication), however, there are no obvious HII regions within the Arecibo beam seen in either Very Large Array (VLA) 20-cm radio or Midcourse Space Experiment (MSX) 8.3 μm images (available from the NASA/IPAC Infrared Science Archive).

The high DM is somewhat surprising given the X-ray absorption quoted by RRK, $n_H=(5.0\pm0.25) \times 10^{21}$ cm^{-2}, where the errors represent the 90% confidence region. The total Galactic HI column density in this direction as estimated from the FTOOL nh, which uses the HI map of Dickey & Lockman

(1990), is 1.2×10^{22} cm^{-2}. This should be a good approximation if the source is truly at the far edge of the outer spiral arm. Noting that the *ASCA* image shows faint, softer emission in the region (Figure 6.2), and given the likely possibility of either associated thermal X-ray flux from a supernova remnant or a nearby massive star, we fit the *ASCA* spectrum of RRK, adding a thermal component to the absorbed power-law model. Accounting for $\sim 4\%$ of the photon flux with a MEKAL thermal plasma model of temperature $kT \sim 0.1$ keV in XSPEC (Arnaud, 1996) statistically improves the fit (F-test chance probability of 2.5%). The best-fit absorption for this three component model is n_H=7.6×10^{21} cm^{-2} with a 90% confidence region of (4.1 – 12.3)×10^{21} cm^{-2}, consistent with the total Galactic column density. The best-fit photon index is $\Gamma = 1.86$, still consistent with the 1.47 – 2.01 range in RRK derived from the simple absorbed power-law model. Hence the X-ray absorption does not force us to adopt a smaller distance than is suggested by the DM.

For a distance $d_{10} = d/10$ kpc, the inferred isotropic X-ray luminosity $L_X = 4.8 \times 10^{34} d_{10}^2$ (2 – 10 keV). The X-ray efficiency $\eta_X = L_X/\dot{E}$ is $0.01 d_{10}^2$. Compared to the total pulsar plus nebula X-ray luminosity of other spin-powered pulsars this is somewhat high, but within the observed scatter (Possenti et al., 2002; Chevalier, 2000).

The pulsar's positional coincidence with the error box of the hard spectrum, low variability *EGRET* γ-ray source GeV J2020+3658 coupled with the high inferred spin-down luminosity strongly suggests this pulsar emits pulsed γ-rays. Unfortunately, confirming this by folding archival *EGRET* data is problematic due to the likelihood of significant past timing noise and glitches, which make the back-extrapolation of the rotational ephemeris uncertain. RRK noted that the chance probability of an X-ray source as bright as AX J2021.1+3651 in the *EGRET* error box was $\sim 10\%$, but the nearby Wolf-Rayet star WR141 was equally bright in X-rays and also a potential γ-ray emitter. However, young pulsars remain the only firmly established class of Galactic *EGRET* sources. The known γ-ray pulsars cluster at the top of pulsar lists rank-ordered by

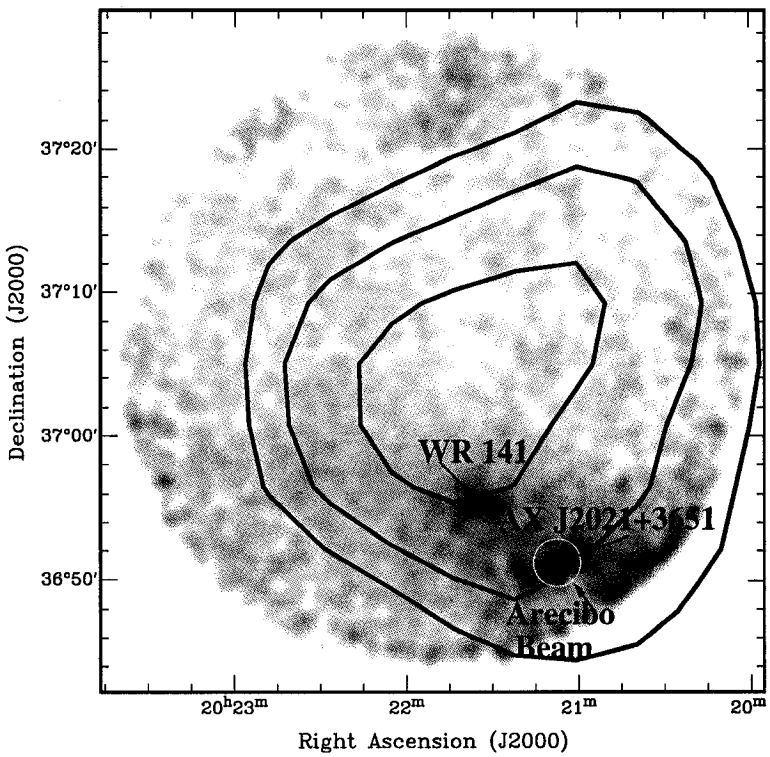

Figure 6.2: ASCA GIS 2-10 keV image of the γ-ray source region. The contours are the 68%, 95%, and 99% confidence regions of the γ-ray source position, derived from the > 1 GeV photons (Roberts et al., 2001). WR 141 is a Wolf-Rayet star also in the field of view. The circle centred on AX J2021.1+3651 indicates the size of the 3′ Arecibo beam.

spin-down flux $\dot{E}/d^2$, with γ-ray efficiencies $\eta_\gamma = L_\gamma/\dot{E}$ mostly between 0.001 and 0.03 (assuming 1 sr beaming) with a tendency to increase with pulsar age (Thompson et al., 1999). The exception is PSR B1055−52, with an apparent γ-ray efficiency $\eta_\gamma \sim 0.2$ given its nominal DM distance of 1.5 kpc. The inferred γ-ray efficiency for PSR J2021+3651 is $\eta_\gamma = 0.15 d_{10}^2$ in the 100 MeV to 10 GeV range. If the pulsar is located within the Perseus arm at a distance of 5 kpc, then the inferred X-ray and γ-ray luminosities would be fairly typical of the other pulsars with Vela-like spin-down luminosities. While there is currently no observational evidence for a distance this close, increased DM from an intervening source in this relatively crowded direction would not be surprising. We note that the DM derived distance for another young pulsar recently discovered within an *EGRET* error box, PSR J2229+6114, also leads to an anomalously high inferred γ-ray efficiency (Halpern et al., 2001).

6.4.2 Upper Limits Toward the Other Sources

Determining the fraction of radio-quiet versus radio-loud pulsars is important for our understanding of γ-ray pulsar emission mechanisms. The two leading classes of emission models, the outer-gap (Romani, 1996) and polar-cap (Daugherty & Harding, 1996) models, make very different estimates of the fraction of γ-ray pulsars that should be seen at radio energies. Out of the 25 brightest sources above 1 GeV not associated with blazars, $\sim$ 10 are now known to either be energetic radio pulsars or contain such pulsars within their error boxes. Searching the brightest unidentified X-ray sources in five GeV error boxes, we detected radio pulsations at the $\sim$ 0.1 mJy level from one of these with Arecibo; this flux density is similar to the limiting sensitivity of the Parkes observations. This is well below the average flux level expected for typical radio luminosities of young pulsars (Brazier & Johnston, 1999) and distances to star forming regions statistically associated with γ-ray sources (Yadigaroglu & Romani, 1997). Two of the sources observed with Parkes, AX J1418.7−6058 (the Rabbit) and AX J1809.8−2333, have radio and X-ray prop-

erties that clearly identify them as pulsar wind nebulae (Roberts et al., 1999; Braje et al., 2002), and the third, AX J1826.1−1300, is an extended hard X-ray source that has few other source class options. Therefore, all three remain viable candidates for γ-ray loud, radio-quiet pulsars. Out of this same sample of 25 bright GeV sources, the total number of reasonable candidate neutron stars within the γ-ray error boxes which have now been searched deeply for radio-pulsations without success is ~ 7. A current "best guess" fraction of radio-loud γ-ray pulsars of $\sim 1/2$ falls in between the predictions of the two main competing models.

Chapter 7

Discovery of an X-ray Pulsar Wind Nebula Associated with PSR J2021+3651

The discovery of PSR 2021+3651, and its likely association with high-energy sources, motivated us to conduct follow-up X-ray imaging, spectroscopy, and timing of this source. In this chapter, we present these observations.

The work presented in this chapter originally appeared in: *Hessels, J. W. T., Roberts, M. S. E., Ransom, S. M., Kaspi, V. M., Romani, R. W., Ng, C-Y, Freire, P. C. C., & Gaensler, B. M. Observations of PSR J2021+3651 and its X-Ray Pulsar Wind Nebula G75.2+0.1. Astrophysical Journal, 612, 389, 2004.* References to this chapter should be considered references to Hessels et al. (2004) as well.

7.1 Introduction

Pulsar wind nebulae (PWNe) allow us to study the basic energetic processes of young, rotation-powered pulsars. It is still unclear how the rotational kinetic energy of these objects is converted into a relativistic particle outflow. The *Chandra X-ray Observatory*'s unprecedented spatial resolution has revealed that the winds from young, energetic pulsars can lead to highly structured PWNe. In some cases these PWNe take the form of an equatorial outflow with polar jets, where the best example of this is the Crab nebula (Weisskopf et al., 2000). These torus plus jet nebulae, of which there are roughly a half-dozen examples, are particularly interesting because a) they allow us to study the interaction of the PWN with its surrounding environment (the location of the bright torus is generally believed to mark the inner termination shock of the pulsar wind) and b) the well-defined morphology of the PWN can constrain the geometry of the pulsar. This is crucial for testing models of high-energy pulsations, such as the outer-gap model (e.g. Romani, 1996) and the polar-cap model (e.g. Daugherty & Harding, 1996).

PSR J2021+3651 (spin period P ~103.7 ms, dispersion measure DM ~369 pc cm^{-3}, and flux density at 1400 MHz S_{1400} ~100 μJy) was discovered by Roberts et al. (2002) with the 305-m Arecibo radio telescope during a targeted search for radio pulsations from X-ray sources proposed as counterparts to unidentified EGRET γ-ray sources (Roberts, Romani, & Kawai, 2001). Timing observations of PSR J2021+3651 revealed that although it is dim, it is young and energetic (characteristic age $\tau_c \equiv P/2\dot{P} = 17$ kyr and spin-down energy $\dot{E} \equiv 4\pi^2 I\dot{P}/P^3 = 3.6 \times 10^{36}$ ergs s^{-1}, assuming moment of inertia $I = 10^{45}$ g cm^2) and a likely counterpart to the *ASCA* X-ray source AX J2021.1+3651 and the EGRET γ-ray source GeV J2020+3658. This discovery bolsters the idea that many of the Galactic unidentified EGRET sources (see Hartman et al., 1999) are young energetic pulsars that were not detected in large-scale radio pulsar surveys.

While the spin properties of PSR J2021+3651 are very similar to those of the known γ-ray pulsars Vela (PSR B0833−45, $P = 89.3$ ms, $\dot{E} = 6.9\times10^{36}$ ergs s^{-1}) and PSR B1706−44 ($P = 102.5$ ms, $\dot{E} = 3.4 \times 10^{36}$ ergs s^{-1}), the 12 kpc distance inferred from its DM using the NE2001 electron model of the Galaxy (Cordes & Lazio, 2002b) places is on the far edge of the outer spiral arm used in this model and would make it much more γ-ray efficient than either Vela or PSR B1706−44. In fact, it would have to be even more γ-ray efficient than the much-less energetic γ-ray pulsars Geminga and PSR B1055−52 (assuming the NE2001 DM distance to PSR B1055−52 of 0.72 kpc). This is contrary to the observation that γ-ray efficiency $\eta_\gamma \equiv L_\gamma/\dot{E}$ increases with age (Thompson et al., 1999) and the theoretical expectation that it is inversely proportional to the square-root of the spin-down luminosity ($\eta_\gamma \propto \dot{E}^{-1/2}$, e.g. Zhang & Harding, 2000). However, since DM distances can be off by a factor of a few, PSR J2021+3651 may be significantly closer (or farther) than its DM implies.

The similarity of PSR J2021+3651 to the Vela pulsar, which is surrounded by a highly-structured pulsar wind nebula (see Helfand, Gotthelf, & Halpern, 2001), prompted us to make X-ray observations of the area surrounding PSR J2021+3651. Only ∼30 of the >1300 known pulsars in the Galaxy are Vela-like (i.e. with $P \sim 100$ ms, $\dot{E} \sim 10^{36} - 10^{37}$ ergs s^{-1}, and characteristic ages τ_c ∼10−20 kyr, see Kramer et al., 2003). Here we present the results of X-ray observations made with the *Chandra* ACIS-S detector. These observations resolve the *ASCA* source into a new PWN, which we name G75.2+0.1, and a thermally emitting point source, likely the neutron-star surface. *Chandra* observations in continuous-clocking mode show a potential detection of X-ray pulsations from PSR J2021+3651. We also present radio timing observations made with the Arecibo telescope, which show that PSR J2021+3651 has glitched and is highly scattered.

7.2 X-ray Observations

7.2.1 X-ray Imaging

We made *Chandra* observations with the ACIS-S detector in VFAINT mode on 2003 February 12 to image PSR J2021+3651 and its surrounding region. To reduce CCD photon pile-up from a potentially bright point source, a quarter sub-array was used. These data were analyzed using CIAO[1] version 3.0.1 and CALDB 2.3. Filtering for good time intervals and accounting for dead-time resulted in a total integration time of 19.0 ks. We subtracted particle background from the image using a 100-ks combination of two ACIS-stowed images from 2002 Sept and 2003 May[2] and then corrected for the different exposure over the chip. The resulting image is shown in Figure 7.1.

This image reveals a point source embedded in an axisymmetric inner nebula $\sim 20'' \times 10''$ across, surrounded by fainter diffuse emission. We refer to this obvious PWN as G75.2+0.1. The point source is at right ascension $20^h21^m05^s.47$ and declination $+36°51'04''.7$ (J2000). We estimate a positional error of $\lesssim 0.5''$ by comparing the position of another bright X-ray point source on the S3 chip (J2000 coordinates: RA $20^h20^m43^s.08$, DEC $+36°49'32''.8$) with the optical point source USNO−B1.0 1268−0448692 (for details on this catalogue see Monet et al., 2003), which is almost certainly the optical counterpart to this other point source. Subtracting the nebular background, the point source has a count rate of 0.0087 ± 0.0008 counts s^{-1} and the nebula has a background-subtracted count rate of 0.080 ± 0.003 counts s^{-1} in the 0.5−10.0 keV range.

The greyscale of Figure 7.1 shows the image smoothed with a $1.2''$ (FWHM) gaussian to bring out the fine structure of the inner nebula. The white contours indicate the position of the point source and are shown to distinguish it from the bright bar running along the axis of the nebula. This bar is the most

[1]See http://cxc.harvard.edu/ciao.
[2]See http://cxc.harvard.edu/contrib/maxim/acisbg.

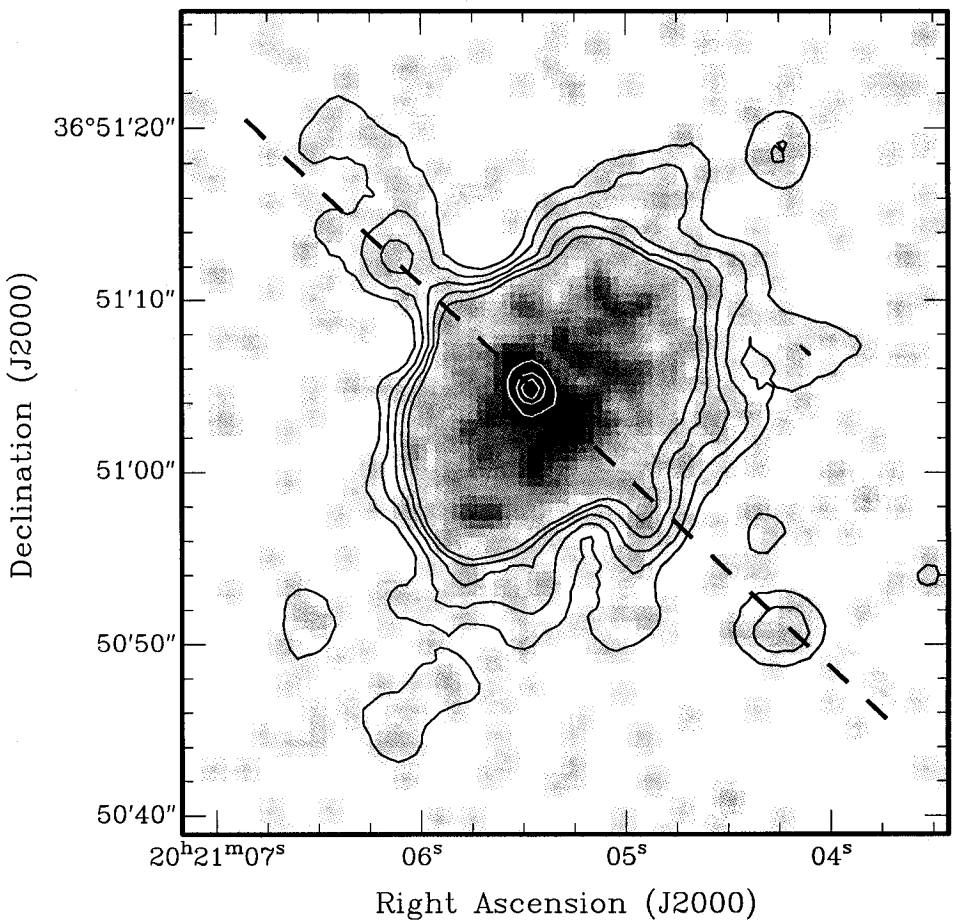

Figure 7.1: A 19.0-ks *Chandra* ACIS-S image (0.3–7.0 keV) of PSR J2021+3651 and its inner nebula. The greyscale shows the image smoothed with a 1.2″ (FWHM) gaussian and scaled to bring out fine structure in the nebula. The black contours are the same image overlaid, but smoothed with a 3.5″ gaussian and scaled to bring out faint extended emission including what may possibly be faint jets along the axis of the nebula. The white contours indicate the point source and are shown to distinguish it from the bright bar running along the axis of the nebula. The dashed line shows the best-fit position angle $\Psi = 47° \pm 1°$ of the torus fit (see §7.4.4), which in analogy with the Crab pulsar and nebula likely corresponds to the projected spin axis of the pulsar.

obvious resolved feature of the nebula. Also overlaid are black contours of the same image smoothed with a 3.5″ gaussian and scaled to bring out what are possibly faint jets along the axis of the nebula. We estimate 62±32 counts may be coming from these putative jets. The nebula appears symmetric about the minor axis, but the point source is clearly offset from the major axis of the nebula. The overall morphology is suggestive of the torus plus weak jet morphologies of the Crab and (likely) Vela nebulae (Weisskopf et al., 2000; Helfand et al., 2001). We discuss the geometry of the PWN further in §7.4.4.

7.2.2 X-ray Spectroscopy

The spectra of the PWN and point source can be measured individually using *Chandra's* excellent spatial resolution. We fit the spectrum of the nebula and point source using CIAO's *Sherpa* environment (version 3.0.1) and XSPEC (version 11.2.0). To isolate the nebula, we used a circular annulus centred on the point source and extending from a radius of 1.6−100 pixels (0.492″ × 0.492″ per pixel) and a circular region from an apparently flux-free area of the S3 chip to estimate the background. We find that the nebula has a hard spectrum (see Figure 7.2) that is well fit (reduced ${\chi_\nu}^2 = 1.1$ for 27 degrees of freedom) by an absorbed power-law model with hydrogen column density $n_H = (7.8^{+1.7}_{-1.4}) \times 10^{21}$ cm^{-2}, photon index $\Gamma = 1.7^{+0.3}_{-0.2}$, and a 0.5−10 keV absorbed flux of $(1.2\pm0.1)\times10^{-12}$ erg cm^{-2} s^{-1} (90% confidence intervals). The best-fit black-body model gives reduced ${\chi_\nu}^2 = 2.3$ for 27 degrees of freedom, a comparatively poor fit to the data.

To isolate the point source, we used a circular extraction region of radius 1.6 pixels, and a surrounding annulus of width 3.4 pixels to subtract the nebular background. Because the wings of the energy dependent PSF extend past 1.6 pixels, we corrected for this by using "mkpsf" to generate model PSFs at several energies between 0.5−6 keV from which we estimated the source minus background enclosed energy fraction. We then fit a linear function to these points which we used to correct the effective area model used in the spectral

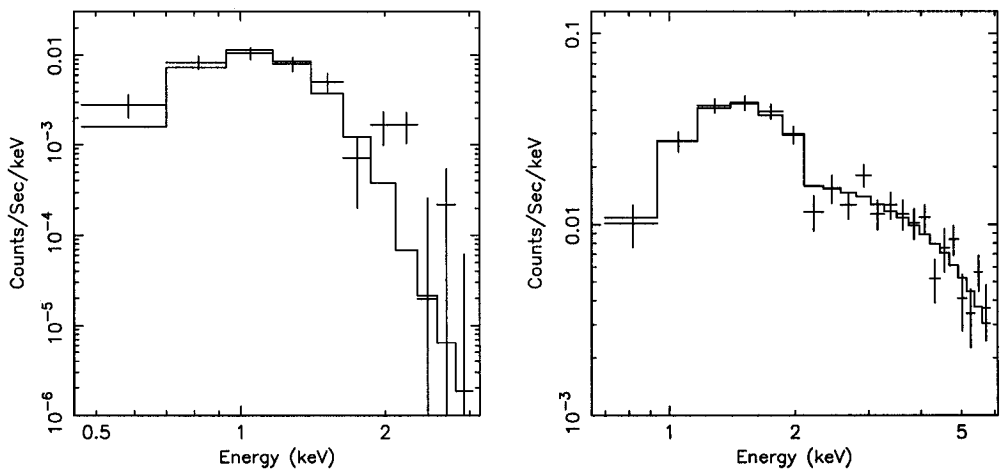

Figure 7.2: *Left*: The background-subtracted spectrum of the point source, fit using an absorbed black-body model. The best-fit temperature and 90% confidence interval is $kT_\infty = 0.15 \pm 0.02\,\mathrm{keV}$ with a 0.5–10.0 keV absorbed flux of $(2.8 \pm 0.2) \times 10^{-14}$ erg cm^{-2} s^{-1}. The n_H was fixed at 7.8×10^{21} cm^{-2}, that found by fitting the nebular spectrum. The energy channels were grouped into bins of 16 channels each. *Right*: The background-subtracted spectrum of the nebula fit with an absorbed power-law model. The best-fit parameters and 90% confidence intervals are $n_H = (7.8^{+1.7}_{-1.4}) \times 10^{21}$ cm^{-2}, $\Gamma = 1.7^{+0.3}_{-0.2}$, and an absorbed flux of $(1.2 \pm 0.1) \times 10^{-12}$ erg cm^{-2} s^{-1} (0.5–10.0 keV). The energy channels were grouped into bins of 16 channels each.

fit. Based on the observed count rate, we estimate a negligible pile-up fraction of ~0.6% using HEASARC's webPIMMs tool[3]. We find that there is very little emission from the point source above 3 keV. Its spectrum is adequately fit (reduced $\chi_\nu{}^2 = 1.7$ for 9 degrees of freedom) by an absorbed black-body model, where we have fixed n_H to the value obtained by fitting the PWN's spectrum. The best-fit black-body model and 90% confidence region is $kT_\infty = 0.15 \pm 0.02$ keV with an absorbed flux of $(2.8 \pm 0.2) \times 10^{-14}$ erg cm^{-2} s^{-1} (0.5–10.0 keV). Since kT_∞ and n_H are highly covariant, we also made a joint fit of an absorbed black body for the pulsar and an absorbed power law for the nebula, tying the n_H of both models together. This gave values and errors that were essentially the same as those from the individual fits. Since we expect non-thermal emission from the magnetosphere of the pulsar, we also fit a black-body plus power-law model to the point source, fixing the photon index at a typical value of 1.5 (there are not enough high energy counts to allow the photon index to be a free parameter in the fit). This did not improve the fit (reduced $\chi_\nu{}^2 = 1.8$ for 7 degrees of freedom), but the temperature and flux of the black-body component were left relatively unchanged. This suggests a maximum non-thermal absorbed flux of $\sim 3 \times 10^{-14}$ erg cm^{-2} s^{-1} (0.5–10.0 keV).

The total flux measured here is a factor of four smaller than seen by *ASCA* (Roberts et al., 2001, 2002). We note that the *ASCA* extraction region has a radius of ~4′, and thus includes areas well outside the 2′-wide field of view of the quarter array used here. A highly smoothed image of the *Chandra* data suggests there may be additional diffuse emission that could extend well beyond the chip. Furthermore, examination of the *ASCA* image suggests there may be additional point sources or structures within the *ASCA* extraction region that are not within the *Chandra* field of view. However, despite the flux discrepancy, the derived n_H, nebular photon index and point source kT_∞ are consistent with the *ASCA* measurements of the source.

[3]See http://heasarc.gsfc.nasa.gov/Tools/w3pimms.html.

7.2.3 X-ray Pulsations

To search for X-ray pulsations from PSR J2021+3651, we also obtained *Chandra* ACIS-S data in continuous-clocking mode, which provides an effective time resolution of 2.85 ms by sacrificing one dimension of spatial resolution. The roll angle of the telescope placed the 1 dimensional image at an angle of ~62° (N-E). The events were filtered for good time intervals and periods of high background, leaving 20.8 ks of integration time. We corrected the read-out times to intrumental times of arrival by removing telescope dither, motion of the detector with respect to the telescope, and the average lag between the readout time and the true times of arrival of the photons. The events were then barycentred using the JPL DE405 ephemeris (Standish, 1998). Given prior knowledge of the point-source spectrum from our imaging observations, we produced an event list with a 0.5−3 keV energy cut and a 3-pixel-radius extraction region. We also produced event lists for a number of other energy cuts and a range of extraction regions. The event lists were folded at the predicted spin frequency of 9.64094861 Hz according to the contemporaneous radio timing ephemeris (see §7.3), which revealed a likely periodic signal (see Figure 7.3). Performing an H-test (De Jager et al., 1989), using *unbinned* events, we find an H-test score of h ~11.7, which corresponds to a chance probability of 8.9×10^{-5} for a single trial. This has an equivalent Gaussian sigma of $3.7\,\sigma$. Searching to a maximum harmonic of 20, the H-test finds the largest significance when two harmonics are summed.

Although this signal is not a certain detection of pulsations from PSR J2021+3651, it is intriguing. If real, these pulsations indicate a pulsed fraction of ~65%, where we define pulse fraction to be the ratio of the number of counts above the 1-σ upper limit on the lowest bin in the light curve (see Figure 7.3) to the total number of background-subtracted counts (in this case, most of the background is from the nebula). From the point source count-rate of our imaging observations, we estimate that ~190 of the counts in the light curve are from the pulsar and that the rest are from the nebula and other

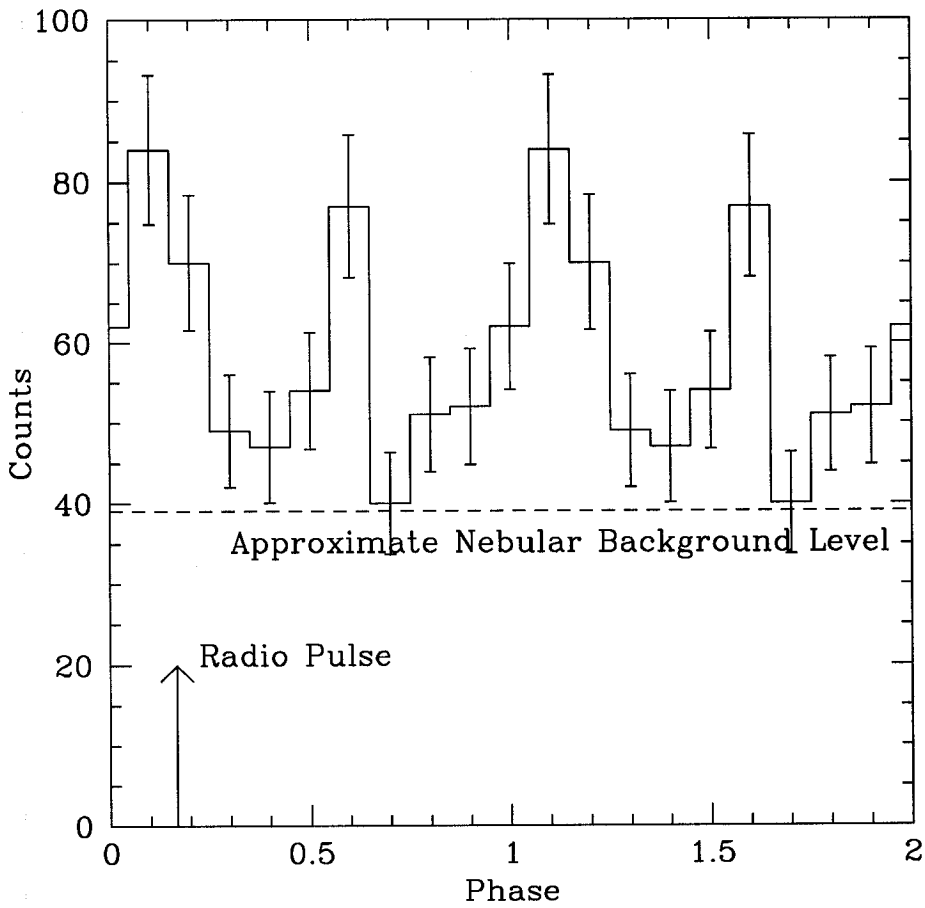

Figure 7.3: *Chandra* continuous clocking data of PSR J2021+3651 folded using a local radio ephemeris for the pulsar. Two cycles are plotted for clarity and there are ten bins across the profile. The phase of the radio pulse is indicated by an arrow. The dashed line indicates the approximate background level. Based on this, there are ~120 pulsed counts and we estimate that ~190 counts are from the pulsar. This gives a pulsed fraction of ~65%.

background. We discuss the pulse shape in §7.4.2.

7.3 Radio Timing

Since the discovery of PSR J2021+3651 in 2002 February, we have been making roughly monthly radio timing observations of the pulsar at 20 cm using the Arecibo radio telescope and multiple Wideband Arecibo Pulsar Processor digital correlator backends (WAPPs, for details see Dowd, Sisk, & Hagen 2000). Each WAPP was configured for 100 MHz of bandwidth, with 512 lags and 200 μs samples. Whenever possible, we used three WAPP backends, typically centred at 1170, 1420, and 1520 MHz. PSR J2021+3651 is significantly scattered (see Figure 7.4). Fitting the profiles with a gaussian convolved with a one-sided exponential ($e^{-t/\tau_{sc}}$) we find a frequency dependence of τ_{sc} that is well fit by a power law of index -4.2 ± 0.6. This is consistent with a pure Komolgorov spectrum (i.e. $\tau_{sc} \propto \nu^{-4.4}$, see Rickett, 1977). Using the measured frequency dependence, we find $\tau_{sc} = 17.7 \pm 0.9$ ms at 1 GHz (90% confidence).

Pulse profiles from each epoch were cross-correlated with a representative high signal-to-noise template to generate times of arrival (TOAs). Using TEMPO[4] we fit these TOAs to a multi-parameter rotational model of the pulsar. The position of the pulsar was fixed at the *Chandra* X-ray position. Our timing analysis reveals that a glitch occured between MJDs 52616 and 52645. We can connect phase across it by fitting an instantaneous jump in frequency and frequency derivative ($\Delta\nu/\nu = 2.587 \pm 0.002 \times 10^{-6}$ and $\Delta\dot{\nu}/\dot{\nu} = 6.2 \pm 0.3 \times 10^{-3}$), which are comparable to those seen in the largest glitches of the Vela pulsar (Dodson et al., 2002). There is only marginal evidence for a glitch decay in the data, which is not surprising given that the typical timescale for such a decay is on the order of days to weeks (Dodson et al., 2002) and is therefore not resolved by our sparse monitoring. The pre- and post-glitch rotational ephemerides of PSR J2021+3651 and the complete

[4]See http://www.pulsar.princeton.edu/tempo.

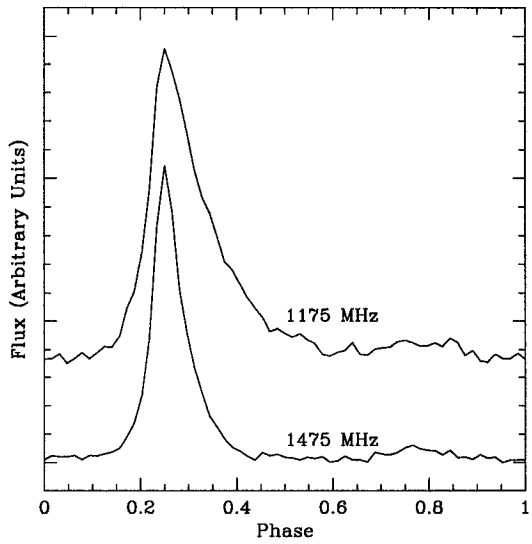

Figure 7.4: Summed pulse profiles of PSR J2021+3651 at centre frequencies of 1175 MHz (top) and 1475 MHz (bottom). The peak fluxes of the two profiles are normalized and the pulse phases aligned at the pulse peak. By fitting the profiles to a gaussian convolved with an exponential we calculate a scattering time $\tau_{sc} = 17.7 \pm 0.9$ ms at 1 GHz.

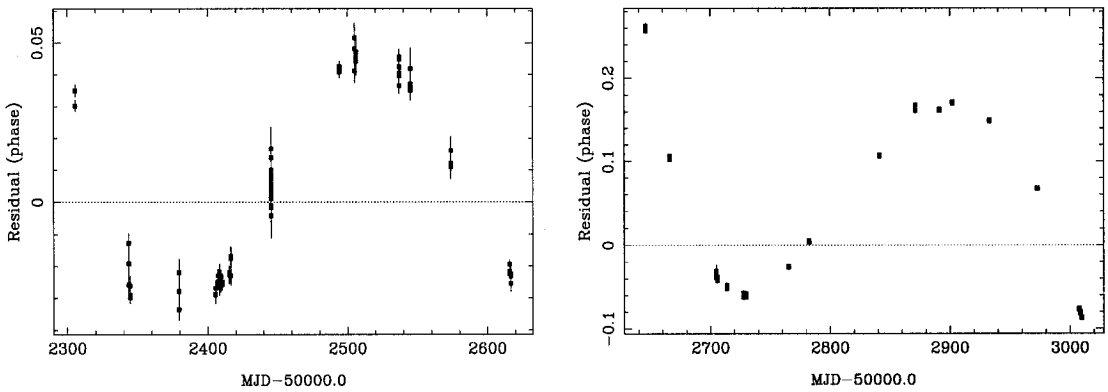

Figure 7.5: Residuals from phase-coherent timing of PSR J2021+3651 fitting only for period and the first period derivative. The residuals can be rendered featureless by fitting for a period second derivative. Alternately, the residuals can be rendered featureless by fitting for position (instead of keeping it fixed at the X-ray position). However, the fitted positions from the pre- and post-fit ephemerides are inconsistent suggesting that timing noise dominates the residuals, rather than an incorrect position. *Left:* pre-glitch residuals. *Right:* post-glitch residuals.

set of glitch parameters are presented in Table 1, along with derived quantities.

The post-fit timing residuals show significant systematics when only the frequency and first frequency derivative are fit (see Figure 7.5). We find that the residuals can be rendered featureless by including a frequency second and third derivative into the fit. Alternately, the residuals can be rendered featureless by allowing TEMPO to fit for position. However, the pre-, post-glitch, and *Chandra* positions are inconsistent, suggesting that timing noise dominates the residuals rather than an incorrect position.

Parameter	Value
Right ascension (J2000.0)[a]	$20^h21^m05^s.46(4)$
Declination (J2000.0)[a]	$+36°51'04''.8(5)$
Galactic longitude l (deg)[a]	75.23
Galactic latitude b (deg)[a]	+0.11
DM (pc cm^{-3})	369.2(2)
Preglitch	
Pulse frequency ν (s^{-1})	9.64113518458(16)
Frequency derivative $\dot{\nu}$ (s^{-2})	$-8.886500(24) \times 10^{-12}$
Epoch (MJD)	52407.389
Range of MJDs	52305–52616
RMS Residuals (ms)	3.0
Postglitch	
Pulse frequency ν (s^{-1})	9.64091197572(12)
Frequency derivative $\dot{\nu}$ (s^{-2})	$-8.932592(12) \times 10^{-12}$
Epoch (MJD)	52730
Range of MJDs	52645–53009
RMS Residuals (ms)	9.3
Glitch Parameters	
Epoch (MJD)	52629.97–52630.16
Frequency jump $\Delta\nu/\nu$	$2.587(2) \times 10^{-6}$
Frequency derivative jump $\Delta\dot{\nu}/\dot{\nu}$	$6.2(3) \times 10^{-3}$
Derived Parameters	
Spin-down Luminosity $\dot{E}^b$ (ergs s^{-1})	3.4×10^{36}
Surface Magnetic Field B^c (G)	3.2×10^{12}
Characteristic Age $\tau_c \equiv P/2\dot{P}$ (kyr)	17

Table 7.1: Measured and Derived Parameters for PSR J2021+3651

[a] Coordinates of the *Chandra* X-ray point source. We estimate a positional error of $\lesssim 0.5''$ by comparing the position of another bright X-ray point source on the S3 chip with a catalogued optical counterpart.
[b] $\dot{E} \equiv 4\pi^2 I \dot{P}/P^3$ with $I = 10^{45}$ g cm^2.
[c] Assuming standard magnetic dipole spindown: $B \equiv 3.2 \times 10^{19}(P\dot{P})^{1/2}$ Gauss.
Note - Figures in parentheses represent uncertainty in the least-significant digits quoted equal to 3 times errors given by TEMPO.

7.4 Discussion

7.4.1 Distance

As discussed in Roberts et al. (2002), the DM distance of PSR J2021+3651 is quite large (~12 kpc using the NE2001 electron density model of the galaxy, see Cordes & Lazio, 2002b) and would place PSR J2021+3651 on the far side of the outer Galactic spiral arm used in this model. This large distance leads to a very high inferred γ-ray efficiency ($\eta_\gamma \equiv L_\gamma/\dot{E} \sim 0.18$ in the 100 MeV−10 GeV range, assuming 1-sr beaming). Cordes & Lazio (2002b) note that the electron density model is seldom off by more than 50% when predicting distances, except when the line of sight intersects a particularly dense scattering screen. We find a scattering measure SM = $(1.5 \pm 0.1)\ d_{10}^{-5/6}$ kpc $m^{-20/3}$ towards PSR J2021+3651, where $\tau_{sc} \equiv 1.10\,\mathrm{ms}\ \mathrm{SM}^{6/5}\nu^{-22/5}d$ (Cordes & Lazio, 2002b), that is two orders of magnitude larger than predicted by the NE2001 model (although PSR J2021+3651 is in the direction of the Cygnus region and pulsars in that direction are often highly scattered). This suggests the presence of a clump of scattering material along the line of sight not accounted for by the NE2001 model. However, small clumps of material that only change the DM by 10−20 pc cm^{-3} (< 5% in the case of PSR J2021+3651) can change the SM by a factor of a hundred. Hence, the large SM does not by itself imply a significantly closer distance. In order for the distance to imply a much smaller γ-ray efficiency, a significant source of dispersion (~200 pc cm^{-3}) unaccounted for by the model is necessary. Such a DM enhancement could come from an ultra-compact HII region or an OB association. An examination of the Midcourse Space Experiment 8.3 μm IR data (available from the NASA/IPAC Infrared Science Archive) and preliminary radio imaging with VLA data we have obtained (work in preparation) show no evidence for an ultra-compact HII region. The OB association Cyg 1,8,9 lies at 1.4 kpc in the direction of PSR J2021+3651(Yadigaroglu & Romani, 1997; Mel'nik & Efremov, 1995), however there is currently no evidence that this is significantly contributing to

the amount of ionized gas along the line of sight or that the pulsar was born in this association. Since the DM distance places PSR J2021+3651 at the very outer edge of the Galaxy one would expect our spectral fit to give an n_H consistent with the total column density in this direction. The X-ray absorption found here, $n_H = (7.8^{+1.7}_{-1.4}) \times 10^{21}$ cm^{-2}, is lower than the total Galactic HI column density in the direction of PSR J2021+3651, 1.2×10^{22} cm^{-2}, estimated using the FTOOL *nh*[5] (which uses the HI map of Dickey & Lockman, 1990). This argues for a distance somewhat closer than the predicted DM distance, but not closer by factor of a few. Hence a distance of ~8 kpc is quite plausible, but a distance of less than 5 kpc, as required to make the γ-ray efficiency similar to that of PSR B1706−44 ($\eta_\gamma = 0.01$, see Roberts, 2003), is hard to justify given current observations of the region. We adopt a nominal distance of 10 kpc to use in scaling quantities ($d_{10} \equiv d/10\,\mathrm{kpc}$) that depend on distance.

7.4.2 Neutron Star Thermal Emission and Pulsations

We find a black-body temperature of $kT_\infty = 0.15 \pm 0.02$ keV for the point source, similar to that found for the Vela pulsar ($kT_\infty = 0.128 \pm 0.003$ keV; Pavlov et al., 2001) and PSR B1706−44 ($kT_\infty = 0.14 \pm 0.02$ keV; Gotthelf et al., 2002). Accounting for the effects of gravitational redshift, this corresponds to a surface temperature $kT_s = 0.20 \pm 0.03$ keV for the canonical neutron-star radius of 10 km and mass of 1.4 $M_\odot$. The point source has an unabsorbed flux $F_X = (4 \pm 1) \times 10^{-13}$ erg cm^{-2} s^{-1} in the range 0.5−10.0 keV. Scaling the luminosity to a distance of 10 kpc, $L_X = 5\ {d_{10}}^2 \times 10^{33}$ erg s^{-1} (0.5−10.0 keV). One can calculate the ratio of the black-body emission radius R_e and the distance to the source using the bolometric flux 6×10^{-13} erg cm^{-2} s^{-1} and the Stefan-Boltzman law. Correcting for gravitational redshift, this gives $R_{10}/d_{10} = 0.9$, where $R_{10} \equiv R_e/10\,\mathrm{km}$. This suggests that for a distance of 10 kpc the emission would be from the entire surface. For a distance smaller than 10 kpc, the simple

[5]See http://heasarc.gsfc.nasa.gov.

black-body model suggests that the emission is coming from hot spots on the surface, rather than from the entire surface. This is not unreasonable, as some high-energy emission models predict hot spots due to back-flowing particles.

Using the non-magnetized neutron-star hydrogen and iron atmosphere models of Gaensicke et al. (2002), which assume a neutron-star radius of 10 km and a mass of $1.4\,M_{\odot}$, changes the temperature significantly. Fixing the n_H to the value derived from the nebular fit, for a hydrogen atmosphere we get a best-fit value of $kT_s = 0.06 \pm 0.01$ keV (which is similar to the hydrogen atmosphere fit of the Vela pulsar, $kT_{\infty} = 0.059 \pm 0.003$ keV; Pavlov et al., 2001) and a flux of 2.9×10^{-14} erg cm^{-2} s^{-1} (0.5–10.0 keV). However, the normalization from this fit implies a $\sim$0.8 kpc distance, which is unreasonable. Again fixing the n_H to the nebular value, for an iron atmosphere model we get a best-fit value of kT_s $= 0.22 \pm 0.01$ keV and a flux of 3.6×10^{-14} erg cm^{-2} s^{-1} (0.5–10.0 keV). The implied distance here is $\sim$13 kpc, which is roughly consistent with the emission coming from the entire surface.

Based on the soft spectrum of the point source, one would expect pulsations to be due primarily to thermal emission. The profile found by folding the X-ray events of our continuous-clocking data with the radio ephemeris shows a somewhat narrow (duty cycle $\sim$0.3) peak and interpulse, which is possible for thermal pulsations given the right geometry. If we are seeing emission from hot spots at both poles then it is possible to get two sinusoidal peaks separated by a plateau of emission (Beloborodov, 2002). In fact, the geometry inferred from the PWN (see §7.4.4) is consistent with the pulse profile seen here. As noted in §7.2.2, a non-thermal component is also allowed by the spectrum. The possible pulsations might be a combination of pulsed thermal and magnetospheric emission, but the number of pulsed counts ($\sim$120) is too large to consist solely of magnetospheric emission. All the known γ-ray pulsars have also been detected as X-ray pulsars with non-thermal emission components to their spectra (Kaspi et al., 2006). We note that a lack of X-ray pulsations would not preclude PSR J2021+3651 from being a γ-ray pulsar. For instance, X-ray pulsations in

PSR B1706−44 are relatively difficult to detect even though PSR B1706−44 is a well-established γ-ray pulsar. Thus, PSR J2021+3651 remains an excellent γ-ray pulsar candidate.

7.4.3 PWN Spectrum

We found that the spectrum of the nebula is well fit by an absorbed power-law model with $n_H = (7.8^{+1.7}_{-1.4}) \times 10^{21}$ cm^{-2} and $\Gamma = 1.7^{+0.3}_{-0.2}$. The photon index Γ is roughly consistent with what is observed from the PWN of other similar pulsars like Vela ($\Gamma = 1.50 \pm 0.04$; Gotthelf, 2003) and PSR B1706−44 ($\Gamma = 1.34^{+0.24}_{-0.30}$; Gotthelf et al., 2002), although it is somewhat higher. The relationship of Gotthelf (2003) between the photon index of the nebula and the spin-down energy of the pulsar (equation 3 of that paper) gives $\Gamma = 1.22 \pm 0.33$, which is marginally consistent with the Γ measured here.

The unabsorbed nebular flux of G75.2+0.1 is $F_X = (1.7 \pm 0.1) \times 10^{-12}$ erg cm^{-2} s^{-1} in the 0.5−10.0 keV range. This corresponds to an X-ray luminosity in the same energy range of $L_X = (2.3\ {d_{10}}^2) \times 10^{34}$ erg s^{-1}. For the 2−10 keV energy range, we calculate an X-ray efficiency ($\eta_X \equiv L_X/\dot{E}$) of 0.004 ${d_{10}}^2$ from the combined point-source and nebular luminosities. This value fits well with the claimed relationship between the spin-down energy of a pulsar and its nebular X-ray efficiency (c.f. Possenti et al., 2002; Chevalier, 2000) even if the distance is as close as 3 kpc. However, note that this is only for the bright inner nebula. If there is significantly more flux coming from diffuse emission (as suggested by the *ASCA* data and in analogy with the Vela nebula, see below) then the efficiency will be higher.

7.4.4 PWN Size and Morphology

Young PWNe are created by a relativistic wind coming from the pulsar, which continuously injects high-enery electrons and positrons, along with magnetic field, at the centre of an expanding supernova remnant (see Kaspi et al., 2006,

and references therein). Given that the characteristic age of PSR J2021+3651 is much larger than the typical time scale for a SNR entering the Sedov phase, it is likely (although not certain since characteristic ages can be off by an order of magnitude or more) that the outer edge of the PWN (at radius R_P) is expanding subsonically into the shocked supernova ejecta. The PWN is bounded at the inner edge (at radius R_T) by the termination of the ultra-relativistic pulsar wind.

The physical size of G75.2+0.1's inner nebula is $\sim (0.5 \times 1)\ d_{10}\,\mathrm{pc}$. As PSR J2021+3651's spin-down energy is within a factor of two of that of the Vela pulsar, one might naively expect the sizes and morphologies of their nebulae to be comparable. Scaling the $\sim 10''$ radius of G75.2+0.1's inner nebula to that of the Vela pulsar's inner nebula, which has a radius of $52.''7$ (Helfand et al., 2001) and whose distance is well known (290 pc, Dodson et al. 2003), places G75.2+0.1 at a distance of $\sim$1.5 kpc, which seems unreasonable given the DM. In fact, G75.2+0.1 would have to be a few times larger than the Vela nebula to put it at a distance that seems at all reasonable based on its DM. However, since the Vela inner nebula is only the central part of a much larger and more luminous nebula, a better comparision between the sizes of these two objects could be made if the true extent of G75.2+0.1 is determined in a deeper observation with a larger field of view.

The bright inner nebulae of Vela and G75.2+0.1 may be directly downstream of the termination shock of the relativistic pulsar wind. The location of the termination shock depends primarily on the energy output of the pulsar and the pressure in the nebula. The pressure in the nebula depends upon the total energy input during the pulsar's lifetime and the losses due to adiabatic and synchrotron processes (possibly complicated by the passage of the SNR reverse shock). The total energy input is highly dependent on the initial spin period, which is unknown and could range from $\sim$10$-$100 ms (Kaspi et al., 2001; Migliazzo et al., 2002). We currently do not know the full extent of G75.2+0.1, which is likely much larger than the inner nebula seen here. While

it is true that the pressure in the PWN should be balanced by the pressure in the surrounding SNR, we know neither the age (as the characteristic age is a poor estimate of the true age for young pulsars) nor the size (since we have not observed a shell) of the potential remnant. Therefore, although the Vela pulsar is twice as energetic as PSR J2021+3651, it is entirely possible that G75.2+0.1 is several times larger than the Vela nebula.

The size of the torus places an upper limit on the termination shock radius R_T. In analogy to Equation 1 in Roberts et al. (2003) (see also Chevalier, 2000) we can estimate the post-shock magnetic field to be

$$B_N \sim 2 \times 10^{-5} \left(\frac{\epsilon_t^{1/2}}{f_t (R_T/r) d_{10}}\right) \mathrm{G},$$

where r is the measured location of the torus, $\epsilon_t \lesssim 1$ is the ratio of the magnetic energy to the total energy in the post-shock flow and $f_t \lesssim 1$ is a geometrical factor allowing for non-spherical outflow. Note that the PWN of PSR B1706−44 (which has a virtually identical $\dot{E}$ to PSR J2021+3651) is both much fainter and smaller than G75.2+0.1. This implies that the magnetic field in PSR B1706−44's nebula is smaller but the density of synchrotron emitting particles is larger. PSR B1706−44 is a known TeV source (Kifune et al., 1995), this suggests PSR J2021+3651 may be an excellent target for ground-based Cerenkov detectors. Our G75.2+0.1 image is rather sparse and Poisson-limited, and so a unique model for its morphology cannot be defined. Nevertheless, the axisymmetry of G75.2+0.1 suggests that the morphology may be that of a torus, with possibly weak jets directed along the axis of symmetry (see Figure 7.1). To investigate the question of G75.2+0.1's morphology quantitatively, we spatially fit the PWN assuming a torus (Figure 7.6), using the fitting technique described in Ng & Romani (2004). Our fiducial model is similar to that of the Vela pulsar PWN: twin tori of radius r, symmetrically spaced by distance d on either side of the pulsar spin equator. The torus axis is at position angle Ψ (N-E) and inclination ζ to the line of sight. The bulk flow velocity down-stream from the termination shock is β_T and a 'blur' parameter

Parameter[a]	Value
Ψ	$47° \pm 1°$
ζ	$83° \pm 1°$
r	$8.6'' \pm 0.3''$
δ^b	$1.2''$
$\beta_T{}^c$	~ 0.8
d	$3.7'' \pm 0.2''$

Table 7.2: Double Torus Fit Parameters

[a] Explanation of parameters in §7.4.4.
[b] Held fixed in the global fit.
[c] The Doppler boosting is likely being dominated by the bright clump to the south-west of the pulsar.

δ is applied to account for the unmodeled shock thickness. For details of the Poisson fit process and caveats about the sensitivity of parameter fitting see Ng & Romani (2004). The derived parameters for the best-fit double torus are given in Table 2, with statistical 1-σ errors. Systematic errors due to un-modeled features are difficult to quantify. To probe this sensitivity, we re-fit excluding an elliptical zone about the pulsar which might be contaminated by an un-modeled jet. All parameters were within 1.5σ of the original fit, except the post-shock β which drops to 0.64 ± 0.02. Ng & Romani (2004) note that this parameter is particularly sensitive to excess (e.g. jet) flux for edge-on tori. We also fit a single torus to see if this is adequate to model the observed PWN. Again, the fit parameters are similar, although δ grows to $1.8''$. The fit statistic for this model is of course larger than that of the two torus model (at a level corresponding to 1σ parameter errors); this does not alone show that a double torus is required as we cannot apply an F-test.

Clearly a deeper image is needed to draw firm conclusions, but we can discuss the geometrical implications of the fit angles. The large ζ implies that we are viewing the pulsar near the spin equator. In the outer magnetosphere picture of Romani & Yadigaroglu (1995) this is indeed where we expect to

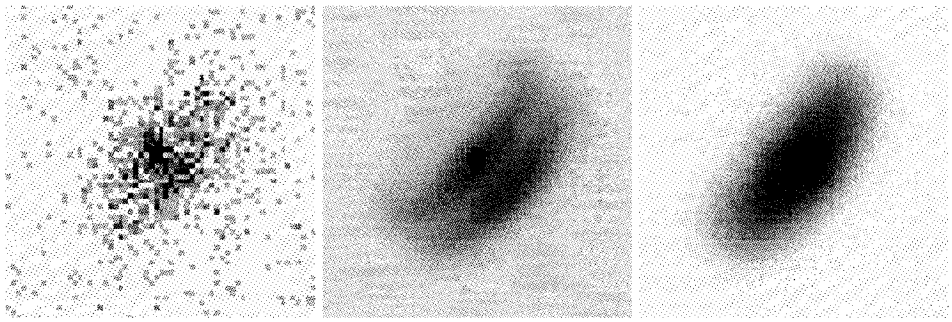

Figure 7.6: *Left*: $32'' \times 32''$ cutout of the central PWN. *Middle*: best-fit double torus plus point source model. *Right*: best-fit single torus plus point source model.

see γ-ray emission. More particularly, Figure 4 of that paper shows that for $\zeta \approx 83°$ and magnetic impact angle β modest (to allow detection of the radio emission), we expect two γ-ray pulses separated by $\sim$180°, with the first lagging the radio peak by $\sim$10°. Intriguingly, McLaughlin & Cordes (2003) found apparently significant pulsations folding the γ-ray photons from this source near the extrapolated P for two viewing periods; the light curves show two narrow peaks separated by 0.5 in phase. It is important to note that for ζ near 90°, such a light curve is also naturally expected in the two pole model of Dyks & Rudak (2003) and may be possible in polar-cap models (Daugherty & Harding, 1996). The separation of the two tori suggest bright emission at spin axis angles $\theta_T = \tan^{-1}(2r\sin\zeta/d) = 77°, 103°$, as viewed from the pulsar. If these represent enhanced $e^{\pm}$ flowing radially from near the magnetic poles then we might infer a magnetic inclination $\alpha \approx 77°$. This would imply an impact parameter $\beta = \zeta - \alpha \approx +6°$. Polarization sweep measurements could test this picture. The unscattered pulse half-power width $\sim$33° of PSR J2021+3651 is substantially wider than the $2.5°(P/1\,\mathrm{s})^{-1/2}/\sin\alpha$ width expected for a core component, but is similar to the $5.8°(P/1\,\mathrm{s})^{-1/2}$ width for an outer cone (Rankin, 1993). Of all the fit geometrical parameters, the most robust is the fit PA of the symmetry axis Ψ. Although difficult to measure,

given the large DM and expected substantial Faraday rotation, the absolute position angle at the polarization sweep maximum would provide an interesting check of the inference that this represents the pulsar spin axis.

7.5 Conclusions and Further Work

We have used the *Chandra X-ray Observatory* to observe the young and energetic pulsar PSR J2021+3651 and have detected a new PWN, G75.2+0.1, as well as an embedded point source near the radio timing position of the pulsar. The morphology of G75.2+0.1 is perhaps best decribed as an equatorial torus, and we have derived geometrical parameters for the orientation of the system by spatially fitting the nebula. Spectral fitting of the nebula shows that it is similar to the nebulae of other energetically-similar pulsars. Spectral fitting of the point source shows that it is adequately fit by an absorbed black-body model or a black-body plus power-law model. Radio timing observations of PSR J2021+3651 have revealed a glitch similar to the largest glitches seen in the Vela pulsar. Analysis of countinuous-clocking data from *Chandra* indicates that there may be weak X-ray pulsations from the source (pulsed fraction of $\sim$65%) at the period predicted by the radio ephemeris. PSR J2021+3651 remains the most likely counterpart to the high-energy EGRET γ-ray source GeV J2020+3651 (which is the 10th brightest γ-ray source above 1 GeV). It is an excellent γ-ray pulsar candidate for the AGILE and GLAST missions, although a contemporaneous ephemeris will be essential, given the large amount of timing noise the pulsar exhibits.

Deeper observations with *Chandra* and *XMM-Newton* are needed to clarify the morphology of G75.2+0.1 and to confirm the presence of pulsations. Such observations are also able to confirm whether the faint outer jet hinted at here is real. Currently, there only about a half dozen PWNe with torus plus jet morphologies, with the Crab and (likely) Vela nebulae as the best examples. With a deeper observation, G75.2+0.1 may prove to be the third best example. Fur-

ther work by our group will also include analysis of radio polarization data we have taken with Arecibo. These data may help bolster the geometrical interpretation described here if the swing of the polarization angle across the pulse is measurable. Proper-motion measurements could check if PSR J2021+3651 is moving along the axis of the nebula, which is the case for both Vela and the Crab. However, measuring the proper motion of PSR J2021+3651 (which will likely be small since the distance is likely large) will be very difficult both through radio timing because of timing noise or through VLBI because the radio source is very faint. We are also analyzing VLA observations (in A, C, and D arrays) of the source region to look for a radio PWN and/or SNR. This is important for characterizing the surrounding medium, which has an important effect on the morphology of the PWN and its size.

Chapter 8

Continuing Surveys of the Galactic Plane

Large-area surveys for radio pulsations continue to produce important scientific insights through their discovery of particularly interesting, and sometimes singular, pulsar systems. A primary goal is to find systems whose properties challenge or elucidate our understanding of the wealth of physical phenomena associated with pulsars. To motivate the rationale behind these surveys, we list some of the most sought-after classes of objects such a survey can hope to find, as well as some of the science these sources can address:

- **Young pulsars**: Young pulsars are spinning down rapidly compared with older, un-recycled pulsars ($\dot{P}_{\rm young} \sim 10^{-11} - 10^{-13}\,{\rm s/s}$ as opposed to $\dot{P}_{\rm old} \lesssim 10^{-14}\,{\rm s/s}$). Consequently, they have significantly higher spin-down luminosities and associated high-energy emission, possibly in the form of high-energy pulsations, thermal emission from the surface, or a pulsar wind nebula. As such, they are important sources for understanding neutron star cooling (for instance Slane et al., 2002), the mechanisms behind high-energy pulsations (Kaspi et al., 2006), and the pulsar's energy budget (Kaspi et al., 2006).

- **High-magnetic-field pulsars**: Five of the known radio pulsars have spindown-inferred magnetar-like surface magnetic fields $B \gtrsim 5 \times 10^{13}\,\mathrm{G}$ (for instance PSR J1847-0130, McLaughlin et al., 2003). Why these systems do not have similar X-ray properties to the persistent magnetars and what relates these two populations of young neutron stars remains unresolved. One possibility is that the high-magnetic-field radio pulsars are quiescent magnetars (Kaspi & McLaughlin, 2005).

- **Binary pulsars**: Some binary pulsars provide an opportunity to precisely constrain neutron star masses and test gravitional theories, like General Relativity, by measuring post-Keplerian orbital effects (Stairs, 2004, and references therein). These provide the most stringent tests of General Relativity in the strong field regime. For instance, recent timing observations of the double pulsar are consistent with General Relativity at the 0.1% level (Kramer et al., 2005). Long-orbital period ($P_{\mathrm{orb}} \gtrsim 100\,\mathrm{d}$), highly circular systems constrain the Strong Equivalence Principle of General Relativity (Lorimer et al., 2005; Stairs et al., 2005). The orbital stability of the binary pulsar B1855+09 has been used to constrain any secular changes in Newton's gravitational constant ($\dot{G}/G = (-9 \pm 18) \times 10^{-12}\,\mathrm{yr}^{-1}$, Kaspi et al., 1994). The precision of pulsar timing also makes it possible to detect planetary-mass companions in orbit around a pulsar. In fact, the first planets discovered outside the Solar System were found around the pulsar B1257+12 by Wolszczan & Frail (1992). Currently we know of only two pulsars with planetary companions - the other being PSR B1620−26 in the globular cluster M4 (Sigurdsson & Thorsett, 2005) - but others must surely exist. The detectable planetary mass limits from pulsar timing are much lower than those probed by the Doppler motion of normal stars.

- **Millisecond pulsars**: The short spin periods and extremely stable rotation rates of millisecond pulsars make them the most precise astro-

nomical clocks known. In addition to well measured orbital parameters, precision timing of these can, in some cases, measure parallax (giving a precise distance), proper motion, as well as DM variations. When used together as a "timing array", millisecond pulsars have the potential to detect nano-Hz gravitational waves (Foster & Backer, 1990; Jenet et al., 2005).

- **Transient sources**: In addition to well defined periodic signals, a pulsar survey can also look for dispersed individual bursts in the time domain (see §3.3). This type of search has lead to the discussion of a class of objects dubbed "rotating radio transients" (RRATs; McLaughlin et al., 2006), which are characterized by radio bursts that repeat on average timescales of minutes to hours. How these sources are related to the normal pulsar population is still not well known, as the current population of roughly only a dozen sources is not completely characterized yet and provides poor statistics.

A well designed survey will be sensitive to all these aforementioned source classes, and potentially new classes of objects as well. The recent discovery of the first double pulsar system, J0737−3039, in a large-area survey of high Galactic latitudes with Parkes (Burgay et al., 2006), is an outstanding example of the windfalls that can result from untargeted searching. Future searches may have the good fortune of uncovering other double pulsar systems, or even the long-sought pulsar-black-hole binary, which could provide an unparalleled test of gravitational theories in the strong-field regime, if the orbital period is on the order of a few hours or less.

In this chapter, we present two complimentary and ongoing surveys of the Galactic Plane using the Arecibo Observatory and the Green Bank Telescope. It is hoped that these surveys will discover interesting individual sources with which to test fundamental physics, as well as provide insight into the pulsar population through their combined statistics. Our knowledge of the Galactic

birthrate and distribution of pulsars - along with distributions in spin period, magnetic field, and velocity - will increase as the known pulsar population grows.

8.1 The Pulsar-ALFA (PALFA) Survey

8.1.1 Introduction

Although the Arecibo telescope's huge single dish provides unparalleled sensitivity, it also results in a very small field of view ($\sim 3'$ across at 1.4 GHz). This is problematic if one wants to cover a significant portion of sky, because ~ 500 pointings will be required to cover just 1 deg^2. However, with a receiver *array*, which samples the focal plane in numerous locations, this problem is somewhat eleviated because the telescope can observe multiple directions simultaneously. This has been done with great success in the Parkes Multibeam Survey (PKMB; Manchester et al., 2001), which employed a 13-element multibeam system to survey a large portion of the southern Galactic Plane.

In the spring of 2004, the Arecibo telescope was equipped with a 7-element multibeam receiver, constructed by the Australia Telescope National Facility, and dubbed the Arecibo L-band Feed Array (ALFA). Operating between 1.2 – 1.5 GHz, this system provides a greater sky coverage rate to expediate deep, large-area sky surveys for pulsars, neutral hydrogen (HI), and extragalactic sources. The 7 beams of the array are spaced approximately two full beamwidths apart when projected onto the sky, and by interleaving this pattern one can cover the sky roughly uniformly.

Shortly after its installation, a consortium of pulsar astronomers[1] began using this receiver for a survey of the Galactic Plane. This survey is commonly referred to as the Pulsar-ALFA or PALFA survey. There are two regions of the Galactic Plane visible from Arecibo, which are referred to as the "inner"

[1]Consortium members: http://alfa.naic.edu/consortia/pulsar_members.html.

Galactic Plane region $32° < l < 77°$ and the "anti-centre" Galactic Plane region $168° < l < 214°$. The goal of this survey is to cover these two regions out to Galactic latitudes $|b| \leq 5°$. In the process, we expect to discover a few hundred pulsars.

Previous large-scale surveys of the Arecibo sky (for example Hulse & Taylor, 1975a; Lorimer et al., 2005) have been conducted at much lower observing frequencies ($\nu_{\rm centre} \lesssim 430\,{\rm MHz}$), where the beam area of the telescope is $\sim 10\times$ larger than at 1.4 GHz, allowing a relatively efficient coverage rate without a multibeam receiver. Although most pulsars have a steep power law spectrum that peaks in brightness at low frequency, the higher frequency used in the 1.4-GHz PALFA survey results in less dispersive smearing and scattering by the interstellar medium. For this reason, and because of the high time and frequency resolution data recorders that are being used, PALFA provides an order of magnitude better sensitivity to fast pulsars ($P < 10\,{\rm ms}$) than previous surveys at Arecibo. PALFA is also significantly more sensitive to fast pulsars than the PKMB Galactic Plane survey (Figure 8.1), which overlaps with the PALFA survey in the $40° < l < 50°$ longitude range. The current PALFA data recorder has a factor of 6 better frequency resolution and a factor of 4 better time resolution than the PKMB filterbank. Furthermore, compared with the 35-min integration times used by the PKMB survey, the $\lesssim$ 5-min pointings being used in the PALFA survey - which can still achieve a lower flux limit than Parkes in this short integration time - have a comparatively lower observational bias against detecting short orbital period binary pulsars. Lastly, re-observing an area of sky that has been surveyed once already has the potential to detect exotic pulsars that were not previously visible, possibly because of precession (in an ultra-relativistic binary), or long radio-quiet periods (consider for instance PSR B1931+24, which has a 10-d active phase, followed by a $\sim 25 - 35$-d period in which it is not visible; Kramer et al., 2006).

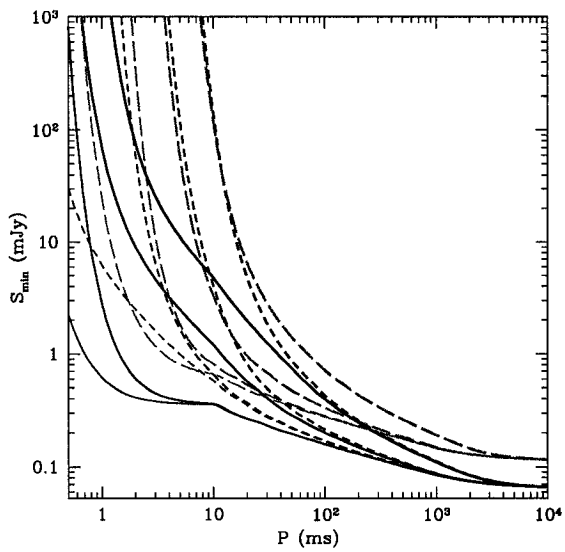

Figure 8.1: The idealized minimum detectable radio flux ($S_{\rm min}$) for the PALFA survey as a function of DM and spin period P. These curves *do not* include the important effects of RFI, red noise, and orbital motion, which are all much more difficult to quantify. The short-dashed lines correspond to the reduced-resolution preliminary "quicklook" processing. The solid curves show the sensitivity of the full-resolution processing. For comparison, the long-dashed, red curves show the sensitivity of the PKMB Galactic Plane survey. Each set of curves shows the varying sensitivity as a function of DM. The curves are, from left to right, for DMs of 1, 200, 500, and 1000 pc cm^{-3}. Figure from Cordes et al. (2006).

8.1.2 Observations

The area covered by the 7 beams of the ALFA receiver is $0.0211\,\mathrm{deg}^2$, and thus 47 pointings are required to survey $1\,\mathrm{deg}^2$ of sky. Given the spacing of ALFA's feed horns, the sky can be covered roughly uniformly by tesselating groups of three pointings that are spaced in the configuration shown in Figure 8.2[2]. If only one of the three pointings in this group is observed, then the sky is sparsely sampled. Simulations[3] by groups at Cornell and McGill indicate that one will find more pulsars early on in the survey by first covering the survey area in the sparse-sampling mode, and then returning to fill in the remaining two pointings of each group. This is because a reasonably bright pulsar can be detected via the gain in the sidelobes of the beams, even if it is outside the nominal FWHMs of the beams themselves. In fact, the sidelobes of the ALFA receiver beams have a similar gain to that of the Parkes telescope main beam, $\sim 1\,\mathrm{K\ Jy}^{-1}$.

For separate pointings to interleave properly, the parallatic angle of the receiver must be adjusted for each observation. The parallatic angle also changes *during* an individual observation. The largest rate of change occurs along the meridian at low zenith angle (where the azimuthmal arm of the receiver platform must move most rapidly to continue tracking a source). This will smear the beam pattern over the sky during the observation, reducing sensitivity. Consequently, to minimize smearing to a small fraction of the beam widths, observations are made only at zenith angles $\gtrsim 5°$. Furthermore, if one observes the same position twice but at significantly different parallactic angles, the beam patterns of the two pointings will be rotated by as much as an arcminute with respect to each other because of projection effects. This also limits how well the pointings will interleave in practice.

Before the start of the "main" survey, a short precursor survey was con-

[2]For a detailed description of this and the other possible tilings see http://www.naic.edu/~pfreire/tiling.

[3]See http://astrosun2.astro.cornell.edu/~cordes/PALFA for simulation descriptions as well as other PALFA-related documents.

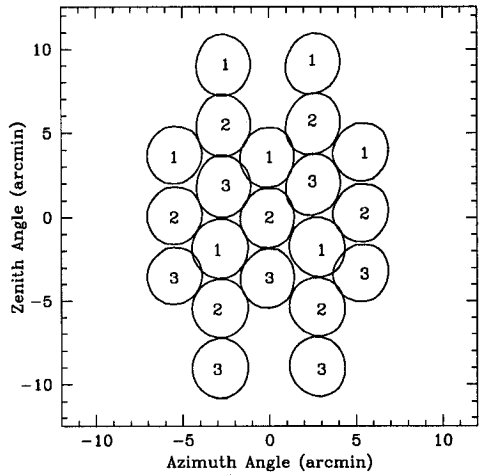

Figure 8.2: The optimal interleaved three-pointing pattern used to cover the sky, as projected onto the sky itself (north at the top). Note that the beam array is elliptical, being 768″ along its major axis, and 658″ along its minor axis. A larger area of sky can be covered roughly uniformly by tesselating this three-pointing pattern. Figure from Cordes et al. (2006).

ducted between August 2004 and January 2005, using the sparse-sampling technique. The precursor survey resulted in the observation of 1200 pointings (where each "pointing" is a set of 7 beam positions) in the inner Galaxy, and 700 pointings in the anti-centre. All of these were within 1° of the Galactic Plane. A total of 25.3 deg^2 and 14.8 deg^2 were covered in the inner and anti-centre regions, respectively. Pointings in the inner Galaxy were integrated for 134 s, while those in the anti-centre were integrated for 67 s. The purpose of these observations was to test the then newly comissioned observing system and to develop the necessary observing, processing, and archiving software. The results of these observations are described in Cordes et al. (2006).

The main survey began in January 2005, and is ongoing. The integration times used in the main survey are double those used in the precursor survey: 268 s in the inner Galaxy and 134 s in the anti-centre. As of May 2006, 3000 pointings have been observed in the inner Galaxy, and 1000 have been observed

in the anti-centre, corresponding to 63.3 deg^2 and 21.1 deg^2 of sky coverage in these two regions, respectively. These pointings are all within 5° of the Galactic Plane (Figure 8.3) and there is some overlap with the area covered previously in the precursor observations. As there is a total of $\sim$ 450 deg^2 of sky in each of the two regions, 14% (5%) of the inner (anti-centre) region have been covered. The lowest Galactic latitudes are being covered first, because this is where most pulsars will be found. Initially, observations were done in sparse sampling mode, although the remaining low latitude pointing positions are now being filled in before higher latitude sparse sampling observations are made.

For both the precursor and main surveys, all four of the Wideband Arecibo Pulsar Processor (WAPP) backends were used to record the data (see §2.2.1 for a description of the WAPPs). They are being used such that each WAPP records 100 MHz of bandwidth from two of the 7 beams with 256 channels and 64-μs time sampling. WAPP4 records the output of the seventh beam, along with a redundant copy of the same data. Each WAPP has a data rate of 16 MB/s, resulting in $\sim$ 230 GB of data per hour from all four WAPPs. It is expected that the total survey data archive will require roughly a petabyte (1 PB = 1024^2 GB) of storage space. This large archiving task is being handled by the Cornell Theory Center[4].

Initially, the central observing frequency was 1420 MHz. However, it became apparent that persistent, strong radio frequency interference from the various nearby airport and military radars operating in the 1220-1370 MHz range, was strongly affecting our data. In November 2005, a high-pass filter was installed in order to mitigate this problem. This also resulted in the central frequency of the observing band being moved up to 1440 MHz. By late 2006 or early 2007, we expect that the WAPPs will be replaced by an FPGA-based backend capable of recording the full 300 MHz bandwidth of the ALFA receiver. It is hoped that this system will also be better at dealing with

[4]See http://www.tc.cornell.edu.

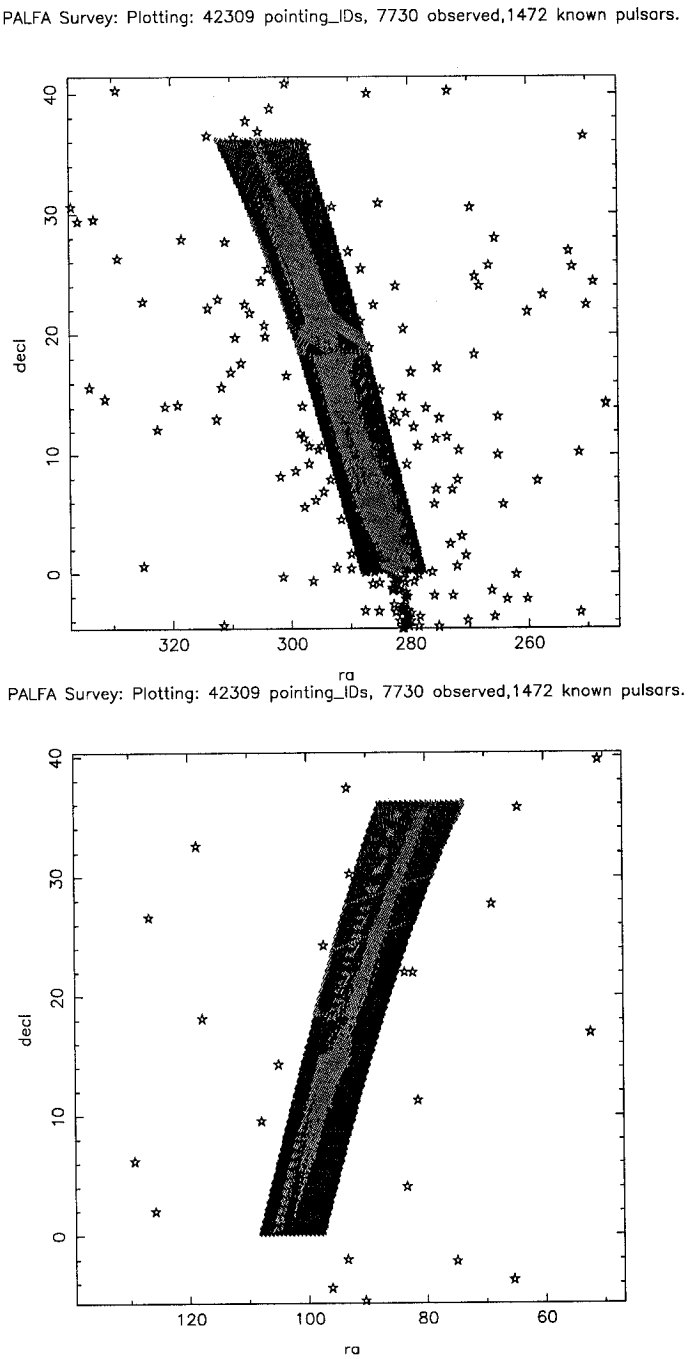

Figure 8.3: Area covered so far by the PALFA survey in the inner (top) and anti-centre (bottom) Galactic Plane regions. The black dots, which are packed very closely together in this zoomed-out view, are the central positions of the roughly 21000 pointings required to cover each of the two regions. The green regions have been observed at least sparsely. See also Figure 8.4, which shows a zoomed-in view of the pointing positions in a small area of sky. The blue stars are know pulsars from the ATNF catalogue (Manchester et al., 2005, http://www.atnf.csiro.au/research/pulsar/psrcat).

narrow-band interference.

8.1.3 Analysis

Survey Database

The management of such a large-scale survey as PALFA is non-trivial. In the two Galactic Plane survey areas, there are approximately 42000 pointings to be made, each with 7 beam positions and other important observational parameters like start time and integration time to record. Furthermore, the storage and organization of analysis results is cumbersome, as numerous candidates (each with a large vector of associated information) per beam will be recorded. My main contribution to this survey thus far (in addition to observing and helping to develop a fully automated search pipeline) has been the creation of a comprehensive database, using the MySQL database system, to record pointing positions, catalogue observations, and store the analysis results. This database resides at Arecibo, and is mirrored at the Cornell Theory Center, through which it can also be accessed via the World Wide Web (http://arecibo.tc.cornell.edu/arecibo/mysql; this interface is password protected).

I have developed a number of scripts that facilitate the entry and extraction of information from the database. For instance, after each observing session, a script is run which parses the observing log written by the telescope's data-taking interface and adds this information into the appropriate fields of the database tables. The database provides an independent record of the observed pointing positions, which are also recorded in the data file headers. This became very useful when it was realized in the summer of 2005 that the positions being written to the data file headers were incorrect, while those written to the database were fine. Using the database positions, it was possible to determine that the positions listed in the file headers were incorrectly rotated by 180° with respect to the centre of the ALFA array.

A script exists to query the database to plot the observed survey pointing positions. This script was used to create Figure 8.3 as well as Figure 8.4, which shows the observed pointings in a small portion of the sky. This script interactively allows one to pan across the survey area and zoom in and out. This has been useful for ensuring that the pointings tesselate properly and to judge the progress of the survey.

When planning an observation, the database is also queried in order to produce a list of pointing positions that have not yet been observed. Given a start MJD and session length, the script will query the database for a set of non-observed survey pointings that are visible at the required epoch, and which satisfy other user-defined criteria. For instance, the user can ask for pointings within a certain range of Galactic latitude, or zenith angle. This formatted list can then be uploaded directly by the telescope's data-taking system to perform automatic catalogue observations.

Search Pipelines

There are two analysis pipelines being applied to the data to search for pulsars. The first, which is called "quicklook" processing, is run during the observations themselves and searches the data in quasi-real-time. This is achieved by first degrading the resolution of the data by a factor of 16 in time and 8 in frequency. The resulting coarser resolution is insufficient to discover millisecond pulsars, but is adequate for finding pulsars with spin periods greater than $\sim 40\,\mathrm{ms}$. As most of the pulsars we will discover will be long period pulsars, this is a valuable tool for discovering these systems quickly and easily.

The second pipeline uses the full time and frequency resolution of the data to maintain maximum sensitivity to the fastest pulsars. Furthermore, acceleration searches are performed on the data in order to look for very highly accelerated pulsars. Although acceleration searches are unecessary for detecting the vast majority of the binary pulsars we expect to find, a potential extreme binary system, like a double neutron star or pulsar-black-hole binary,

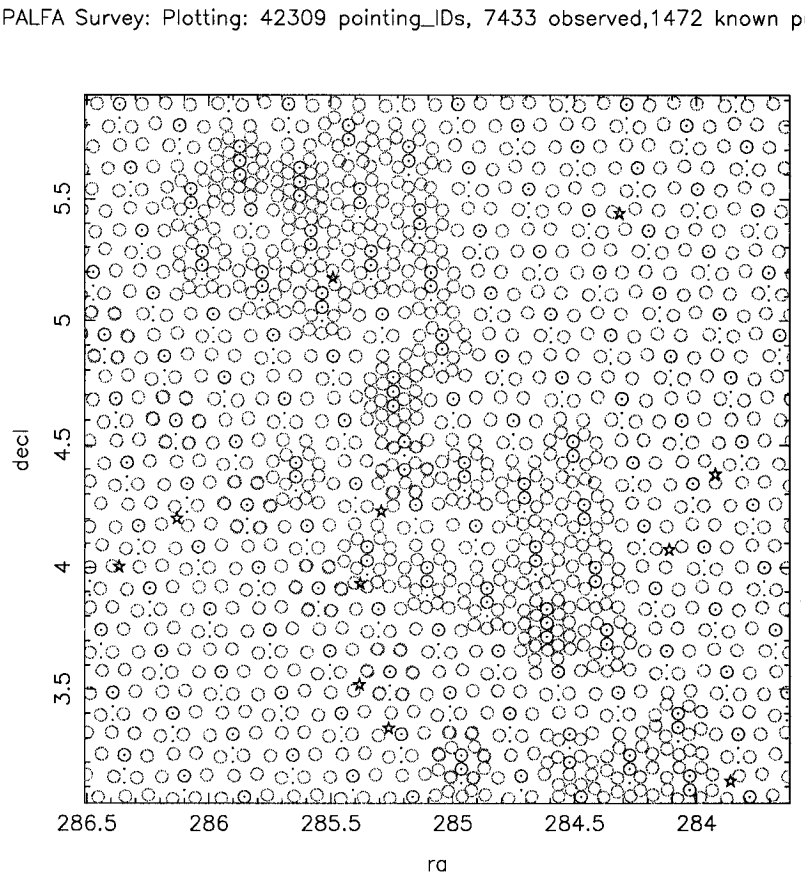

Figure 8.4: Pointings in the PALFA database from a small $\sim 3° \times 3°$ portion of the sky. The red circles indicate the central beam position of each 7-beam pointing. The green circles indicate the positions of the 6 outer beams. The blue stars are the positions of known pulsars in the ATNF catalogue (Manchester et al., 2005, http://www.atnf.csiro.au/research/pulsar/psrcat). In most cases, only one of the three pointings in each cluster has been observed, in accordance with the sparse sampling strategy. In a few cases, two or all three of the pointings in the cluster have been observed, showing how the beams interleave.

can easily have an acceleration that will smear out its signal over the course of the 268-s integration time, unless this is accounted for.

8.1.4 Results

As of August 2006, 28 pulsars and 2 single-pulse (i.e. RRAT) sources have been found in the PALFA survey (Table 8.1). 11 (17) of these were found in the precursor (main) survey. All of these were found by the quicklook processing. Some of the interesting sources found thus far include:

- **PSR J1928+1746**: This was the first pulsar to be discovered by the PALFA survey, and was fortuitously found by the quicklook processing within the first hour of the very first observing session (Cordes et al., 2006). It is a 69-ms pulsar with a relatively young characteristic age of 82 kyr. The spin-down luminosity is $\dot{E} = 1.6 \times 10^{36}\,\mathrm{erg\ s^{-1}}$. Multi-frequency observations between $1 - 9\,\mathrm{GHz}$ show that the spectral index is near zero (i.e. the spectrum is almost flat within this range). It is spatially coincident with the unidentified *EGRET* γ-ray source 3EG J1928+1733, and presents a plausible low-energy counterpart to this source.

- **PSR J1906+0746**: The first binary pulsar to be discovered by the PALFA survey, it is also the youngest known pulsar binary system (Lorimer et al., 2006b). The pulsar is un-recycled, has a spin period of 144 ms and a characteristic age of only 112 kyr. The orbit is relativistic, with an orbital period of 3.98 hr and eccentricity of 0.09. The coalescence time due to gravitational waves is estimated at 300 Myr. It is unclear whether the companion star is another neutron star or a white dwarf, but the total system mass is $2.61 \pm 0.02\,\mathrm{M_\odot}$.

- **PSR J1856+0244**: This is an 80-ms pulsar with a characteristic age of $\sim$ 20 kyr (Hessels et al., in prep.). As such, it is the youngest pul-

sar found in the PALFA survey so far. PSR J1856+0244 is also visible in archival Parkes Multibeam survey data, although faintly. It is plausibly associated with the *ASCA* Galactic Plane Survey faint source AX J185651+0245, which appears to be a point source plus extended structure (B. Gaensler, private communication).

Timing observations of these and the other discoveries have begun with Arecibo, Jodrell Bank, and soon potentially other radio telescopes as well.

8.2 The GBT350 Survey

8.2.1 Introduction

Compared with the Arecibo-visible declination range and the area covered by the various Parkes multibeam surveys (Manchester et al., 2001; Edwards et al., 2001; Jacoby, 2005; Burgay et al., 2006) and the Parkes Southern Pulsar Survey (Manchester et al., 1996; Lyne et al., 1998), the northern sky has not been deeply surveyed, particularly for fast pulsars. Previous surveys of the northern sky at $300 - 500\,\mathrm{MHz}$ include an all-sky survey above $\delta \gtrsim 38°$ using the Jodrell Bank telescope at 428 MHz, which, largely due to RFI, discovered only one pulsar (Nicastro et al., 1995) and a survey at Green Bank using the 140-ft (43-m) equatorially mounted telescope at 370 MHz, which found eight new pulsars (two of which are recycled; Sayer et al., 1997). Another survey, using the Green Bank 300-ft (91-m) transit telescope (which was only capable of moving in altitude) at 390 MHz provided partial coverage of the northern sky and discovered 20 pulsars (Stokes et al., 1986). This survey had relatively poor sensitivity to MSPs and the fastest pulsar found had a spin period of $\sim 100\,\mathrm{ms}$. The sky above $\delta \gtrsim 38°$ comprises roughly a fifth of the total celestial sphere, yet there are only two pulsars with spin periods faster than 40 ms known in this region: PSR J0218+4232 ($P_{\mathrm{spin}} = 2.32\,\mathrm{ms}$) and PSR J1012+5307 ($P_{\mathrm{spin}} = 5.26\,\mathrm{ms}$). Finding more fast pulsars in this part of

Pulsar Name	Spin Period (ms)	DM (pc cm^{-3})	Notes
	Galactic Anti-Centre		
J0540+3207	524.0	62	
J0628+09	413.7	110	
	Inner Galaxy		
J1855+02	246.8	850	
J1856+02	80.90	630	Young, Likely X-ray Assoc.
J1858+03	256.8	420	
J1901+0621	831.7	94	Also found by PKMB
J1904+07	209.0	280	
J1905+08	218.2	450	
J1906+0746	144.0	220	Relativistic Binary
J1909+07	118.6	540	
J1916+12	227.4	250	
J1919+13	571.4	620	
J1925+13	132.5	790	
J1928+1746	68.72	180	Young, Possible γ-ray Assoc.
J1937+20	687.0	310	
J1940+23	546.9	240	
J1941+25	2306	320	
J1946+25	515.2	240	
J1948+25	196.6	280	Bright
J1949+23	1319	280	
J1953+27	1334	300	
J2006+31	163.7	110	
J2007+31	608.2	200	
J2009+33	1438	250	
J2010+28	565.4	110	
J2010+32	1442	440	
J2011+33	931.7	310	
J2018+34	387.7	210	

Table 8.1: Discoveries made by the PALFA survey.

the sky, especially ones that can be timed precisely, could be very interesting for adding to a timing array of millisecond pulsars (Manchester, 2006), which can be used to detect nano-Hz gravitational waves. The sensitivity of such an array depends partly on there being a roughly isotropic distribution of timing sources on the sky.

The GBT's large collecting area and maneuverability make it the most sensitive radio telescope on Earth over a large portion of the sky. The beamwidth of the GBT at 350 MHz is $\sim 0.6°$, large enough to permit very efficient large-scale surveys of the sky using the telescope at this frequency. This motivated us[5] to commence a 350-MHz survey, which we will refer to as the GBT350 survey, of the Galactic Plane in the region north of that visible by the Arecibo telescope: $\delta \gtrsim 38°$, corresponding to Galactic longitudes $65° < l < 170°$. Initial precursor data for this survey were taken in the summer of 2004, and data continue to be collected. Here we present the observational setup, analysis pipeline, and preliminary results.

8.2.2 Observations

Precursor data were taken from July to September 2004, between Galactic longitudes $76° < l < 116°$ and latitudes $8° < b < 18°$. Approximately 1300 pointings were observed. The primary purpose of these observations was to prove the capability of the Spigot system for performing large-scale low-frequency surveys and to develop the necessary software to interface the Spigot with the primary telescope control software, so that the observing sessions, which involve making many hundreds of individual short pointings, could be automated. Before these observations began, there was no way for the telescope pointing software to communicate with the Spigot.

Following the precursor survey, we began a Galactic Plane survey with the intention of covering the entire Galactic Plane north of the Arecibo-visible

[5]The other members of the GBT350 survey collaboration are D. J. Champion, V. M. Kaspi, S. M. Ransom, and M. S. E. Roberts.

declination range $65° < l < 170°$ and within 5° of the Plane. Data collection began in April 2005 and is almost complete. A total of ~ 3800 pointings will be observed in all. The spacing of the pointing centres is such that there is a 10% overlap in the FWHM of the beams at some points in the sky. This ensures that all points in the survey area are covered to at least the beam half-power. The survey coverage is shown in Figure 8.5.

Data are recorded using the GBT Pulsar Spigot (see §2.3.1 for a description) in a 50 MHz bandwidth mode centred at 350 MHz. The dual linear polarizations of the PF1 receiver ($T_{\rm sys} \sim 40$ K, $G \sim 2$ K/Jy) are summed in quadrature and sampled every 81.92 μs. There are 1024 lags across the observing band, resulting in a residual dispersive smearing of 100 (1000) μs at DM = 10 (100) pc cm^{-3}. The integration time per pointing is 120 s. Accounting for time lost due to slewing between pointings, settling and other overhead, the total time spent per pointing is roughly 150 s, resulting in a very respectable 80% observing efficiency.

In Figure 8.6, we compare the sensitivity of this survey to some selected past large-scale surveys. The GBT350 survey is a factor of $\gtrsim 4$ times more sensitive to slow pulsars and $\gtrsim 10$ times more sensitive to fast pulsars at moderate to high DMs than previous surveys of the same area. Furthermore, the current RFI environment at Green Bank in this frequency range is remarkably good. This allows us to use a very low signal-to-noise threshold when investigating candidates from the periodicity and single pulse searches. Given that these "clean skies" are unlikely to persist indefinitely, we are also archiving all the raw data from this survey (roughly 10 TB of data) for use by future projects. The archived data will be listed on a website.

8.2.3 Analysis

As discussed in Chapter 3, when one is searching for pulsars and the DM is unknown, numerous trial dedispersed time series at a range of DMs must be generated and each must be searched for potential pulsations. The spacing of

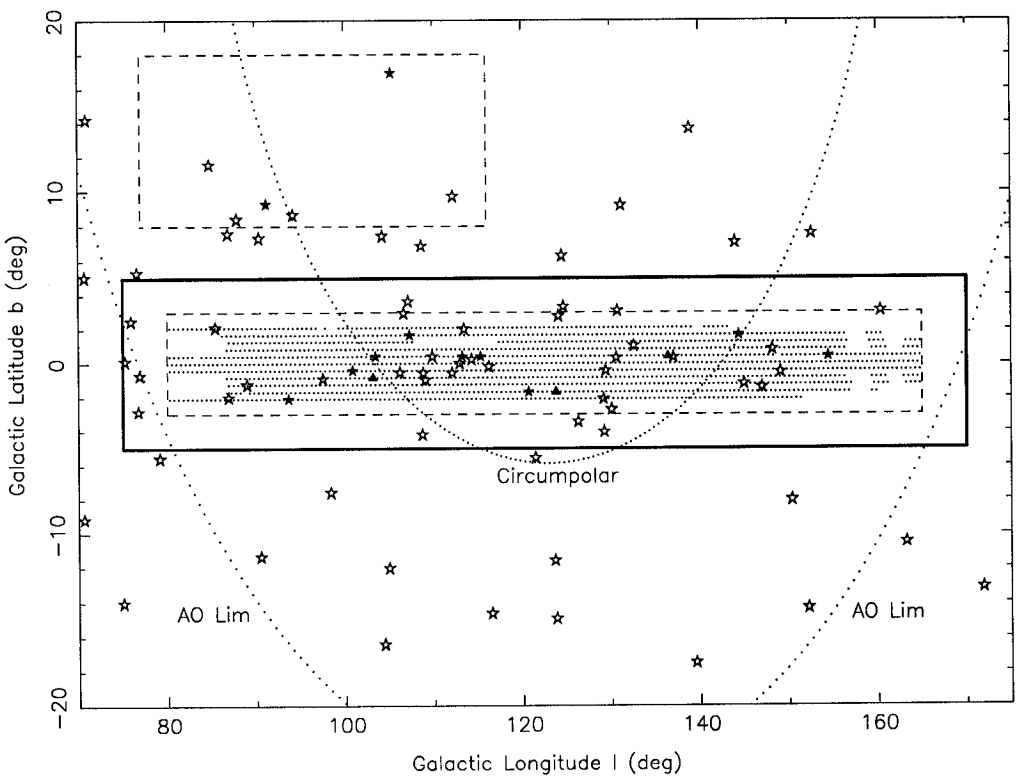

Figure 8.5: Sky coverage of the GBT350 Galactic Plane survey. The two dashed rectangles show regions which have been already covered (one along the Galactic Plane, and another region off the Plane, which was covered during precursor observations for this survey). The dots indicate which Galactic Plane survey pointings have been processed. The entire precursor dataset has been processed as well. The solid rectangle shows the full extent of the Galactic Plane survey, when it will be completed. Un-filled stars indicate the positions of previously known pulsars, and filled stars indicate pulsars discovered in this survey. Sources which were detected in the single pulse search are marked with filled triangles. Dotted lines indicate the region of the sky which is circumpolar as seen from the GBT, as well as the northern limit of the sky visible from Arecibo.

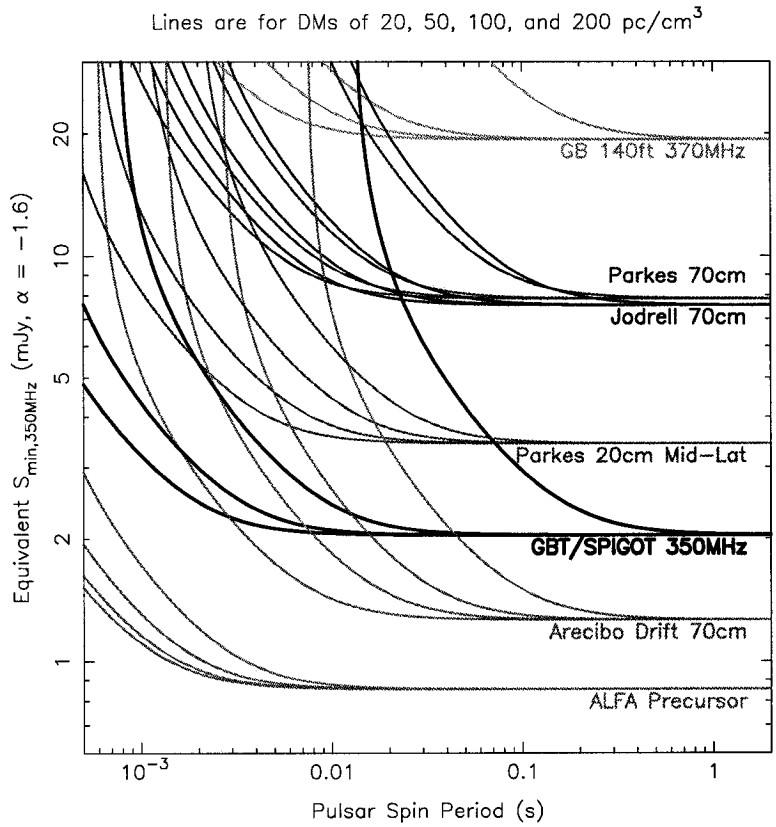

Figure 8.6: Search sensitivity of the GBT350 survey compared with those of other large-scale pulsar surveys with Arecibo, Parkes, Green Bank and Jodrell Bank.

the time series DMs must be fine enough so that the true DM of the pulsar one hopes to find is well approximated. If the DMs of the time series differ significantly from the true DM of the putative pulsar, then dispersive smearing may be large enough to wash out the signal, especially in the case of millisecond pulsars. Because of the quadratic dependence of dispersive smearing on observing frequency, this makes correcting for DM a much more computationally intensive task at low frequencies. Given the observing parameters of the GBT350 survey, in order to keep dispersive smearing below 1 ms for DMs up to 100 pc cm^{-3}, we must generate roughly 2600 trial DMs for our blind searches. The dedispersion plan, and resulting smearing as a function of DM, which also comes from the finite time and frequency resolution of the data, is shown in Figure 8.7. Thus, if one wants to maintain sensitivity to the fastest pulsars, searching the low-frequency data of the GBT350 survey is necessarily extremely computationally intensive. To fully search a single 2-minute pointing requires roughly 12 hr using a 64-bit, 2.2 GHz Opteron processor (i.e. the search time is 360 times longer than the observation time).

Our search pipeline for the GBT350 data is fully automated. The raw data are stored on the RAIDs of the Borg file servers (see §2.7) and information about the various observations, including their location on the Borg system and processing status, is stored in a MySQL database tailored specifically to this survey. A script is run which interfaces with the GBT350 database and the batch server of the Borg cluster to spawn processing jobs. This script queries the database for unprocessed pointings and then queries the Borg batch system for free processing resources. The data from individual observations are then sent to a free Borg node and processing begins. The processing itself consists of the following routine. First the data are converted from auto-correlation format to filterbank format (i.e. the spectral channels are formed). This filterbank version of the data is used for all subsequent processing. The data are then searched and masked for RFI in a manner identical to that described in §4.3.1. Dedispersion is done in two steps. First, a set of 64 subbands is created

by combining groups of 16 contiguous frequency channels from the initial 1024-channel data. Each subband is dedispersed to some central DM. Subsequently, time series with DMs close to the central DM of the subbands are generated and then searched. This process is repeated for various subband DMs until the desired range of DMs has been covered. After all the periodicity searches are complete, the candidates are collated to identify promising sources that appear at numerous DMs and are above the signal-to-noise threshold. These candidates are then folded and stored for inspection. A single pulse search is also performed on the time series, and the results of these searches are collated into a plot (see for instance Figure 8.9). Processed pointings are indicated in Figure 8.5.

8.2.4 Results

Approximately half of all the GBT350 pointings have already been run through our search pipeline. Thus far, we have discovered 14 pulsars (Table 8.2, Figure 8.8, and Figure 8.10). Of these, 11 were discovered in the standard periodicity search. The other 3 pulsars were found uniquely in the single pulse searches (Figure 8.9). These pulsars have been identified through a preliminary inspection of the candidate lists from our search processing. A deeper look at the results of the processing will likely result in the identification of other new pulsars, which were initially overlooked because of their lower signal-to-noise ratio. Also, because our initial inspection of the candidate lists focussed mostly on identifying the easiest-to-find slow pulsars, we may have missed millisecond pulsars in our first pass. Simulations by our group suggest we will find $1-2$ new millisecond pulsars in the survey area. This remains a primary goal of this survey.

The current batch of discoveries are all slow pulsars, with periods between $\sim 0.5-3\,\mathrm{s}$. Owing to the $\sim 0.6^\circ$ beam width of the GBT at 350 MHz, the positions of these pulsars were initially poorly constrained. Timing observations of these sources with the GBT at 350 and 820 MHz began in mid June 2006.

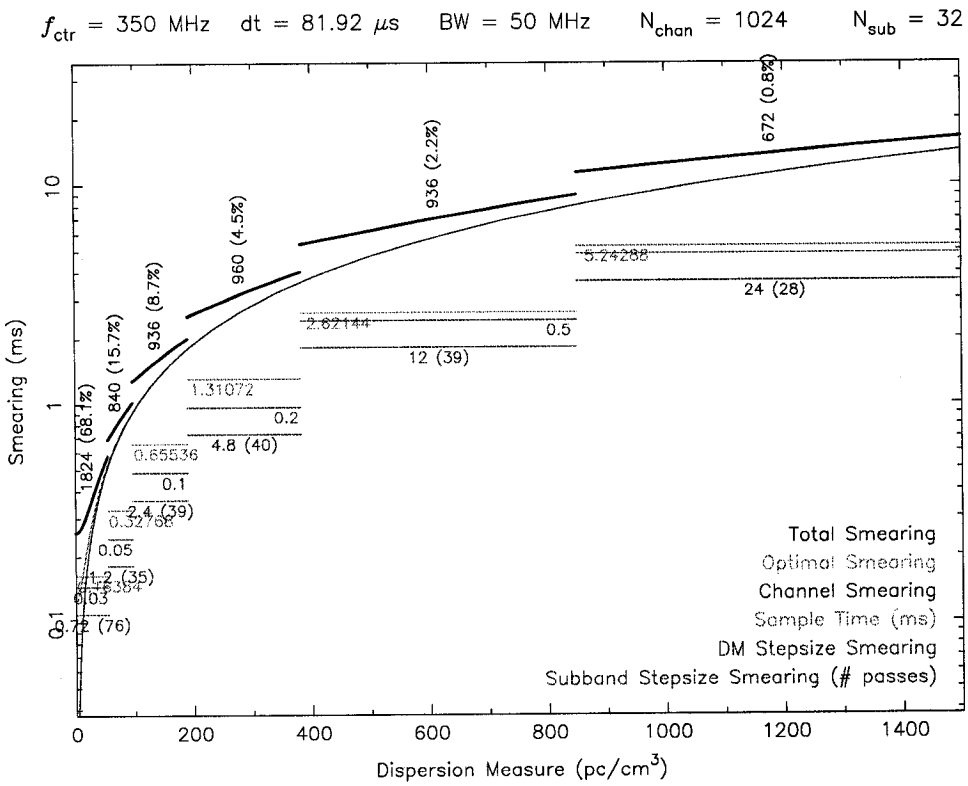

Figure 8.7: The dedispersion plan used in the GBT350 survey. Horizontal colored bars indicate the amount of smearing from various sources. The jumps are where a new downsampling in time is applied to the data. The thick black lines indicate the total smearing as a function of DM. The number of trial DMs and the fraction of the total work load is indicated above each segment. Roughly two thirds of the entire workload is dedicated to searching between DM = 0 − 50 pc cm^{-3}, where the spacing between trial DMs is only 0.03 pc cm^{-3}. This is done to maintain maximum sensitivity to fast-spinning, low-DM pulsars.

Pulsar Name	Spin Period (ms)	DM (pc cm^{-3})	Notes
Galactic Plane Survey			
J0033+61	912	37	
J0341+57	1888	100	
J0426+49	922	85	
J2136+49	696	168	
J2206+55	933	105	
J2218+57	1057	130	
J2239+60	3070	182	
J2328+61	790	33	
J2345+62	1799	117	
Precursor Survey			
J2045+70	588	57	
J2030+55	579	60	
Single-Pulse Sources			
G10319-084	1336	168	Periodic nuller?
G12380-168	637	129	Extreme nuller.
G13643+042	1473	141	

Table 8.2: Discoveries made by the GBT350 survey so far.

Gridding the pulsars with the smaller 820-MHz beam has resulted in improved positions, which will be used in our timing models. The timing solutions we are currently building will provide precise astrometric and rotational properties, and will determine if any of the new pulsars are in a long-orbital-period binary system. We will also be looking into the emission properties of these objects to see if there is any interesting behaviour, such as drifting pulses or periodic nulling.

Our searches for bright, dispersed single pulses revealed three promising candidates (Figure 8.9), which we confirmed in June 2006. These have no associated candidate in the periodicity searches (although some of the brighter sources identified by the periodicity searches also appear in the single pulse search). However, close examination of the times between bursts led to the identification of the pulsar spin periods of all three sources. In the case of the sources G10319−084/J2222+56 and G12380−168/J0058+61, the failure of the periodicity search in detecting these sources is likely due to nulling. PSR J2222+56 appears to null periodically (Figure 8.10), and during the discovery observation, it was nulled for more than half the observation. PSR J0058+61 is an even more extreme nuller (Figure 8.10), and during the discovery observation the emission is completely dominated by only a few bright pulses. G13643+042/J0243+60 appears to be a more steady emitter (Figure 8.10), and was likely missed in the periodicity searches because it is relatively faint and has a very short duty cycle of $\sim 1.3\%$. As our searches sum only the first 16 harmonics, it is likely that we are missing faint, very narrow pulsars. We plan to re-analyze the data using at least 32-harmonic summing.

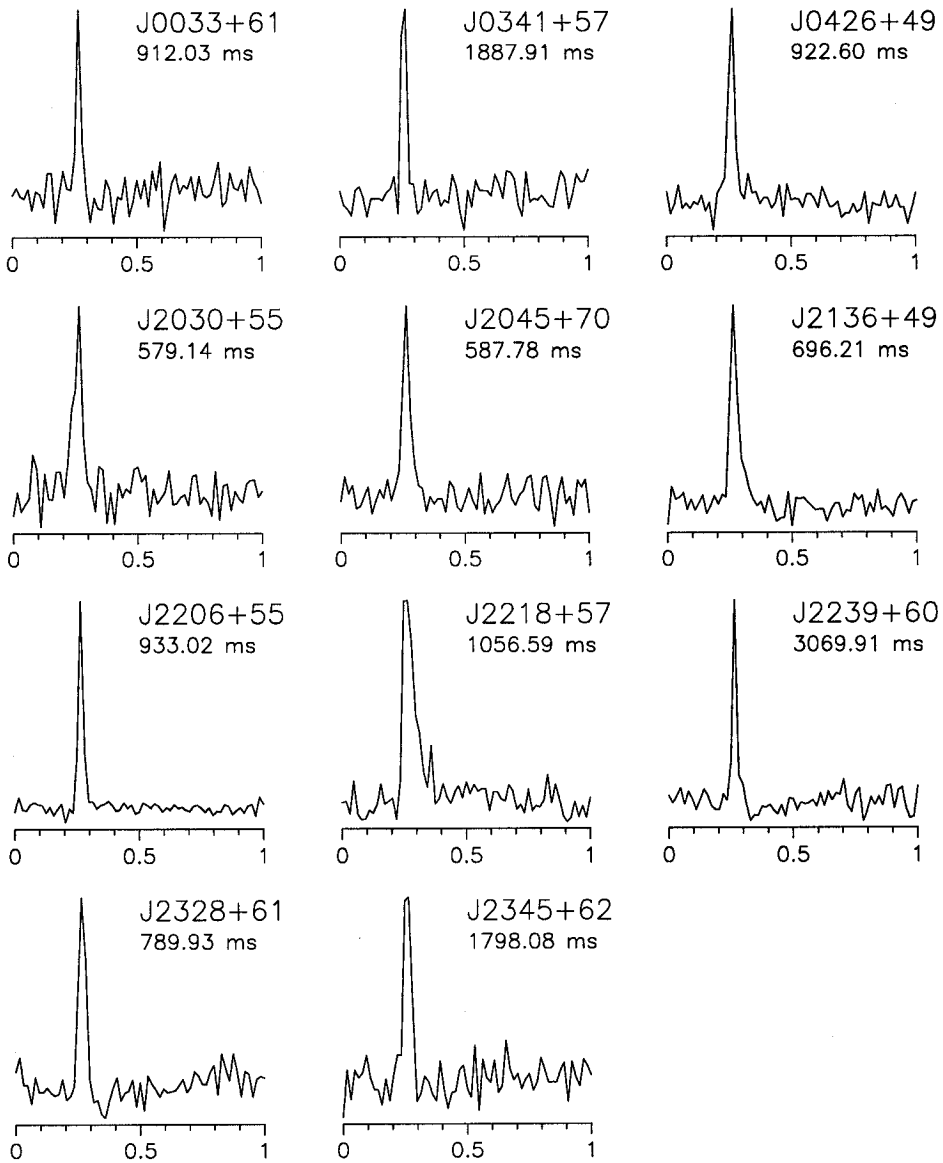

Figure 8.8: Pulses profiles of the 11 pulsars discovered thus far in the GBT350 survey, using the standard periodicity search. These are from the 120-s discovery observations of each pulsar. One full pulse cycle is shown.

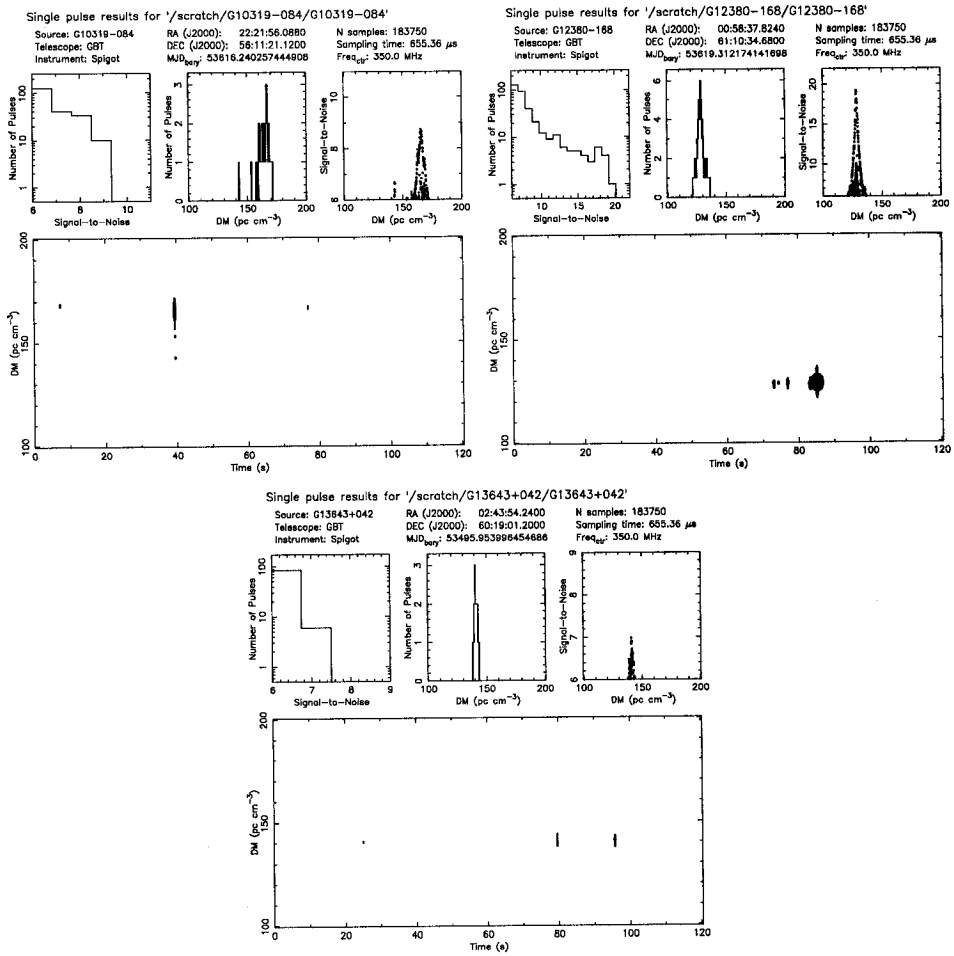

Figure 8.9: Single pulse discovery plots for three sources: G123.8−1.7, G103.2−0.8, and G136.4+0.4 (clockwise from top left). The bottom panel of each plot shows observation time on the abcissa and dispersion measure on the ordinate. Single pulses with significance above 6σ are plotted as circles, with larger circles indicating higher signal-to-noise pulses. Notice the lack of RFI in these observations, which greatly aids in the identification of faint single pulses. The top panels of each plot show, from left to right, number of pulses versus signal-to-noise ratio, number of pulses versus dispersion measure, and signal-to-noise ratio versus dispersion measure.

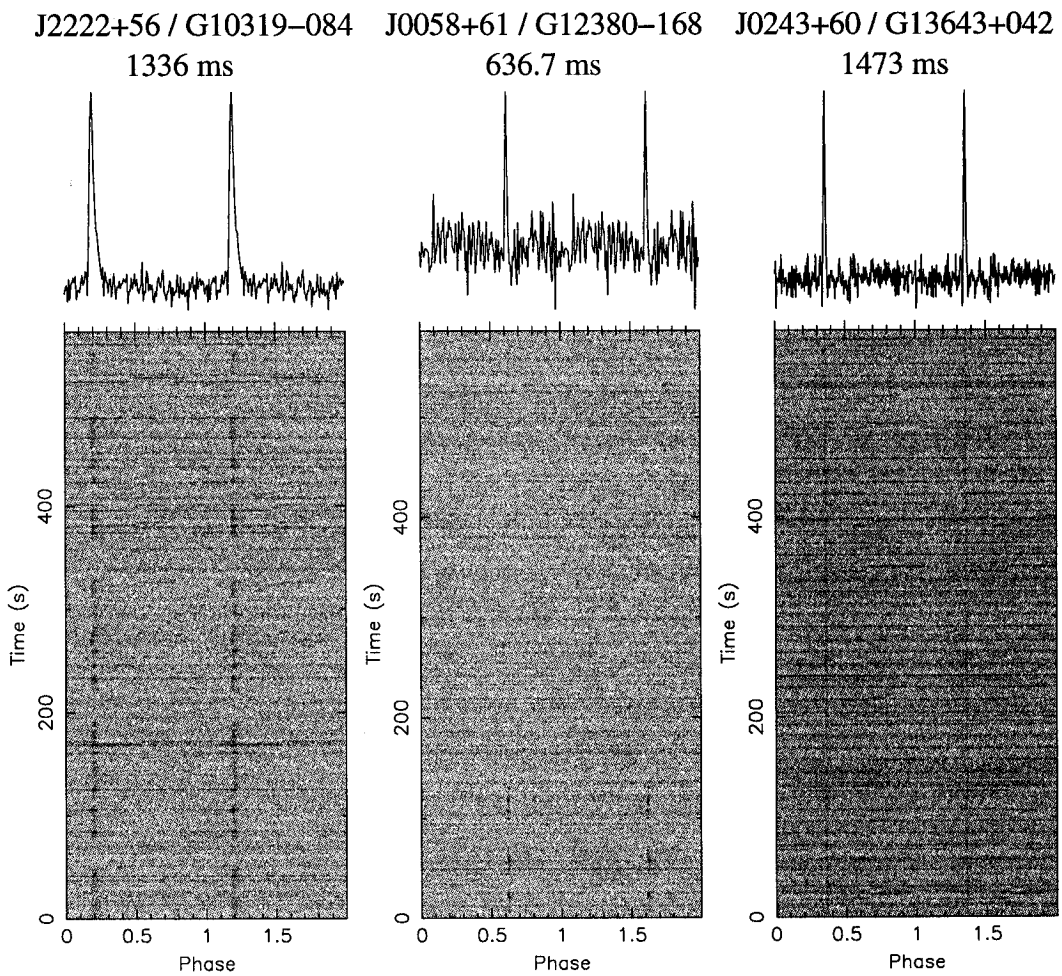

Figure 8.10: Folds of three roughly 600-s GBT follow-up observations of the single pulse discoveries shown in Figure 8.9. The observations are all at 350 MHz. The periods of these pulsars were determined by examining the spacing between single pulse events. *Left:* one sees what looks like periodic nulling from J2222+56. *Centre:* J0058+61 is on intermittently and only for roughly the first quarter of the observation. *Right:* the emission from J0243+60 is more steady; the duty cycle is very small, only ∼1.3%.

Chapter 9

Conclusions and Future Work

♫ *TV dinner by the pool, I'm so glad I'm finished school* ♫
– Frank Zappa, "Brown Shoes don't Make It",
from the album "Tinseltown Rebellion".

9.1 Conclusions

In this thesis, we have presented several successful searches for exotic radio pulsars, as well as follow-up work on our new discoveries. Here we summarize these results and comment on the potential for future work in these areas.

In Chapter 4, we presented a 1.4-GHz survey of all 22 known globular clusters observable with the Arecibo radio telescope that are within 50 kpc of the Earth. This survey discovered 10 binary and one isolated millisecond pulsar in 5 clusters. Three of the new binaries are in compact $2-4$-hr orbits, and show eclipses. This survey discovered a much higher fraction of very fast-spinning ($P_{\rm spin} \lesssim 3$ ms) and binary pulsars than previous searches of these clusters at 430 MHz, demonstrating our improved sensitivity to such systems. We comment on the characteristics of the globular cluster pulsar population in general, and discuss the luminosity and spin period distributions.

Given the unparalleled size of the Arecibo dish, it is unlikely that a more sensitive survey of these clusters will be performed in the near future with a different telescope. Indeed, some of the known pulsars in these clusters are too faint to be detectable with any other radio telescope. With Arecibo itself, there is the possibility of re-observing certain clusters at other frequencies. With multiple WAPP backends, it is possible to achieve 400 MHz (or potentially even 800 MHz) of bandwidth - although finding such a large spectral window that is relatively RFI-free will be challenging. This opens the possibility of observing the clusters with higher DMs at higher observing frequencies (> 2 GHz), while still maintaining enough sensitivity to detect faint, steep spectrum sources. Conversely, the 327-MHz receiver provides 50 MHz of bandwidth and will soon be better cooled. This receiver could be used to observe the low-DM clusters from our survey, using 4 WAPPs across the 50 MHz of bandwidth to minimize dispersive smearing. Continued timing of the most interesting pulsars in these clusters is also warranted.

In Chapter 5, we presented the discovery of the fastest-spinning pulsar currently known, PSR J1748−2446ad. Located in Terzan 5, PSR J1748−2446ad has a spin rate of 716 Hz and is in a 26-hr eclipsing binary with a $0.14\,M_\odot$ (minimum mass) companion. One can use PSR J1748−2446ad's spin rate to constrain its non-rotating radius, which must be less than 16 km if the star's mass is less than $2\,M_\odot$. The existence of PSR J1748−2446ad, and the strong observational biases against detecting such a system, suggest that other very-fast-spinning pulsars remain to be found. As 5 of the 10 fastest-spinning pulsars show eclipses, many of the fastest-spinning binary pulsars may be obscurred for a significant fraction of their orbit. The globular cluster Terzan 5 is now known to contain 5 of the 10 fastest-spinning pulsars in the Galactic globular cluster system, suggesting that this cluster is particularly good at manufacturing very fast-spinning pulsars.

Thanks to the hard work of Paulo Freire, we now have a phase-connected timing solution for PSR J1748−2446ad. Numerous orbital period derivatives

are required to smooth the residuals, which is unsurprising given the interaction that may be happening between the pulsar and its bloated companion. The timing position shows that PSR J1748−2446ad is likely associated with a *Chandra* X-ray point source identified by Heinke et al. (2006). This source is one of the hardest in the field. Timing of this source and the other 32 pulsars known in Terzan 5 is continuing with the GBT. We have also begun timing observations of the Terzan 5 pulsars using the Westerbork Synthesis Radio Telescope (WSRT) and the coherent data recorder PUMAII.

In Chapter 6, we presented deep radio pulsation searches of 5 promising *ASCA* X-ray counterparts to unidentified *EGRET* γ−ray sources. These observations culminated in the discovery of PSR J2021+3651, a 104-ms, young, energetic, Vela-like pulsar. This pulsar is plausibly the source of the γ−rays observed from 3EG J2021+3716, and potentially solves the long-standing mystery of this source's nature. No radio pulsar counterpart was detected in the other 4 *ASCA* sources we searched.

In Chapter 7, we presented follow-up X-ray observations of the area around PSR J2021+3651, using the *Chandra* satellite. These observations discovered an X-ray point source - likely thermal emission from the surface of the neutron star - and a compact pulsar wind nebula (PWN). X-ray timing observations using *Chandra*'s continuous clocking mode revealed possible X-ray pulsations when the data were folded with the radio ephemeris. Radio timing revealed a pulsar glitch.

We have received follow-up time with the European Space Agency's *XMM-Newton* observatory in order to image the faint, extended X-ray emission surrounding the compact PWN found with *Chandra*, and to verify whether jets hinted at in the *Chandra* data are real. These data are in hand and are currently being analyzed. A deep, $\sim$ 100-ks integration has also been approved for *Chandra* - although to a competing group - in order to derive better spectral parameters and to better ascertain the nebula's morphology.

In Chapter 8, we presented two on-going, large-scale surveys of the Galactic

Plane for radio pulsars. The first, the 1.4-GHz PALFA multibeam survey with Arecibo, will cover the Galactic Plane between $32° < l < 77°$ and $168° < l < 214°$ out to $b < |5°|$ and expects to find several hundred new pulsars in the coming years. So far, 28 new sources have been discovered, including the youngest pulsar binary system known, PSR J1906+0746. Full-resolution processing of this data has recently begun. The second, the 350-MHz GBT350 Galactic Plane survey, has almost completed observations between $75° < l < 165°$ out to $b < |5°|$. So far, 14 new sources have been discovered. Processing of this data will likely be completed in the next few months.

9.2 Future Work

In September 2006 I am off to the Netherlands to join Ben Stappers' pulsar group at the Universiteit van Amsterdam. There I will continue some of the survey work presented in this thesis, but also investigate new directions of pulsar research. I look forward to working with the Westerbork Synthesis Radio Telescope (WSRT) and the PUMA II coherent backend. This system has the potential for doing some very nice pulsar studies. I am also becoming involved with the LOw Frequency ARray for radio astronomy (LOFAR), setting the stage for an all-sky survey for pulsars with this instrument.

Bibliography

Alpar, M. A., Cheng, A. F., Ruderman, M. A., & Shaham, J. 1982, Nature, 300, 728

Anderson, S. B. 1993, Ph.D. Thesis, California Institute of Technology

Anderson, S. B., Gorham, P. W., Kulkarni, S. R., Prince, T. A., & Wolszczan, A. 1990, Nature, 346, 42

Andersson, N. 1998, ApJ, 502, 708

Andersson, N., Glampedakis, K., Haskell, B., & Watts, A. L. 2005, MNRAS, 361, 1153

Andersson, N., Kokkotas, K., & Schutz, B. F. 1999a, ApJ, 510, 846

Andersson, N., Kokkotas, K. D., & Stergioulas, N. 1999b, ApJ, 516, 307

Arnaud, K. A. 1996, in ASP Conf. Ser. 101: Astronomical Data Analysis Software and Systems V, ed. G. H. Jacoby & J. Barnes, 17

Baade, W. & Zwicky, F. 1934, PNAS, 20, 254

Backer, D. C., Kulkarni, S. R., Heiles, C., Davis, M. M., & Goss, W. M. 1982, Nature, 300, 615

Bailes, M. 1989, ApJ, 342, 917

Beloborodov, A. M. 2002, ApJL, 566, L85

Bhat, N. D. R., Cordes, J. M., Camilo, F., Nice, D. J., & Lorimer, D. R. 2004, ApJ, 605, 759

Bhattacharya, D. & van den Heuvel, E. P. J. 1991, Phys. Reports, 203, 1

Bietenholz, M. F., Kassim, N. E., & Weiler, K. W. 2001, ApJ, 560, 772

Bildsten, L. 1998, ApJL, 501, L89

Bildsten, L., Chakrabarty, D., Chiu, J., Finger, M. H., Koh, D. T., Nelson, R. W., Prince, T. A., Rubin, B. C., Scott, D. M., Stollberg, M., Vaughan, B. A., Wilson, C. A., & Wilson, R. B. 1997, ApJS, 113, 367

Bildsten, L. & Ushomirsky, G. 2000, ApJL, 529, L33

Bionta, R. M., Blewitt, G., Bratton, C. B., Caspere, D., & Ciocio, A. 1987, PhRvL, 58, 1494

Bracewell, R. N. 2000, The Fourier transform and its applications (McGraw-Hill series in electrical and computer engineering)

Braje, T. M., Romani, R. W., Roberts, M. S. E., & Kawai, N. 2002, ApJL, 565, L91

Brazier, K. T. S. & Johnston, S. 1999, MNRAS, 305, 671

Breton, R. P., Roberts, M. S. E., Ransom, S. M., Kaspi, V. M., Durant, M., Bergeron, P., & Faulkner, A. J. 2007, ApJ, in press

Burgay, M., Burderi, L., Possenti, A., D'Amico, N., Manchester, R. N., Lyne, A. G., Camilo, F., & Campana, S. 2003, ApJ, 589, 902

Burgay, M., Joshi, B. C., D'Amico, N., Possenti, A., Lyne, A. G., Manchester, R. N., McLaughlin, M. A., Kramer, M., Camilo, F., & Freire, P. C. C. 2006, MNRAS, 368, 283

Camilo, F., Bell, J. F., Manchester, R. N., Lyne, A. G., Possenti, A., Kramer, M., Kaspi, V. M., Stairs, I. H., D'Amico, N., Hobbs, G., Gotthelf, E. V., & Gaensler, B. M. 2001, ApJL, 557, L51

Camilo, F., Lorimer, D. R., Freire, P., Lyne, A. G., & Manchester, R. N. 2000, ApJ, 535, 975

Camilo, F. & Rasio, F. A. 2005, in ASP Conf. Ser. 328: Binary Radio Pulsars, ed. F. A. Rasio & I. H. Stairs, 147

Camilo, F., Stairs, I. H., Lorimer, D. R., Backer, D. C., Ransom, S. M., Klein, B., Wielebinski, R., Kramer, M., McLaughlin, M. A., Arzoumanian, Z., & Müller, P. 2002, ApJL, 571, L41

Carroll, B. W. & Ostlie, D. A. 1996, An Introduction to Modern Astrophysics (Reading, MA: Addison-Wesley)

Chakrabarty, D. 2005a, in ASP Conf. Ser. 328: Binary Radio Pulsars, ed. F. A. Rasio & I. H. Stairs, 279

Chakrabarty, D. 2005b, in ASP Conf. Series 328: Binary Radio Pulsars, ed. F. Rasio & I. Stairs, 279

Chakrabarty, D., Morgan, E. H., Muno, M. P., Galloway, D. K., Wijnands, R., van der Klis, M., & Markwardt, C. B. 2003, Nature, 424, 42

Chandler, A. M. 2003, Ph.D. Thesis, California Institute of Technology

Chandrasekhar, S. 1931, ApJ, 74, 81

Chevalier, R. A. 2000, ApJL, 539, L45

Cohn, H. N., Lugger, P. M., Grindlay, J. E., & Edmonds, P. D. 2002, ApJ, 571, 818

Cook, G. B., Shapiro, S. L., & Teukolsky, S. A. 1994, ApJL, 423, L117

Cordes, J. M. & Chernoff, D. F. 1997, ApJ, 482, 971

Cordes, J. M., Freire, P. C. C., Lorimer, D. R., Camilo, F., Champion, D. J., Nice, D. J., Ramachandran, R., Hessels, J. W. T., Vlemmings, W., van Leeuwen, J., Ransom, S. M., Bhat, N. D. R., Arzoumanian, Z., McLaughlin, M. A., Kaspi, V. M., Kasian, L., Deneva, J. S., Reid, B., Chatterjee, S., Han, J. L., Backer, D. C., Stairs, I. H., Deshpande, A. A., & Faucher-Giguere, C.-A. 2006, ApJ, 637, 446

Cordes, J. M. & Lazio, T. J. W. 2002a, (astro-ph/0207156)

—. 2002b, (astro-ph/0207156)

—. 2003, (astro-ph/0301598)

Cordes, J. M. & McLaughlin, M. A. 2003, ApJ, 596, 1142

Cottam, J., Paerels, F., & Mendez, M. 2002, Nature, 420, 51

Cutler, C. 2002, PhRvD, 66, 084025

D'Amico, N., Kaspi, V. M., Manchester, R. N., Camilo, F., Lyne, A. G., Possenti, A., Stairs, I. H., Kramer, M., Crawford, F., Bell, J. F., McKay, N. P. F., Gaensler, B. M., & Roberts, M. S. E. 2001a, ApJL, 552, L45

D'Amico, N., Possenti, A., Fici, L., Manchester, R. N., Lyne, A. G., Camilo, F., & Sarkissian, J. 2002, ApJL, 570, L89

D'Amico, N., Possenti, A., Manchester, R. N., Sarkissian, J., Lyne, A. G., & Camilo, F. 2001b, ApJL, 561, L89

Daugherty, J. K. & Harding, A. K. 1996, ApJ, 458, 278

De Jager, O. C., Swanepoel, J. W. H., & Raubenheimer, B. C. 1989, 221, 180

Demorest, P., Ramachandran, R., Backer, D., Ferdman, R., Stairs, I., & Nice, D. 2004, American Astronomical Society Meeting Abstracts, 205

Dewey, R. J., Taylor, J. H., Weisberg, J. M., & Stokes, G. H. 1985, ApJL, 294, L25

Dickey, J. M. & Lockman, F. J. 1990, ARA&A, 28, 215

Dodson, R. G., McCulloch, P. M., & Lewis, D. R. 2002, ApJL, 564, L85

Dotani, T., Asai, K., & Greiner, J. 1999, PASJ, 51, 519

Dowd, A., Sisk, W., & Hagen, J. 2000, in ASP Conf. Ser. 202: IAU Colloq. 177: Pulsar Astronomy - 2000 and Beyond, ed. M. Kramer, N. Wex, & R. Wielebinski, 275

Dyks, J. & Rudak, B. 2003, ApJ, 598, 1201

Edwards, R. T., Bailes, M., van Straten, W., & Britton, M. C. 2001, MNRAS, 326, 358

Faulkner, A. J., Stairs, I. H., Kramer, M., Lyne, A. G., Hobbs, G., Possenti, A., Lorimer, D. R., Manchester, R. N., McLaughlin, M. A., D'Amico, N., Camilo, F., & Burgay, M. 2004, MNRAS, 355, 147

Ferdman, R. D., Stairs, I. H., Backer, D. C., Ramachandran, R., Demorest, P., Nice, D. J., Lyne, A. G., Kramer, M., Lorimer, D., McLaughlin, M., Manchester, D., Camilo, F., D'Amico, N., Possenti, A., Burgay, M., Joshi, B. C., & Freire, P. C. 2004, American Astronomical Society Meeting Abstracts, 205

Foster, R. S. & Backer, D. C. 1990, ApJ, 361, 300

Freire, P. C., Gupta, Y., Ransom, S. M., & Ishwara-Chandra, C. H. 2004, ApJL, 606, L53

Freire, P. C., Kramer, M., Lyne, A. G., Camilo, F., Manchester, R. N., & D'Amico, N. 2001, ApJL, 557, L105

Freire, P. C. C. 2005, in ASP Conf. Ser. 328: Binary Radio Pulsars, ed. F. A. Rasio & I. H. Stairs, 405

Freire, P. C. C., Hessels, J. W. T., Nice, D. J., Ransom, S. M., Lorimer, D. R., & Stairs, I. H. 2005, ApJ, 621, 959

Friedman, J. L. & Morsink, S. M. 1998, ApJ, 502, 714

Gaensicke, B. T., Braje, T. M., & Romani, R. W. 2002, VizieR Online Data Catalog, 338, 61001

Gaensler, B. M., Arons, J., Kaspi, V. M., Pivovaroff, M. J., Kawai, N., & Tamura, K. 2002, ApJ, 569, 878

Gaensler, B. M., van der Swaluw, E., Camilo, F., Kaspi, V. M., Baganoff, F. K., Yusef-Zadeh, F., & Manchester, R. N. 2004, ApJ, 616, 383

Gavriil, F. P., Kaspi, V. M., & Woods, P. M. 2002, Nature, 419, 142

Ghosh, P. & Lamb, F. K. 1979, ApJ, 234, 296

Gold, T. 1968, Nature, 218, 731

Goldreich, P. & Julian, W. H. 1969, ApJ, 157, 869

Gotthelf, E. V. 2003, ApJ, 591, 361

Gotthelf, E. V., Halpern, J. P., & Dodson, R. 2002, 567, L125

Gotthelf, E. V., Ueda, Y., Fujimoto, R., Kii, T., & Yamaoka, K. 2000, ApJ, 543, 417

Halpern, J. P., Camilo, F., Gotthelf, E. V., Helfand, D. J., Kramer, M., Lyne, A. G., Leighly, K. M., & Eracleous, M. 2001, ApJL, 552, L125

Halpern, J. P. & Holt, S. S. 1992, Nature, 357, 222

Harris, W. E. 1996, AJ, 112, 1487

Hartman, R. C., Bertsch, D. L., Bloom, S. D., Chen, A. W., Deines-Jones, P., Esposito, J. A., Fichtel, C. E., Friedlander, D. P., Hunter, S. D., McDonald, L. M., Sreekumar, P., Thompson, D. J., Jones, B. B., Lin, Y. C., Michelson, P. F., Nolan, P. L., Tompkins, W. F., Kanbach, G., Mayer-Hasselwander, H. A., Mucke, A., Pohl, M., Reimer, O., Kniffen, D. A., Schneid, E. J., von Montigny, C., Mukherjee, R., & Dingus, B. L. 1999, ApJS, 123, 79

Heggie, D. C. 1975, MNRAS, 173, 729

Heinke, C. O., Wijnands, R., Cohn, H. N., Lugger, P. M., Grindlay, J. E., Pooley, D., & Lewin, W. H. G. 2006, astro-ph/0606253

Helfand, D. J. 1994, MNRAS, 267, 490

Helfand, D. J., Gotthelf, E. V., & Halpern, J. P. 2001, ApJ, 556, 380

Hessels, J. W. T., Ransom, S. M., Stairs, I. H., Freire, P. C. C., Kaspi, V. M., & Camilo, F. 2006, Science, 311, 1901

Hessels, J. W. T., Roberts, M. S. E., Ransom, S. M., Kaspi, V. M., Romani, R. W., Ng, C.-Y., Freire, P. C. C., & Gaensler, B. M. 2004, ApJ, 612, 389

Hewish, A., Bell, S. J., Pilkington, J. D., Scott, P. F., & Collins, R. A. 1968, Nature, 217, 709

Hibschman, J. A. & Arons, J. 2001, ApJ, 554, 624

Hirata, K., Kajita, T., Koshiba, M., Nakahata, M., & Oyama, Y. 1987, PhRvL, 58, 1490

Hulse, R. A. & Taylor, J. H. 1975a, ApJL, 201, L55

—. 1975b, ApJL, 195, L51

Hut, P., McMillan, S., Goodman, J., Mateo, M., Phinney, E. S., Pryor, C., Richer, H. B., Verbunt, F., & Weinberg, M. 1992, PASP, 104, 981

Jacoby, B. A. 2005, Ph.D. Thesis, California Institute of Technology

Jenet, F. A., Hobbs, G. B., Lee, K. J., & Manchester, R. N. 2005, ApJL, 625, L123

Johnston, H. M. & Kulkarni, S. R. 1991, ApJ, 368, 504

Jouteux, S., Ramachandran, R., Stappers, B. W., Jonker, P. G., & van der Klis, M. 2002, A&A, 384, 532

Kaplan, D. L., Escoffier, R. P., Lacasse, R. J., O'Neil, K., Ford, J. M., Ransom, S. M., Anderson, S. B., Cordes, J. M., Lazio, T. J. W., & Kulkarni, S. R. 2005, PASP, 117, 643

Kaspi, V. M. & McLaughlin, M. A. 2005, ApJL, 618, L41

Kaspi, V. M., Roberts, M. S. E., & Harding, A. K. 2006, Isolated neutron stars (Compact stellar X-ray sources. Edited by Walter Lewin & Michiel van der Klis. Cambridge Astrophysics Series, No. 39. Cambridge, UK), 279–339

Kaspi, V. M., Roberts, M. S. E., Vasisht, G., Gotthelf, E. V., Pivovaroff, M., & Kawai, N. 2001, 560, 371

Kaspi, V. M., Taylor, J. H., & Ryba, M. 1994, 428, 713

Kifune, T., Tanimori, T., Ogio, S., Tamura, T., Fujii, H., Fujimoto, M., Hara, T., Hayashida, N., Kabe, S., Kakimoto, F., Matsubara, Y., Mizumoto, Y., Muraki, Y. ., Suda, T., Teshima, M., Tsukagoshi, T., Watase, Y., Yoshikoshi, T., Edwards, P. G., Patterson, J. R., Roberts, M. D., Rowell, G. P., & Thornton, G. J. 1995, 438, L91

King, I. R. 1966, AJ, 71, 64

Kramer, M., Bell, J. F., Manchester, R. N., Lyne, A. G., Camilo, F., Stairs, I. H., D'Amico, N., Kaspi, V. M., Hobbs, G., Morris, D. J., Crawford, F.,

Possenti, A., Joshi, B. C., McLaughlin, M. A., Lorimer, D. R., & Faulkner, A. J. 2003, MNRAS, 342, 1299

Kramer, M., Lorimer, D. R., Lyne, A. G., McLaughlin, M., Burgay, M., D'Amico, N., Possenti, A., Camilo, F., Freire, P. C. C., Joshi, B. C., Manchester, R. N., Reynolds, J., Sarkissian, J., Stairs, I. H., & Ferdman, R. D. 2005, astro-ph/0503386

Kramer, M., Lyne, A. G., O'Brien, J. T., Jordan, C. A., & Lorimer, D. R. 2006, Science, 312, 549

Kulkarni, S. R., Anderson, S. B., Prince, T. A., & Wolszczan, A. 1991, Nature, 349, 47

Kulkarni, S. R., Goss, W. M., Wolszczan, A., & Middleditch, J. 1990, ApJL, 363, L5

Lamb, R. C. & Macomb, D. J. 1997, ApJ, 488, 872

Lattimer, J. M. & Prakash, M. 2004, Science, 304, 536

Levin, Y. & Ushomirsky, G. 2001, MNRAS, 324, 917

Li, B. & Steiner, A. 2005, nucl-th/0511064

Lindblom, L., Owen, B. J., & Morsink, S. M. 1998, PhRvL, 80, 4843

Lorimer, D. R., Faulkner, A. J., Lyne, A. G., Manchester, R. N., Kramer, M., McLaughlin, M. A., Hobbs, G., Possenti, A., Stairs, I. H., Camilo, F., Burgay, M., D'Amico, N., Corongiu, A., & Crawford, F. 2006a, (astro-ph/0607640)

Lorimer, D. R. & Kramer, M. 2004, Handbook of Pulsar Astronomy (Handbook of pulsar astronomy, by D.R. Lorimer and M. Kramer. Cambridge observing handbooks for research astronomers, Vol. 4. Cambridge, UK: Cambridge University Press, 2004)

Lorimer, D. R., Stairs, I. H., Freire, P. C., Cordes, J. M., Camilo, F., Faulkner, A. J., Lyne, A. G., Nice, D. J., Ransom, S. M., Arzoumanian, Z., Manchester, R. N., Champion, D. J., van Leeuwen, J., Mclaughlin, M. A., Ramachandran, R., Hessels, J. W., Vlemmings, W., Deshpande, A. A., Bhat, N. D., Chatterjee, S., Han, J. L., Gaensler, B. M., Kasian, L., Deneva, J. S., Reid, B., Lazio, T. J., Kaspi, V. M., Crawford, F., Lommen, A. N., Backer, D. C., Kramer, M., Stappers, B. W., Hobbs, G. B., Possenti, A., D'Amico, N., & Burgay, M. 2006b, ApJ, 640, 428

Lorimer, D. R., Xilouris, K. M., Fruchter, A. S., Stairs, I. H., Camilo, F., Vazquez, A. M., Eder, J. A., McLaughlin, M. A., Roberts, M. S. E., Hessels, J. W. T., & Ransom, S. M. 2005, MNRAS, 359, 1524

Lyne, A. G., Biggs, J. D., Brinklow, A., McKenna, J., & Ashworth, M. 1988, Nature, 332, 45

Lyne, A. G., Burgay, M., Kramer, M., Possenti, A., Manchester, R. N., Camilo, F., McLaughlin, M. A., Lorimer, D. R., D'Amico, N., Joshi, B. C., Reynolds, J., & Freire, P. C. C. 2004, Science, 303, 1153

Lyne, A. G., Johnston, S., Manchester, R. N., Staveley-Smith, L., & D'Amico, N. 1990, Nature, 347, 650

Lyne, A. G., Johnston, S., Manchester, R. N., Staveley-Smith, L., D'Amico, N., Lim, J., Fruchter, A. S., & Goss, W. M. 1990, Millisecond pulsar in Terzan 5

Lyne, A. G., Manchester, R. N., Lorimer, D. R., Bailes, M., D'Amico, N., Tauris, T. M., Johnston, S., Bell, J. F., & Nicastro, L. 1998, MNRAS, 295, 743

Lyne, A. G., Manchester, R. N., & Taylor, J. H. 1985, MNRAS, 213, 613

Lyne, A. G., Mankelow, S. H., Bell, J. F., & Manchester, R. N. 2000, MNRAS, 316, 491

Malofeev, V. M., Gil, J. A., Jessner, A., Malov, I. F., Seiradakis, J. H., Sieber, W., & Wielebinski, R. 1994, A&A, 285, 201

Manchester, R. 2006, astro-ph/0604288

Manchester, R. N., Hobbs, G. B., Teoh, A., & Hobbs, M. 2005, AJ, 129, 1993

Manchester, R. N., Lyne, A. G., Camilo, F., Bell, J. F., Kaspi, V. M., D'Amico, N., McKay, N. P. F., Crawford, F., Stairs, I. H., Possenti, A., Kramer, M., & Sheppard, D. C. 2001, MNRAS, 328, 17

Manchester, R. N., Lyne, A. G., D'Amico, N., Bailes, M., Johnston, S., Lorimer, D. R., Harrison, P. A., Nicastro, L., & Bell, J. F. 1996, MNRAS, 279, 1235

Maron, O., Kijak, J., Kramer, M., & Wielebinski, R. 2000a, A&AS, 147, 195

—. 2000b, A&AS, 147, 195

McConnell, D., Deshpande, A. A., Connors, T., & Ables, J. G. 2004, MNRAS, 348, 1409

McLaughlin, M. A. & Cordes, J. M. 2003, astro-ph/0310748

McLaughlin, M. A., Lyne, A. G., Lorimer, D. R., Kramer, M., Faulkner, A. J., Manchester, R. N., Cordes, J. M., Camilo, F., Possenti, A., Stairs, I. H., Hobbs, G., D'Amico, N., Burgay, M., & O'Brien, J. T. 2006, Nature, 439, 817

McLaughlin, M. A., Stairs, I. H., Kaspi, V. M., Lorimer, D. R., Kramer, M., Lyne, A. G., Manchester, R. N., Camilo, F., Hobbs, G., Possenti, A., D'Amico, N., & Faulkner, A. J. 2003, ApJL, 591, L135

Mel'nik, A. M. & Efremov, Y. N. 1995, 21, 10

Meylan, G. & Heggie, D. C. 1997, A&ARv, 8, 1

Middleditch, J. & Kristian, J. 1984, 279, 157

Migliazzo, J. M., Gaensler, B. M., Backer, D. C., Stappers, B. W., van der Swaluw, E., & Strom, R. G. 2002, ApJL, 567, L141

Monet, D. G., Levine, S. E., Canzian, B., Ables, H. D., Bird, A. R., Dahn, C. C., Guetter, H. H., Harris, H. C., Henden, A. A., Leggett, S. K., Levison, H. F., Luginbuhl, C. B., Martini, J., Monet, A. K. B., Munn, J. A., Pier, J. R., Rhodes, A. R., Riepe, B., Sell, S., Stone, R. C., Vrba, F. J., Walker, R. L., Westerhout, G., Brucato, R. J., Reid, I. N., Schoening, W., Hartley, M., Read, M. A., & Tritton, S. B. 2003, AJ, 125, 984

Morgan, E., Kaaret, P., & Vanderspek, R. 2005, The Astronomer's Telegram, 523, 1

Mott, A. J. & Freire, P. C. 2003, in Bulletin of the American Astronomical Society, 1292

Muno, M. P., Clark, J. S., Crowther, P. A., Dougherty, S. M., de Grijs, R., Law, C., McMillan, S. L. W., Morris, M. R., Negueruela, I., Pooley, D., Portegies Zwart, S., & Yusef-Zadeh, F. 2006, ApJL, 636, L41

Ng, C.-Y. & Romani, R. W. 2004, ApJ, 601, 479

Nicastro, L., Lyne, A. G., Lorimer, D. R., Harrison, P. A., Bailes, M., & Skidmore, B. D. 1995, MNRAS, 273, L68

Nice, D. J. & Sayer, R. W. 1997, ApJ, 476, 261

Ozel, F. 2006, astro-ph/0605106

Pacini, F. 1967, Nature, 216, 567

Pavlov, G. G. & Bezchastnov, V. G. 2005, ApJL, 635, L61

Pavlov, G. G., Teter, M. A., Kargaltsev, O., & Sanwal, D. 2003, ApJ, 591, 1157

Pavlov, G. G., Zavlin, V. E., Sanwal, D., Burwitz, V., & Garmire, G. P. 2001, ApJL, 552, L129

Pooley, D., Lewin, W. H. G., Anderson, S. F., Baumgardt, H., Filippenko, A. V., Gaensler, B. M., Homer, L., Hut, P., Kaspi, V. M., Makino, J., Margon, B., McMillan, S., Portegies Zwart, S., van der Klis, M., & Verbunt, F. 2003, ApJL, 591, L131

Possenti, A., Cerutti, R., Colpi, M., & Mereghetti, S. 2002, A&A, 387, 993

Possenti, A., D'Amico, N., Manchester, R. N., Camilo, F., Lyne, A. G., Sarkissian, J., & Corongiu, A. 2003, ApJ, 599, 475

Radhakrishnan, V. & Srinivasan, G. 1982a, CurSci, 51, 1096

—. 1982b, 51, 1096

Rankin, J. M. 1993, ApJ, 405, 285

Ransom, S. M. 2001, Ph.D. Thesis, Harvard University

Ransom, S. M., Cordes, J. M., & Eikenberry, S. S. 2003, ApJ, 589, 911

Ransom, S. M., Eikenberry, S. S., & Middleditch, J. 2002, AJ, 124, 1788

Ransom, S. M., Hessels, J. W. T., Stairs, I. H., Freire, P. C. C., Camilo, F., Kaspi, V. M., & Kaplan, D. L. 2005a, Science, 307, 892

Ransom, S. M., Hessels, J. W. T., Stairs, I. H., Freire, P. C. C., Kaspi, V. M., & Camilo, F. 2005b, American Astronomical Society Meeting Abstracts, 207

Ransom, S. M., Hessels, J. W. T., Stairs, I. H., Kaspi, V. M., Freire, P. C. C., & Backer, D. C. 2005c, in ASP Conf. Ser. 328: Binary Radio Pulsars, ed. F. A. Rasio & I. H. Stairs, 199

Ransom, S. M., Stairs, I. H., Backer, D. C., Greenhill, L. J., Bassa, C. G., Hessels, J. W. T., & Kaspi, V. M. 2004, ApJ, 604, 328

Rickett, B. J. 1977, ARA&A, 15, 479

Roberts, M. S. E. 2003, in ASP Conf. Ser. 302: Radio Pulsars, 337

Roberts, M. S. E., Hessels, J. W. T., Ransom, S. M., Kaspi, V. M., Freire, P. C. C., Crawford, F., & Lorimer, D. R. 2002, ApJL, 577, L19

Roberts, M. S. E., Romani, R. W., Johnston, S., & Green, A. J. 1999, ApJ, 515, 712

Roberts, M. S. E., Romani, R. W., & Kawai, N. 2001, ApJS, 133, 451

Roberts, M. S. E., Tam, C. R., Kaspi, V. M., Lyutikov, M., Vasisht, G., Pivovaroff, M., Gotthelf, E. V., & Kawai, N. 2003, ApJ, 588, 992

Romani, R. W. 1996, ApJ, 470, 469

Romani, R. W. & Yadigaroglu, I.-A. 1995, ApJ, 438, 314

Rutledge, R. E., Bildsten, L., Brown, E. F., Pavlov, G. G., & Zavlin, V. E. 2002, ApJ, 577, 346

Sayer, R. W., Nice, D. J., & Taylor, J. H. 1997, ApJ, 474, 426

Scheuer, P. A. G. 1968, Nature, 218, 920

Sigurdsson, S. & Phinney, E. S. 1993, ApJ, 415, 631

Sigurdsson, S. & Thorsett, S. E. 2005, in ASP Conf. Ser. 328: Binary Radio Pulsars, ed. F. A. Rasio & I. H. Stairs, 213

Sipior, M. S., Portegies Zwart, S., & Nelemans, G. 2004, MNRAS, 354, L49

Slane, P. O., Helfand, D. J., & Murray, S. S. 2002, ApJL, 571, L45

Smarr, L. L. & Blandford, R. 1976, ApJ, 207, 574

Stairs, I. H. 2004, Science, 304, 547

Stairs, I. H., Faulkner, A. J., Lyne, A. G., Kramer, M., Lorimer, D. R., McLaughlin, M. A., Manchester, R. N., Hobbs, G. B., Camilo, F., Possenti, A., Burgay, M., D'Amico, N., Freire, P. C., & Gregory, P. C. 2005, ApJ, 632, 1060

Standish, E. M. 1998, Interoffice Memo. 312.F-98-048. Pasadena: JPL

Stappers, B. W., Gaensler, B. M., Kaspi, V. M., van der Klis, M., & Lewin, W. H. G. 2003, Science, 299, 1372

Staveley-Smith, L., Wilson, W. E., Bird, T. S., Disney, M. J., Ekers, R. D., Freeman, K. C., Haynes, R. F., Sinclair, M. W., Vaile, R. A., Webster, R. L., & Wright, A. E. 1996, Pub Astro Soc of Aus, 13, 243

Stokes, G. H., Segelstein, D. J., Taylor, J. H., & Dewey, R. J. 1986, ApJ, 311, 694

Tam, C. & Roberts, M. S. E. 2003, ApJL, 598, L27

Tavani, M. 1991, ApJL, 379, L69

Taylor, J. H. & Cordes, J. M. 1993, ApJ, 411, 674

Thompson, C. & Duncan, R. C. 1995, MNRAS, 275, 255

—. 1996, ApJ, 473, 322

Thompson, D. J. 2001, in ASSL Vol. 267: The Nature of Unidentified Galactic High-Energy Gamma-Ray Sources, ed. A. Carramiñana, O. Reimer, & D. J. Thompson, 349–352

Thompson, D. J., Bailes, M., Bertsch, D. L., Cordes, J., D'Amico, N., Esposito, J. A., Finley, J., Hartman, R. C., Hermsen, W., Kanbach, G., Kaspi, V. M., Kniffen, D. A., Kuiper, L., Lin, Y. C., Lyne, A., Manchester, R., Matz, S. M., Mayer-Hasselwander, H. A., Michelson, P. F., Nolan, P. L., Ogelman, H., Pohl, M., Ramanamurthy, P. V., Sreekumar, P., Reimer, O., Taylor, J. H., & Ulmer, M. 1999, ApJ, 516, 297

Thorsett, S. E., Arzoumanian, Z., Camilo, F., & Lyne, A. G. 1999, ApJ, 523, 763

Voges, W., Aschenbach, B., Boller, T., Brauninger, H., Briel, U., Burkert, W., Dennerl, K., Englhauser, J., Gruber, R., Haberl, F., Hartner, G., Hasinger, G., Pfeffermann, E., Pietsch, W., Predehl, P., Schmitt, J., Trumper, J., & Zimmermann, U. 2000, VizieR Online Data Catalog, 9029

Wagoner, R. V. 1984, ApJ, 278, 345

Weisskopf, M. C., Hester, J. J., Tennant, A. F., Elsner, R. F., Schulz, N. S., Marshall, H. L., Karovska, M., Nichols, J. S., Swartz, D. A., Kolodziejczak, J. J., & O'Dell, S. L. 2000, ApJL, 536, L81

Wijnands, R. 2005, astro-ph/0501264

Wijnands, R. & van der Klis, M. 1998, Nature, 394, 344

Wolszczan, A. 1991, Nature, 350, 688

Wolszczan, A., Anderson, S., Kulkarni, S., & Prince, T. 1989a, IAU Circ., 4880, 1

Wolszczan, A. & Frail, D. A. 1992, Nature, 355, 145

Wolszczan, A., Kulkarni, S. R., Middleditch, J., Backer, D. C., Fruchter, A. S., & Dewey, R. J. 1989b, Nature, 337, 531

Woods, P. M. & Thompson, C. 2004, astro-ph/0406133

Yadigaroglu, I.-A. & Romani, R. W. 1997, ApJ, 476, 347

Zhang, B. & Harding, A. K. 2000, ApJ, 532, 1150

Zoccali, M., Renzini, A., Ortolani, S., Bragaglia, A., Bohlin, R., Carretta, E., Ferraro, F. R., Gilmozzi, R., Holberg, J. B., Marconi, G., Rich, R. M., & Wesemael, F. 2001, ApJ, 553, 733